



# LIFT & ESCALATOR SYMPOSIUM

## 11TH SYMPOSIUM ON LIFT & ESCALATOR TECHNOLOGIES

**Volume 11**

September 2020

ISSN 2052-7225 (Print)

ISSN 2052-7233 (Online)

[www.liftsymposium.org](http://www.liftsymposium.org)



## **Legal notices**

The rights of publication or translation are reserved.

No part of this publication may be reproduced, stored in a retrieval system or transmitted in any form or by any means without prior permission of the copyright holders. Requests for republication should be made via [www.liftsymposium.org](http://www.liftsymposium.org).

© 2020 The Lift and Escalator Symposium Educational Trust, The University of Northampton, The CIBSE Lifts Group, LEIA and the authors.

No representation is made with regard to the accuracy of the information contained in these proceedings. No legal responsibility or liability is accepted by in relation to errors or omissions. Any commercial products included within this publication are included for the purpose of illustration only and their inclusion does not constitute endorsement or recommendation.

## **Management Team**

Professor Lutfi Al-Sharif, The University of Jordan  
Eur-Ing David Cooper, The CIBSE Lifts Group, The University of Northampton (Charity Trustee)  
Mrs Elizabeth Evans, The CIBSE Lifts Group  
Professor Stefan Kaczmarczyk, The University of Northampton (Charity Trustee)  
Mr Nick Mellor, LEIA, The University of Northampton (Charity Trustee)  
Dr Richard Peters, The CIBSE Lifts Group, The University of Northampton (Charity Trustee)  
Dr Rory Smith, The CIBSE Lifts Group, The University of Northampton

## **UK Organizing Committee**

Dr Jonathan Adams, The University of Northampton  
Eur Ing David Cooper, The CIBSE Lifts Group, The University of Northampton  
Mrs Elizabeth Evans, The CIBSE Lifts Group  
Professor Stefan Kaczmarczyk, The University of Northampton (Co-Chair)  
Mr Nick Mellor, LEIA, The University of Northampton  
Dr Richard Peters, The CIBSE Lifts Group, The University of Northampton (Co-Chair)  
Dr Rory Smith, The CIBSE Lifts Group, The University of Northampton

## **Scientific Committee**

Professor Xabier Arrasate, Mondragno University, Spain  
Dr Rosa Basagoiti, University of Mondragón, Spain  
Mrs Theresa Christy, Lerch Bates Inc, USA  
Dr Stefan Gerstenmeyer, thyssenkrupp Elevator, Germany  
Dr Lee Gray, UNC Charlotte, USA  
Mr Philip Hofer, Schindler Elevator Ltd, Switzerland  
Professor Ignacio Herrera, University of Extremadura, Spain  
Mr Ben Langham, London Underground, U.K.  
Dr Ana-Maria Lorente Lafuente, Aachen University, Germany  
Dr Mike Pentney, Peters Research Ltd, UK.  
Dr Bruce A Powell, Bruce Powell Company, Inc, USA  
Dr Gabriela Roivainen, Kone, Finland  
Mr Adam J Scott, Sweco, UK  
Dr Marja-Liisa Siikonen, Kone, Finland  
Dr Janne Sorsa, Kone, Finland  
Dr Seiji Watanabe, Mitsubishi Electric Corp., Japan  
Mr Jochem Wit, Deerns, Netherlands

# FOREWORD

It is with great pleasure that we present the proceedings of the 11<sup>th</sup> Symposium on Lift and Escalator Technologies, 23-25 September 2020, organised by The Lift and Escalator Symposium Educational Trust. The Covid 19 pandemic necessitates this year's Symposium to take place on-line, but we have strived to retain many characteristics of the traditional meeting. We hope to meet next year, face to face.

The objective of The Lift and Escalator Symposium Educational Trust is to advance education in lifts, escalators and related technologies. The Trust is a Registered Charity No: 1170947 and is supported by The University of Northampton, The Chartered Institution of Building Services Engineers (CIBSE) and The Lift and Escalator Industry Association (LEIA).

Proceedings from the full conference series (since 2011) are available to download from [www.liftsymposium.org](http://www.liftsymposium.org). The proceedings are indexed in Scopus as "Symposium on Lift and Escalator Technologies", starting from the 2015 Symposium. Scopus is the world's largest abstract and citation database of peer-reviewed literature (scientific journals, books and conference proceedings), see <https://blog.scopus.com/about>.

The Lift Engineering programme offered at The University of Northampton includes postgraduate courses at MSc/ MPhil/ PhD levels that involves study of the advanced principles and philosophy underlying lift and escalator technologies. The programme aims to provide a detailed, academic study of engineering and related management issues for persons employed in lift making and allied industries.

The CIBSE Lifts Group is a specialist forum for members who have an interest in vertical transportation. The group meets regularly to promote technical standards, training and education, publications and various aspects of the vertical transportation industry. The CIBSE Lifts Group directs the development of CIBSE Guide D: Transportation systems in buildings, the de facto reference on vertical transportation.

LEIA is the UK trade association and advisory body for the lift and escalator industry with a membership covering some 95% of the lift and escalator industry. LEIA members supply passenger and goods/service lifts, stairlifts, homelifts, lifting platforms, escalators, passenger conveyors and a range of component parts for such products. LEIA members undertake the maintenance and modernisation of more than 250,000 products falling within the scope of the Association. LEIA provides advice on health, safety and standards matters, promotes education and training especially through its distinctive distance learning programme.

The Symposium brings together experts from the field of vertical transportation, offering an opportunity for speakers to present peer reviewed papers on the subject of their research. Speakers include industry experts, academics and post graduate students.

The papers are listed alphabetically by title. The requirement was to prepare an extended abstract, but full papers were accepted from the invited speakers where they preferred to offer them. The submissions are reproduced as they were submitted, with minor changes in formatting, and correction of obvious language errors where there was no risk of changing meaning.

*Professor Stefan Kaczmarczyk, and Dr Richard Peters*  
*Co-Chairs and Proceeding Editors*

# CONTENTS

<b>A Design Methodology of Rope Tension Meter Used for Lift Automatic Door Assembly</b>	<b>1</b>
Anup Balharpure <sup>1</sup> , Rohit Nehe <sup>2</sup>	
<sup>1</sup> Rewale Engineering Pvt Ltd, India	
<sup>2</sup> Creestaa Elevator (India) Pvt Ltd, India	
<b>A MATLAB/Simulink Journey-Based Lift Energy Consumption Model</b>	<b>2</b>
Lutfi Al-Sharif, Mohammad Al-Ahdab	
The University of Jordan, Jordan	
<b>Call-Giving Devices in Lift Traffic Design with a Destination Control System</b>	<b>3</b>
Janne Sorsa <sup>1</sup> , Mikko Kontturi <sup>1</sup> and Mirko Ruokokoski <sup>2</sup>	
<sup>1</sup> KONE Industrial Ltd, Finland	
<sup>2</sup> KONE Corporation, Finland	
<b>Computational Environment for Simulating Impact of Building Sway on High Rise Lifts</b>	<b>4</b>
Jaakko Kalliomäki, Jarkko Saloranta, Joonas Sorvari, Sakari Mäntylä, Mikko Puranen	
KONE Corporation, Finland	
<b>Computer-Aided Structural Analysis of the Lift Car – Frame System Under Emergency Arrest Operational Conditions</b>	<b>5</b>
Mohammad Ghaleeh, Stefan Kaczmarczyk, Shafqat Rasool, Jonathan Adams, Nawar Al-Esawi	
University of Northampton, UK	
<b>Feasibility of An Energy Efficient Fuel Cell Hybrid Lift: the Main Concept and Design</b>	<b>6</b>
Stefan Kaczmarczyk <sup>1</sup> , Janusz Blaszczyk <sup>2</sup> , H. Lei <sup>2</sup> , Rory Smith <sup>1</sup>	
<sup>1</sup> University of Northampton, UK	
<sup>2</sup> Shanghai Everpower Technologies Ltd, China	
<b>Feasibility Study of Using a Coupler Skate Encoder System for Monitoring the Real Time Status of Lift Door Operation</b>	<b>7</b>
Rohit Nehe, Chetan Mahale, Babasaheb Patil	
Creestaa Elevators India Pvt Ltd, India	
<b>IOT, Magic or Myth</b>	<b>8</b>
Rory Smith, University of Northampton, UK	

<b>Research of Real Time Video Monitoring and Remote Control System of Escalators</b>	<b>9</b>
Yantai Luo Shanghai Mitsubishi Elevator Corporation, Japan	
<b>Study on a Vibration Reduction System for Lift Roller Guides</b>	<b>10</b>
Yosuke Shima and Osamu Furuya Tokyo Denki University, Japan	
<b>Study on Behavior of Escalator During Earthquake</b>	<b>11</b>
Nayuta Sudo <sup>1</sup> , Satoshi Fujita <sup>1</sup> Keisuke Mori <sup>2</sup> , Izumi Nakamura <sup>3</sup> Shigeki Okamura <sup>4</sup> <sup>1</sup> Tokyo Denki University, Japan <sup>2</sup> Mitsubishi Electric Corporation Advanced Technology R&D Center, Japan <sup>3</sup> National Research Institute for Earth Science and Disaster Resilience, Japan <sup>4</sup> Toyama Prefectural University, Japan	
<b>Study on Evacuation Route in Case of Disaster Considering the Fragility of Mechanical Structures</b>	<b>12</b>
Kazusada Natsu, Osamu Furuya Tokyo Denki University, Japan	
<b>The Maximum Number of Passengers Boarding a Lift in Office Buildings Based on Automated Passenger Counts</b>	<b>13</b>
Tiina Laine, Janne Sorsa KONE Industrial Ltd, Finland	
<b>The Passenger Input to Escalator Accidents</b>	<b>14</b>
David Cooper LECS (UK) Ltd University of Northampton, UK	
<b>The Round Trip Time Simulation: Monte Carlo Implementation and Consistency with Other Techniques</b>	<b>15</b>
Matthew Appleby, Richard Peters Peters Research Ltd, UK	
<b>The Use of Lifts in Offices in Social Distancing Environments</b>	<b>16</b>
Jochem Wit Deerns, The Netherlands	

**Using the Inter-Linked Monte Carlo Simulation Method (iL-MCS) to  
Calculate the Value of the Elevator Round Trip Time to Reflect the Random  
Nature of Passenger Destinations**

**17**

Lutfi Al-Sharif, Noor Toghoj, Ammar Hakam  
The University of Jordan, Jordan

# A Design Methodology of Rope Tension Meter Used for Lift Automatic Door Assembly

Anup Balharpure<sup>1</sup> and Rohit Nehe<sup>2</sup>

<sup>1</sup>Rewale Engineering Pvt Ltd, India

<sup>2</sup>Creestaa Elevator (India) Pvt Ltd, India

**Keywords:** rope tension, load cell, lift automatic door, automatic door operator

**Abstract.** The present work demonstrates a low-cost open-source design of a rope tension meter specifically designed for measuring rope tension of lift door assembly. The potential use of such an easy to use, economical and handy unit could be in a door operator production plant and on installation site for measuring rope tension.

The rope tension meter consists of a sensor unit and the embedded system equipped with a signal conditioning circuit, digitization circuit, microcontroller, and interactive display. The sensor unit is designed such that the load cell is mounted on a custom-designed mechanical structure. The sensor unit can *clip* onto a rope using an attached hand screw. While measuring the rope tension, the sensor unit *clipped* on the rope gives an analog output signal proportional to the load applied on the load cell. The analog output signal of the load cell is fed to the microcontroller through the signal conditioning and digitization circuit, and the corresponding load value is displayed on a screen as per the desired units of the load. To evaluate whether the rope tension meter was working, tests were performed on an automatic door operator setup. In this test, the rope tension meter showed a proportional response for any changes in the tension and high repeatability in its results. To calibrate the rope tension meter signal against the rope tension in units of Newton [N], calibration tests were performed.

The study described in this document tries to fill in the gap in the literature in regards to the development of rope tension meters used for measuring rope tension of lift automatic door assemblies. The design and the procedure discussed could be utilized by lift manufacturing and service companies for developing a portable and low-cost rope tension meter tool for factory or on-site use.

## 1. INTRODUCTION

The *lift automatic door assembly* is one of the important components of the lift. A typical lift automatic door mechanism consists of car door assembly and landing door assembly. In the lift door mechanism, the car door assembly is an active driving component while landing door assembly is a passive driven component i.e. car doors are power operated through drive and motor while landing doors simply follow the car door motion through a mechanical linkage. This mechanical tie consists of a vertical vane also called as coupler skate (or a pair of vanes, depending on the type of doors) mounted on the car door assembly (see Figure 1(A)) and pair of rollers mounted on the landing door interlock. During the door opening and closing operation, the vanes are engaged with the landing door lock rollers resulting in a simultaneous movement of car and landing doors [1].

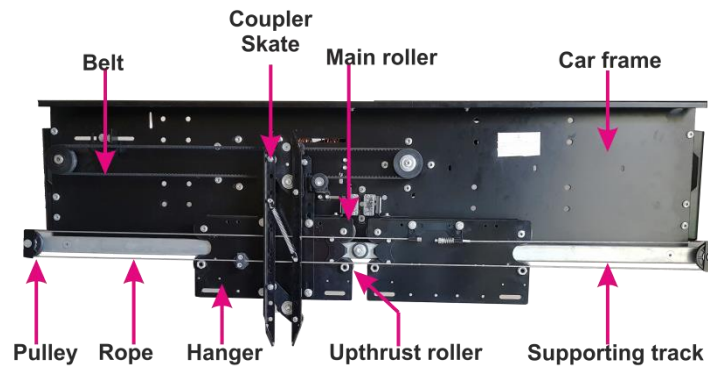


**Figure 1(A) Car door operator assembly**

Figure 1(B) shows the side view of door operator assembly excluding the interlocking mechanism which is typically used to interlock car and landing doors. In general door operator mechanism

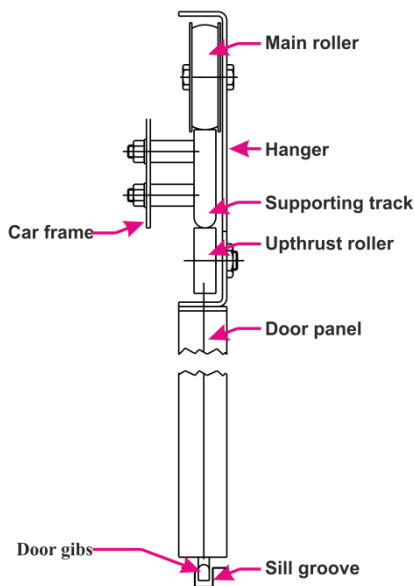


**Figure 1(B) Door hanger assembly**

includes door hangers, door panels, pulleys, rope, hanger track, sill groove, and door gibs, etc. Each panel of horizontal sliding doors is hanged on hangers also called a carriage and guided on a hanger track at the top and by a sill groove at the bottom as shown in Figure 1(B) [1]. During the door operation (opening and closing motion), the door panels move in the opposite direction in the case of centre opening mechanisms (further details about the types of door and roping system can be referred from reference [1]). The linkage between the door panels is established through a simple roping system of two pulleys. The smooth movement of the door panels can be obtained by maintaining the required tension in the rope. Over time, due to wear and tear during normal usage, the rope tension needs to be re-adjusted. To reduce the breakdown due to door panel related problems, periodic maintenance of its components and rope tension adjustment of the lift door mechanism is important.

Various types of analog and digital rope tension meters are available in the market, but these measurement tools are not specifically designed for lift door operator ropes. To adjust a rope tension, on-site or in a production plant many engineers estimate rope tension by hand/feel. Determination of rope tension by feel (pushing/pulling the rope by hand) is more of an art form than a learned skill [2] and is not an accurate method, due to which rope tension will vary from person to person. To address this issue, present work demonstrates a low-cost open-source design of a rope tension meter specifically designed to measure rope tension of lift automatic door assembly.

In the present work, we are using off the shelf components such as, low-cost open-source Arduino Uno board as processing unit, HX711 module as a signal conditioning unit, Nextion 4.3 inch display and customized sensor unit which consist of mechanical structure and load cell. Further details about the rope tension meter calibration and its demonstration to measure the rope tension of door operator mechanism is discussed in detail in section 2 and section 3 respectively.

## 2. ROPE TENSION METER DESIGN AND EXPERIMENTAL SET UP

The rope tension meter discussed in this paper is designed such that it can be used as a portable and easy to operate service tool on site as well as during the door operator manufacturing process. In this section, details about rope tension meter design, load cell calibration setup, sensor unit calibration and lift automatic door operator test jig are discussed.

### 2.1 Rope tension meter design and its working principle

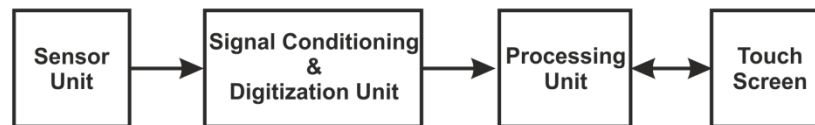


**Figure 2 Block diagram of rope tension meter**

Figure 2 shows the block diagram of the rope tension meter discussed in this paper. It consists of a sensor unit, signal conditioning and digitization unit, processing unit, and a touch screen.

#### 2.1.1 Sensor unit

The sensor unit consists of an *LFT-25 Miniature Compression and Tension 50Kg Load Cell* housed within the mechanical structure assembly. *LFT-25 Miniature Compression and Tension 50Kg Load Cell* utilizes bridge type sensors with strain gauge technology [3].

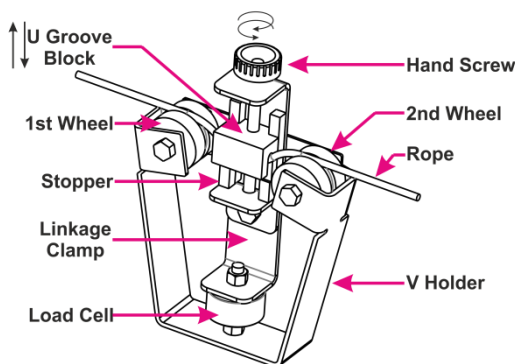


**Figure 3 Customized sensor unit with rope**

The sensor unit is designed such that the load cell is fitted within a custom design mechanical structure. The main purpose of the mechanical structure is to provide housing for load cell and to transform the tension from rope to the load cell. The mechanical structure consists of two wheels, U-groove block, V-holder, linkage clamp, stopper, and hand screw. Figure 3 shows the CAD image of the rope tension meter designed and discussed in this paper. The 1st and the 2nd wheel discussed in Figure 3 acts as a guiding wheel, ensuring the correct placement of the rope within the sensor unit. The U-groove block works as a traversing clamping element. By using a hand screw, the U-groove block can be moved such that it can clamp the rope until the movement of the U-groove block is stopped by the stopper. The sub-assembly of U-groove block, stopper and hand screw is mounted on the *linkage clamp*, wherein the linkage clamp facilitates the transfer of the rope tension to load cell.

Following is the procedure which describes the working of the sensor unit i.e. the working of *mechanical structure assembly* and the *load cell* to measure the tension of the rope:

1. Adjust the rope and the sensor unit such that rope is placed within the groove of the 1st and 2nd wheel.

2. Once the rope is placed in the sensor unit, the U-groove clamp is moved through hand screw such that U-groove clamps the rope tightly until the movement of the U-groove clamp is stopped by the stopper.
3. Due to the clamping of the rope by U-groove clamp, the tension of the rope is transferred to the load cell through a linkage clamp.
4. The resultant analog output voltage given by the load cell proportional to rope tension is fed to the electronic circuitry to process and provide the output data in the required format.

### 2.1.2 Signal conditioning unit

HX711 amplifier and 24-bit analog to digital converter (ADC) module is used as a signal conditioning unit for the rope tension meter. It is based on Avia Semiconductor's patented technology, specially designed for weighing scale and industrial control applications to interface directly with a bridge sensor. It has two channels A and B with an inbuilt low-noise programmable gain amplifier (PGA) with a selectable gain of 64 and 128 for channel-A and constant gain of 32 for channel-B [4]. It is low cost and easily available in the open market. This module gives output in a serial format with two-wire serial communication.

### 2.1.3 Processing unit

Arduino Uno is an open-source and easily available development board. It is used as a processing unit in the presented work. For further details of the board see the reference [5].

### 2.1.4 Touch Screen

Nextion make model-NX4827K043\_011R of size 4.3-inch resistive touch screen [6] is used as the human-machine touch-based interface for the rope tension meter described in this paper. NX4827K043\_011R display is a very easy to use display available in the market and it is serially interfaced with the processing unit of the rope tension meter. The output data processed by the processing unit is displayed on the custom made GUI of the Nextion 4.3-inch display.

## 2.2 Load cell calibration setup

Figure 4 depicts the load cell calibration set up used to study the characteristics of the load cell. The set up consists of a four-legged aluminium extrusion structure with a level screw, built in such a way that the load cell is fixed on one of the top members of the structure. The load cell is fitted with a holder which can hold multiple calibrated weights.

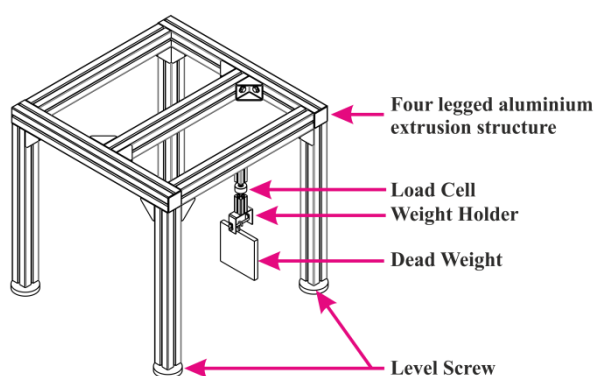


**Figure 4 Load cell calibration setup**

To calibrate the response of the load cell against various known weights, calibration experiments are performed. The dead weights used for calibration experiments are of F1 precision class and are calibrated in the NABL (National Accreditation Board for Testing and Calibration Laboratories, India) accredited laboratory. During the calibration experiments, the load cell is provided by ~ 5-volt excitation voltage from

the HX711 module. To calibrate the load cell, the load cell holder is fixed with a known weight and the proportional response in terms of the analog output voltage is measured and processed by the processing unit. The calibration experiment is performed such that the load cell response is measured for various weights resulting in a look-up table data of load cell output (analog voltage signal) versus weights in desired units (N) or (kgf). The results of load cell calibration experiments are discussed in section 3.1.

### 2.3 Sensor unit calibration setup

A sensor unit as described in section 2.1, consists of a load cell mounted within a mechanical structure assembly. The construction of the sensor unit is designed such that the tension or the load to be measured is transferred to the load cell via a linkage clamp; unlike the loading of load cell described in section 2.2 wherein the load cell is directly loaded with weights without any intermediate member attenuating the loading force. To calibrate the sensor unit analog output data against the weight in the desired unit (N) or (kgf), the sensor unit calibration experiments are performed using set up highlighted in Figure 5.

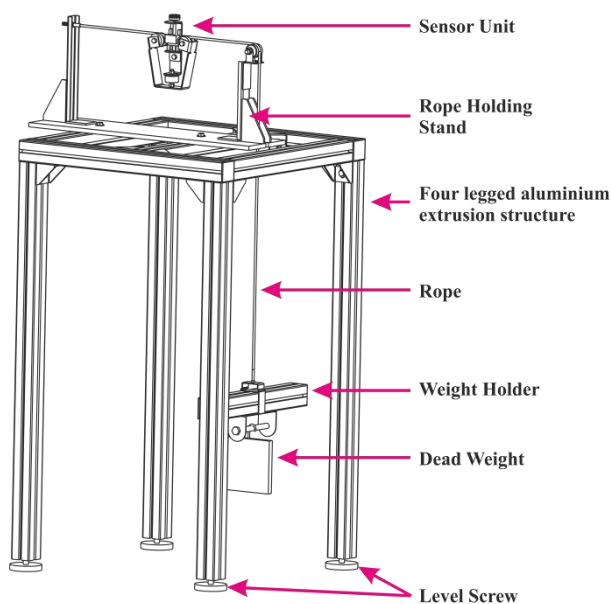


**Figure 5** Sensor unit calibration setup

holder, as shown in Figure 5. The sensor unit is clipped on a rope by using the hand screw as explained in section 2.1.1. The rope tension is varied by adding various calibrated dead weights on the weight holder. The raw ADC count to be recorded is sent to the PC using the Arduino board. The detailed results and discussion in regards to the sensor unit calibration experiment are highlighted in section 3.2.

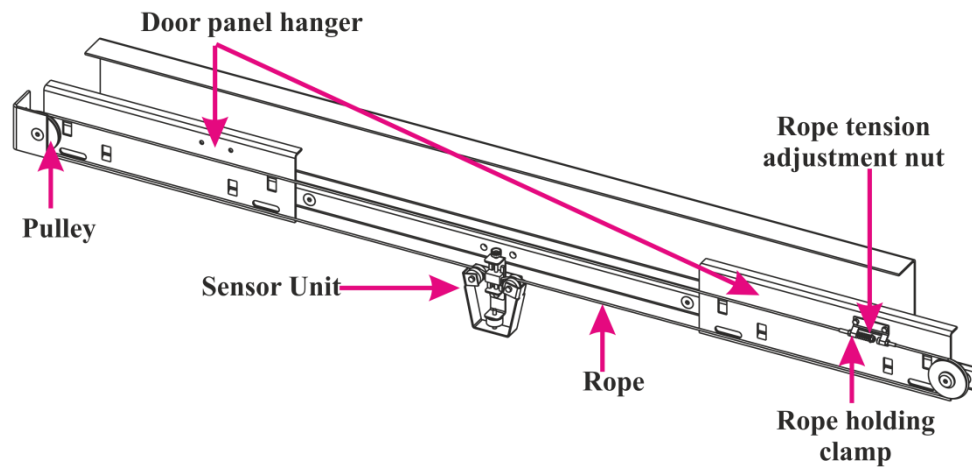
### 2.4 Lift automatic door operator test jig

Figure 6 highlights a particular type of lift automatic door operator mechanism used in the experimental set up described in this paper to demonstrate the working of rope tension meter (sensor unit and electronic circuitry). This mechanism involves door panel hangers, ropes, pulleys and tracks for the movement of door panel hangers. To adjust the rope tension, a rope tension

Sensor unit calibration set up consists of the four-legged mounting table made from aluminium extrusion members, rope holding stand with a rope guiding pulley at one end, weight holder to hang the dead weights, rope and calibrated dead weights. The rope used for the calibration setup is the same as the rope used for lift automatic door operator assembly (rope material: SS wire rope, material grade: SS304, OD: 3mm, construction: crossley pattern with 7 cores, minimum braking force: 1570 (N/mm<sup>2</sup>)). The dead weights used in calibrations setup are the same as the dead weights used in section 2.2.

To calibrate the sensor unit on calibration setup, rope is fixed at one end of the rope holding stand and another end is connected to the weight

adjustment nut is provided. By turning the nut clockwise or anticlockwise, rope tension can be increased or decreased.



**Figure 6 CAD design of lift automatic door operator test jig along with the rope tension meter unit clipped on rope**

The rope tension meter described in section 2.1 is calibrated for various nut positions i.e. for various rope tension settings of door operator mechanism. This experiment provides a lookup table of rope tension meter analog output data versus multiple rope tension nut positions. By utilizing the data sets obtained from experimental set-ups shown in Figure 4 and Figure 5, the rope tension meter is calibrated in the desired units (N) or (kgf) for multiple rope tension nut settings. The detailed data analysis and discussion of the data is explained in section 3.3.

(Note: Figure 6 depicts the lift automatic car door operator assembly. For simplicity some parts of assembly like motor, belt, coupler skate, etc. are not showing in figure)

### 3. RESULTS AND DISCUSSION

In this section results of the load cell calibration setup, sensor unit calibration setup and rope tension meter testing on lift automatic door test jig are discussed.

#### 3.1. Load cell calibration results

Load cell calibration experiments are performed using the set up described in section 2.2 and the results are highlighted in Figure 7. To calibrate the load cell, calibrated weights of ~9.81 (N) are gradually added and corresponding results in terms of ADC counts are recorded. The readings are recorded for the weights in the range of 50 (N) to 180 (N). To obtain a statistically averaged data, each data point highlighted in Figure 7 is calculated by averaging the data over the sampling window of 50 data points.

In Figure 7, the x-axis represents the weights (N) and the y-axis represents ADC counts. The plot shows two data sets, one is the load cell output ADC count recorded from the experimental work which is shown by black colour marker and the other data set is the load cell output data obtained from the datasheet [3] supplied by the manufacturer (shown in red colour). This experiment is carried out to verify the linearity of the load cell as mentioned in the datasheet. As seen in the plot

highlighted in Figure 7, the experimental readings follow the expected linear behaviour with the highest deviation of less than 1.5 % compare to the data set provided by the manufacturer.

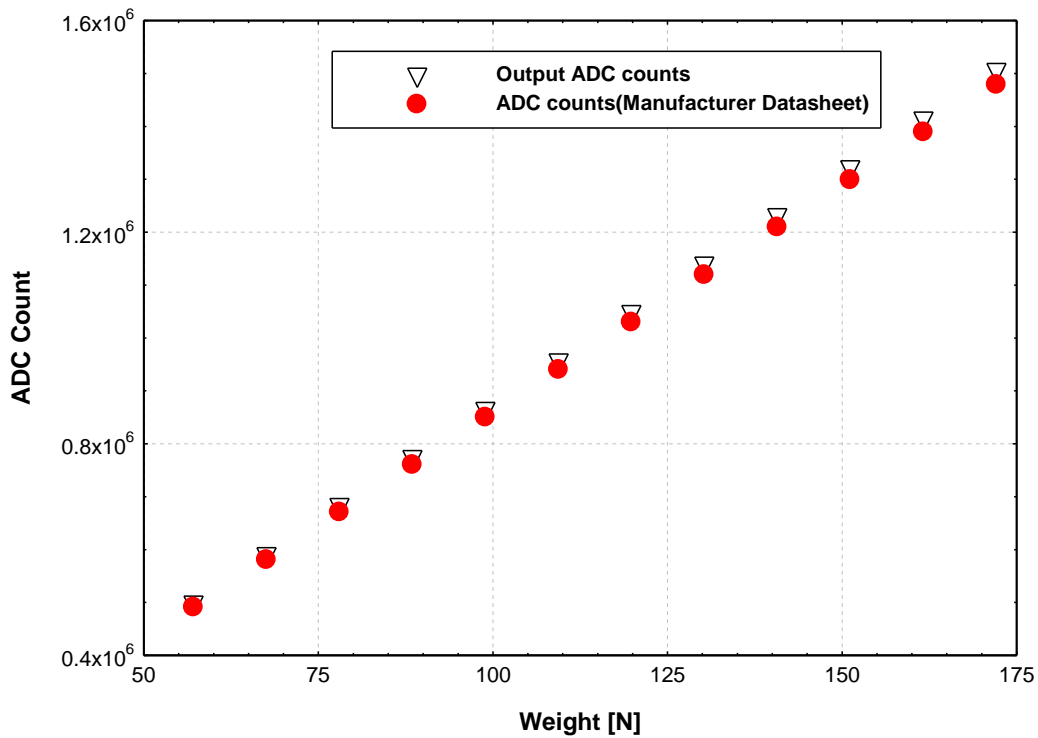


**Figure 7 Load cell calibrations results (Weights (N) vs ADC counts)**

### 3.2. Sensor unit calibration results

Figure 8 shows the experimental calibration data of the sensor unit as discussed in section 2.3. The load cell used in the sensor unit is not directly loaded with the rope tension, instead, it is loaded with the help of a linkage clamp. The design of the sensor unit (mechanical structure and linkage clamp) happens to be such that it transfers the attenuated rope tension to the load cell. In the case of a sensor unit, the load cell needs to be re-calibrated to account for the attenuated loading effect induced by mechanical structure on a load cell.

In Figure 8, the x-axis represents the rope tension (N) and the y-axis represents output ADC count. To obtain a statistically averaged data, each data point highlighted in Figure 8 is calculated by averaging the data over the sampling window of 50 data points. The plot shows the sensor output in terms of ADC counts in red circles corresponding to calibrated weights in the range of 120 (N) to 320 (N).

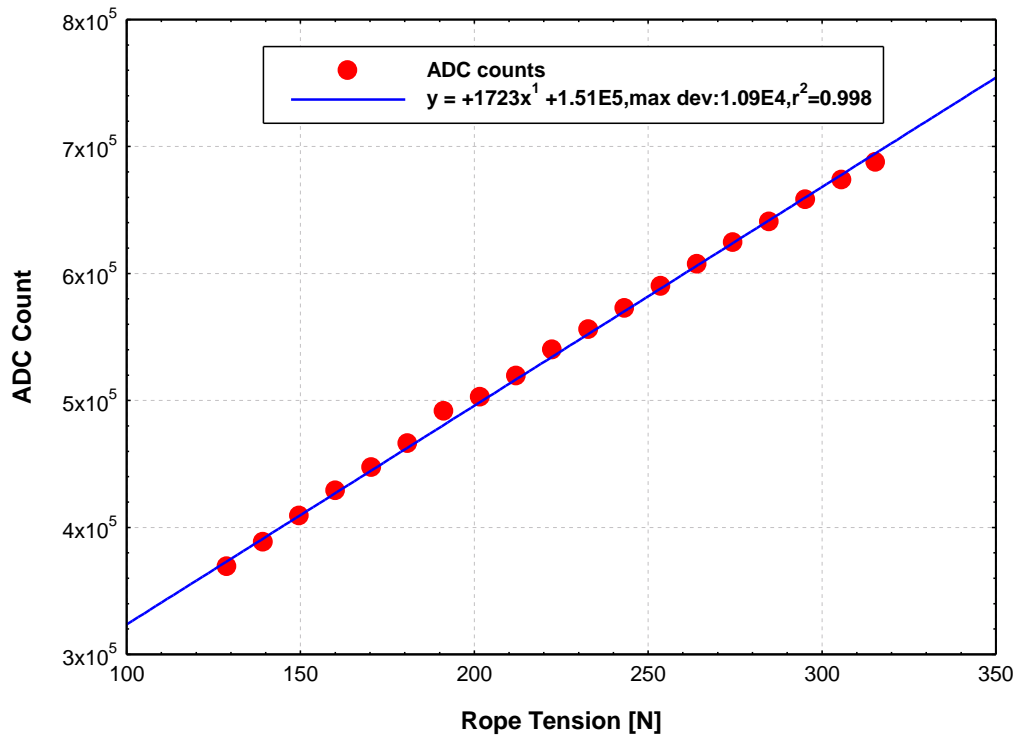


**Figure 8 Sensor unit calibration result (Rope tension (N) vs ADC count)**

The data highlighted in Figure 8 shows the linear response of the sensor unit similar to the linear response trend seen in Figure 7. However as expected, due to attenuation affect the response of the sensor unit compared to the bare load cell response (see Figure 7) corresponding to the same load is of lower value. For example, when the load cell is directly loaded with 150 (N) then the output is  $\sim 13 \times 10^5$  (1321328) ADC counts and when the load cell is indirectly loaded with the help of linkage clamp and mechanical structure in the sensor unit, the output decreases such that ADC counts recorded are  $\sim 4 \times 10^5$  (408777). Such lower bound values of the sensor unit highlights the mechanical structure caused attenuation effect on a load cell.

### 3.3. Demonstration of rope tension meter

To evaluate and demonstrate the rope tension meter working (sensor unit and electronic circuitry), tests were performed on a lift automatic door operator setup (see section 2.4). As discussed in section 2.4, one of the sub-assemblies of the automatic door operator set up consists of a roping system (roping and pulley system) to drive both the door panels (see section 1). During the experiments, the rope tension of the roping system was varied by adjusting the tension nut at various positions. Note, the tension adjustment nut position is the distance between the rope holding clamp and the nut itself. To vary the rope tension, the rope tension adjustment nut is rotated manually and its position from the rope holding clamp is measured using a vernier scale.

Figure 9 shows the results of the experiments discussed in this section. In Figure 9, rope tension meter output in the units of ADC count is represented on the y-axis while the tension adjustment nut position is shown on the x-axis. The experiment wherein the rope adjustment nut position was varied in the range 39 (mm) to 36.5 (mm) and the corresponding rope tension meter response is

measured and is defined as test 1. To test the repeatability of results, such experiments were conducted 5 times and the corresponding data sets are labelled as TEST 1 to TEST 5(see Figure 9).

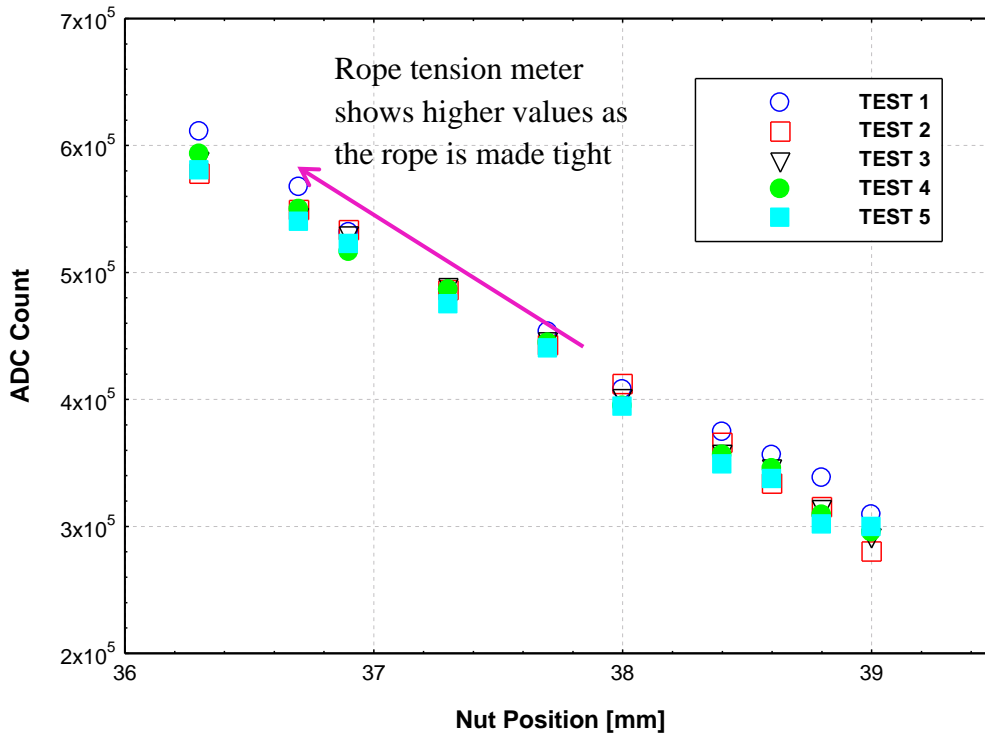


**Figure 9 Plot between nut positions (mm) and ADC count to demonstrate the working of rope tension meter**

From Figure 9 it is observed that for the same nut position, the rope tension meter always showed repeatable results when the multiple tests were performed i.e. TEST 1 to TEST 5. The repeatability result of the rope tension meter is seen for all the nut positions i.e. from 39 (mm) to 36.5 (mm). Thus, this result confirms the repeatable behaviour of the rope tension meter discussed in this paper.

Another observation from Figure 9 to be discussed is the trend of increasing ADC counts as we change the nut position from 39 (mm) to 36.5 (mm). The rope tension meter shows a higher tension value as we tightened the rope using a rope tension adjustment nut. This trend of results demonstrates the correct working of the rope tension meter designed in this paper.

Figure 9 shows the rope tension meter output in the units of *ADC counts*. To convert the rope tension meter output from the units of *ADC count* to *Newton (N)*, the calibration data set highlighted in Figure 8 is utilized (the linear fit equation is utilized). The resultant data set of rope tension meter output in the units of *Newton (N)* against the nut position is highlighted in Figure 10. Thus, this demonstrates the basic working and data reduction procedure of the rope tension meter designed and discussed in this paper.

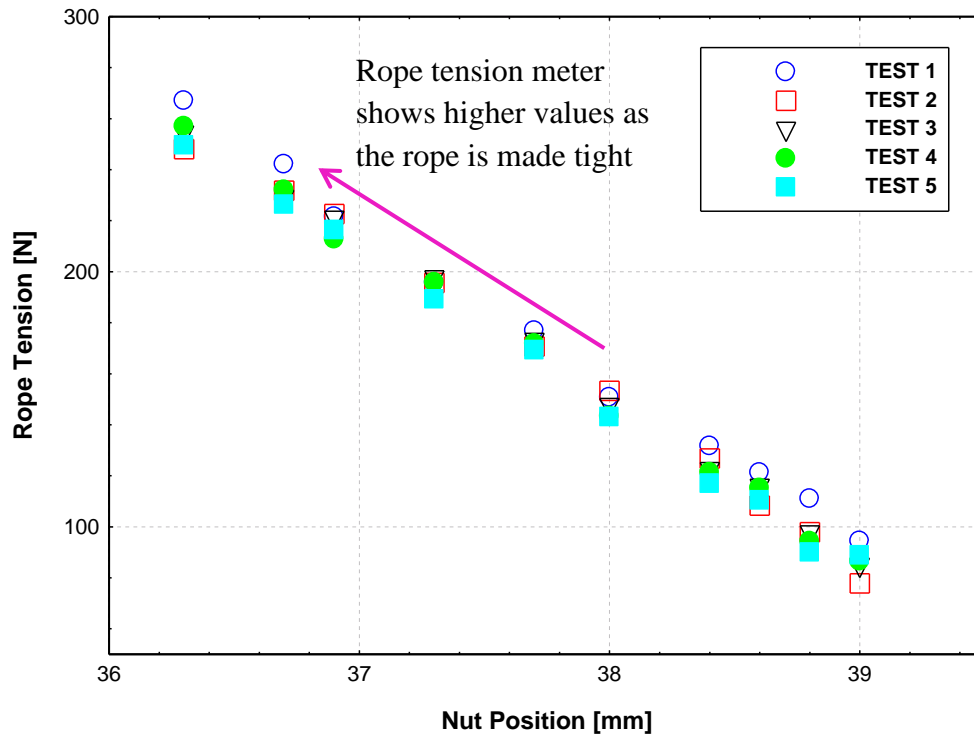


**Figure 10 Plot between nut positions (mm) and Rope tension (N) to demonstrate the working and outcome of rope tension meter**

#### 4. CONCLUSION

A rope tension meter design methodology was explored in the paper. The rope tension meter discussed in the paper is specifically designed for the ropes used in the lift automatic door mechanisms. The load cell used in the rope tension meter sensor unit design is based on strain gauge technology. To calibrate the load cell and the sensor unit, the calibration experiments were performed. The calibration experiments result highlighted the linear and repeatable response of the load cell used in the rope tension meter. To demonstrate the working of the rope tension meter, experiments were conducted on lift automatic door mechanism set up. The results from these experiments exhibit and confirm the repeatability and easy to use operation of rope tension meter for checking the rope tension of door mechanism roping system. The instrument also exhibits robustness in measuring data such that repeatable results were obtained at multiple position of door operator roping system.

#### ACKNOWLEDGEMENT

The authors are thankful to Mr. Samadhan Kadam (Application Engineer, Creestaa Elevator (India) Pvt. Ltd), Mr. Baba Patil (Research and Development Engineer, Creestaa Elevator (India) Pvt. Ltd) and Mr. Pratik Patil (Design Engineer, Rewale Engineering Pvt. Ltd.) for support to carry out the present work.

## REFERENCES

- [1] L. Janovsky, *Elevator mechanical design (Third Edition)*. Elevator world, Inc., U.S (1999)
- [2] Michael A., V. Dohre and T. Cecere, “DOOR OPERATORS”. EDUCATIONAL FOCUS, ELEVATOR WORLD (2003)
- [3] LFT-25-50Kg load cell details available at [online], <http://en.ligentcn.com/a/chanpinzhanshi/zuqiuqicai/48.html> (accessed 07 Jun 2020)
- [4] HX711 module datasheet available at[online], [https://cdn.sparkfun.com/assets/b/f/5/a/e/hx711F\\_EN.pdf](https://cdn.sparkfun.com/assets/b/f/5/a/e/hx711F_EN.pdf) (accessed 07 Jun 2020)
- [5] Arduino Uno details available at [online], <https://store.arduino.cc/usa/arduino-uno-rev3> (accessed 07 Jun 2020)
- [6] Nextion make model-NX4827K043\_011R details available at [online], <https://nextion.tech/datasheets/nx4827k043/> (accessed 07 Jun 2020)
- [7] C.Slattery and M. Nie, “A Reference Design for High-Performance, Low-Cost Weigh Scales”. Analog Dialogue, Vol. 39, No. 12, 1-6 (2005).

## BIOGRAPHICAL DETAILS

Anup Balharpure is Sr. Project Engineer at Rewale Engineering Pvt. Ltd. He obtained his M.Sc degree in Electronics Science in 2011 from Rashtasant Tukadoji Mahraj Nagpur University, Nagpur (RTMNU). Later, he obtained his PhD degree in Electronics Science and Technology in 2016 from same university. He is actively involved in various research activity and product development projects at Rewale Engineering Pvt. Ltd.

Rohit Nehe is the Head of Electrical and Electronics department at Creestaa Elevators (India) Pvt. Ltd. He obtained his M.S. degree in Mechanical and Aerospace Engineering in 2008 from Syracuse University, NY, USA. Later he obtained his PhD degree in Mechanical Engineering in 2013 from Michigan State University, East Lansing, USA. He has a strong research and academic background in developing diagnostic instruments involving interdisciplinary engineering fields. His current activity at Creestaa Elevators involves research and product development in regards to vertical transportation systems.



# A MATLAB/Simulink Based Journey-Based Lift Energy Consumption Model

Lutfi Al-Sharif, Mohammad Al-Ahdab

Mechatronics Engineering Department, School of Engineering,  
The University of Jordan, Amman 11942, Jordan

**Keywords:** modular simulator; elevator, lift, modelling, energy consumption, mechanical design, elevator traffic.

**Abstract.** A number of different approaches have been used in order to calculate the energy consumption of lifts. Such approaches have ranged from simple rules of thumb, to lookup tables, more detailed equation-based models and simulation-based models. This paper presents an approach based on the use of MATLAB/Simulink to model the various components used in a lift in order to calculate the power drawn during the lift journey as well as the total energy consumption. The model comprises a number of modular blocks, such as the variable speed drive, the induction motor, the gearbox, the ropes, the lift car, the counterweight as well as the passenger load.

The main advantage of this model is that it models the energy accurately based on the mechanical and electrical design of the system, as well as the kinematic parameters. Moreover, the model is open source, transparent and intuitive (as it is based on the dragging and dropping of modules). The model offers a platform for any lift system designer to calculate the energy consumption of the system based on the electrical and mechanical components of the system.

## 1. INTRODUCTION

Much work has been carried on the topic of lift energy consumption. The basis for these pieces of work can be categorised into three categories: simple rules of thumb, lookup tables, equation-based models and simulation-based models. Some of these use analytical equations developed from first principles [1], others employ measurements of real systems [2], and there are models that use the measurements of real systems to calibrate the analytical equation based models [3, 4]. A general overview of the different energy consumption models and research can be found in ([5], [6], [7]). An example of using the energy measurement in order to find the parameters of the lift system can be found in [8]. An analysis that analyses the payback period that could result from adding a variable frequency drive to a lift system can be found in [9]. Energy consumption has also been suggested as a performance parameter to be compared between different systems [10].

The motivation for modelling energy consumption in lifts is to allow the user of such a model to predict the instantaneous, daily or annual energy consumption of the lift without the need to carry out actual measurements on the lift, for the following reasons [2]:

1. Convenience: It is much easier and more convenient to be able to calculate the expected energy consumption under different scenarios without the need for measurement.
2. Restriction or difficulty of access and the requirement for resources: access to assets is often restricted due to operational requirements. Carrying out measurements requires specialised equipment and much care during the process of measurement (e.g., measuring at the correct incoming point of the supply; distinguishing between the main asset and the ancillary equipment; using three-phase equipment in cases where the load on the three phases is not balanced). Moreover, the results from the measurement are only applicable to the specific

conditions prevalent at the time of the measurement (e.g., number of passengers on that specific day; mechanical condition of the asset at the time of measurement).

3. The lift might not have been built yet: this is especially true for product designers who need to assess the effect that their design decisions will have on the expected future energy consumption of the product. An example of a study looking at the effects of mechanical design on power consumption can be found in [11]. A good example of such a system is a hypothetical two-dimensional lift system in a large building [21, 22].
4. The proposed modification or operational change has not been implemented on the asset yet: this is especially true where a client is offered a design modification or an operational change on the asset and he/she needs to determine the expected effect that such a change will have on the energy consumption. The expected energy saving can be weighed against the cost and risk of the proposed design modification or the operational change (e.g., the effect of lift traffic is analysed in [12], the effect of the group control algorithm can be found in [24, 25], the effect of passenger traffic on escalator energy consumption can be found in [13]; and the effect of lift velocity can be found in [14]). Another good example is for a system that attempts to feed electrical power from one lift to another in order to avoid passenger entrapments in case of a power failure [4].

As with all other means of transport, the energy consumption of lifts does not solely depend on the asset itself (mainly defined by its electrical and mechanical design). The energy consumption of any means of transportation asset depends on the following four important factors:

1. The electrical and mechanical design of the asset (e.g., the effect of the mechanical design on escalator energy consumption [15]).
2. The quality of asset maintenance: maintenance has an important effect on the efficiency of a mechanical asset and associated frictional losses.
3. The methods of control and operation: this factor has great importance in lift systems. It is well known that the energy consumption of a group of lifts depends on the method of allocation of the landing calls to the lifts [24, 25].
4. The characteristics of the passengers using the asset (e.g., number of daily passengers, their arrival pattern, and their behaviour) [12]. For this reason, any lift energy consumption tool would need to be intricately linked to a lift traffic simulator. Research has been carried out to link the energy consumption to passenger demand response [23].

It is thus meaningless to talk about the energy consumption of an asset solely based on its electrical and mechanical design, without taking into consideration the level of maintenance, the method of operation and control as well as the characteristics and behaviour of the passengers using it.

This paper used MATLAB/Simulink for lift energy modelling and simulation. The blocks can be adapted to suit the actual components used within the lift being analysed. Simulink has been widely used to model and simulate electrical machines in general ([16], [17]). It was also used to Mechatronic system education by modelling the operation of a DC motor operated lift [18].

Section 2 provides a high-level overview of the model and the rationale for using it. Section 3 describes the components of the model in detail. Section 4 provides some representative results.

## 2. OVERVIEW OF THE MODEL

This paper develops a Simulink based model for the evaluation of the energy consumption of a traction lift system. It is mainly based on the model that can be found in [19]. A similar approach was used in [20] but with a different set of equations. The model in [20] calculates the required value of the torque, while the model described here divides the net torque by the second moment of mass and then feeds back the resultant rotational speed. The model uses a widely available installation of lifts on the market that assumes the following:

1. The lift system uses a squirrel cage induction motor.
2. The induction motor is driven by a variable frequency drive system. The variable frequency drive system employs an uncontrolled six pulse rectifier, followed by a capacitor and then a six pulse IGBT inverter. The inverter employs flux-vector control. It is acknowledged that lift variable speed drive systems employ different types of inverters, such as flux vector control, direct torque control (DTC) and scalar control. By changing the block used, it is possible to simulate the different types of drives as well as their effect on the energy consumption.
3. The system runs under closed loop control and it is assumed that some form of feedback for the motor speed is provided to the controller (e.g., using an incremental shaft encoder).
4. The ropes have been modelled within the system. Only the suspension ropes have been modelled. It is possible in a future version to include the compensation ropes as well.
5. It has been assumed that the system employs a gearbox to match the speed and torque from the motor to the load.
6. The car mass has been assumed to be equal to the passenger rated load, and the counterweight ratio can be changed by the user. The user can easily change the assumption about the mass of the car and the rated load being equal. This is just a simplification.
7. Other mechanical aspects are incorporated into the model, such as the viscous friction and the gearbox efficiency.

In order to initialise all the parameters, a MATLAB script file is used that will be run at the beginning and assign all the parameters their intended value.

Some of the blocks have been used without any change from Simulink, but other models have been built from scratch. This feature from Simulink allows any user to adapt the model to his/her application. The following are two of the limitations of this model:

- It only provides the energy consumed for one journey. So, it would need to be linked to a traffic simulator in order to aggregate the energy consumed over a day or a year.
- The parameters of the mechanical model are embedded inside the blocks, rather than being modelled as mechanical components.

The model is effectively open source, and this gives it a great educational advantage. A link is given at the end of this paper for those interested in downloading it. The next section provides a detailed description of the blocks of the model.

### 3. DESCRIPTION OF THE BLOCKS IN THE SIMULINK MODEL

This section describes the simulation model used in detail. A block diagram of the whole model is shown in Figure 1. It shows a modular approach to building the model. The main advantage of this method of energy modelling is that it takes into consideration the dynamic characteristics of the system. This offers the advantage of being able to alter the control algorithm in order to optimise the energy consumption. The model comprises the following eight modules:

1. The speed time profile generator: this block generates the speed time profile for the lift journey. It uses four parameters, namely: the journey distance, the rated speed, the rated acceleration, and the rated jerk. This forms the basis of the operation of the model, as the system uses the speed-time profile curve as the set value for the closed loop speed control system. This block specifically mirrors a similar block that is available in all variable speed drive systems in modern lift speed controllers.
2. The Flux Vector Control: this block contains the PI parameters. It forms the controller for the closed loop control system that controls the motor in order to produce the required torque and speed. Although PID (proportional-integral-differential) controllers are widely used in many industrial control systems, lift controllers usually only use PI (proportional-integral) due to the slowly changing nature of the reference signal generated by the speed time profile.
3. The rectifier block: this block contains the six-pulse uncontrolled rectifier that converts the supply from the three phase source into dc. It also contains the components necessary for the regenerative feature.
4. The Inverter Block (IGBT inverter): this unit contains the six IGBT's the control the squirrel cage induction motor (SCIM). The firing pulses for the six-IGBT's are received from the Flux Vector Control unit.
5. The motor block which contains the model of squirrel cage induction motor (SCIM) used as the hoisting motor and the processing necessary to extract the torque from the motor and feed the actual speed.
6. The Mechanical System block which contains the details of the system inertia (second moment of mass) referred to the low speed shaft (LSS), the passenger mass, the frictional model and the implementation of the rotational equivalent of Newton's second law applied on the low speed shaft (LSS). Even though MATLAB/Simulink contains some advanced dedicated mechanical component blocks (in SimMechanics), these have not been used in this model due to their drastic impact on the running time of the simulation.
7. The power supply: This comprises the three-phase source and contains components that enable the regenerative feature.
8. The Power Meter: This unit measures the real power flowing from the power source to the lift system.

It is worth mentioning that the model allows for full regeneration back into the power supply when the lift is over-hauling. The voltage of the dc link (i.e., the voltage on the capacitor of the dc bus) is continuously monitored and compared to a pre-set value of 725 V. It is assumed that rated three phase supply voltage is 400 V rms (line to line), based on a phase voltage of 230 V rms. This gives an average dc link voltage from the output of the six-pulse uncontrolled rectifier of 538 V dc. Thus, the threshold for the dc link has been set higher than this value assuming that the voltage rating of the dc link capacitor is 1000 V dc.

Whenever the voltage on the dc link exceeds this pre-set value, the regenerative unit starts operating. An inverter starts producing a three phase AC voltage from the dc bus and feeding the three phase AC voltage back to the supply. A low pass filter comprising a series inductor and a shunt capacitor is used to filter the voltage. A controlled current source is then used to feed the energy back into the supply. This feature can be used to show the effect of selecting a fully regenerative drive system.

#### 4. SOME REPRESENTATIVE RESULTS

The model was setup for a typical small size lift installation. It was run for one single journey of 4.5 m. Some results are shown below to illustrate the possible outputs that can be extracted from the model.

The system is set up to log the following: three phase currents drawn by the motor, the power drawn by the system from the three phase source, the motor speed, the torque from the motor, the displacement against time, the speed against time, the acceleration against time and the jerk against time, the voltage on the dc bus (i.e., on the capacitor), whether the system requires braking or driving at one point.

Figure 2 shows the instantaneous values of the three-current drawn by the motor during the full lift journey. It is obvious how the frequency of the current is low at the beginning, high in the middle of the journey and then low again at the end of the journey, corresponding to the speed of the motor during the journey. It can also be seen how the magnitude of the current is large at the beginning due the large torque required at the beginning to accelerate the translational and rotational masses.

Figure 3 shows the plot against time of the active (real) power drawn by the system from the source. It is worth noting that for most of the time the power is drawn from the supply, but for a short period of time no power is drawn. This is the period of braking. Figure 4 shows the speed-time profile (reference speed and actual speed) against time. It shows how close the two values are similar to each other, showing how effective the closed loop control system is in keeping the speed equal to the reference value



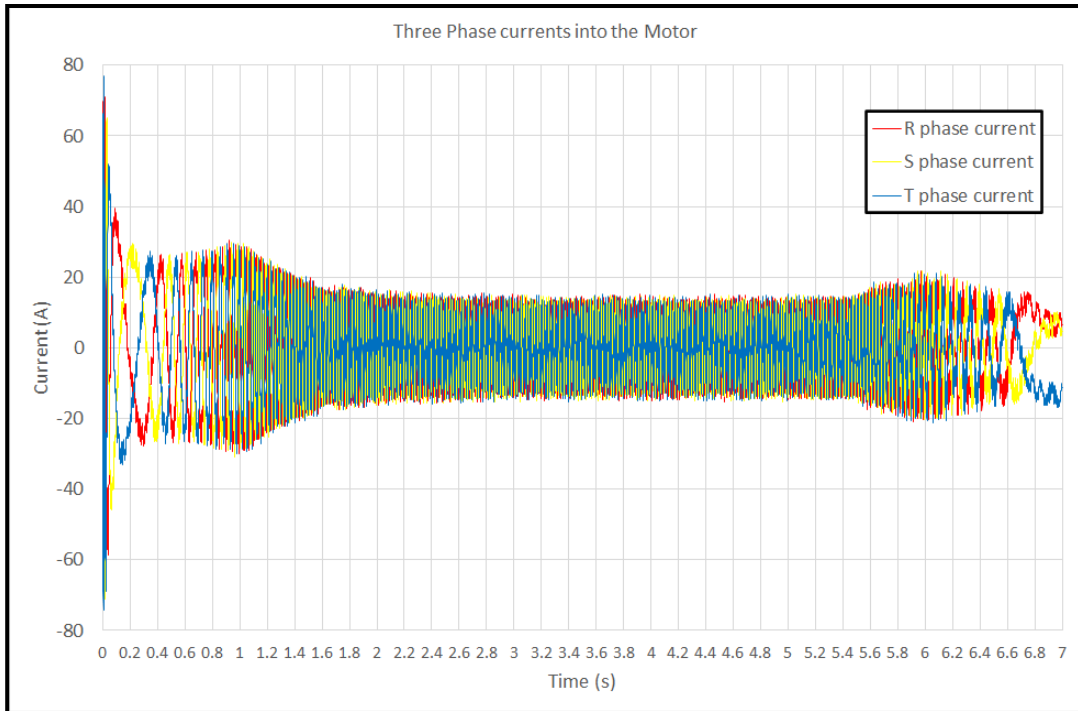


Figure 2: The three phase currents drawn during the journey.

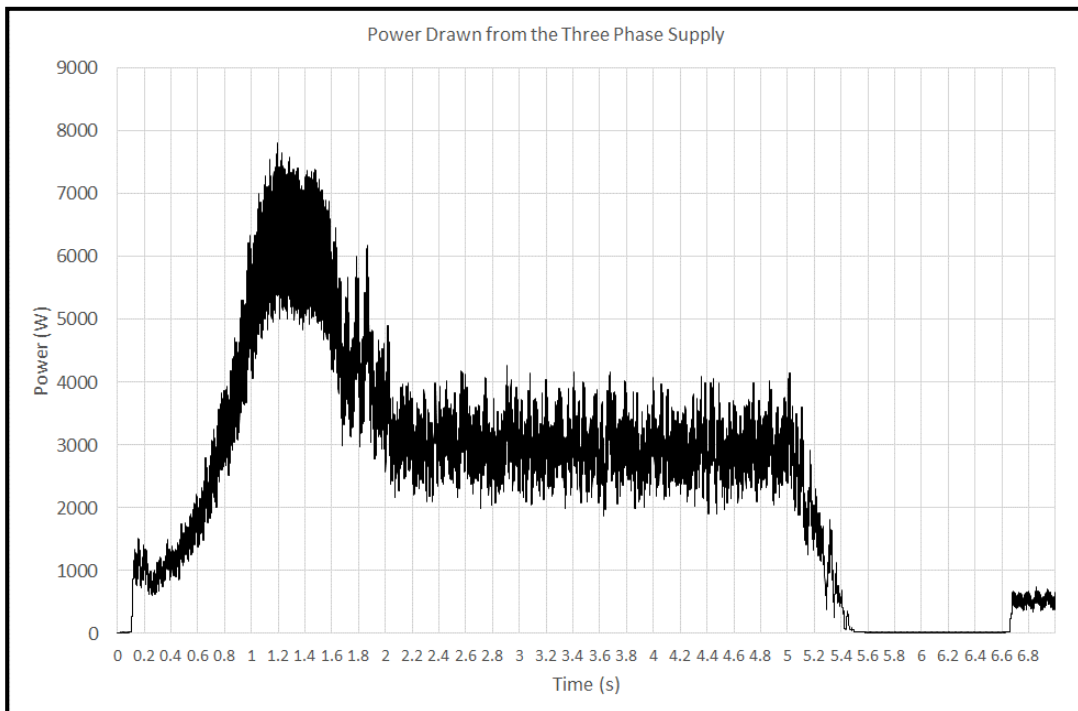
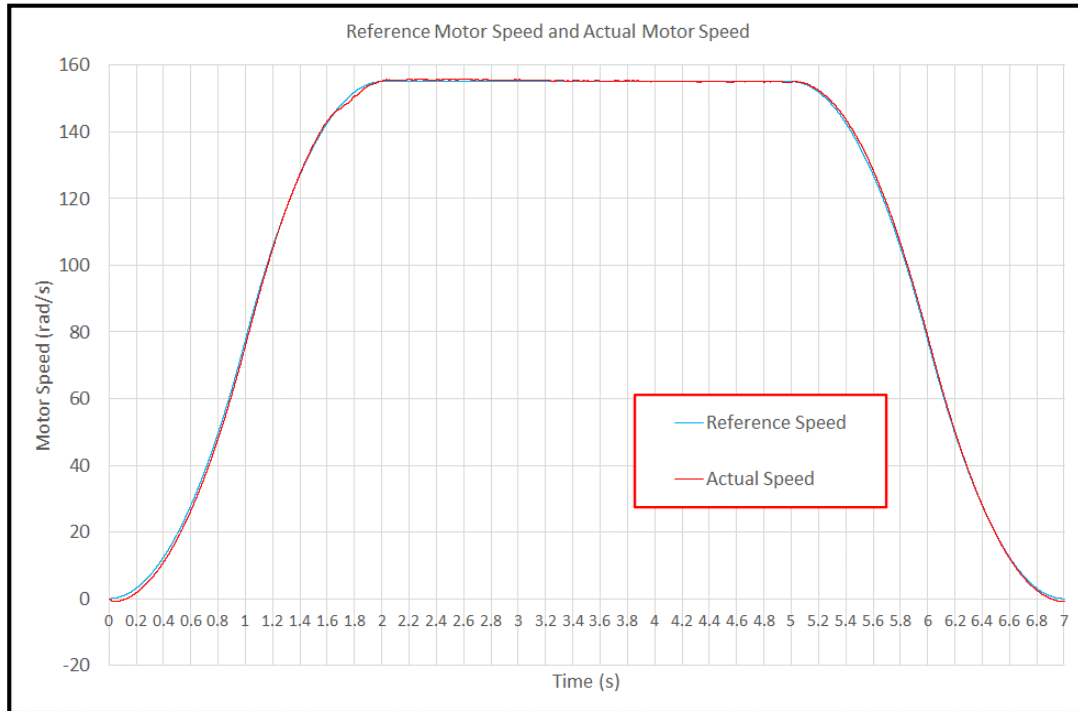


Figure 3: Power drawn by the motor during the journey.



**Figure 4: Reference motor speed and actual motor speed in rad/s.**

## 5. CONCLUSIONS

A component-based energy lift model has been designed and tested in Simulink. The main components were explicitly represented in the model including the squirrel cage induction motor, the variable frequency drive (including the rectifier, the capacitor on the dc bus and the inverter), the regenerative unit (that is used to feed power back into the mains), the closed loop feedback controller (PI controller in this case), the viscous friction, the inertia of the rotating and translating masses, the ropes, the mass of the car, passengers and counterweight. The model simulates the full system in real time, timeslice by timeslice, thus providing a micro-scale view of the flow of energy, as well as faithfully representing the dynamic response of the system.

The model contains a speed time profile generator, that produces the exact speed profile that the system should follow. The output from this block becomes the reference value and is used in the closed loop control system to drive the speed of the motor and thus the lift. Such a system captures the dynamics of the system very accurately.

One of the main advantages of a component-based-model is that it clearly segregates each component of the model mathematically and even graphically, which makes it easy and transparent for the user to change the parameter of each component or even change the complete component. Although in real life systems, a time-lag exists between the consecutive blocks, this has not been simulated in this model. It is possible in the future to use one or more timeslice delay blocks ( $z^{-1}$ ) between the consecutive models.

A numerical example of a lift system was run and samples of results were shown in the paper, including the reference and actual speed time profiles against time, the power drawn from the supply and the instantaneous three phase currents drawn by the motor.

Further work will be carried out in carrying out detailed comparisons between the model results and logging data from real lift sites.

**Source Code:** The following is the link to the Simulink file and the associated script file: DOI: 10.13140/RG.2.2.33365.65762

## BIOGRAPHICAL NOTES

Lutfi Al-Sharif is currently Professor of Electrical Engineering at Al-Hussein Technical University in Amman/Jordan and jointly Professor of Building Transportation Systems at of the Department of Mechatronics Engineering, The University of Jordan. He received his Ph.D. in elevator traffic analysis in 1992 from the University of Manchester, U.K. He worked for 10 years for London Underground, London, United Kingdom in the area of elevators and escalators.

In 2002, he formed Al-Sharif VTC Ltd, a vertical transportation consultancy based in London, United Kingdom. He has over 30 papers published in peer reviewed journals the area of vertical transportation systems and is co-inventor of four patents and co-author of the 2<sup>nd</sup> edition of the Elevator Traffic Handbook.

He is also a visiting professor at the University of Northampton (UK), member of the management committee of the annual Symposium on Lift & Escalator Technologies and a consultant for Peters Research Ltd.

He is a passionate believer in making higher education simple and accessible for engineering students and has a You Tube channel on engineering that has more than 55 000 subscribers and around 8 million views. He has also been working as a member of the METHODS Erasmus+ Project that aims to improve teaching methods in higher education in Jordan and Palestine. He is also the author of the Mechatronics Engineering Module on Saylor.org.

## REFERENCES

- [1] So A T P. Computer simulation-based analysis of elevator drive systems. *HKIE Transactions*. 1992, no. 3.
- [2] Doolaard D. Energy consumption of different types of lift drive system. 1992, in Elevator Technology 4: Proceedings of Elevcon '92, Editor Dr. G. Barney, The International Association of Elevator Engineers.
- [3] Al-Sharif, L., Peters, R., Smith, R., Elevator (2014) Energy Simulation Model *Elevator World*.
- [4] Smith R, Peters R D and Al-Sharif L. *Elevator system to minimize entrapment of passengers during a power failure*. Patent number US7967113, Publication date, 26th June 2011.
- [5] Al-Sharif L. Elevator and Escalator Energy Consumption. *The CIBSE/ASHRAE Joint National Conference*, 29 Sept. - 1 Oct., 1996, Harrogate, UK. Volume 1, pp.231-239.
- [6] Al-Sharif, L., Peters, R., Smith, R., Elevator (2004), Elevator Energy Consumption: General Overview (1974-2001) *Elevator World*
- [7] CIBSE. *Transportation Systems in Buildings. Guide D*, Section 13: Lift and Escalator Energy Consumption, November 2000.
- [8] Tyni, T., Kontturi, R., Perälä, P. *Electric Site Survey- on Quest of Elevator Parameters*. Kone Corporation, Finland. EP 2774885 A1, 2014.
- [9] McGlashan H S. M.Sc. dissertation. What is The Pay Back Period When Modernising a Lift System to a Variable Frequency Drive? The University of Northampton, Northampton, United Kingdom, September 2002.

- [10] So A T P. Parameters to Evaluate Elevator Performance. *Elevator World* in January, 2005.
- [11] Stawinoga R. Designing for reduced energy elevator costs. Lift Technology 1, *Proceedings of LiftTech 94*, Editor Dr. G.C.Barney, The International Association of Elevator Engineers, 1994. Appendix A: Table showing relative power consumption of various drive systems.
- [12] Siikonen, Marja–Liisa. Sorsa J. Hakala, H. Impact of traffic on annual elevator energy consumption. *Elevator Technology 18*, editor A. Lustig, 2010, p344-353.
- [13] Al-Sharif L. Modelling of Escalator Energy Consumption. *Energy & Buildings* 2011; 43(6):1382-1391.
- [14] Lunki T. *The effect of changes in the velocity profile into overall energy consumption*. Master of Science in Elevator Engineering. The University of Northampton, 2003.
- [15] Al-Sharif L. Experimental Investigation into the Effect of Mechanical Design of an Escalator and Passenger Loading on its Energy Consumption. The World Congress on Engineering, London, UK 2008; 2: 1542-1547.
- [16] Miklosevic K, Spoljaric Z and Jerkovic V. Analysis of Electric DC Drive Using Matlab Simulink and SimPowerSystems. Department of Electromechanical Engineering, Faculty of Electrical Engineering, J. J. Strossmayer University of Osijek, Osijek, Croatia.
- [17] Chee-Mun Ong, “Dynamic Simulation of Electric Machinery Using MATLAB/Simulink”, Prentice Hall, 1997.
- [18] Al-Sharif, L., Tutunji, T., Ragab, D, Kayfi, R. (2014). Using Elevator System Modeling and Simulation for the Integrated Learning Process of Multiple Courses in Mechatronics Engineering, REM 2014, The 15<sup>th</sup> International Workshop on Research and Education in Mechatronics, Elgouna, Egypt, 9<sup>th</sup> to 11<sup>th</sup> September 2014
- [19] Al-Ahdab M. Energy Based Model for Elevators. Final Year Graduation project, Mechatronics Engineering Department, The University of Jordan, Amman 11942, Jordan. Supervisor: Lutfi Al-Sharif. May 2016.
- [20] Haddad M. Dynamic Modelling and Simulation of an Electric Elevator. M.Sc. Thesis, The University of Northampton, January 2016.
- [21] So A, Al-Sharif L and Hammoudeh A. Traffic analysis of a simplified two-dimensional elevator system. *Building Services Engineering Research and Technology*. 2015; 36(5): 567-579. doi:10.1177/0143624414568728.
- [22] So A, Al-Sharif L and Hammoudeh A. Concept design and derivation of the round trip time for a general two-dimensional elevator traffic system. *Journal of Building Engineering* 2016; 5(2016): 165-177.
- [23] Tukia T. Models for Evaluating the Power Consumption of Elevators - The Perspective of Power Systems and Demand Response. Doctoral thesis, Aalto University, 2019.
- [24] Tyni T and Ylinen J. Evolutionary bi-objective optimisation in the elevator car routing problem. *European Journal of Operational Research*, 2006; 169(3): 960-977.
- [25] Kobori S, Iwata M, Suzuki N and Yamashita S. Energy saving techniques of elevator group control system. *Elevator technology* 18, 2010. pp 167-176.

# Call-Giving Devices in Lift Traffic Design with a Destination Control System

Janne Sorsa<sup>1</sup>, Mikko Kontturi<sup>2</sup> and Mirko Ruokokoski<sup>3</sup>

<sup>1</sup>KONE Industrial Ltd, Keilasatama 3, FI-02150 Espoo, Finland

<sup>2</sup>KONE Industrial Ltd, Hissikatu 3, FI-05830 Hyvinkää, Finland

<sup>3</sup>KONE Corporation, Keilasatama 3, FI-02150 Espoo, Finland

**Keywords:** lift traffic design, destination control system, call-giving device, queuing theory, simulation

**Abstract.** In a Destination Control System (DCS), passengers use specific terminals in lift lobbies to give their calls. Often, a building security system is integrated with the lift control system: after having granted access at a security gate, passenger's home floor is automatically sent to the lift control system as a passenger call. Immediately after registering the call, the lift control system allocates a lift to the call and announces it on a display attached to the terminal or the gate. So far, passenger interaction with these call-giving devices has been overlooked in lift traffic simulation, which typically assumes an infinite-capacity queue for the devices and does not model passenger walking from the devices to the lifts. Standard passenger service quality parameters such as waiting time are defined from when a passenger either registers a call on a landing or joins a queue. Thus, in the case of the DCS, service quality measures include queueing, interaction and walking time. This paper introduces a queue-theoretic model for call-giving devices based on average interaction time and verifies it by simulations. The model predicts queue saturation, which allows to define handling capacity of call-giving devices with 80% utilization factor. The effect of walking distance on passenger service quality is studied by gradually increasing the distance from zero up to a remote location corresponding to security gates. Usage data of call-giving devices from operational lift groups with the DCS is analysed and compared to the current practices of lift traffic design.

## 1 INTRODUCTION

A Destination Control System (DCS) was introduced to the market in the 1990s and is nowadays provided by all major lift manufacturers. In the original concept, lift lobbies were equipped with passenger terminals with a keypad and display, which passengers used to input their destination floors [1]. The terminals have evolved into touchscreen displays with customizable user interfaces. Often, the building security system and security gates are integrated with the lift control system and act as call-giving devices. Also new call-giving and guidance concepts different from the original ones have been developed [2,3]. Given that the DCS is in use in numerous high-rise buildings and the *de facto* standard for new offices, it is surprising to find that practically nothing has been published about call-giving devices and passengers' interaction with them [4].

Passenger's interaction with call-giving devices starts before operating them by choosing a device, approaching it and preparing to use it. The passenger may need to swipe an access card to unlock the device. When using a typical terminal, the passenger first reads and interprets instructions to use it and, then, inputs the destination floor. The interaction is simplified if the security system automatically sends the destination floor to the lift control system after granting access to the passenger at a gate. The lift control system allocates a lift to the passenger and immediately shows it on the display attached to the call-giving device. After correctly interpreting the shown information, the passenger walks to the allocated lift and waits for its arrival. The display may still show the allocated lift for some time, the duration of which may be required by accessibility standards [5]. The shown information may delay the next passenger to start the interaction.

Current practice in lift traffic design neglects passenger interaction with call-giving devices. However, more realistic assessment of lift group performance could be obtained if lift lobbies and passenger interaction with the devices were considered properly in lift traffic simulations. Building Traffic Simulator (KONE BTS™) is capable of modelling call-giving device queues and lobby layout, which makes it a unique tool to study the effect of interaction and walking on lift group performance [6]. Standard measures for passenger service quality include *walking time* to the allocated lift and *standing time* in front of it [7,8]. Fig. 1 adds *queueing time* and *interaction time* to the beginning of a passenger journey from the moment when a passenger joins a call-giving device queue until registering a call. While lift traffic simulations can be conducted without considering the time spent before standing in front of a lift, it is always present in DCS installations. Therefore, this paper aims at bridging the gap between simulation and real-world installations as well as establishing guidelines about how call-giving devices should be considered in lift traffic design.

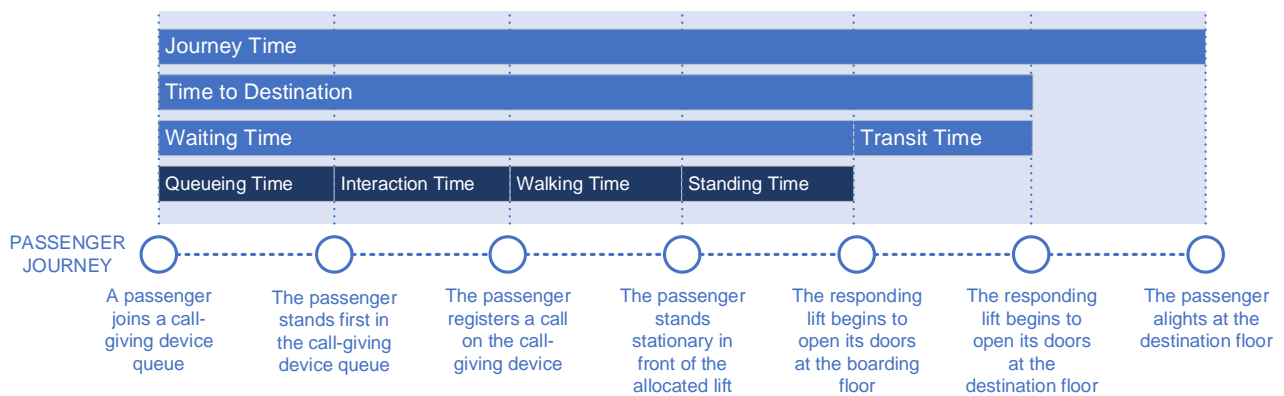


**Figure 1 A passenger journey in a lift group with a destination control system**

The rest of this paper is organized as follows. Section 2 presents a queue-theoretic model of call-giving devices and numerically shows queue saturation. Section 3 aims at validating the saturation in lift traffic simulation. In Section 4, the effect of passenger walking time on lift group performance is studied systematically. Section 5 utilizes lift monitoring system data to derive real-world evidence on passenger interaction with call-giving devices. Section 6 concludes the paper.

## 2 CALL-GIVING DEVICE QUEUES

Call-giving devices in a lift lobby can be considered as a multi-server queueing system. Lift passengers first arrive at the queue and then interact with the devices for some time. In office buildings, passenger arrivals have been found to follow a Poisson process during morning uppeak [9,10]. For simplicity, an M/M/c queue model is adopted for call-giving devices, where passengers arrive according to a Poisson process and are served by a single queue on  $c$  servers with exponentially distributed service times [11]. In practice, lift passengers form separate queues in front of each device, i.e.,  $c$  single-server M/M/1 queues, and, upon arrival at the lobby, choose one based on queue length, for example. On the other hand, a passenger standing in a queue may jockey to another queue [12]. Thus, passenger behaviour may differ from the model assumptions in practice.

Utilization factor  $\rho$  in an M/M/c queue is related to arrival rate  $\lambda$  passengers per five minutes, service rate  $\mu$  passengers per five minutes and the number of servers,

$$\rho = \lambda/(c\mu), \quad (1)$$

where service rate  $\mu$  is the inverse of average interaction time  $T$  given in seconds,  $\mu = 300/T$ . The queue is stable if utilization factor  $\rho$  is less than one. Mean queue length  $L_q$  is given by [11],

$$L_q = P_0 \rho \left( \frac{\lambda}{\mu} \right)^c / c! (1 - \rho)^2, \quad (2)$$

where  $P_0$  is the probability of no passengers in the system, i.e., a passenger can be served immediately,

$$P_0 = 1 / \left[ \left( \sum_{m=0}^{c-1} \frac{(c\rho)^m}{m!} \right) + \frac{(c\rho)^c}{c!(1-\rho)} \right]. \quad (3)$$

The mean queue length can be expressed as a function of the utilization factor and the number of servers if the relationship of arrival and service rate in Eq. 2 is substituted by  $c\rho$  according to Eq. 1. Table 1 illustrates mean queue lengths for up to six servers with varying utilization factors. The mean queue lengths start to increase uncontrollably when utilization factor exceeds 80%, which can then be used as the definition of a saturation point.

**Table 1 Mean queue lengths for M/M/c queues**

Utilization factor $\rho$ [%]	Mean queue length $L_q$ for $c$ servers [persons]					
	1	2	3	4	5	6
20	0.05	0.02	0.01	0.00	0.00	0.00
40	0.27	0.15	0.09	0.06	0.04	0.03
60	0.90	0.68	0.53	0.43	0.35	0.29
80	3.20	2.84	2.59	2.39	2.22	2.07
90	8.10	7.67	7.35	7.09	6.86	6.66
95	18.05	17.59	17.23	16.94	16.68	16.45

Mean queue waiting time  $W_q$  in seconds can be derived from the mean queue length by Little's rule,

$$W_q = 300 \times L_q / \lambda. \quad (5)$$

Table 2 shows mean queue waiting times for M/M/c queues, which increase when varying interaction times from 0.001 to 5.0 seconds and utilization factors from 80% to 95%. The results clearly demonstrate exponentially increasing mean queue waiting times for utilization factors higher than 80%, which indicates queue saturation. Interaction time 0.001 seconds is impossible in practice but is included here to demonstrate how a queue with infinite capacity results in zero mean queue waiting time as currently assumed in lift traffic simulations.

The saturation point can be used to define handling capacity for a set of call-giving devices as a maximum sustainable number of passengers that can use the devices in five minutes,

$$HC5 = 0.8 \times c \times \mu = 0.8 \times 300 \times c / T. \quad (4)$$

The 80% saturation point is typically not considered in security gate handling capacities [e.g. 13].

### 3 CALL-GIVING DEVICE QUEUES IN LIFT TRAFFIC SIMULATION

Building Traffic Simulator models passenger journeys in a multi-storey building of any complexity by a network of building hotspots, through which virtual agents navigate from their origins to their destinations [6,14]. In the case of the DCS, each call-giving device in a lift lobby is associated with a hotspot having three-dimensional coordinates. An agent first chooses the starting point of her journey from the available call-giving devices. Device interaction time  $T$  is modelled as a constant delay, after which the agent registers the call, lift control system allocates a lift to it and the agent

walks to the allocated lift. Walking times from the devices to the lifts constrain call allocation for subsequent passenger arrivals on a particular floor. A new passenger can be allocated to a lift if her estimated time of boarding occurs before a specified maximum stopping time has elapsed since the first passenger on the same floor boarded the lift. Thus, maximum stopping time sets the limit to how long a lift may wait for new passengers before closing its doors and departing. In the simulations that follow, maximum stopping time is set at 15 seconds.

**Table 2 Mean queue waiting times with varying interaction time and utilization factor**

Interaction time $T$ [s]	Utilization factor $\rho$ [%]	Mean queue waiting time $W_q$ for $c$ servers [seconds]					
		1	2	3	4	5	6
0.001	80	0.004	0.002	0.001	0.001	0.000	0.000
	90	0.009	0.004	0.003	0.002	0.002	0.001
	95	0.019	0.009	0.006	0.005	0.004	0.003
1.0	80	4.0	1.8	1.1	0.7	0.6	0.4
	90	9.0	4.3	2.7	2.0	1.5	1.2
	95	19.0	9.3	6.0	4.5	3.5	2.9
2.0	80	8.0	3.6	2.2	1.5	1.1	0.49
	90	18.0	8.5	5.4	3.9	3.1	2.5
	95	38.0	18.5	12.1	8.9	7.0	5.8
3.0	80	12.0	5.3	3.2	2.2	1.7	1.3
	90	27.0	12.8	8.2	5.9	4.6	3.7
	95	57.0	27.8	18.1	13.4	10.5	8.7
4.0	80	16.0	7.1	4.3	3.0	2.2	1.7
	90	36.0	17.1	10.9	7.9	6.1	4.9
	95	76.0	37.0	24.2	17.8	14.0	11.5
5.0	80	20.0	8.9	5.4	3.7	2.8	2.2
	90	45.0	21.3	13.6	9.8	7.6	6.2
	95	95.0	46.3	30.2	22.3	17.6	14.4

Call-giving device queues are studied for a five-car group that has a handling capacity of 14% of population per five minutes with the DCS (detailed building and lift parameters can be found in [15]). The number of call-giving devices and interaction times with a device are varied. With an interaction time of five seconds, a call-giving device can handle 48 passengers in five minutes. Passenger walking times are kept at zero by positioning all call-giving devices and lifts at the same coordinates. Pure uppeak traffic is simulated with increasing passenger demands from 10% to 16% of population per five minutes. Each passenger demand is simulated for 240 minutes, from which quantities occurring in the first 15 minutes and the last five minutes are excluded to avoid the statistical effects of initial and end transients [16]. Simulations are repeated 20 times to improve the accuracy of the results. For each simulated passenger demand, Table 3 shows queue utilization factors ( $\rho$ ) calculated using Eq. 1, average number of passengers in the car at departure from the main entrance floor ( $P$ ), average roundtrip time ( $RTT$ ), average queueing time ( $QT$ ), average standing time ( $ST$ ), average waiting time ( $WT$ ) and average time to destination ( $TTD$ ).

In the cases, where passenger interaction time with call-giving devices are set at zero seconds, call-giving device queues do not show any sign of saturation as can be expected. Average queueing time increases uncontrollably only if passenger demand exceeds handling capacity and the lift group itself saturates. Passenger demand 15% provides interesting insights when studying the repeated simulations in detail. Due to the timing of random passenger arrivals, the lift group saturated in three out of the 20 simulations, resulting in very long average queueing and standing times. The remaining 17 simulations experienced no queueing at call-giving devices and average standing time was only about 35 seconds. Thus, depending on the random sequence of passengers, the lift group may be able to handle passenger demands above handling capacity without showing any alarming values in passenger service quality measures.

**Table 3 Lift group performance in uppeak traffic with varying interaction times**

	<i>T</i> [s]	<i>c</i>	Passenger demand [% / 5 min]						
			10	11	12	13	14	15	16
<i>ρ</i> [%]	0	3	0.0	0.0	0.0	0.0	0.0	0.0	0.0
		6	0.0	0.0	0.0	0.0	0.0	0.0	0.0
	5	3	72.2	79.4	86.7	93.9	101.1	108.3	115.6
		6	36.1	39.7	43.3	46.9	50.6	54.2	57.8
<i>P</i> [N]	0	3	9.7	11.1	12.6	14.2	16.1	18.1	19.9
		6	9.7	11.2	12.6	14.3	15.9	18.1	19.9
	5	3	9.7	11.2	12.7	14.3	15.6	15.7	15.6
		6	9.7	11.2	12.6	14.3	16.0	17.9	19.9
<i>RTT</i> [s]	0	3	112.2	116.9	121.7	126.5	132.3	140.1	159.8
		6	112.0	117.0	121.7	126.9	131.4	140.2	158.8
	5	3	112.1	117.7	122.3	127.4	130.8	131.7	130.9
		6	112.0	117.1	121.8	127.0	131.8	137.7	155.2
<i>QT</i> [s]	0	3	0.0	0.0	0.0	0.0	0.0	29.4	529.3
		6	0.0	0.0	0.0	0.0	0.0	32.5	459.5
	5	3	2.5	3.8	6.2	15.7	167.3	630.0	1047.5
		6	0.2	0.2	0.3	0.5	0.6	9.4	393.8
<i>ST</i> [s]	0	3	20.9	22.3	23.7	25.7	28.8	47.6	120.1
		6	21.1	22.3	23.8	25.7	29.0	47.2	119.4
	5	3	21.2	22.3	23.8	25.3	26.6	26.6	26.9
		6	21.0	22.2	23.8	25.5	28.5	39.0	101.8
<i>WT</i> [s]	0	3	20.9	22.4	23.7	25.7	28.8	81.0	678.1
		6	21.1	22.4	23.8	25.7	29.0	87.7	637.3
	5	3	28.7	31.1	35.0	46.0	198.9	661.7	1079.4
		6	26.2	27.5	29.2	31.0	34.1	54.9	526.5
<i>TTD</i> [s]	0	3	71.2	75.0	78.6	83.0	88.9	145.5	753.2
		6	71.4	75.0	78.7	83.1	88.9	152.3	711.6
	5	3	78.9	83.8	89.8	103.5	257.9	721.0	1138.5
		6	76.5	80.2	84.0	88.5	94.0	118.2	598.7

Lift group performance with six call-giving devices and five-second interaction time closely follow the results with zero-second interaction time, which follows from the fact that six call-giving devices even with a five-second interaction time have much higher handling capacity than the lift group, 22% of population per five minutes. Furthermore, average waiting time and time to destination are slightly more than five seconds longer than in the cases with zero interaction time. Thus, the modelling of passenger interaction with call-giving devices adds a constant delay almost equal to the parameter value to both passenger service quality measures.

Three call-giving devices with an interaction time of five seconds have a handling capacity of only 11% of population per five minutes. The results show the saturation of device queues in many ways. First, queue utilization factor for 11% passenger demand is about 80%, which indicates approaching saturation. Second, average queueing time for call-giving devices is already on a higher level for 12% passenger demand but clearly saturated for 13% passenger demand. Third, with high passenger demands from 14% to 16% per five minutes, lift group performance measures and passenger standing time stop increasing but remain at the level reached by 14% passenger demand. In this case, congestion at call-giving devices makes lift group performance look better since call registration stalls and lift control system cannot allocate the lifts to their capacities. Thus, in the case of too few call-giving devices, lift group saturation may go unnoticed.

#### 4 PASSENGER WALKING TIME IN LIFT TRAFFIC SIMULATION

The impact of walking distances between call-giving devices and lifts on lift group performance and passenger service quality is studied by the same simulation setup as in the previous section. In all cases, interaction time  $T$  is kept at zero seconds and the number of call-giving devices at six. The walking distance is varied from 0 to 60 meters in 5-meter steps, and it is translated to a walking time by assuming a constant walking speed of 1.0 m/s. Simulation results are shown in Table 4.

Average number of passengers in the car at departure from the main entrance floor ( $P$ ) and average roundtrip time ( $RTT$ ) indicate that lift group handling capacity remains at 14% of population per five minutes up to a walking distance of 20 meters. Both measures are about the same for distances between 0 and 20 meters while, for the distances of 40 and 60 meters, they become clearly higher. Based on average roundtrip time with 14% passenger demand, a walking distance of 40 meters reduces handling capacity by 8.4 % and 60 meters by 16.3 %. The results indicate that the lift control system starts to lose its ability of allocating passengers going to the same destination to the same elevator due to walking time and maximum stopping time constraints in call allocation.

For passenger demands up to lift group handling capacity, 14% of population per five minutes, and for walking distances between 0 and 20 meters, average standing time ( $ST$ ) remains about the same and average waiting time ( $WT$ ) increases about as much as average walking time. In addition, average standing time decreases with walking distances longer than 20 meters. This indicates that the earlier the call is given to the lift system, the better for user experience, regardless of the loss in handling capacity. Average time to destination ( $TTD$ ), on the other hand, increases slightly more than the distance grows for walking distances longer than 20 meters, which results from longer roundtrips.

The situation changes when passenger demand exceeds handling capacity: average waiting time increases much faster than the distance grows as lift group saturates and passengers start to queue for a call-giving device. The saturation can be seen in dramatically increasing average queueing times ( $QT$ ) on call-giving devices especially for 40-meter and 60-meter walking distances.

As a short summary, call-giving devices can safely be located at distances up to 20 meters from lifts, and it may not be necessary to take the distances into account in simulations to correctly evaluate the

performance of a lift group with a destination control system. Nevertheless, walking distances longer than 20 meters should be considered in simulations since they influence handling capacity.

**Table 4 Passenger service quality in uppeak with different walking distances**

	Walking distance [m]	Passenger demand [% / 5 min]						
		10	11	12	13	14	15	16
<i>P</i> [N]	0	9.6	11.0	12.4	14.0	15.8	17.7	19.9
	5	9.3	10.7	12.1	13.7	15.5	17.5	19.9
	10	9.4	10.8	12.3	13.8	15.6	18.3	19.9
	20	9.6	11.0	12.4	14.0	15.7	18.7	20.0
	40	10.1	11.6	13.2	15.0	17.4	19.9	20.0
	60	11.7	13.3	15.0	16.7	19.0	20.0	20.0
<i>RTT</i> [s]	0	112.0	117.0	121.7	126.9	131.4	140.2	158.8
	5	107.5	112.3	116.6	121.4	127.3	135.3	160.0
	10	108.5	112.9	118.1	122.8	128.6	143.2	160.7
	20	110.4	114.8	119.4	123.8	129.7	147.4	161.2
	40	116.8	122.0	127.3	133.3	143.5	160.8	161.7
	60	135.2	139.2	144.0	148.7	157.0	161.6	162.4
<i>QT</i> [s]	0	0.0	0.0	0.0	0.0	0.0	32.5	459.5
	5	0.0	0.0	0.0	0.0	0.0	14.2	467.3
	10	0.0	0.0	0.0	0.0	0.0	56.0	543.2
	20	0.0	0.0	0.0	0.0	0.0	57.3	582.0
	40	0.0	0.0	0.0	0.0	0.2	215.2	646.0
	60	0.0	0.0	0.0	0.0	2.7	278.5	710.8
<i>ST</i> [s]	0	21.1	22.4	23.8	25.7	29.0	47.2	119.4
	5	21.5	23.1	25.1	27.1	30.2	41.8	117.5
	10	21.5	23.7	25.3	27.8	31.1	62.8	117.3
	20	19.3	21.3	23.0	25.1	28.8	67.7	109.2
	40	17.6	19.7	22.1	25.8	36.7	87.5	92.2
	60	13.2	15.0	17.9	22.7	42.1	71.6	73.4
<i>WT</i> [s]	0	21.1	22.4	23.8	25.7	29.0	87.7	637.3
	5	25.6	27.1	29.2	31.4	34.6	63.8	649.9
	10	30.2	32.4	34.1	36.8	40.3	146.1	735.4
	20	37.1	39.2	41.0	43.3	47.4	167.8	778.5
	40	54.2	56.6	59.4	63.8	76.7	402.4	850.3
	60	66.4	68.9	72.7	79.0	111.3	477.4	918.8
<i>TTD</i> [s]	0	71.3	75.0	78.7	83.1	88.9	152.3	711.6
	5	74.1	77.8	82.0	86.7	92.9	126.4	725.0
	10	78.9	83.4	87.6	93.0	99.5-	212.9	811.0
	20	87.0	91.2	95.2	100.0	107.2	236.9	854.4

	<b>40</b>	107.7	112.7	118.2	125.9	144.0	478.3	926.8
	<b>60</b>	128.9	133.0	139.0	147.6	184.7	554.0	995.8

## 5 CALL-GIVING DEVICE USAGE BASED ON LIFT MONITORING SYSTEM DATA

Call-giving usage patterns and passenger interaction time at a device are derived from lift monitoring system data of two lift groups. Group 1 has automatic call-giving at four parallel security gates that lead to the lift lobby. Gate 1 is the nearest and Gate 4 the furthest from the main building entrance. Group 2 has six touchscreen passenger terminals, where users manually select the desired destination floor from a list. The terminals are located around the lift lobby. Terminal 1 and 6 are the closest to the main entrance while Terminal 4 and 5 are the furthest. Table 5 shows walking distances between each call-giving device and lift for both lift groups.

**Table 5 Walking distances between call giving devices and lifts**

Group / Device	Walking distance from a call giving device to a lift [m]							
	Lift 1	Lift 2	Lift 3	Lift 4	Lift 5	Lift 6	Lift 7	Lift 8
1/1	6	8	11	13	6	8	11	13
1/2	6	8	11	13	6	8	11	13
1/3	6	8	11	13	6	8	11	13
1/4	6	8	11	13	6	8	11	13
2/1	7	9	10	18	20	22	N/A	N/A
2/2	10	7	4	7	9	13	N/A	N/A
2/3	13	9	7	5	8	11	N/A	N/A
2/4	22	20	18	10	9	7	N/A	N/A
2/5	18	15	12	7	7	7	N/A	N/A
2/6	8	7	7	13	16	19	N/A	N/A

Samples of more than 2000 calls placed at the main lobby were gathered from both lift groups for the period of one working week during the most intense period of morning uppeak traffic. Call-giving interval and time difference between two consecutive calls at the same device closely corresponds to passenger interaction time at a device if one passenger immediately follows another to the device and gives a call. Thus, an exceptionally long call-giving interval does not necessarily mean that a passenger was somehow troubled with the call-giving. More likely, the device was unused for a moment before the next passenger approached it or, in the case of security gates, the counter-flow of outgoing passengers blocked the incoming flow for a while.

Fig. 2 shows the distributions of call-giving intervals for each device in both lift groups, which clearly resemble gamma distributions with long tails extending greatly above 16 seconds. However, the least used devices have almost flat distributions probably arising from long periods, during which they are not used. Most frequently, call-giving intervals fall around 4.5 and 5.0 seconds for security gates and terminals, respectively. Some of the distributions have slightly raised peaks around 10 seconds, which may correspond to passengers whose first attempts to use a device failed.

Table 6 summarizes passenger call statistics for each device. Calls are not distributed evenly to the available devices but clearly chosen by the proximity of the device along passengers' paths from the entrance to the lift lobby. This behaviour should be considered already in the design stage when

positioning devices to maximize their usage, to ensure enough devices and to enable efficient use of lift groups.

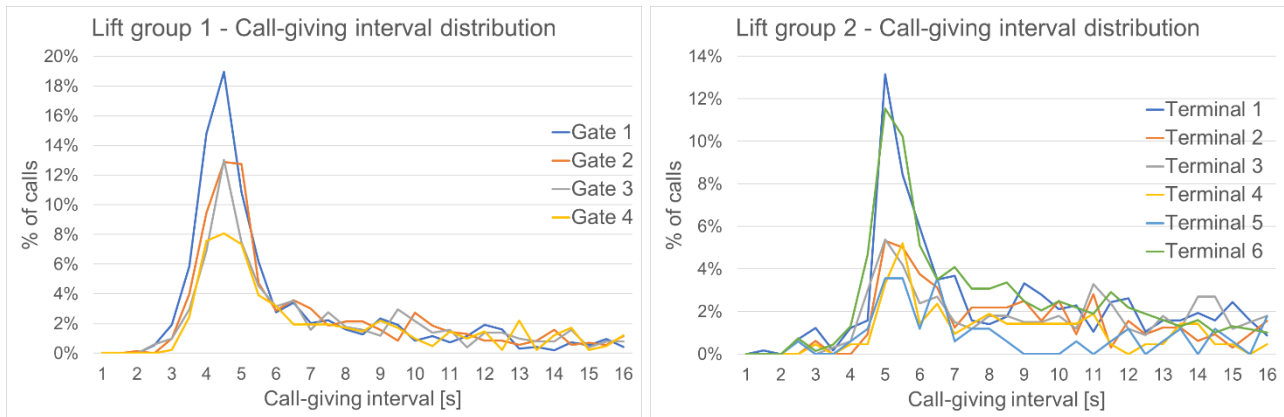


**Figure 2 Call-giving interval distributions for each device**

Call-giving intervals indicate possible interaction times with devices for design purposes. Mean call-giving intervals are high due to the long tails. Median values are lower than means but still too high to represent typical interaction times except possibly in the case of Gate 1 in Group 1. The shortest call-giving intervals are about two seconds for almost all devices, which indicates that experienced users can, at least in theory, use the devices quickly. However, such short intervals were rare exceptions in the data and cannot be considered typical interaction times. For design purposes, four seconds can be assumed for security gate interaction time and five seconds for touchscreen passenger terminals based on the observed statistics. With these interaction times, handling capacity of a security gate becomes 60 passengers in five minutes and, respectively, 48 passengers in five minutes for touchscreen passenger terminals by using Eq. 4.

**Table 6 Call statistics for the call giving devices at the main lobby**

Group / Device	Number of calls	% of calls	Call-giving interval [s]			Walking time [s]	Standing time [s]	Waiting time [s]
			Mean	Median	Min			
1/1	939	36.8	8.0	4.9	2.1	9.4	14.4	22.7
1/2	698	27.3	10.9	6.3	1.8	9.4	15.2	23.5
1/3	507	19.9	14.9	8.2	2.1	9.3	13.9	21.9
1/4	409	16.0	18.5	11.6	2.9	9.3	14.7	22.8
2/1	570	24.9	13.2	9.4	1.5	13.7	11.5	22.8
2/2	319	14.0	28.4	18.1	2.6	8.5	11.0	17.4
2/3	334	14.6	25.7	15.4	2.2	8.5	12.2	19.0
2/4	211	9.2	37.2	26.4	3.0	12.2	12.3	22.8
2/5	168	7.3	50.0	30.3	2.3	9.7	12.9	20.7
2/6	684	29.9	13.7	8.3	2.2	11.2	11.1	20.0

Finally, passenger service quality statistics demonstrate the effect of walking time. First, walking time seems to mostly explain the differences between the devices with respect to average waiting times. Average standing times are rather constant and independent on device locations, 14-15 seconds for Group 1 and 11-12 seconds for Group 2, which indicates that walking distances do not affect call allocation. Second, in these lift groups, average passenger waiting times are excellent, below 25

seconds, but, average standing times are even better, less than 15 seconds. Since standing times can be taken as a measure of user experience, waiting times reported by a lift monitoring system may lead to incorrect conclusions about lift group performance.

## 6 CONCLUSIONS

This paper studied the effect of call-giving devices on the destination control system by explicitly modelling passenger interaction with a device and walking between the devices and lifts. A queueing-theoretic model and lift traffic simulations showed that a call-giving device queue saturates when utilization factor exceeds 80%, which can be used to define call-giving device handling capacity. The simulations showed an important result that time to interact with a device and walking to the allocated lift do not negatively affect lift group handling capacity and passenger service quality if walking distances between the devices and the lifts remain below a practical limit of 20 meters. However, if walking distances are increased beyond 20 meters, the lift control system starts to lose its ability of allocating passengers traveling to the same destinations to the same lifts, which reduces lift group handling capacity. Finally, call-giving intervals, i.e., times between consecutive passenger calls, were derived from lift monitoring system data for the most intense morning uppeak traffic to determine typical passenger interaction times for call-giving devices. In lift traffic design, interaction times of four seconds for a security gate and five seconds for a touchscreen passenger terminal could be assumed as realistic design parameters.

Based on the results, lifts with a destination control system could be designed and commissioned in three steps, which would evaluate lift group performance independent of call-giving device locations and actual passenger demands:

- 1) Carry out lift traffic design according to the current practice and design criteria, if walking distances between the lifts and call-giving devices does not exceed 20 meters. Otherwise, account for the distances in design criteria or simulate vertical transportation along with detailed lobby layouts and passenger walking paths.
- 2) Select the number of call-giving devices by assuming realistic interaction time to match passenger demand and position them in attractive locations with respect to building entrances.
- 3) Verify lift group performance by simulating the same traffic patterns as in the design stage with a real-time simulator, where virtual passengers travel in the actual lift system.

The results of this paper directly apply to the studied destination control system. Nevertheless, also other destination control systems need to cope with call-giving device locations and passenger interaction with them, although practical control system implementations most likely vary and affect options available to fine-tune lift group performance. As the effect of call-giving devices on lift group performance is largely unknown, they should also be incorporated into other simulation models and design standards.

## REFERENCES

- [1] J. Schröder, “Elevating Calculation – Probable Stops and Reversal Floor “M10” Destination Hall Calls + Instant Car Assignment”. *Elevator World*, Vol. 38, No. 4, 40-46 (1990).
- [2] M-L. Siikonen, J. Sorsa, and T. Susi, KONE Polaris Hybrid. *Elevator World*, Vol. 60(7), 2012, 108-112.
- [3] R. Barker, “Harmonized Elevator Dispatching and Passenger Interfaces”. *Elevator World*, Vol. 66, No. 11, 82-90 (2018).

- [4] J. Sorsa, and M-L. Siikonen, "Double-Deck Destination Control System. *Elevatori*, Vol. 37(5), 2008, 42-56.
- [5] CBSC, *2019 California Building Code*. California Building Standards Commission, The United States of America (2019).
- [6] M-L. Siikonen, T. Susi, and H. Hakonen, "Passenger traffic flow simulation in tall buildings". *Elevator World*, Vol. 49, No. 8, 117-123 (2001).
- [7] ISO, *ISO 8100-32:2020 – Lifts for the transportation of persons and goods – Part 32: Planning and selection of passenger lifts to be installed in office, hotel and residential buildings*. International Organization for Standardization, Switzerland (2020).
- [8] G. Barney, "Towards agreed traffic design definitions". *Elevator World*, Vol. 53, No. 2, 108 (2015).
- [9] N.A. Alexandris, *Statistical models in lift systems*. Ph.D. thesis, The Victoria University of Manchester, Institute of Science and Technology (1977).
- [10] J-M. Kuusinen, J. Sorsa, M-L. Siikonen, and H. Ehtamo, "A study on the arrival process of lift passengers in a multi-storey office building". *Building Services Engineering Research and Technology*, Vol. 33, No. 4, 437-449 (2012).
- [11] S.M. Ross, *Introduction to Probability Models*. Academic Press, San Diego, CA, USA (2014).
- [12] E. Koenigsberg, "On Jockeying in Queues". *Management Science*, Vol. 12, No. 5, 412-436 (1966).
- [13] M. McGovern, "How to Calculate Turnstile Lane Needs for Any Facility". <https://www.linkedin.com/pulse/how-calculate-turnstile-lane-needs-any-facility-mike-mcgovern/> (accessed 15.02.2020)
- [14] J. Sorsa, "Lift traffic design: calculation or simulation?". *Proceedings of 10<sup>th</sup> Symposium on Lift and Escalator Technologies*, Northampton (2019).
- [15] H. Hakonen, and M-L. Siikonen, "Elevator traffic simulation procedure". *Elevator World*, Vol. 57, No. 9, 180-190 (2009).
- [16] T. Susi, J. Sorsa, and M-L. Siikonen, "Passenger Behavior in Elevator Simulation". *Elevatori*, Vol. 34, No. 5, 28-37 (2005).

## BIOGRAPHICAL DETAILS

Janne Sorsa is the head of People Flow Planning in KONE Major Projects. He obtained the degree of D.Sc. (Tech.) in operations research in 2017 from Aalto University School of Science. He has developed optimization models and numerical algorithms for lift group control systems. His research interests include all aspects of modelling people flow in buildings such as transport planning, simulation, behaviour, human factors and evacuation.

Mikko Kontturi studied computer science at Tampere University of Technology, Finland and works as people flow planning expert in KONE Major Projects organization. He has been with KONE for more than a decade, and during the last 12 years has globally been responsible for people flow analysis and solutions for high rise buildings as well as training of people flow planning.

Mirko Ruokokoski graduated from the Department of Engineering Physics and Mathematics, Helsinki University of Technology in 2008. Currently, he is finalizing his doctoral thesis at Systems

Analysis Laboratory in the Aalto University, School of Science and Technology. He joined KONE in 2012 and has been working for R&D.

# Computational environment for Simulating Impact of Building Sway on High Rise Lifts

Jaakko Kalliomäki, Jarkko Saloranta, Joonas Sorvari, Sakari Mäntylä,  
Mikko Puranen

KONE Corporation, Finland, jaakko.kalliomaki@kone.com

**Keywords:** high rise lift, sway, traffic, simulation

**Abstract.** In high wind conditions, tall buildings are subjected to sway, which creates a challenge in maintaining passenger comfort and safety. The lift performance may need to be reduced or the lift service may even need to be suspended in severe conditions; however, since the lifts are a key service of a building, any reduction in their performance may cause substantial loss of revenue. Therefore, there is a strong demand on the one hand to maximize the lift service availability as long as it is safe, and on the other hand, to demonstrate the impact of sway countermeasures on the performance of the lift system in advance. This article explains how a computational environment that models a lift system in building sway conditions is built based on a segmented approach. The first part consists of the *main lift model*, which utilises the building and lift data and is able to run the lift, based on recorded or simulated lift calls. It also implements the operational mode it receives from the *real-time rope sway calculator*. This model forms the second part of the environment and it calculates rope amplitudes based on recorded or simulated building motion and car position from the main model and determines the appropriate operational model. The third part consists of the *rope sway analysis tool*, which provides precalculated amplification data for the real-time calculation model, the *full-scale rope sway simulation tool*, which acts as a reference for result validation, and the *building motion calculator*. All simulations are based on the modelling of the physical events. This environment can be used to predict lift system performance on future buildings and to test the efficiency of different sway control strategies, and the visualisation of results allows effective communication between different parties in high rise building projects.

## 1 INTRODUCTION

The trend of building taller has been combined with a trend of creating super-slender buildings. This later trend is driven by high city-centre land value, its scarce availability, development in engineering techniques and aesthetic trends [1]. The trend for tall and slender buildings creates unique challenges in maintaining a good lift service while also preserving high passenger comfort and safety. The problem is particularly challenging because it involves multiple disciplines; e.g. mechanical, electrical and control system design of the lift, lift traffic planning, wind engineering and building structural engineering.

Caporale described in his dissertation in 2000 the challenges of traditional approaches by lift engineers to tackle rope sway [2]; either the rope sway in lift ropes is dampened by hardware, or the speed of the lifts is reduced by software. The drawback of the hardware solution is that effective dampening of suspension and compensation ropes on both the car and counterweight side requires complex arrangements, which are costly to produce, install and maintain. Whereas, the speed reduction by software, and ultimately the cessation of lift service in severe conditions, can lead to loss of revenue and make areas of the building less desirable and less valuable to building owners. As a conclusion, Caporale anticipated that the hardware dampening strategy would become the preferred option, but the experience of the Authors suggests that the software solutions have become the industry standard.

Since then, different ways of simulating the dynamic response of high rise lift systems have been published e.g. by Crespo et al. [3] and the work to reduce the impacts of the software-based solution has continued to this day. For instance, an approach which aims to optimise between passenger ride comfort, traffic and building and rope sway has been presented [4], as well as an approach where rope sway is estimated in real-time based on car location to minimize impact on lift system performance [5]. But a way is needed to test and demonstrate the effectiveness of different sway control strategies and to help the communication of experts in different fields.

This paper describes how a computational environment is built from segments to achieve these targets. Building motion data can be reproduced using a mathematical model and rope amplification data is generated based on the physical properties of the ropes, the lift system and the building. The lift and building properties are also used to populate lift running information. The rope sway amplitudes are then calculated based on these variables. As a final step, the processed data can be exported into various output formats.

While different aspects of this computational environment have been studied elsewhere, combining the different elements together is what provides the means to simulate different kinds of configuration changes quickly and to visually assess their impact on the performance of the lift system. The accuracy of the simulation may also be improved by substituting some of the computational elements with actual recorded data, if such information is available.

## 2 THE COMPUTATIONAL ENVIRONMENT

The computational environment is a context that combines several calculation elements together and enables to create visualisations that illustrate the impact of changes of input parameters or boundary conditions.

### 2.1 Dynamically Changing Lift Operation

One of the main reasons why a new computational environment was built was the fact that the lift operation changes dynamically based on building motion, calculated rope sway and selected operation mode. For instance, decreasing lift speed is one common way to alleviate rope sway problems, and the decision of reducing lift speed can be made based on calculated rope amplitudes. The speed reduction in turn affects the sequence of calls that can be served and subsequently how the rope sway evolves.

Furthermore, even if there were different kinds of tools available for assessing lift traffic, the traffic analysis focuses traditionally on peak traffic and on the handling capacity of the lifts [6]. Therefore, these tools are targeted for estimating the required speed and quantity of the lifts in normal operational mode and are, as such, unsuitable for simulating the lift operation in building sway conditions. Also, traffic analysis normally ignores service lifts. Service lifts are more likely to serve the floors where rope resonance is present, and may be assigned as firefighting and evacuation lifts, in which case basic safety must be ensured even in extreme sway conditions.

### 2.2 Structure of the Environment

The structure of the computational environment is presented in Fig.1. The inputs for the computational sway environment are the Building Motion Data (2), which consist of acceleration and amplitude levels of the building, Lift Data (3), which consist e.g. of masses and lengths of lift components, Building Data (4), which consist of building characteristics such as natural frequencies and information such as quantity and positions of served floors and Lift Call Data (5), which is a log of calls assigned to the lift. Alternatively, building motion can be artificially populated using Building Motion Calculator (1) and the call data using Main Lift Model (8) within the computational environment.

The Building Motion Data and Building Data is typically received from the wind engineering consultant of the builder. Preliminary lift data is received from the lift engineering team. A simplified

summary of these data sets is shown in table 1. Lift call data can be extracted from a lift monitoring system such as KONE E-Link.

**Table 1. A sample summary of Building Motion Data, Building Data and Lift Data**

Data from wind engineer			Data from lift engineer			
Highest occupied floor	[m]	220.0	Counterweight location (Rear / Side)		Rear	
Natural freq. x-direction	[Hz]	0.21231	Travel	[m]	200	
Natural freq. y-direction	[Hz]	0.24938	Roping		1:1	
Peak to RMS factor		3.82415	Height of lowest landing	[m]	5.0	
<b>Max amplitude</b> Return period [years]	x-direction	y-direction	Pit	[m]	5.0	
	[mm]	[mm]	Headroom (SH)	[m]	11.5	
	1	21.9	58.1	Sling height (E)	[m]	3.6
	5	30.4	80.6	Rated speed	[m/s]	8.0
	10	36.5	96.9	Rated acceleration	[m/s <sup>2</sup> ]	1
	50	52	138	Total Car Weight KTQ [kg]	[kg]	6400
100	59.8	158.7	Rated Load Q [kg]	[kg]	2000	
<b>Deflection shape</b> Height	x-direction	y-direction	CWT Total weight	[kg]	5600	
			Rope compensator mass	[kg]	1100	
	0	0.000	0.000	Overspeed governor tension weight	[kg]	250
	1/4	0.125	0.125	Hoisting roping		8xd16 PAWO F3
	1/2	0.354	0.354	Total suspension rope weight	[kg/m]	7.87
	3/4	0.650	0.650	Compensation ropes		7xd16 PAWO F3
	1/1	1.000	1.000	Total compensation rope weight	[kg/m]	6.89
				OSG-rope		d10 PAWO F3
					[kg/m]	0.38
				Travelling cables	[kg/m]	3.29

The lift data, floor information and natural frequencies of the building are fed to the Building Sway Analysis Tool (6), which generates the rope amplification data (7) needed by the real-time sway calculator (9).

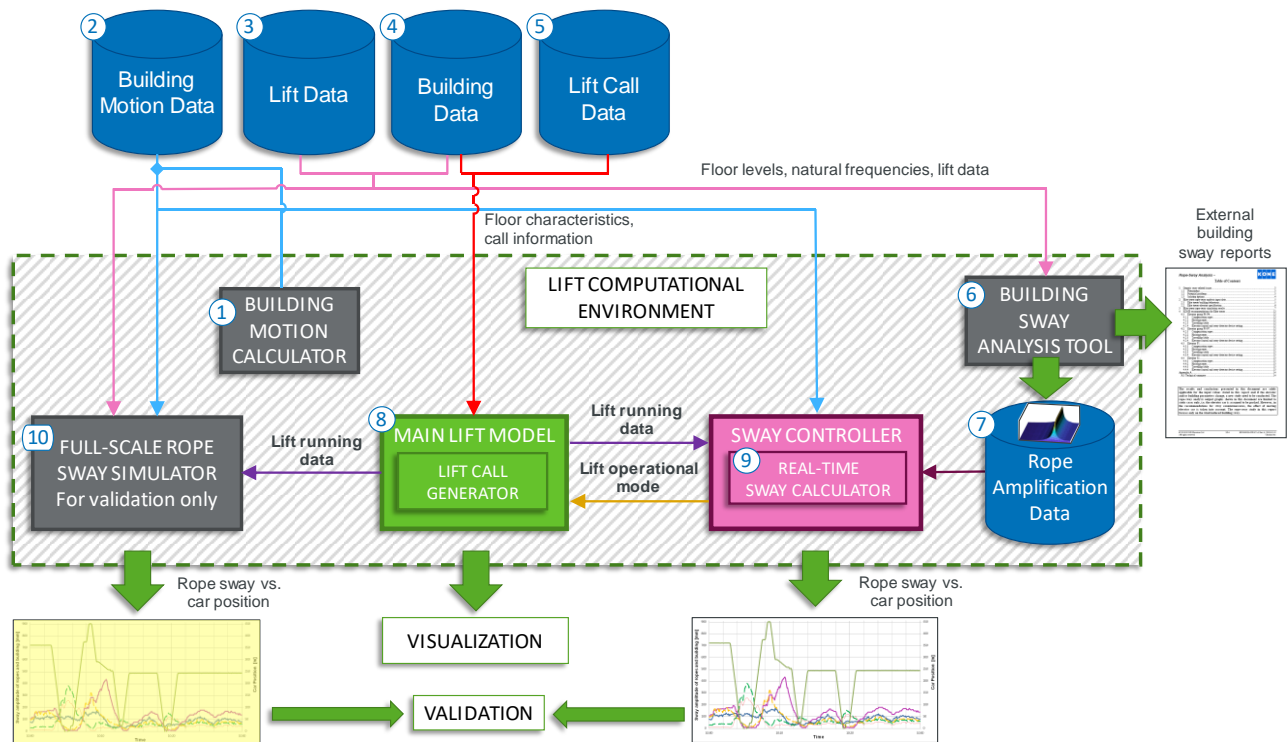


**Figure 1. Structure of the computational environment.**

The main model (8) is in charge of the lift operation. It utilises the building (4) and call data (5) to calculate the lift running data (i.e. speed and position of the lift). The main model feeds the lift running data to the real-time sway calculator (9), which returns the lift operational mode according to the predefined sway amplitude thresholds. The main model changes the operational mode at the next possible time step and feeds the new speed and position information back to the real-time sway calculator, consequently starting the loop again.

The log of lift running data can also be sent to the Full-Scale Rope Sway Simulator (10) for validation. In theory, the full rope sway simulator provides exactly the same information as the computational environment depicted above, but it requires a lot of processor capacity. The computational environment has been optimised for performance, thus offering a possibility to carry out extensive simulations in a reasonable amount of time.

### **3 ELEMENTS OF THE COMPUTATIONAL ENVIRONMENT**

#### **3.1 Main Model and Lift Call Generator**

The purpose of the main lift model is to replicate the functions of the actual lift controller. It controls the acceleration and the target speed of the lift, assigns different drive profiles and calculates the position of the car at each time step. Furthermore, the main model is the entity responsible for implementing the operational modes – as requested by the sway controller – at the next possible time step according to their priority. For example, the lift controller can actuate the lift parking mode only after it has ended serving the current call.

The main model simulates the running of the lift by utilising the floor characteristics (type and position) of the building and stored lift call data, which can be either actual data from an existing building or data for a future building generated by a traffic simulation software. Alternatively, the lift call generator within the main model can populate random calls based on given probability distribution (e.g. half of the calls to or from the main floor), or call data from a previous simulation can be reutilised for comparison purposes.

Based on the lift calls, the main model calculates car speed and position, which are governed by the rated acceleration and the applicable operational mode of the lift. Other parameters, such as loading time to calculate the total waiting time between calls, are also utilised. The time step length for car position calculation has to be shorter by an order of magnitude compared to the real-time sway calculation.

#### **3.2 Sway Controller Model and Real-Time Sway Calculator**

The sway controller model collects the needed inputs (e.g. building acceleration, car position), determines the suitable operational mode and maintains the timers, which define how long a given mode must be maintained. The objective of the lift operational mode selection is to maximize the service rate without sacrificing ride comfort or safety of the passengers. The correlation between speed profile selection and ride comfort has been demonstrated earlier by Roivainen et al. [4], and here the focus is to limit the rope amplitudes without quantifying the lateral vibrations in the car in order to maintain high performance level.

##### **3.2.1 Operational Modes**

At each given time, the sway controller determines the most suitable operational mode to the lift. The basic operational mode alternatives, in a prioritised order from lowest to highest, are normal, variable speed (VAS), performance selection (PES) and park (PARK). VAS drive profile assigns reduced speed to top or bottom part of the shaft. PES profile adjusts the maximum driving speed to a lower level for a set period of time. PARK parks the car to a pre-defined park position for a set period of time. Only one mode can be active at a time. VAS and PES drive profiles are illustrated in Fig.2.

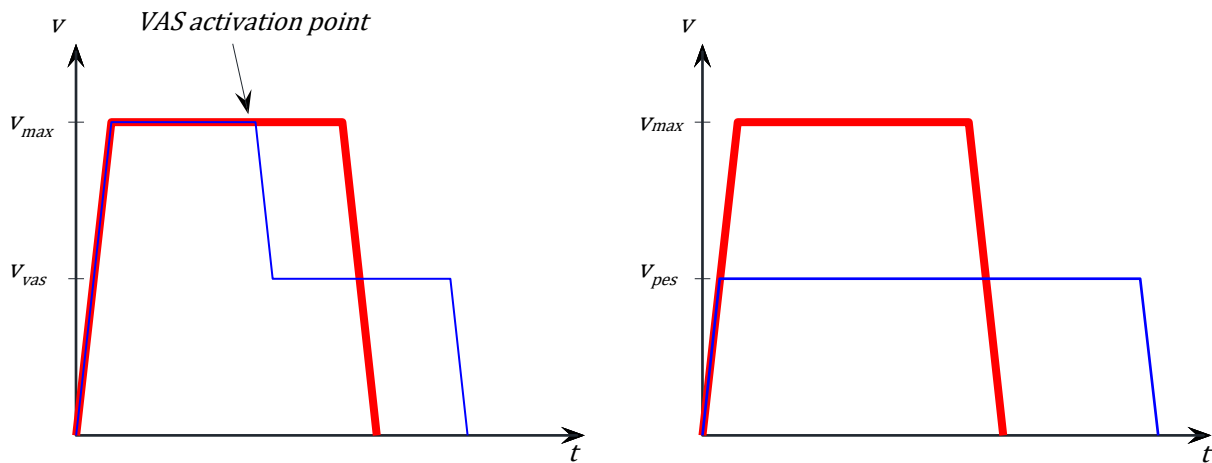


**Figure 2.** Velocity as a function of time when lift travels from the bottommost floor to the topmost floor. Left side: VAS versus normal drive. Right side: PES versus normal drive.

### 3.2.2 Real-Time Rope Sway Calculation

The real-time rope sway calculation occurs within the sway controller model. Rope amplitudes are estimated using lift car position information, building acceleration amplitudes and rope-specific data tables for each period of building acceleration. The method has been inspired by the paper by Arai et al. [5].

The advantage of calculating rope amplitudes based on predefined tables is that the calculation is light and fast. This means that in actual lift installation this kind of calculation can be executed by lift group controller in real-time without overburdening its resources, while taking into consideration that the calculation has to be done for both primary building modes (x- and y- directions) and for each lift separately. In the case of simulation, the efficient calculation makes it possible to calculate long periods in a short amount of time.

### 3.2.3 Building Acceleration Amplitudes

Building acceleration amplitudes are determined from periodic acceleration data. The effective amplitude  $\hat{a}$  is calculated from the peak-to-peak amplitude. That is, the effective amplitude  $\hat{a}$  is defined as half the difference between the highest and the lowest value in the acceleration period. See Fig.3 and Fig.4.

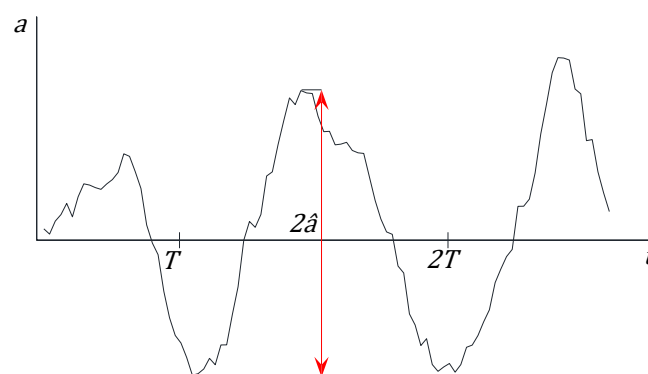


**Figure 3.** Acceleration amplitude  $\hat{a}$  for acceleration data with period  $T$ .

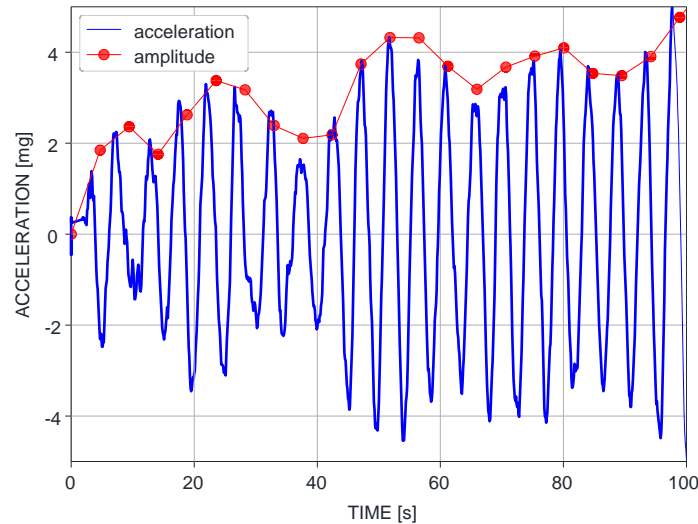


**Figure 4.** Acceleration amplitude for building acceleration data. Acceleration period  $T = 4.71$  s.

### 3.2.4 Rope Amplification Table

Rope amplification table is a two-dimensional array, denoted hereafter as  $A$ , where each row represents a floor level and each column an acceleration period, see Fig.5 for illustration. Table values are precalculated by solving a second-order damped wave equation, with constant acceleration amplitude. When the rope tension is assumed to not change due to rope displacement, the resulting equation is linear. Thus, the rope amplitudes  $u$  are directly proportional to acceleration amplitude, i.e.  $u \sim \hat{a}A$ . Consequently, once the table has been generated for a single acceleration amplitude, it can be used for any acceleration amplitude by employing scaling. Table cell value  $A_{ij}$  is the amplification factor in the considered rope after  $j$  acceleration periods when lift car is at rest at  $i^{\text{th}}$  floor level.

Hereafter, it is assumed that the rope amplification data tables are generated using unit acceleration amplitude. It should be noted that calculation floor levels do not need to coincide with car landing levels. A data table is visualised in Fig.6.

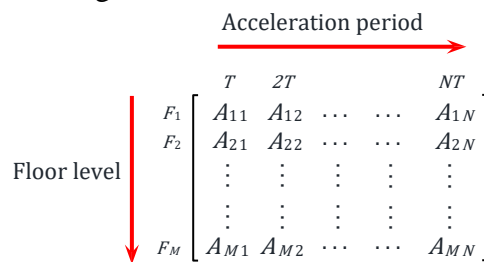


**Figure 5.** Rope amplification table illustration.  $F_i$  is the position of  $i^{\text{th}}$  floor level and  $T$  is the acceleration time period.

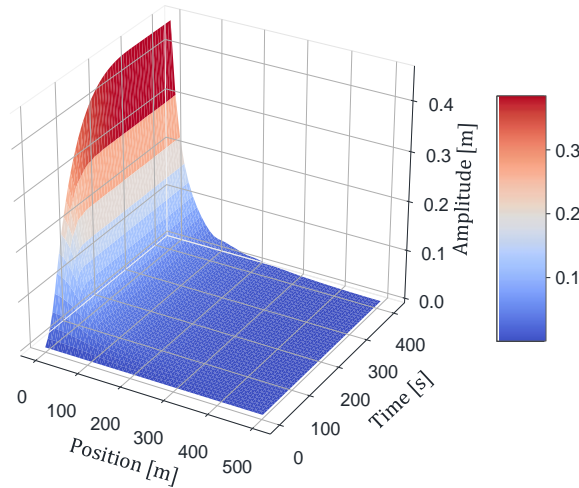


**Figure 6. Data table visualisation. Rope amplitude as a function of time and car position.**

Rope amplitudes are updated at discrete time steps  $t_0, t_1, t_2, \dots$  such that  $t_n - t_{n-1} = T$ . Suppose that at time  $t_n$  the nearest floor to lift car, in direction of travel, is the  $i^{\text{th}}$  floor. Furthermore, let  $\hat{a}(t_n)A_{ij}$  be the amplitude value in row  $i$  which is closest to previously calculated amplitude  $u(t_{n-1})$ . Then amplitude at time  $t_n$  is calculated as

$$u(t_n) = u(t_{n-1}) + du, \quad (1)$$

where the amplitude increment is given by

$$du = \hat{a}(t_n)(A_{ij+1} - A_{ij}), \quad (2)$$

where  $\hat{a}(t_n)$  is the acceleration amplitude of the  $n^{\text{th}}$  acceleration period. However, if the previous amplitude is higher or equal to the maximum table value in row  $i$ , the amplitude decays exponentially or stays the same:

$$u(t_n) = \max(u(t_{n-1})e^{-2\pi p_i \zeta}, \hat{a}(t_n)A_{iN}), \quad (3)$$

where  $p_i$  is the precalculated ratio between building period and rope period when car is at the floor position  $F_i$  and  $\zeta$  is the damping ratio value.

### 3.3 Building Motion Time-series Calculator

The time series data for building motion is calculated by the means of a narrow-band process [7], [8] shown in Fig.7. The building motion  $w_0(t)$  is calculated from Gaussian white noise  $\zeta(t)$  by a two-step filter. The filter consists of a low-pass filter and a band-pass filter.

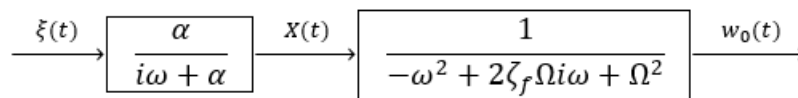


**Figure 7. Narrow-band process.**

The filter parameters are chosen such, that the building motion  $w_0(t)$  has the desired statistical properties. The filter parameter  $\alpha$  is calculated as

$$\alpha = \Omega \left( -\zeta_f + \sqrt{\zeta_f^2 + \frac{\zeta_f \Omega^3 A_0^2}{\pi S_0 - \zeta_f \Omega^3 A_0^2}} \right), \quad (4)$$

where  $\Omega$  is equivalent to the building natural frequency and corresponds to band-pass filter center frequency,  $\zeta_f$  is the band width of the band-pass filter,  $A_0$  is the amplitude of a harmonic sinusoidal

time series that has the same RMS value as the building motion  $w_0(t)$  and  $S_0$  is the constant level of the power spectrum of white noise  $\zeta(t)$ .

The building motion time-series is created with pre-defined RMS value, peak-to-RMS ratio and building natural frequency. The value for peak-to-RMS ratio is estimated as [9]

$$\frac{Peak}{RMS} = \sqrt{2 \ln(\Omega T_{obs})} + \frac{0.5772}{\sqrt{2 \ln(\Omega T_{obs})}}, \quad (5)$$

where  $T_{obs}$  corresponds to observation time period, typically 600 s or 3600 s in wind engineering practice. It should be noted that obtaining a pre-defined value of peak-to-RMS ratio for building motion  $w_0(t)$  time series is not guaranteed by the narrow-band process described above. However, it can be easily obtained for typical peak-to-RMS values by running the process with new random Gaussian white noise  $\zeta(t)$  time-series until the desired value is obtained.

### 3.4 Full-scale Simulation Model

The full-scale model is based on second-order damped wave-equation and the governing PDE-equation is solved numerically by the means of finite-difference method. The simulation model used in the computational environment is a KONE in-house developed code. A very similar approach to solve the rope sway for a moving lift system with finite-difference method has been presented in [10]. In the full-scale model, more complex events can be easily considered, e.g. ropes hitting shaft equipment or shaft wall or the application of the hardware solutions mentioned in Chapter 1.

The full-scale model is a collection of scripts, which offers high degree of freedom, but also requires an experienced user with in-depth knowledge of the problem that is being studied. In the case of the computational environment under discussion, the full-scale model is used as a reference model to make sure that the rope amplitude calculation logic using the amplification data tables is producing accurate results.

### 3.5 Rope Amplification Data Table Calculation

Rope amplification data tables described in Chapter 3.2 are generated using the rope sway analysis tool. This tool applies the same finite difference approach as the full-scale model, but it uses a dedicated input file and runs only limited scripts to produce specific output files. This tool is also used to generate calculation results for external rope sway analysis reports.

In the beginning of the simulation, the rope displacement is set to zero and the building starts to sway with given period  $T$  and with unit acceleration amplitude of 1 milli-g. The unit acceleration amplitude of the building is set to building height, where the lift specific building accelerometer is located, i.e. typically the machine room height. The lift car remains stationary at given shaft location  $F_i$  during one simulation run. The maximum absolute displacements of the different rope segments are recorded as a function of time and stored with building period  $T$  interval as a row in the corresponding rope amplification data tables. When the above mentioned simulation is repeated for all lift car positions  $F_i$  for the studied lift, the rope amplification data tables are obtained. The simulation time for each lift car location  $F_i$  needs to be long enough, so that converged maximum amplitudes are found for each rope segments.

## 4 OUTPUTS

The computational environment can be configured to generate various outputs. This chapter presents the three basic outputs and their usages.

### 4.1 Model Comparison

For validation purposes, the lift running data, building data and building motion data can be fed to the full-scale rope simulator, which calculates the “accurate” amplitudes that can then be compared to the “estimated” results provided by the real-time sway calculator. Fig.8 shows the results of one of

such validations. As noted, it is possible to achieve good correlation between the results based on the predefined tables (Real-time model) and the finite-difference method (Full-scale model).

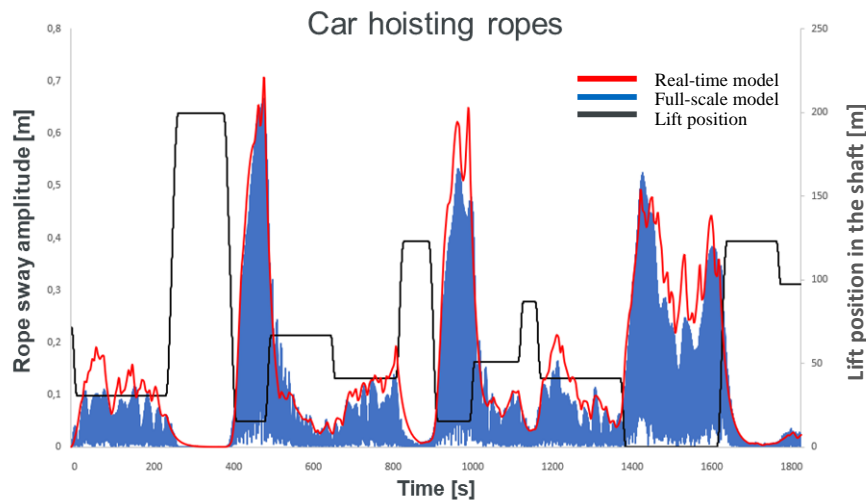


**Figure 8. Sample validation between Real-time and full-scale models**

#### 4.2 Numerical data for analysis

The numerical data produced by the computational environment is demonstrated using a sample lift with a travel of 200 m, a rated speed of 8 m/s and with 34 landings. The minimum times the lift spends in PES or PARK are 10 and 15 minutes correspondingly. Two scenarios were analysed, one where the lift is running as a shuttle service between the lowest and the highest floor, and the other where there are also intermediate floors and the lift serves random calls. Both scenarios are further assessed with the assumption that the total waiting time is 180 s or 10 s at the landings where the lift stops. The results are presented with three conditions: “Ideal” represents the situation where no sway control features are present, “Old” represents the situation where sway control is based on building acceleration only and “New” represent the situation where sway control is based on real-time rope amplitude calculation. The results are presented in Table 2.

**Table 2. Simulation results of sample case from the computational environment.**

		Shuttle						Random					
		Waiting time 180s			Waiting time 10s			Waiting time 180s			Waiting time 10s		
		Ideal	Old	New	Ideal	Old	New	Ideal	Old	New	Ideal	Old	New
<b>Run info</b>	Calls	402	382	395	1908	1595	1865	440	431	434	3230	2985	3177
	Utilisation [%]	100.0	95.0	98.3	100.0	83.6	97.7	100.0	98.0	98.6	100.0	92.4	98.4
	Normal time [%]	100.0	50.3	90.2	100.0	50.0	94.9	100.0	50.4	86.7	100.0	50.3	94.1
	PES time [%]	0.0	48.6	8.8	0.0	49.0	4.1	0.0	48.5	12.3	0.0	48.7	4.8
	PARK time [%]	0.0	1.0	1.0	0.0	1.0	1.0	0.0	1.0	1.0	0.0	1.0	1.0

#### 4.3 Animation

The main model can directly create animations to visualise the numerical data from the computational environment. Fig.9 shows a simple and effective way to demonstrate the correlation between different aspects of the rope sway problem. The upper left corner shows the relative position of the car and counterweight at each time step, the upper right corner shows the building acceleration and the bottom part shows the calculated rope amplitudes of each rope segment.

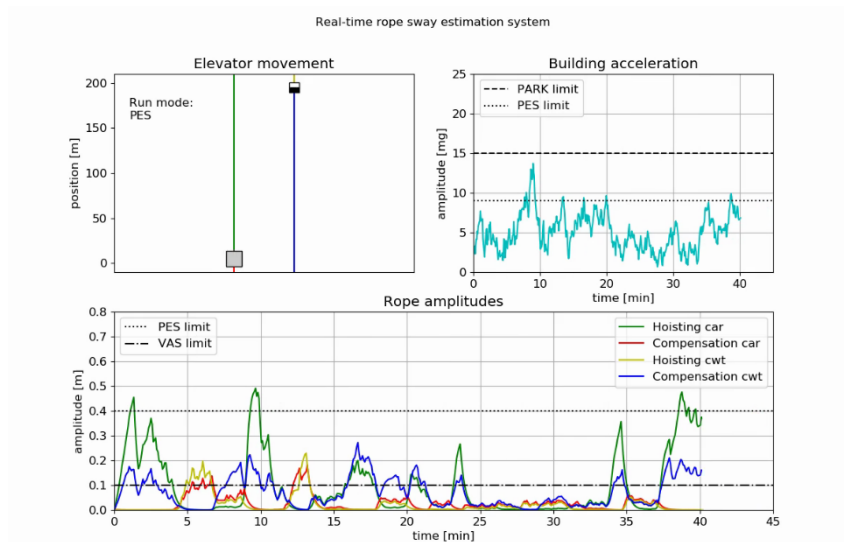


**Figure 9.** Visualisation generated using the computational environment.

## 5 DISCUSSION

In his dissertation, Caporale predicted that mechanical countermeasures would prevail over software solutions, because the customers would outweigh the higher initial expense over the reduction in lift system performance. Based on the experience of the Authors, the development has not proceeded as Caporale anticipated. There are a number of reasons for this – the most obvious being the quick advancements in software based control systems. In addition, the advancements in building technology have made buildings less sensitive to sway. One of the less apparent reasons has been the lack of tools that could be used to easily demonstrate the effectiveness of different sway control strategies – whether software or hardware based – to the customer. This deficiency has left customers without proper justification in making the decision between short-term investment cost and long-term profitability.

The introduction of the computational environment for simulating the impact of building sway on high rise lifts eliminates this short-coming and gives the customers the possibility to make educated decisions. The visualisation of results also allows effective communication between different parties in high rise building projects, who may not have in-depth knowledge of the intricacies of lift engineering. For lift engineers, the computational environment enables the testing and refining of different sway control strategies in different kinds of buildings and in varying weather conditions.

These types of tools are needed to answer the ever-tightening expectations of the super tall and super slender buildings.

## 6 REFERENCES

- [1] S. Marcus, "The New Supers: Super-Slender Towers of New York," Chicago, 2015.
- [2] R. S. Caporale, "The Effect of Building Sway on Lift Ropes and Cables," in *Vertical Transportation Review*, Elevator World Inc..
- [3] R. S. Crespo, S. Kaczmarczyk, P. Picton, H. Su and M. Jetter, "Modeling and simulation of a high-rise elevator system to predict the dynamic interactions between its components," in *Symposium on Lift and Escalator Technologies*, Northampton, 2013.
- [4] G. Roivainen, J. Saloranta, M. Ruokokoski, J. Kalliomäki and V. Sreenath, "Transient Dynamic Computation for Mega-High Rise Lifts," Northampton, UK, 2018.
- [5] Y. Arai, K. Tanaka, J. Koizumi and S. Sasaki, "Application of Seismic Design to Elevators for Skyscrapers," in *Elevator Technology 22, Proceedings of Elevcon 2018, 22nd International Congress on Vertical Transportation Technologies*, Berlin, The International Association of Elevator Engineers, 2018.
- [6] G. S. Strakosch and R. S. Caporale, *The Vertical Transportation Handbook*, 4th Edition, New York: John Wiley & Sons, Inc., 2010.
- [7] J. W. Larsen, R. Iwankiewicz and S. K. R. Nielsen, "Nonlinear stochastic stability analysis of wind turbine wings by Monte Carlo simulations," *Probabilistic Eng. Mech.* 22, 181-193., 2007.
- [8] S. Kaczmarczyk, R. Iwankiewicz and Y. Terumichi, "The dynamic behaviour of a non-stationary elevator compensating rope system under harmonic and stochastic excitations," *Journal of Physics: Conference Series* 181, 2009.
- [9] A. G. Davenport, "Note on the distribution of the largest value of a random function with application to gust loading.," *Proceedings, Institution of Civil Engineering*, 28(2):187-196, 1964.
- [10] H. Kimura, H. Ito and T. Nakagawa, "Vibration Analysis of Elevator Rope – Forced Vibration of Rope with Time-Varying Length," *Journal of Environment and Engineering*. Vol. 2, No 1, pp. 87-96, 2007.
- [11] P. Andrew and S. Kaczmarczyk, *Systems Engineering of Elevators*, Mobile: Elevator World, Inc., 2011.

**BIOGRAPHICAL DETAILS****Jaakko Kalliomaki****Education**

2003 Master of Science (M.Sc.) in Mechanical Engineering, Helsinki University of Technology, Finland

**Work Experience**

2003 – 2005 Mechanical Designer, ABB Oy (Drives and Power Electronics), Finland

2005 – 2007 Designer, Delta Energy System (Finland) Oy

2007 – 2014 (Senior) Chief Design Engineer, KONE Corporation, Finland

2014 onward Global Platform Manager (High Rise Platforms), KONE Corporation, Finland

**Jarkko Saloranta****Education**

2006 Master of Science (M.Sc.) in Aeronautics/Aviation/Aerospace Science and Technology, Helsinki University of Technology, Finland

**Work Experience**

2006 – 2008 PhD Student/Researcher, Helsinki University of Technology, Finland

2008 – 2010 Design Engineer (numerical models) KONE Corporation, Finland

2010 – 2013 Technical Specialist, WinWinD Oy

2013 – 2020 Entrepreneur/ Technical Specialist, UpWind (assigned to KONE Corporation)

2020 onward Calculation and Analysis Expert, KONE Corporation, Finland

**Sakari Mäntylä****Education**

2017 Master of Science (M.Sc.) in Mechanical Engineering, Aalto University, Finland

**Work Experience**

2014 – 2017 Structural Analysis Engineer, Etteplan Oyj (Assigned to KONE Corporation)

2018 onward Platform Engineer, Neteram Oy (Assigned to KONE Corporation)

**Joonas Sorvari****Education**

2009 Doctor of Philosophy (PhD) in Technical Physics, University of Kuopio, Finland

**Work Experience**

2004 – 2007 Research assistant / Researcher, University of Kuopio

2007 – 2013 Researcher, Technical Research Centre of Finland

2013 – 2017 Assistant Professor, Lappeenranta University of Technology

2017 onward Senior Specialist, Etteplan Oyj

**Mikko Puranen****Education**

2009 Doctor of Science (D.Sc.) in Electrical Engineering, Helsinki University of Technology, Finland

**Work Experience**

2004 – 2008 Research scientist, Helsinki University of Technology, Finland

2008 – 2012 Design Engineer, KONE Corporation, Finland

2012 – 2015 Senior Specialist, KONE Corporation, Finland

2016 onward Expert, High Rise Electrification, KONE Corporation, Finland

# Computer-Aided Structural Analysis of the Lift Car – Frame System Under Emergency Arrest Operational Conditions

Mohammad Ghaleeh, Stefan Kaczmarczyk, Shafqat Rasool, Jonathan Adams, Nawar Al-Esawi

Faculty of Arts, Science and Technology (FAST), University of Northampton, University Drive, Northampton NN1 5PH United Kingdom

**Keywords:** Car, Frame, Buffering, Dynamics, Bending, Deflections, Permissible Stress

**Abstract.** The paper presents Computer-Aided Analysis (CAA) model of a lift car - frame system. Structural analysis is carried out by the application of the Finite Element Method (FEM) to predict the responses and stresses arising in the system arising under the emergency conditions. The emergency scenario presented in the paper involves a buffer strike event which occurs during the car overtravel. The model can then be used to optimise the design to ensure safe operation of the system.

## 1 INTRODUCTION

Vertical transportation systems (VTS) such as lifts (elevators) are key elements in the built environment, especially in the high-rise building environment. It is important that the design of VTS provides efficient and safe service to building occupants and users [1].

Various dynamic loads act upon components of the lift system during the normal operation and the emergency conditions. High levels of dynamic stresses in the lift car-frame structure might then occur. In order to satisfy the requirements of safety standards and to meet the criteria for acceptable service, thorough understanding of engineering principles and models applied is of paramount importance in conducting the system calculations [2].

The aim of this work is to demonstrate a computer aided solution and analysis of the dynamic responses that arise during an emergency scenario. The emergency arrest is initiated when the car overtravels the designated terminal floor at the bottom of the hoistway. The dynamic loads that arise during the event are determined and applied in the FEM structural analysis of the car frame structural components.

## 2 CAR OVERTRAVEL AND EMERGENCY ARREST

The overtravel arrest mechanism consists of buffers beneath the car (and often beneath the counterweight) [2]. Three types of buffer are permitted by safety codes [3]: linear, energy accumulation type buffers, non-linear energy accumulation buffers, and energy dissipation buffers. Consider a scenario when the car is striking an energy dissipation buffer (see Fig. 1).

The equation of motion describing the dynamics of the system when the car travelling at speed  $V$  has engaged an energy dissipation buffer (buffering event) is given as

$$M\ddot{x} + c\dot{x} + kx = Mg \quad (1)$$

where  $g$  is the acceleration of gravity,  $x$  is the displacement,  $M$  is the mass of the car-frame assembly,  $c$  represents the coefficient of damping and  $k$  denotes the coefficient of stiffness of the buffer. The buffer acting at the buffer striking plate is determined as

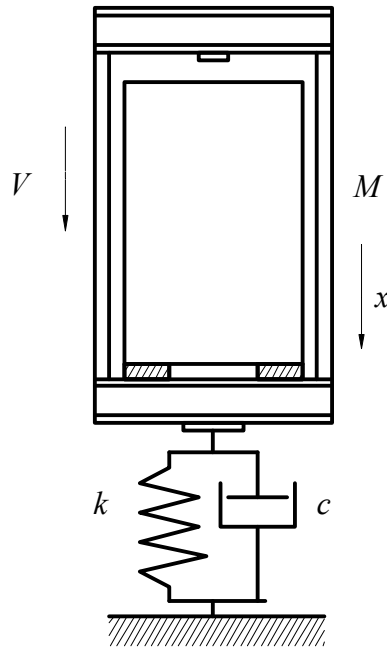


**Figure 1** Descending car striking a buffer of energy dissipation type.

$$F_b = c\dot{x} + kx \quad (2)$$

In this model of the car-frame – buffer dynamics is represented by the fundamental mode with the car-frame treated as a rigid body. By solving the equation of motion (1) the buffer force can then be readily evaluated from equation (2).

### 3 STRUCTURAL ANALYSIS OF THE CAR-FRAME ASSEMBLY

To determine the dynamic deformations and stress levels of the car-frame assembly, the system can be analyzed by the application of Finite Element Method (FEM). The behaviour of the structure is then represented by the following equation [4]

$$[M]\ddot{\bar{x}} + [C]\dot{\bar{x}} + [K]\bar{x} = \bar{F} \quad (3)$$

where  $[M]$  is the mass matrix,  $[C]$  is the damping matrix,  $[K]$  is the stiffness matrix,  $\bar{F}$  is the load vector and  $\bar{x}$  denotes the displacement vector.

#### 3.1 CAD model

The lift car-frame assembly is a combination of three distinct components: car bodywork (enclosure), sling (frame) and car platform. A CAD model used in the study is shown in Fig. 3.

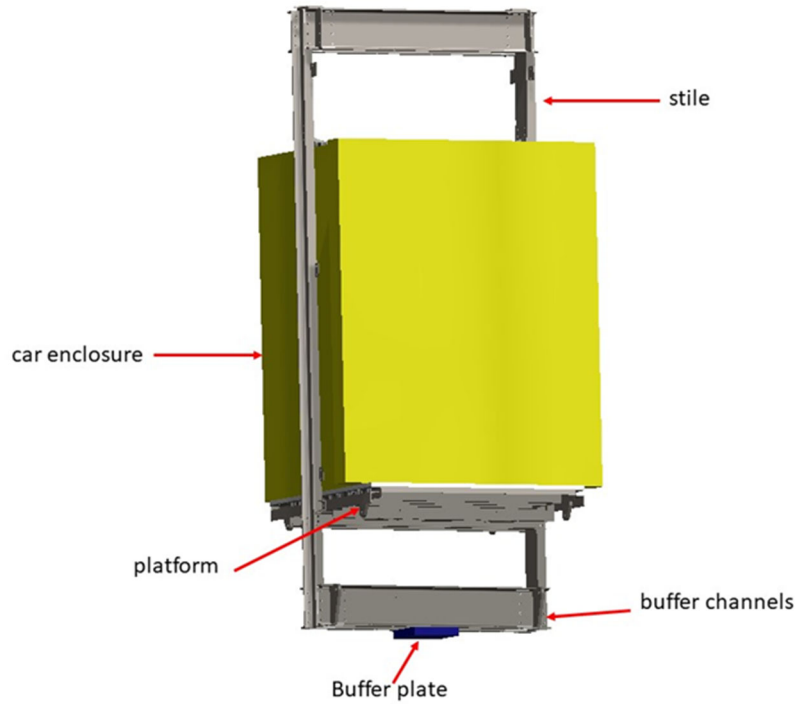


**Figure 2** CAD model of the car-frame assembly

### 3.2 Fundamental mode analysis of the car-frame - buffer system

Equation (1) can be re-formulated in terms of the fundamental mode parameters as

$$\ddot{x} + 2\zeta\omega\dot{x} + \omega^2x = g \quad (4)$$

where  $\zeta$  is the damping ratio and  $\omega$  represents the fundamental frequency of the car-frame - buffer system.

Equation (4) is then solved by considering the car speed of 2 m/s, the damping ratio  $\zeta = 0.25, 0.75$ , and the fundamental frequency assumed as 1.63 Hz, respectively. The results are shown in Fig. 3.

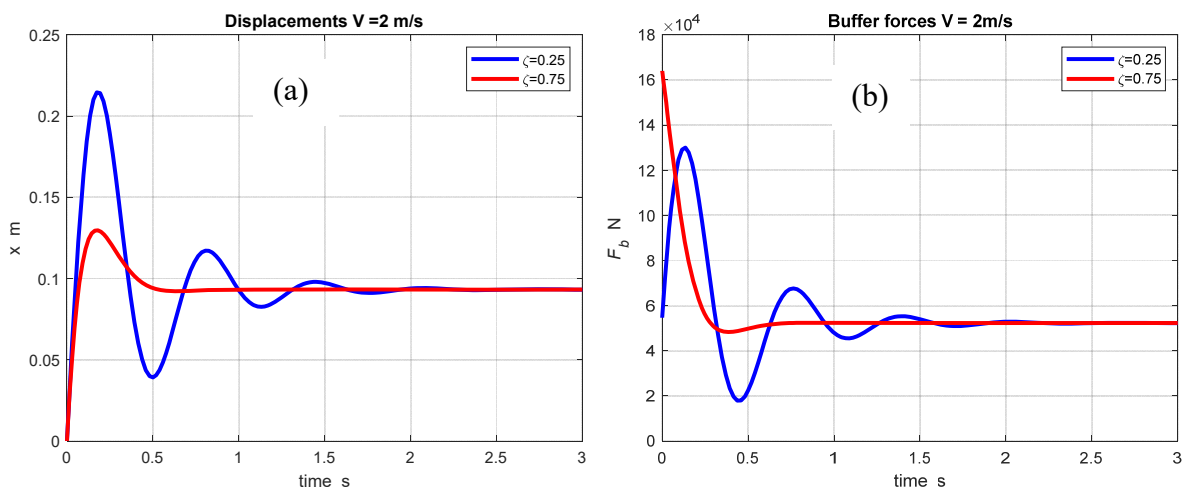


**Figure 3** Fundamental mode displacements and the corresponding buffer forces

The dynamic deflections are shown in Fig. 3(a) and the buffer forces are illustrated in Fig. 3(b), respectively.

The rating of buffers is based on arresting the car from 115% rated speed (the overspeed governor electrical trip speed). Safety codes [4] stipulate that the total possible stroke of energy dissipation buffers shall be at least equal to the gravity stopping. Considering that the car strikes the buffer at rated speed and the gravity stopping distance, for the rated speed of  $V = 2$  m/s, is calculated as  $\frac{(1.15 \times V)^2}{2g} = 0.2696$  m it is evident that the maximum deflections of the buffer are smaller than the minimum buffer stroke.

### 3.3 FEM Simulation and results

In the FEM simulation of the car-frame assembly the buffer channel beam structure is selected. The bending stresses (see Fig. 4) and the deflection levels (see Fig. 5) are determined under the maximum load conditions as illustrated in Fig. 3b.

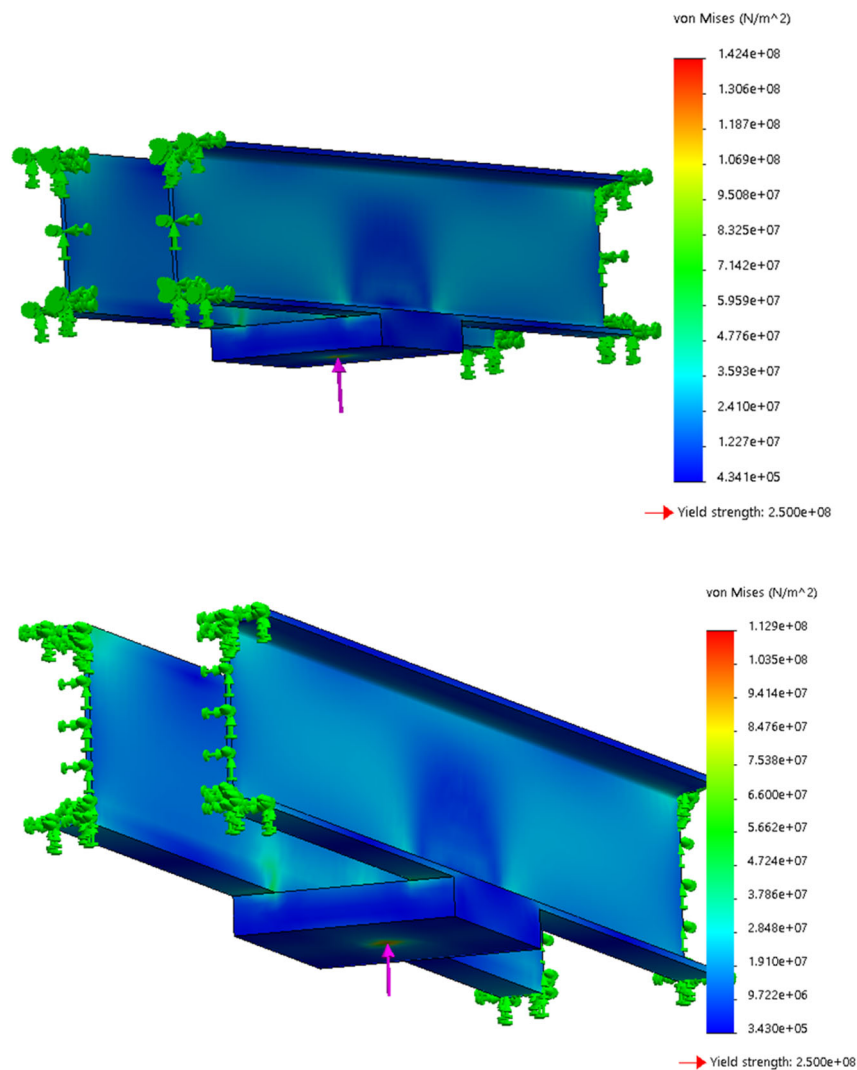
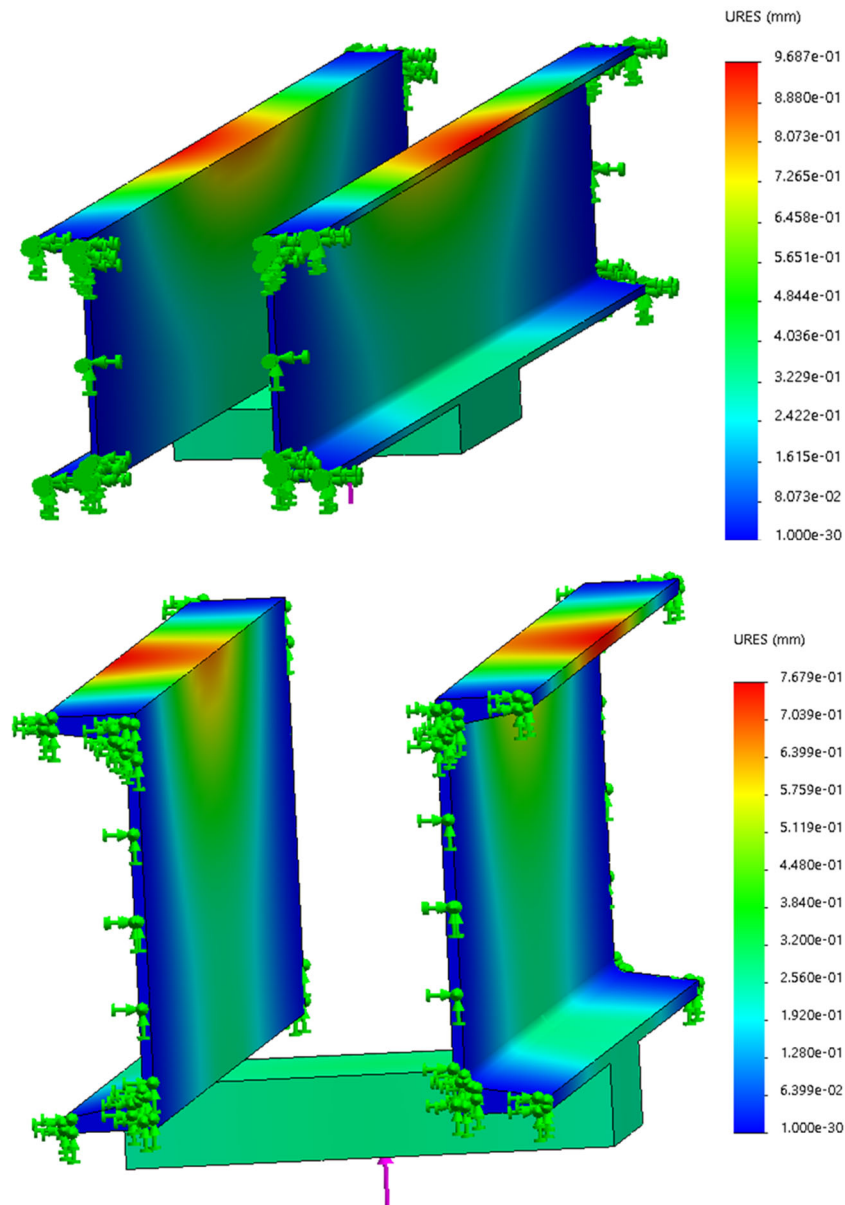


Figure 4 FEM simulation results: bending stresses



**Figure 5** FEM simulation results: bending deflections

Maximum permissible stresses in car frame buffer plank under buffering conditions specified in ASME A17.1 are given as 189.6 MPa (27,500 psi). It is evident that under the loading conditions considered the maximum stress levels (determined as 142.4 MPa and 112.9 MPa, respectively) do not exceed the permissible value. Normal practice for dealing with loads that act at the buffer channel beam (safety plank) structure is to ensure that the deflections shall be no more than  $\frac{1}{1000}$  th of the channels' span. Considering the span length of 2350.7 mm the maximum deflections (determined as 0.9687 mm and 0.7679 mm, respectively) are within the acceptable range.

#### 4 CONCLUSIONS

The analysis and results presented in this paper demonstrate that large deformations and stress levels may occur in a lift system during an emergency arrest event triggered by car overtravel. The stresses and deflections in the buffer channels need to be assessed for the worst case of operation. This should be carried out for the buffering events, as demonstrated in the paper.

## REFERENCES

- [1] S. Mirhadizadeh, S. Kaczmarczyk, N. Tongue, H. Al-Jelawy P. Feldhusen, W Delk, K. Anderson, F. Dudde, “Modelling and Computer Simulation of aerodynamic Interactions in High-Rise Lift Systems”. *Proceedings of the 5th Symposium on Lift and Escalator Technologies*. Volume 5, September 2015, Northampton, UK, pp. 117–123.
- [2] J.P. Andrew and S. Kaczmarczyk, *Systems Engineering of Elevators*. Elevator World, Mobile, AL (2011).
- [3] British Standards Institution, *Safety rules for the construction and installation of lifts — Lifts for the transport of persons and goods Part 20: Passenger and goods passenger lifts*. BS EN 81-20:2014.
- [4] S.S Rao, *Mechanical Vibration*. Prentice Hall, Singapore (2005)

## BIOGRAPHICAL DETAILS

Mohammad Ghaleeh is Senior Lecturer in Engineering at the University of Northampton. He received his PhD in the durability of solder joints under thermo-mechanical loading: application to Sn-37Pb and Sn-3.8Ag-0.7Cu lead-free replacement alloy from Heriot-Watt University. He is an expert in Finite Element Analysis as applied to problems in structural mechanics, multiple Experience in material design engineering, materials and structural analyst in Oil & Gas, Automotive industries, etc. Research interests related to the project include the durability of structural joints under thermo-mechanical loading; with design engineering, engineering materials and structural analysis/ FEM modelling.

Stefan Kaczmarczyk is Professor of Applied Mechanics and Postgraduate Programme Leader for Lift Engineering at the University of Northampton. His expertise is in the area of applied dynamics with particular applications to vertical transportation and material handling systems. Professor Kaczmarczyk is a Chartered Engineer, a Fellow of the Institution of Mechanical Engineers and a Fellow of the Higher Education Academy.

Shafqat Rasool is Lecturer in Engineering (Mechanical Engineering and Design) at the University of Northampton. He received his PhD from Delft University of Technology for his research in durability of thermoplastic composites under fatigue loading. He has also worked as post doc researcher on projects focusing on powder resin processing and structural health monitoring of thick composites. His research interests are durability and structural integrity of composites materials and structures. He has border experience in the context of experimental investigation, design and development of testing fixture, testing and measurements, and failure analysis.

Jonathan Adams graduated from the University of Bradford in 1990 with a B.Eng. degree in Electrical and Electronic Engineering. He holds a Certificate in Education from the University of Leicester, and an M.A. in Continuing Education from the University of Warwick. He also holds a PhD in Engineering Education. His industrial background is in the lift-making industry where he spent nearly 10 years. He has been employed at The University of Northampton for over 20 years specialising in distance education for the lift industry. He is currently Head of Department of Engineering & Technology. His research interests include teaching and learning strategies used in continuing and engineering education, and in the use of electronic methods for delivery, assessment and support. He is a Teaching Fellow of The University of Northampton.

# Feasibility of An Energy Efficient Fuel Cell Hybrid Lift: the Main Concept and Design

S. Kaczmarczyk<sup>1</sup>, J. Blaszczyk<sup>2</sup>, H. Lei<sup>2</sup> and R. Smith<sup>1</sup>

<sup>1</sup>Dept of Engineering, Faculty of Arts, Science and Technology, The University of Northampton, UK

<sup>2</sup>Shanghai Everpower Technologies Ltd, 1000 Jinsui Road, Pudong, Shanghai, China, 201206

**Keywords:** regenerative, reversible, fuel cell, hydrogen, solar panels, hybrid elevator, hybrid lift.

**Abstract.** The latest progress in Fuel Cell (FC) technologies have led to rapid developments in ground vehicle transportation. These technologies could also be considered for deployment in vertical transportation (VT) systems. This paper presents a feasibility study concerning the application of a reversible fuel cell power supply for a solar panel powered lift system operating in a high-rise building. It is assumed that all energy needed to power the elevator system will originate from the solar panels. Energy needed for operation at the low-irradiation periods will be generated from the Hydrogen stored in medium-pressure tanks. The Hydrogen will be produced in a Unitized Reversible Fuel Cell (URFC). When the Grid access is possible the grid will provide emergency power for peak operations or for longer periods of low solar panels output. The URFC unit shall operate in a tandem with a lithium-ion battery, while the size of URFC and battery shall be optimized for overall system minimum cost. The overall conclusion is that the grid-independent lift energy supply system is possible, however the cost and space requirements are major limitations in the seasonal energy storage in Hydrogen form.

## 1 INTRODUCTION

In the modern high-rise built environment electric motor driven traction elevators are applied for efficient Vertical Transportation (VT) of people and goods. In the traditional system the power to the electric motor is provided by the public mains supply (grid). When the system is raising the out of balance load in the car or in the counterweight the power is taken from the grid. Part of the supplied energy is then stored in the mechanical system as potential energy. On the other hand, when the system is lowering the out of balance in the car or the out of balance of the counterweight the potential energy is being returned to the drive system. This returned energy is referred to as 'regenerated'. Thus, the elevator drive is capable of transferring energy in both directions and is termed as 'reversible' [1].

The recent progress in Fuel Cell (FC) technologies have led to rapid developments in ground vehicle transportation. This paper presents the results of a study concerning the feasibility of a reversible fuel cell power supply system for solar panel powered lift operating in a high-rise building. It is assumed that all energy needed to power the elevator system will originate from the solar panels. Two geographic locations are considered: the best possible solar irradiation in Kampala (Equator) and mid-Europe 52° N parallel (London). The solar irradiation [ $\text{W}/\text{m}^2$ ] curves have been derived from available data [2] and are shown in Fig. 1.

In both cases the lift daily energy needs are balanced with the energy stored in a buffer battery set, which has to satisfy two main requirements: store enough energy for daily operations (with reasonable margin for the cloudy weather) and the capability of charge/discharge current at peak power periods (e.g. motor start power, break energy accumulation).

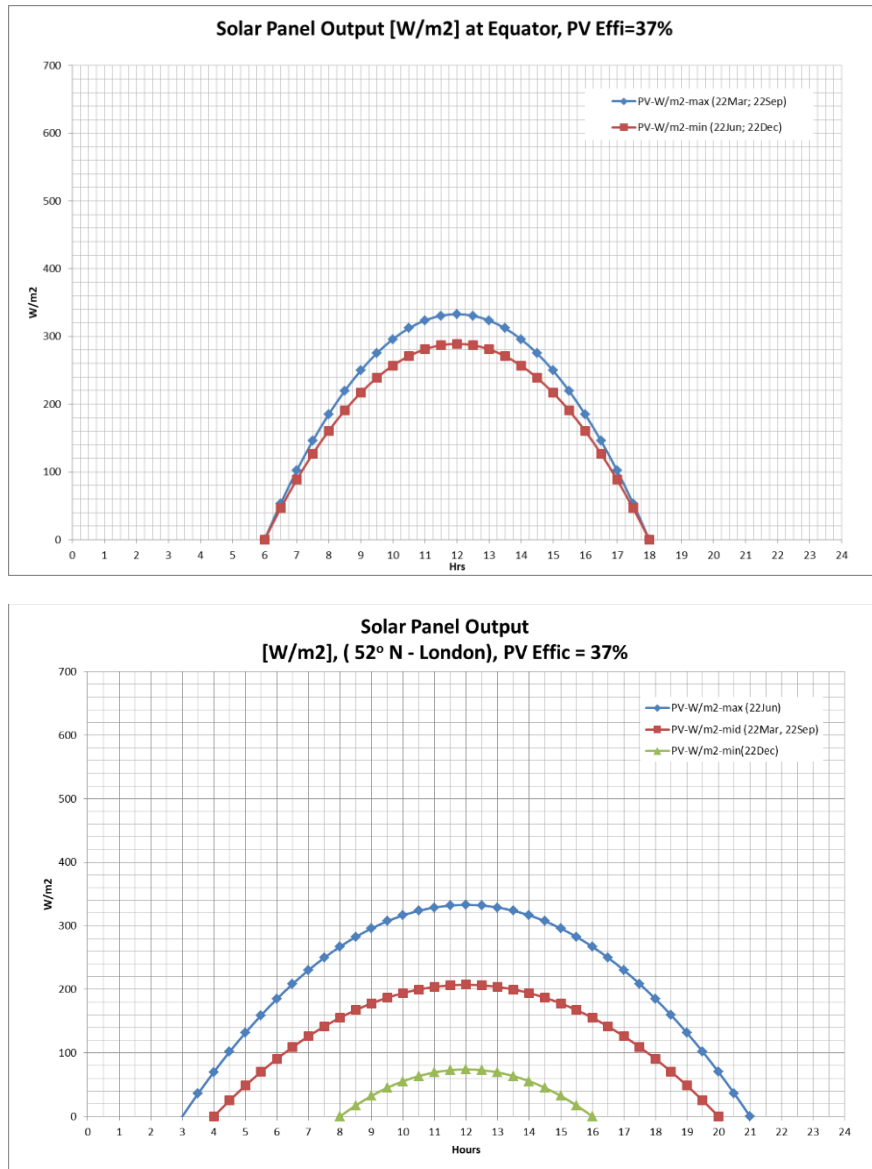


**Figure 1 Solar power seasonal fluctuations**

## 2 ENERGY REQUIREMENTS

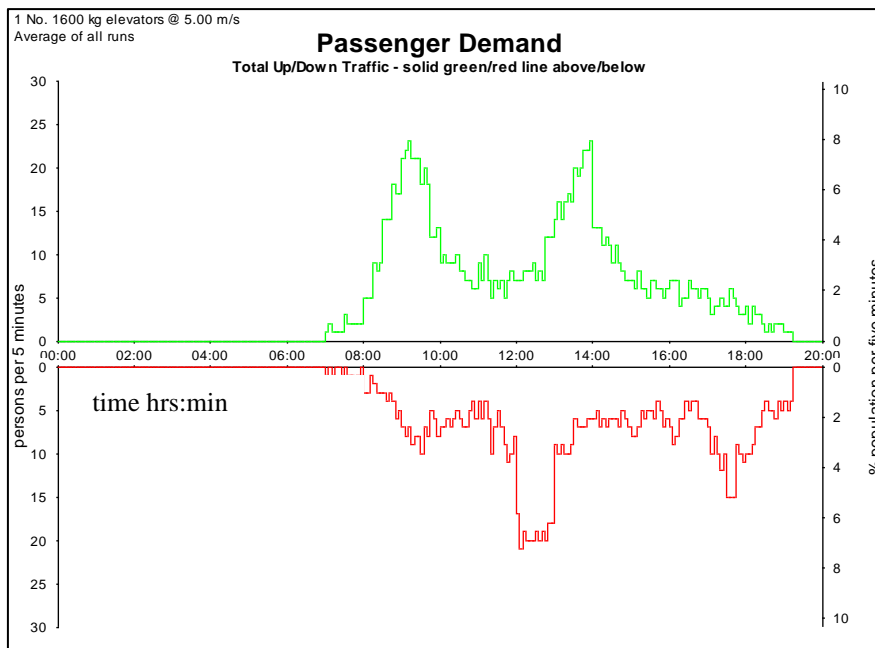
A simplified model of high-rise lift installation has been considered to generate the lift power requirements and energy consumption. The corresponding building data and the lift installation parameters are shown in Table 1. The lift energy simulation model implemented in a commercial simulation software package Elevate™ [3] has been used to determine the lift power requirements and energy consumption. Siikonen full day office template was used to generate the passenger demand data [4] (see Fig. 2).

Fig. 3 illustrates the simulated cumulative energy consumption data and Fig. 4 shows the averaged power requirements. The lift energy requirements over time is then derived from the cumulative energy data and the corresponding curve is shown in Fig. 5.

The available Sun energy depends on the daily and seasonal irradiation fluctuations. Different energy storage strategies have been adopted to adapt the lift operation scenarios to these cases.

**Table 1 Main model data**

PARAMETERS	UNIT	VALUE
<b>Building:</b>		
Total building height	[m]	112.4
Average floor height	[m]	3.75
Number of floors		30
Total resident population		300
Average population/floor		10
<b>Lift installation:</b>		
Number of lifts		1
Rated load	[kg]	1600
Car area	[m <sup>2</sup> ]	2.84
Door open time	[s]	1.8
Door close time	[s]	2.9
Rated speed	[m/s]	5.0
Acceleration	[m/s <sup>2</sup> ]	1.0
Jerk	[m/s <sup>3</sup> ]	1.4



**Figure 2 Siikonen full day office passenger demand curves**

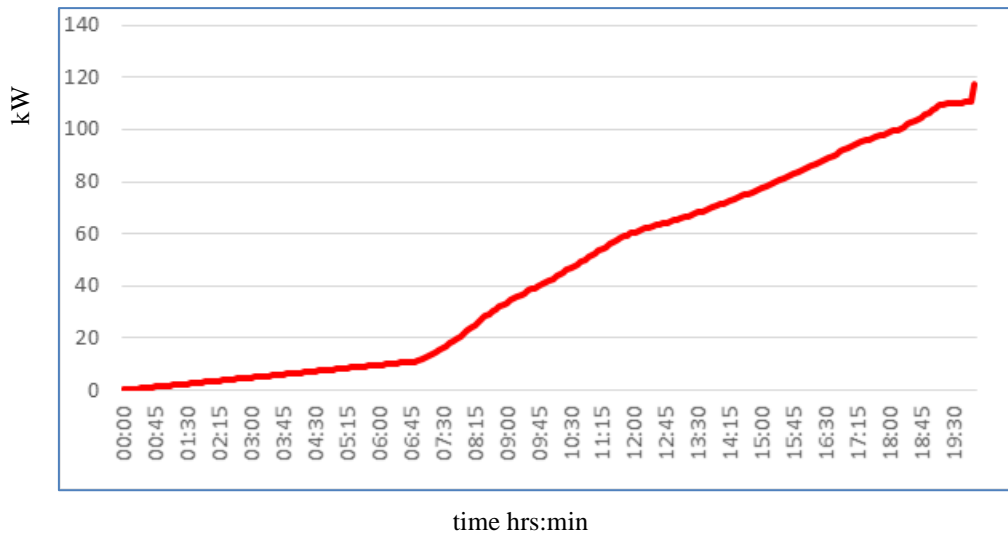


**Figure 3 Cumulative energy consumption**

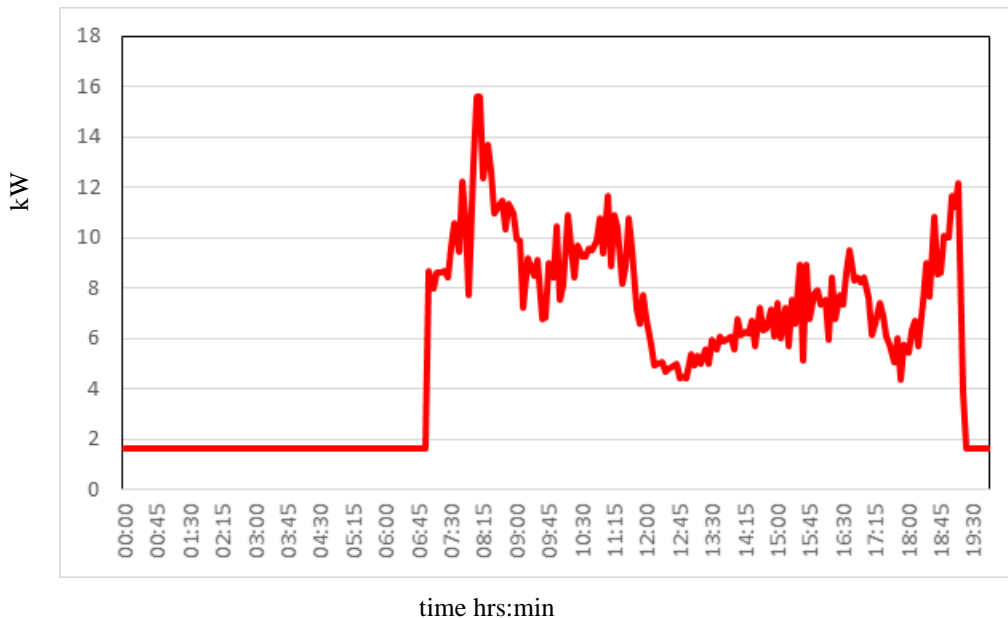


**Figure 4 Averaged power requirements**

These scenarios are outlined as follows.

- A) The energy required is balanced with the energy stored in a daily buffer battery sized for the available Sun energy on:
- a. 22 June at the Equator location
  - b. 22 Sep at the 52°N location.

It is considered that the seasonal energy imbalances/ fluctuations can be covered in the following ways.

- B) The Grid access is possible
- a. The Sun excess energy is stored in the grid at times when the excess energy occurs
  - b. The Lift energy deficits are covered from the grid at times when the Sun energy is inadequate
- C) The Grid access is not possible
- a. The Sun excess energy is stored in the seasonal battery bank when the excess energy occurs, while the energy deficits are covered from the battery bank when the Sun energy is not adequate

- b. The Sun Excess energy is stored in the Hydrogen gas generated (Water Electrolysis) when the excess energy occurs, while the energy deficits are covered from the Fuel Cell operations through Hydrogen conversion into electricity.

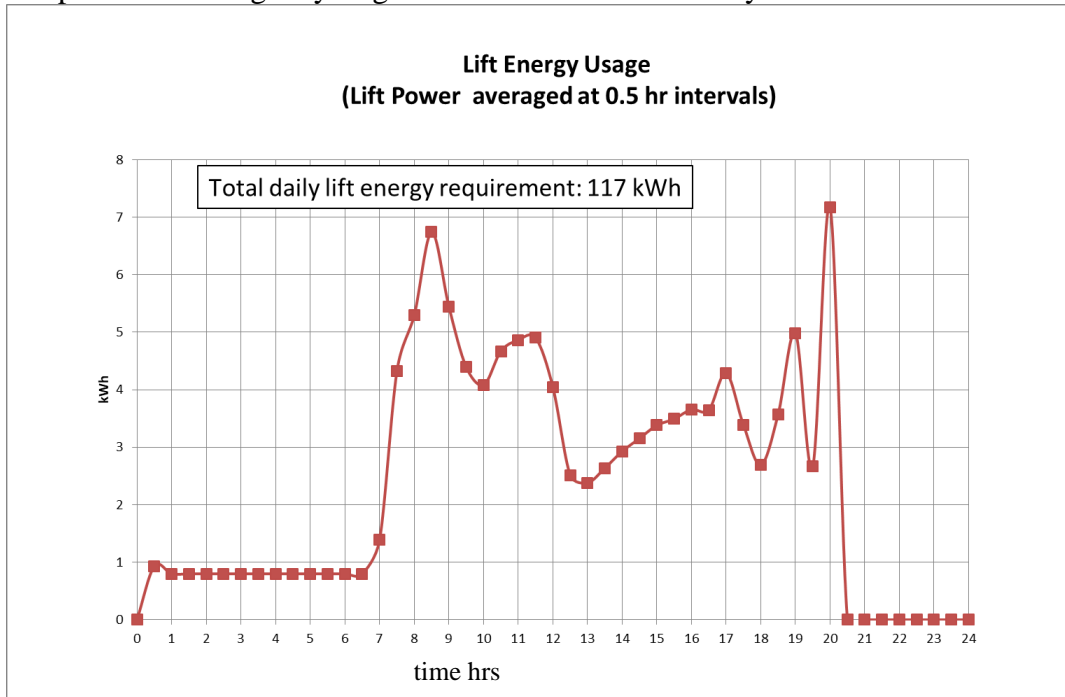


Figure 5 Lift energy consumption

**3 POWER SUPPLY SYSTEMS FOR ENERGY STORAGE STRATEGIES**

Considering the seasonal energy imbalance/ fluctuations the following lift power supply systems are considered. The diagrams in Fig. 6 and Fig. 7 illustrate the power supply system for scenario B and scenario C, respectively. It should be noted that the diagram in Fig. 7 covers two cases: C)a and C)b, respectively.

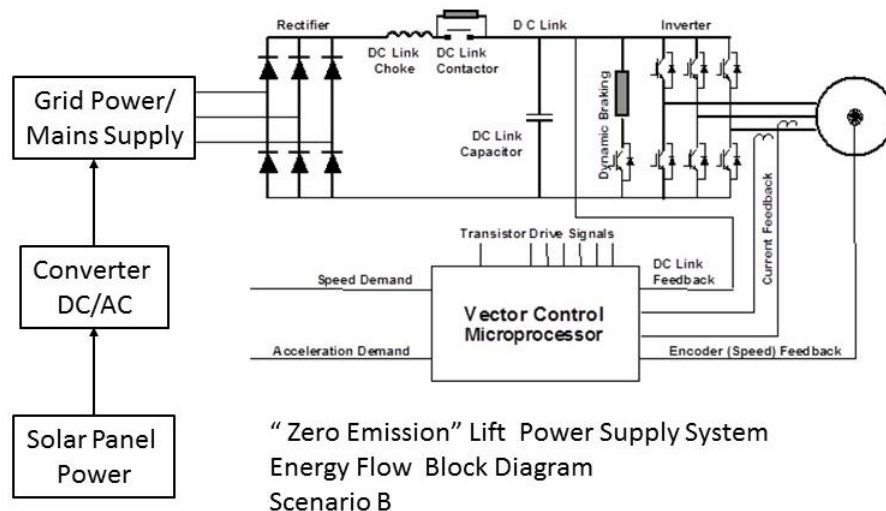
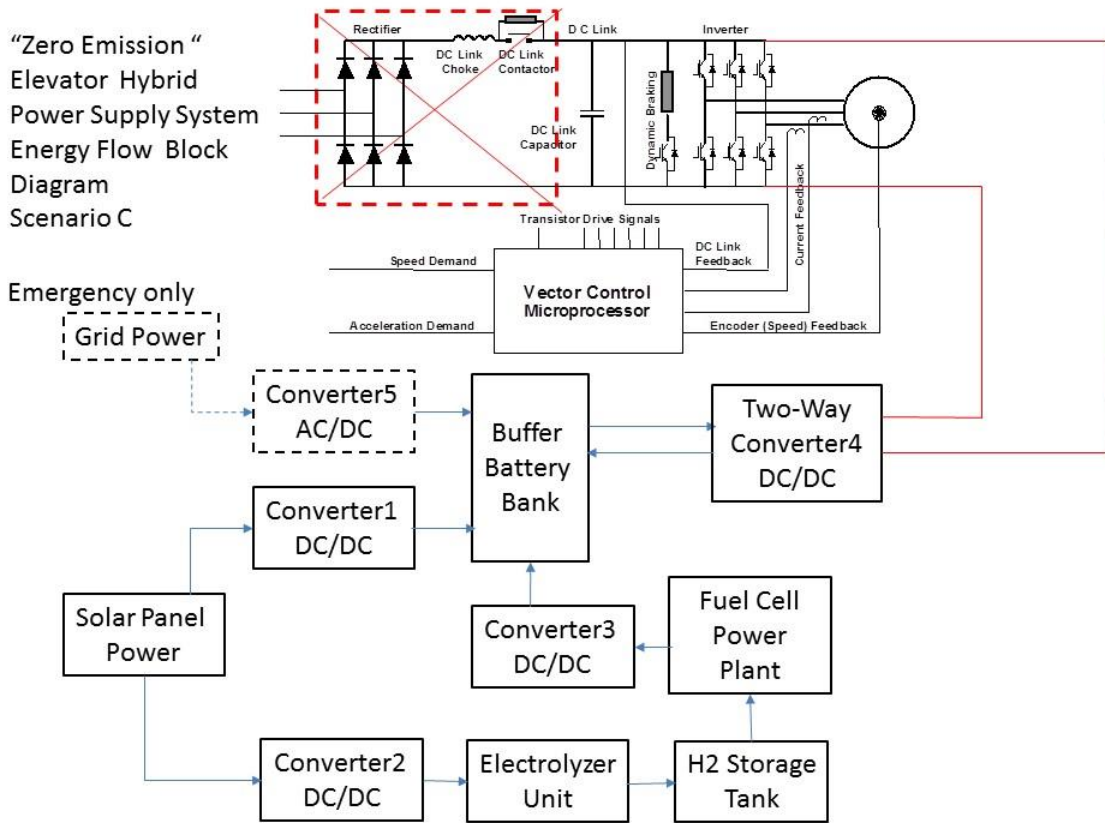


Figure 6 Energy Flow Block Diagram – Scenario B



**Figure 7 Energy Flow Block Diagram – Scenario C**

The Case C)a can be realized when the Fuel Cell/Electrolyser loop is omitted and when the Buffer Battery Bank size is increased to cover the seasonal Sun power fluctuations.

#### 4 BUFFER BATTERY SIZE – DAILY ENERGY FLUCTUATIONS

##### 4.1 Battery Size for Daily Lift Operations

Considering that the lift power requirements don't correspond to the available Sun energy periods (e.g. day-night) the buffering battery bank is proposed. In this scenario the battery is sized for charging from photovoltaics (PV) solar panels to cover the daily lift energy requirement. The minimum required battery size for daily operations is estimated at 79 [kWh] based on the data shown in Fig. 8 (assuming 100% capacity margin for a "cloudy" day). It should be noted that the lift power requirement is related to the unit area (1m<sup>2</sup>) of PV panels.

The diagram in Fig. 8 presents the comparison of the Sun's available energy on the minimum energy day (area below the red line) with the lift's daily energy requirement (area below the purple line) for locations near the Equator. Sizing PV panels for the minimum energy day is likely to result in a cheaper solution than sizing the PV panels between the blue and red lines and installing any seasonal energy fluctuation compensation device.

For locations near the 52°N parallel the situation is dramatically different. By comparing the graphs in Fig. 1 it becomes clear that the PV panel surface would need to be very large in order to cover the daily lift power requirement on the minimum Sun energy day (22 Dec) –green line, bottom graph. In this case a seasonal energy fluctuations compensation device will likely be required, while the PV panels would be sized to match the annual energy requirement need.

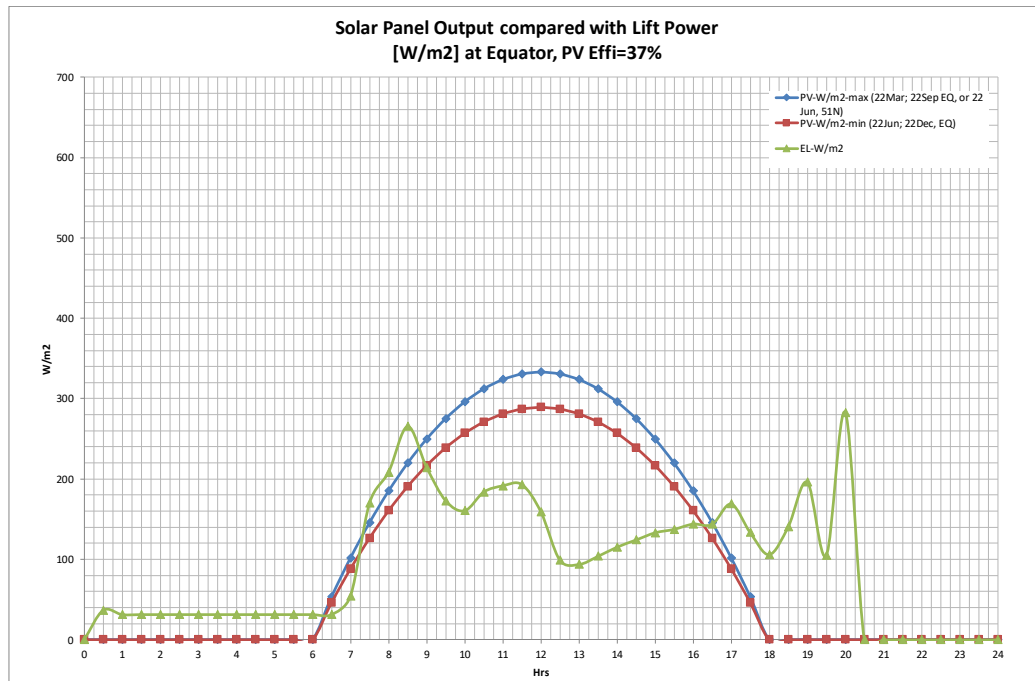


**Figure 8 Lift daily energy requirement balanced with PV daily energy on 22 Jun at equator**

## 4.2 Battery Size for Lift Maximum Power Operations

The battery size is also linked to the load power and charge current limitation. A typical 3C Li-Ion battery's current limitation is 300 [A]. For the selected 100 [Ah], 12 V battery and 165 [kW] peak lift power the minimum buffer battery size is 55 [kWh].

Comparing the battery sizes from cases 4.1 and 4.2, the 79 [kWh] battery bank size is suitable to cover both the daily Sun power fluctuations and the battery charge current requirements.

## 5 PV PANELS SIZE AND BUFFER BATTERY SIZE

### 5.1 PV panels size for operations near the equator

The required PV panels surface area for operations near the Equator is determined to be 51 m<sup>2</sup> assuming the PV conversion efficiency at 37%. The comparison of major component costs is provided in Table 2. There will be no need for the seasonal energy storage – see the maximum (blue) and minimum (red) irradiation curves in Fig. 8.

### 5.2 Buffer battery size – seasonal energy fluctuations (52°N)

One of the seasonal energy storage options is to use the battery bank. The required battery capacity calculations that have been carried out indicate that this option is not a plausible solution – the energy storage would require 9,906 batteries of 100 Ah each, while the PV Panel surface area would be 50 m<sup>2</sup>. The cost of batteries would then be of about USD 2,000,000.

## 6 H<sub>2</sub> STORAGE AND FUEL CELL SIZE – SEASONAL ENERGY FLUCTUATIONS (52°N)

Some other seasonal energy storage option is the Electrolyser-H<sub>2</sub> Storage-Fuel Cell Power System. The main system components are presented in Fig. 7. The operating strategy involves harvesting the Sun energy during high-irradiation periods, converting it into Hydrogen through water Electrolysis, storing Hydrogen in pressurized tanks and converting the Hydrogen back to electricity in the Fuel Cell at the low-irradiation periods. The Electrolysis/Fuel Cell round trip efficiency is around 45 %

which impacts on the required PV panel size/ surface area during the high-irradiation energy harvesting. In this case the needed PV panel surface area is determined as 80 m<sup>2</sup>.

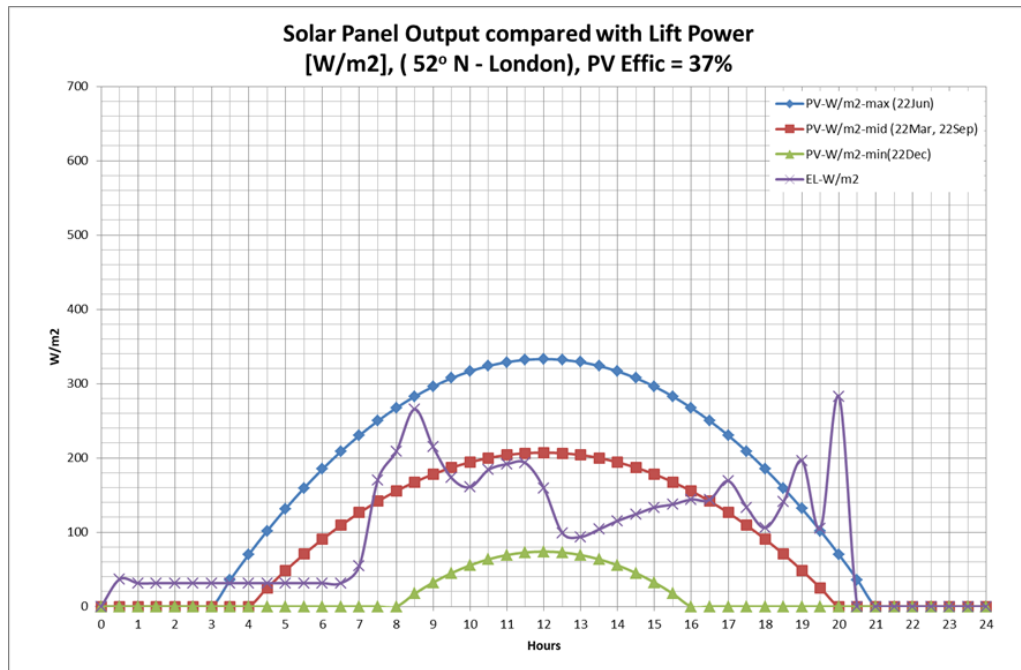


**Figure 9 PV Panel Output compared with daily lift power need (PV Panels sized for energy harvesting between 22 March and 22 September)**

It should be noted that the lift power requirement is per the unit area (1m<sup>2</sup>) of PV panels. The required Hydrogen amount for energy storage is 7,925 [Nm<sup>3</sup>]. The maximum H<sub>2</sub> storage pressure is 130 [barg] due to the Electrolysis process limitations [5]. However, at this point only prototypes of such Electrolysers are available. But bearing in mind the rapid progress in FC technology it can be assumed that the commercial 130 [barg] electrolysers will be available soon and that the high-pressure H<sub>2</sub> compressors will not have to be used due to their high cost.

The required H<sub>2</sub> tanks volume (to store water) is 66 m<sup>3</sup>, which might be not practical for installation in the high-rise building. The cost of tanks would exceed USD100,000. The cost of 4 [Nm<sup>3</sup>/hr], 30 [barg] PEM Electrolyser is around USD200,000. The cost of Fuel Cell for H<sub>2</sub> conversion is comparable to the PEM Electrolyser cost.

The Unitized Reversible Fuel Cell technology, which combines Electrolyser and Fuel Cell in one device, is in the prototyping stage and once developed it might cut the H<sub>2</sub> conversion hardware cost by 50%.

Assuming that the required advanced technology is commercially available today, the cost of H<sub>2</sub> production infrastructure would exceed USD 300,000.

## 7 CONCLUSION

A comparison of the scenarios considered in this study is presented in Table 2. Two geographic locations have been considered in the analysis: near the Equator and at 51°N, which corresponds to London location.

The analysis carried out shows that there is no need for the seasonal energy storage in the areas close to the Equator due to the high solar power availability through the entire year. The daily energy balancing can be covered with a battery pack which is much cheaper than the Electrolyser-

Fuel Cell system of the comparable energy storage capacity (USD 25,000 vs USD 200,000), refer to the cases A)a; B)-C), respectively. The need for seasonal energy storage arises at the locations away from the Equator. The simplest and most cost-effective way to deal with the seasonal energy storage in these locations is the Grid energy storage (see the case A)b; B, respectively).

When the Grid energy storage is not available (case A)b; C)a and C)b.), the cheaper solution is Energy Storage in Hydrogen rather than in Li-hydrate Battery, however, the size of H2 storage tanks (66 m3) might result in safety concerns if located near a high rise building. Considering 2 m diameter tanks the total length of tanks would be about 21 m.

A careful layout planning will be required if such solution is adopted, assuming that the high cost is not an issue. Seasonal energy storage in a Battery Pack is the most expensive of all considered scenarios. It is relatively safe, but still requires considerable amount of real estate space to house the batteries. The expected battery mass is 214 tons while the battery storage volume would be around 200 m3, including the space for connections and cooling.

The overall conclusion is that the grid-independent lift energy supply system is possible, however the cost and space requirements are major limitations in the seasonal energy storage in Hydrogen form.

It should also be noted that there are hazards associated with the application of fuel cell technology in the built environment. The main hazards involved are related to the hazardous properties of hydrogen and its storage [6]. The hazards include fire and explosion as well as electrical hazards. Therefore, controlling the risks involved need to be considered.

**Table 2 Comparison of Scenarios**

Category	Unit	Scenarios			
		A)-a. Equator Locations	A)-b. 52° N Locations		
		B)-C) No Grid Storage Required	B) Grid Storage Possible	C) Grid Storage Not Possible	
				a. Energy in Battery	b. Energy in H2
<b>Technical Data</b>					
Lift Peak Power	[kW]	165	165	165	165
Buffer Battery Size	[kWh]	79	79	10698	79
PV Panels Total Surface	[m2]	51	63	63	80
H2 Storage Size (130 bar)	[m3]	NA	NA	NA	66
H2 Production/Conversion Hardware (Reversible Fuel Cell - projection )	[kW]	NA	NA	NA	24
<b>Cost Estimate</b>					
Buffer Battery Cost	[USD]	14,103	14,103	> 2 mln	14,103
PV Panels Cost (@ \$0.65/W)	[USD]	10,988	13,556	13,556	17,220
H2 Storage Cost	[USD]	NA	NA	NA	> 100,000
H2 Production/Conversion Hardware Cos	[USD]	NA	NA	NA	>200,000
Total Cost Estimate	[USD]	25,091	27,659	> 2 mln	> 300,000

**REFERENCES**

[1] J.P. Andrew and S. Kaczmarczyk, *Systems Engineering of Elevators*. Elevator World, Mobile, AL (2011).

[2] Worldatlas.com <https://www.worldatlas.com/articles/how-long-is-a-day-at-the-equator.html> ((Accessed 15 February 2020))

- [3] L. Al-Sharif, R. Peters, R. Smith, "Elevator energy simulation model". *Elevator Technology 14. Proceedings of ELEVCON 2004*, Istanbul, Turkey, April 2004, 11-20.
- [4] M.L. Siikonen, "On Traffic Planning Methodology". *Elevator Technology 10. Proceedings of ELEVCON 2000*, Berlin, Germany, May 2000, 267–274.
- [5] V.N. Fateev et al., *High pressure PEM water electrolysis and corresponding safety issues*. International Journal of Hydrogen Energy 36(3) • February 2011.
- [6] Health and Safety Guidance HSG243, *Fuel cells. Understand the hazards, control the risks*. Health and Safety Executive, 2004.

## BIOGRAPHICAL DETAILS

Dr Stefan Kaczmarczyk is Professor of Applied Mechanics and Postgraduate Programme Leader for Lift Engineering at the University of Northampton, UK. His expertise is in the area of applied dynamics and vibration with particular applications to vertical transportation and material handling systems. He has published over 100 journal and international conference papers in this field. He is a Chartered Engineer, elected Fellow of the Institution of Mechanical Engineers and a Fellow of the Higher Education Academy.

Dr Janusz Blaszczyk is a Mechanical and Power Engineering graduate. For the past 40 years he was developing and improving technologies and products related to power generation and alternative energy: thermal processes (heat exchange & combustion), internal combustion engines, steam power boilers and fuel cell power units for various applications - automotive engines, backup power units, portable power units and auxiliary power units. His functions and positions included: Research Development Engineer, Product Development Engineer, Performance Engineer, Process Engineer, Lecturer (Thermal Subjects), Project/Program Manager, Product Development Technical Leader, Functional Manager – Mechanical Engineering, Principal Applied Scientist and Chief of Engineering. Dr Blaszczyk spent 17 years in academia environment lecturing at Silesian Technical University (Poland), University of Zimbabwe (Zimbabwe) and University of British Columbia (Canada). His recent career years were devoted to the new technologies development while working for Utility & Recovery Engineering Ltd. (Canada), Ballard Power Systems Inc. (Canada), PowerCell Ltd. (Volvo subsidiary, Sweden) and Shanghai Everpower Technologies Ltd. (China). Dr. Blaszczyk have overseen entire lifecycle of new product development – from conceptualization and R&D, through prototyping and testing to transfer for production.

Dr H. Lei Mr. his Ph.D. degree in Power Electronics from the Zhejiang University in China. He has twenty years of research and development experience, including outstanding achievements related to the development of "multi-frequency power converter topology and control" and "1-2kW UPS digital control" electronic boards. Dr. Hu Lei has worked several years as a team leader at the Fuel Cell Division at Samsung, accomplishing "2W passive Fuel Cell charger system for a cellphone" and "25W portable Fuel Cell Power Supply" for military application. Recently Dr. Hu Lei has been promoted to the position of Director of Transportation Division at Shanghai Everpower Technologies, Ltd.

Dr Rory Smith has over 49 years of experience in all aspects of the lift industry including sales, installation, maintenance, manufacturing, engineering, research & development. He has worked for ThyssenKrupp Elevator for the last 23 years. Prior to becoming involved in ThyssenKrupp's Internet of Things, he was Operations Director, ThyssenKrupp Elevator Middle East. His scientific interests include, operations management, high rise - high speed technology, ride quality, traffic analysis, dispatching. To date he has been awarded numerous patents in these areas and has many pending patents.

# Feasibility Study of Using a Coupler Skate Encoder System for Monitoring the Real Time Status of Lift Door Operation

Rohit Nehe, Chetan Mahale and Babasaheb Patil

Creestaa Elevators India pvt ltd, A3 The Fifth Avenue, 5th Floor, Dhole Patil Road,  
Pune – 411001, India.

**Keywords:** Coupler Skate, Encoder, Preventive Maintenance, Automatic Lift Door, Hall-Effect Sensor.

**Abstract.** This work presents a proof-of-concept study of the encoder system developed for monitoring the health of coupler skate assembly used in automatic door header system of lifts. The motivation of developing a coupler skate encoder system is to provide real-time information on coupler skate status and its performance which could be further used for developing a preventive maintenance program of door header system.

The coupler skate encoder system consists of a Hall effect-based sensor, microcontroller board, and power supply unit. The Hall effect sensor measures the real-time angular rotation of coupler skate assembly. The microcontroller is flashed with the firmware which evaluates the time series data, and as a result, it sends a digital signal in case of any deviation in expected performance of coupler skate assembly. A benchtop sensor calibration set up is constructed to prepare a look-up table for calibrating analog voltage signal against angle in degrees.

The coupler skate encoder system is tested on automatic lift door test jig for evaluating its various parameters like accuracy and repeatability of sensor and real-time data analysis by the microcontroller. The results obtained from the experiments are found to be encouraging such that the coupler skate encoder system resolves the smallest angular rotation which is required to detect an erroneous condition of coupler skate assembly operation.

The proof of concept study highlighted in this document introduces a new concept of real-time monitoring of sub-assembly of door header system, which could be a guiding document in developing preventive maintenance technologies specially designed for lift automatic doors. The preventive maintenance technologies of such kind as discussed in this paper would be a significant development for smooth and error-free operations of lift doors.

## 1 INTRODUCTION

### 1.1 Background

A lift is sometimes described as the driverless vehicle, transporting passengers on a fixed route i.e. along the fixed trajectory. To perform such an autonomous driving function, typically, a microprocessor based lift controller uses multiple electro-mechanical subsystems (assemblies) with real-time monitoring of safety sensors. In the case of a lift, one of the important “electro-mechanical” subsystems is an automatic door assembly. The automatic door assembly involves large numbers of linkages and parts (i.e. mechanical and electrical parts) which work in a synergic manner. For a lift to make a successful ride from one floor to the other floor, it is of paramount importance to have robust and well maintained automatic door assembly.

The automatic door assembly of a lift can be considered to be made up of two parts i.e. car door assembly and landing door assembly. The car door assembly is a power-operated mechanism while

the landing door assembly is driven by car door assembly. Simultaneous movement of car door and landing door is made possible by the mechanical interlocking mechanism. The mechanical interlocking consists of pair of fins (also known as coupler skates) fixed on a car door assembly (See figure 1-1) and a pair of rollers fixed on a landing door lock assembly (See figure 1-2). The main role of the interlocking mechanism is to act as a link between car and landing doors. When the car door arrives in the unlocking zone, during the lift door operation (i.e. opening and closing of doors) coupler skates located on a car door spread out such that landing lock rollers are pressed causing the landing lock to open. As soon as the car door is power operated through door drive for a door opening or closing command, landing door mechanism follows the car door movement i.e. the car door horizontal movement is transmitted to the landing door through interlocked coupler skates and landing lock rollers. The opening and closing of car and landing door mechanisms are monitored through electrical safety switches.

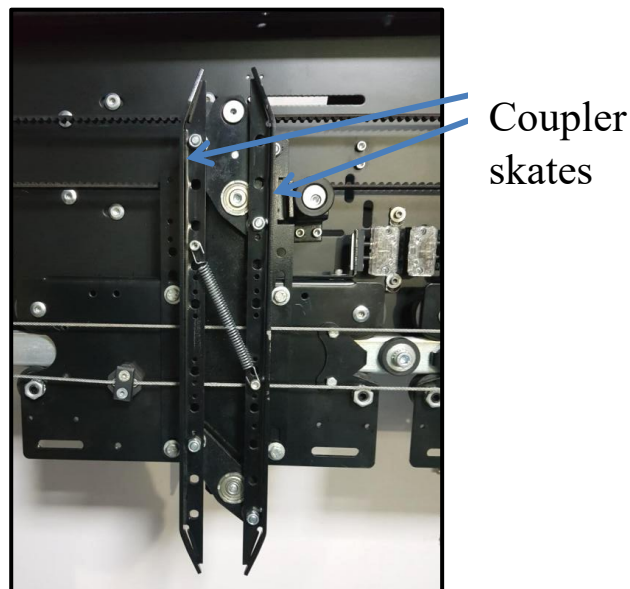


**Figure 1-1** Picture of car door coupler skate assembly

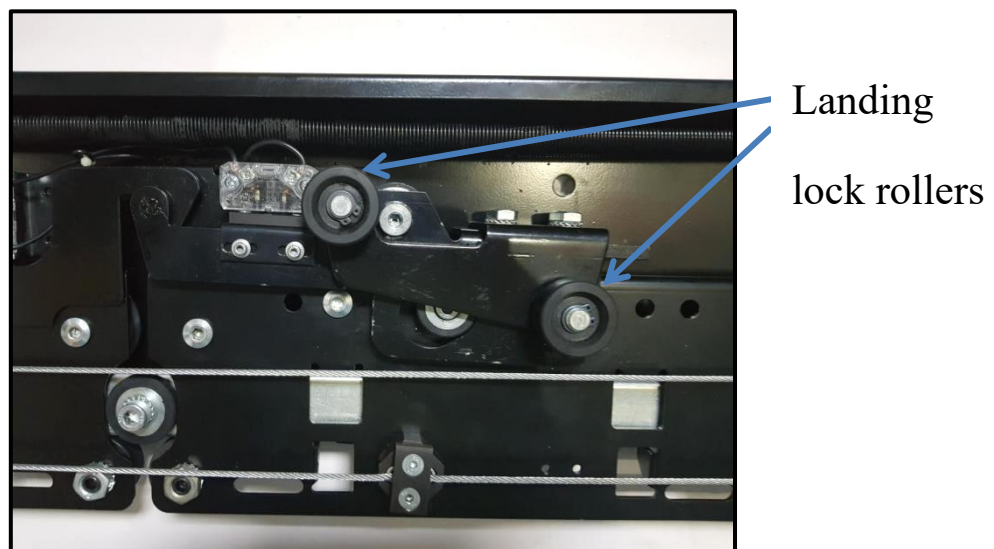


**Figure 1-2** Picture of landing door lock assembly

The working principle of automatic door assembly discussed in this article is the most commonly used design by elevator companies. In general, most of the door assemblies will have a similar working principle but they might be different in terms of material specification, size, duty cycle and many other functional parameters which depend upon the application for which it is to be used. Readers are also referred to three articles published in the book “Educational Focus” by Elevator World magazine [1,2,3]. These articles provide a comprehensive introduction about the basics of elevator automatic doors.

One interesting point to be highlighted about the working principle of automatic door assemblies discussed in this article is the “driver” role played by car door mechanism and the “driven” role of multiple landing door mechanisms installed at various stops. For a lift to successfully open the doors, the car door mechanism should always be healthy and in a perfect operating condition such that it can align itself correctly at every floor for the mechanical interlocking to take place; followed by simultaneous movement of car and landing door. It is imperative to always maintain door assemblies and operator wear and tear-free and also in a healthy condition for the error-free operation of automatic doors which will lead to minimum lift breakdowns. Indeed, it has been a challenge for many elevator companies as the maximum number of breakdowns in a lift are typically encountered in the door assemblies. Some of the principal reasons for door related break downs are highlighted in the reference [1] such as dirt, grease and oil accumulation on rollers, pulleys, cables, switches and other sub-assemblies. Also, change in the adjustment of mechanical components and assemblies due to wear and tear over the time of normal usage can cause a breakdown.

Considering the intricacy of the door assembly, the elevator companies need to have a preventive maintenance program. A proof of concept is presented in this article, wherein a sensor is used to monitor the functional accuracy of one of the door sub-assembly which would aid in taking preventive actions rather than reactive maintenance efforts. The function of the sensor described in this document is to monitor the correct working of coupler skate assembly, its wear and tear and the change in dimensional settings during opening and closing operation of the car door assembly. The idea here is to keep monitoring the health of a car door sub-assembly and whenever the data shows a deviation from a threshold value, a flag is raised by the onboard firmware to indicate the need for initiation of preventive action. Note that, the preventive maintenance idea described in this article is a “proof of concept” study, so the experiments and its scope is limited to only coupler skate pre-failure detection scheme. But, for the preventive maintenance program of a complete door assembly to be effective, a comprehensive system should be developed with multiple sensors for monitoring various sub-assemblies of a door.

## 1.2 Objectives:

The main focus of the work mentioned in this article is to provide a proof of concept of a car door mounted coupler skate pre-failure diagnostic system. In this regard, following are some of the questions that are addressed through this paper:

1. What type of sensor would monitor the health of coupler skate assembly?
2. What is the working principle of proposed “Coupler skate encoder system”?
3. Is the coupler skate encoder system sensitive enough to diagnose the deviation in the working of coupler skate assembly?

4. What are the results from the proof of concept experiments of “coupler skate encoder system” in regards to its application to detect coupler skate assembly pre-failure condition?

The paper is organized such that the details about the coupler skate sensor design, experimental set-up, results and conclusions are described in sections 2, 3, 4 and 5 respectively.

## 2 DESIGN OF COUPLER SKATE ENCODER

The coupler skate studied in this document is shown in figure 2-1 (a, b). As discussed in the introduction section, during the opening of the door, coupler skates (vanes) spreads out to open the landing lock and close-in at the end of the door closing motion. The assembly of coupler skate is designed in such a way that if we connect a linkage connecting both the skates of a coupler, the linkage will be seen making rotational movement about a fixed point. By tracking the rotational motion of the linkage connecting the skates using a sensor, we can monitor the degree of movement of the coupler skates. This concept is the basic working principle of the “Coupler skate encoder” system demonstrated in this document.

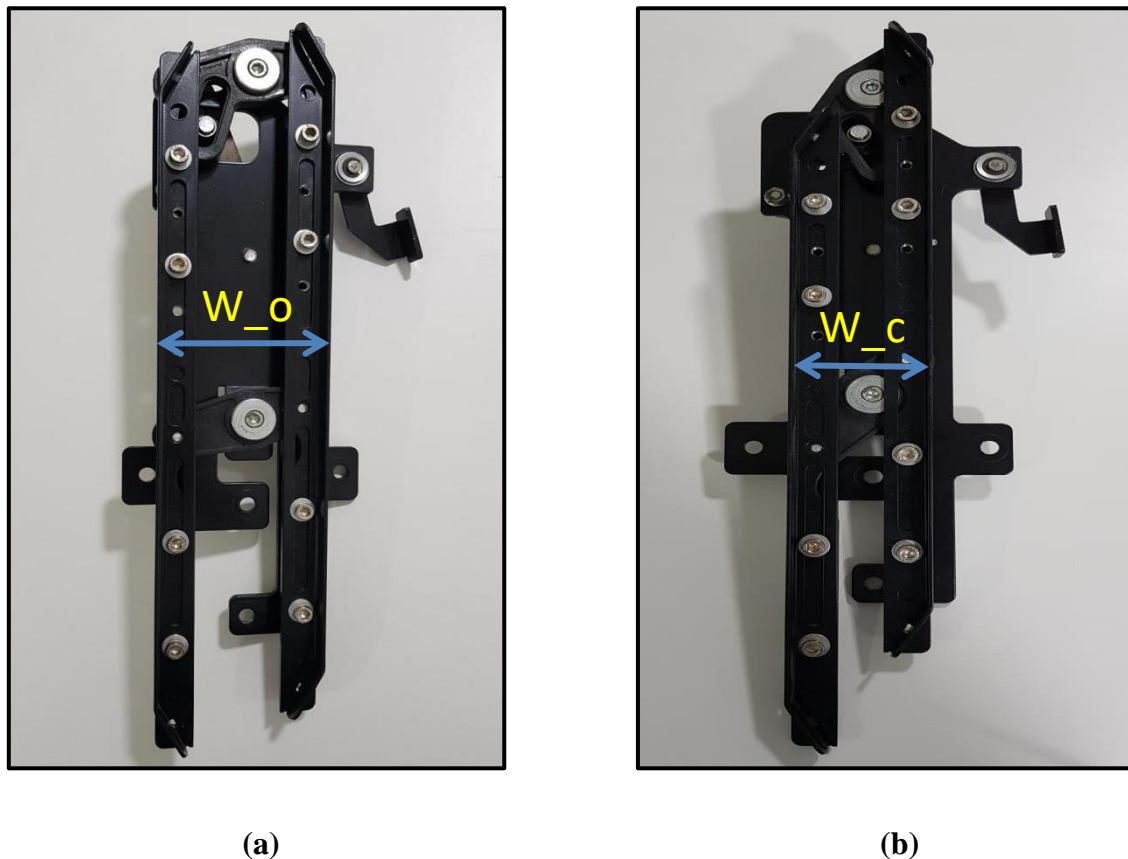


**Figure 2-1 Picture of the coupler skate assembly ; (a) Coupler skate open condition (b) Coupler skate close condition**

Figure 2-2 shows the CAD drawing of the angle position sensor installed on a coupler skate assembly. The angle position sensor (Asahi Kasei, make EM-3242 IC) uses the Hall effect principle to measure the angle. The sensor and the magnet are assembled such that sensor IC PCB is fixed on the coupler skate assembly base plate while the magnet is fixed on the linkage connecting both of the coupler skates. The magnet is oriented and placed in such a way that the rotating magnetic vector from the magnet is in the parallel plane to the sensor IC which is the essential condition for the sensor to measure the degree of rotational motion. During the door operation, as the coupler skates spread out,

a proportional rotation is made by linkage which is measured in real-time by the angle position sensor. The analog voltage data measured by the sensor is fed to a microcontroller board (Arduino Uno) which is powered by a DC power supply (Meanwell, Model PSC-60-R4) module. The microcontroller board performs the signal conditioning process to amplify the signal as well as to filter out the noise. The lookup table i.e. analog voltage signal against angle is utilized by a microcontroller to convert the measured sensor signal into the units of “degrees”.

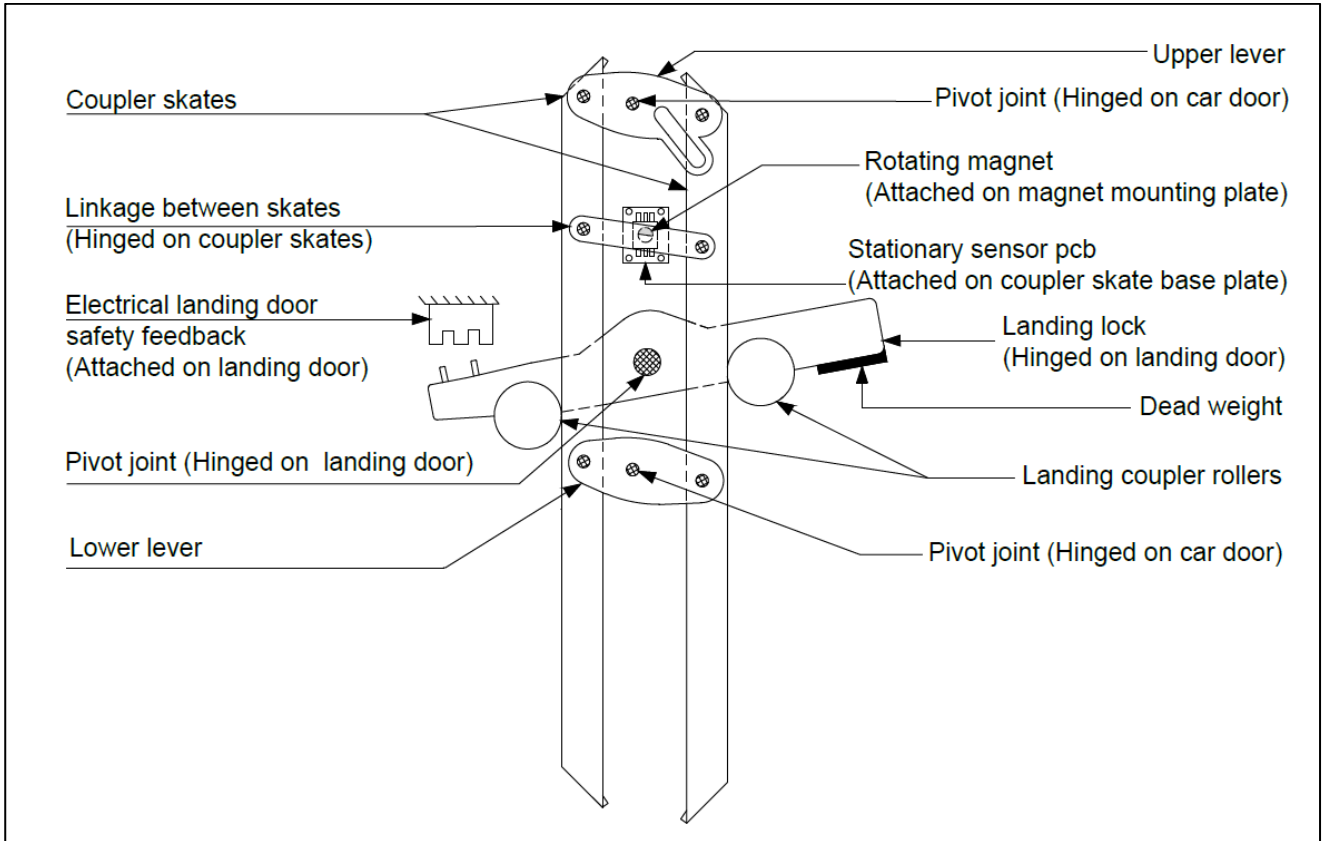


**Figure 2-2 CAD drawing of coupler skate encoder system installed on coupler skate assembly**

To detect any deviation in coupler skate assembly desired performance level, an algorithm is embedded in the microcontroller to signal the preventive maintenance flag. The desired performance of the coupler skate assembly is defined such that coupler skate assembly should spread out during door open command and the distance between the skates (vanes) should be observed in the range  $W_o = 87.5$  to  $90$  mm. Similarly, during the door close operation, the coupler skate assembly should close the skates wherein the distance between the vanes should be in the range  $W_c = 63$  mm to  $65$  mm. Based on these threshold values of  $W_o$  and  $W_c$ , corresponding angles ( $\theta_o$ ,  $\theta_c$ ) are calibrated and saved in the microcontroller memory. The preventive maintenance algorithm is designed in such a way that whenever the threshold angles ( $\theta_o$ ,  $\theta_c$ ) are not achieved by the coupler skate assembly during the door operation, a flag is raised by the microcontroller signaling a need for preventive maintenance of the coupler skate assembly.

Note, that the optimum working range of  $W_o = 87.5$  mm to  $90$  mm and  $W_c = 63$  to  $65$  mm is defined through an independent characteristic study of coupler skate assembly and landing lock assembly wherein the said threshold values of  $W_o$  and  $W_c$  ensures smooth opening and closing of landing locks. If the threshold values are not met, the landing lock unlocking and locking operation is not smooth and also sometimes it's unsuccessful.

### 3 EXPERIMENTAL SET UP

#### 3.1 Sensor calibration set up

The sensor EM-3242 is a non-contact angle positioning IC used in the coupler skate encoder system to detect instantaneous angle. The EM-3242 provides an absolute position in the units of “voltage”. To convert the angle data from the units of “voltage” to the units of “degree”, a calibration set up is constructed. Figure 3-1 and 3-2 highlights the calibration set up. The calibration set up is constructed such that a rotating magnet is placed in parallel plane of the IC so that a rotating magnetic field is generated above the sensor IC. Whenever a known rotation of magnet is made in degrees, a corresponding voltage is measured as an output from the IC. This forms the basic idea for creating a calibration lookup table for the sensor IC.

The construction of a calibration unit is such that the angle measurement scale is fixed on the mounting table (see figure 3-1 and 3-2). The sensor PCB is fixed on top of the angle scale supported by studs. A magnet is held above the sensor IC using a lever which can be freely rotated in the clockwise and anticlockwise direction. Any rotation made by the lever or say magnet is measured by eyeballing the angle pointer fixed on the lever. The angle pointer rotates above the angle scale through which degrees of magnet rotation can be easily measured. The analog voltage signal of the sensor IC for the calibration experiments is measured by an oscilloscope (Tektronix, Model - TBS1000B, Vertical resolution 8 bits). The results of the sensor calibration and its characteristics are discussed in section 4.

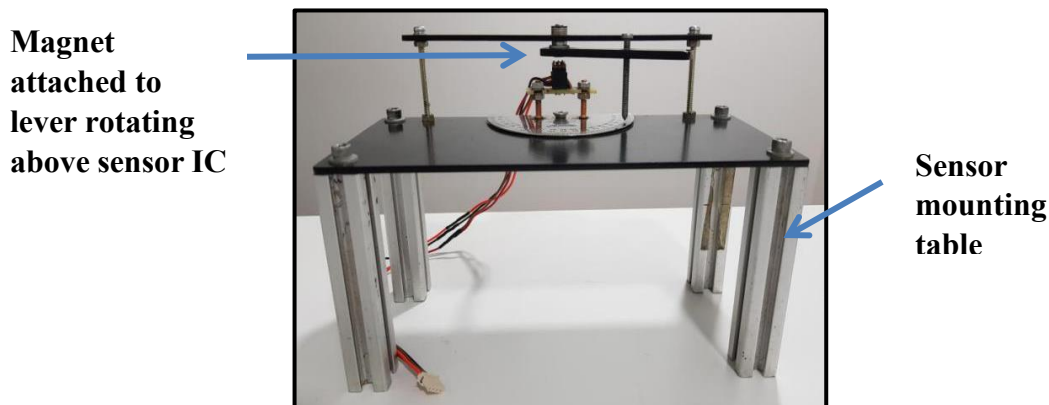


Figure 3-1 Sensor IC EM-3242 calibration set-up

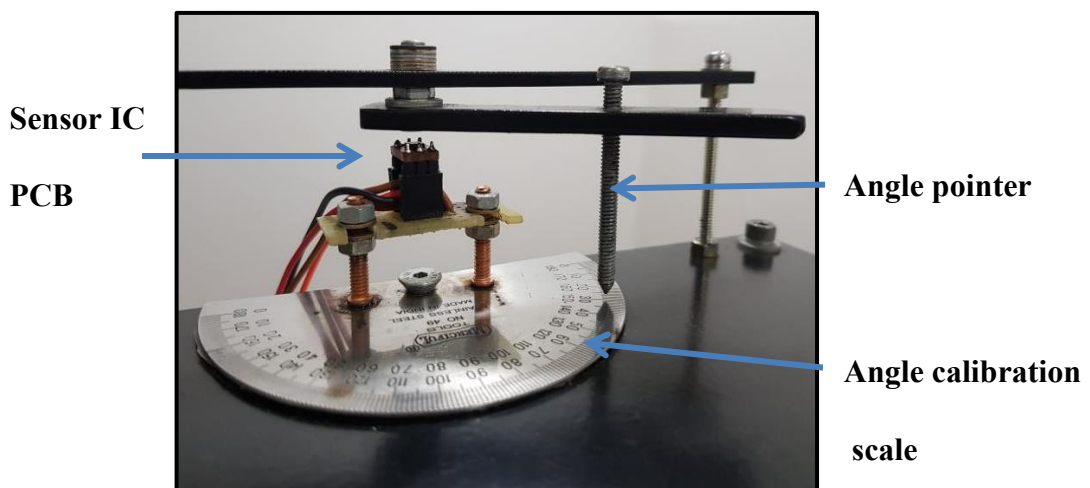


Figure 3-2 Sensor IC EM-3242 calibration set-up (close-up view)

### 3.2 Elevator automatic door test jig

An automatic lift door test jig is used to evaluate the working of the coupler skate encoder system. On this test jig, landing header and car header are mounted with their respective door panels attached through hangers. Car door header assembly is operated through a door drive unit and the coupler skate system of the car door assembly drives the landing door assembly, simulating the closest possible automatic door operation typically seen for elevators.

To simulate the erroneous operation of the coupler skate assembly, an adjustable screw-based obstruction is provided on the coupler skate assembly. Through the obstruction screw, the spread-out distance between the skates ( $W_o$ ) is restricted which simulates the faulty operation of the coupler skate assembly during the door opening cycle. The proof of concept of coupler skate encoder system and the fault detection algorithm is verified by performing experiments using obstruction screw attached to an above-mentioned test jig. The results of the experiments are discussed in section 4.

## 4 RESULTS AND DISCUSSION

The results and discussion section describes the outcome from the calibration experiments and the proof of concept experiments performed on the test jig.

Figure 4-1 depicts the sensor (coupler skate encoder) calibration data which is obtained using a calibration set up described in section 3.1. The figure 4-1 shows the degree of rotation of the magnet on the x-axis while the sensor output analog voltage signal is highlighted on the y-axis. The calibration experiment was performed such that the sensor is calibrated for the angle in the range 0 to 100 degrees. The magnet angle was incremented in the step of 2 degrees. To minimize the random error and to get statistically accurate reading, the calibration for each angle increment was repeated 10 times. Thus, each data highlighted in figure 4-1 through the red colour symbol is an average of 10 experiments.

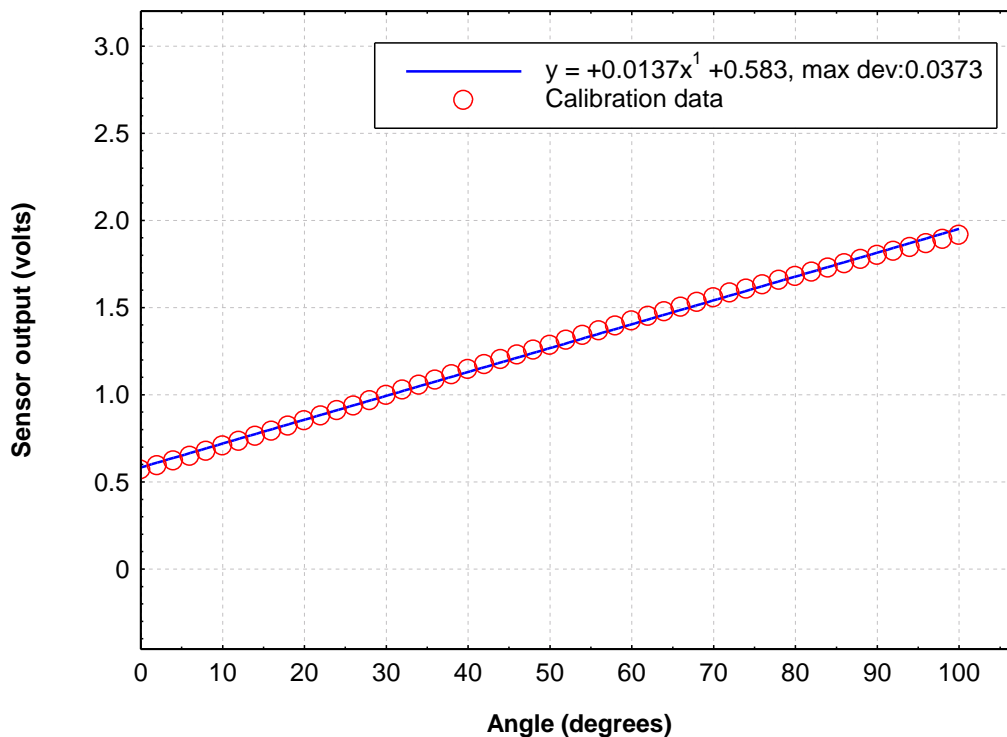
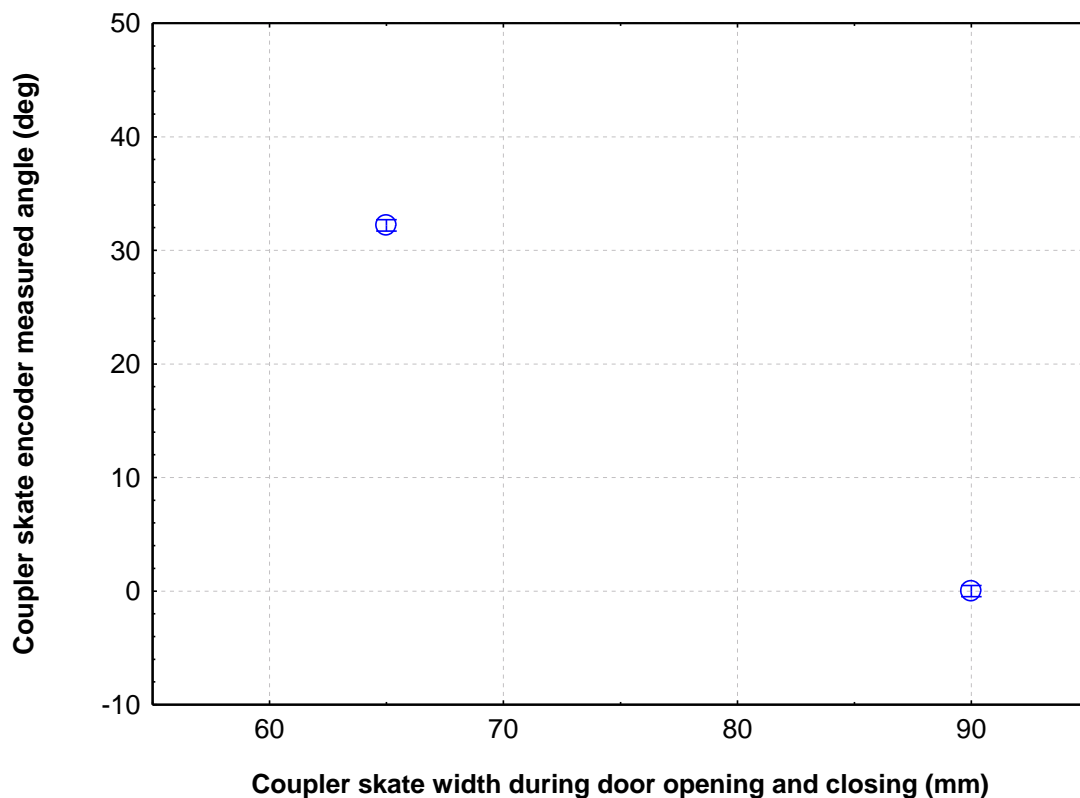


Figure 4-1 Calibration curve of coupler skate sensor ( angle against analog voltage signal)

A linear response of the sensor output is observed for rotation of magnet in the range 0 to 100 degrees (see figure 4-1). This result concurs with the behaviour described in the data-sheet of the sensor (EM - 3242). As the sensor shows the linear behaviour a linear equation based data fitting line is also highlighted in figure 4-1. The linear equation obtained through the fitting line enables the conversion of sensor output voltage signal to the units of angle in degrees.

The AKM sensor EM-3242 is a very accurate sensor such that its accuracy is defined in the datasheet as 0.36 deg [4]. For the experiments described in this document, the accuracy is limited by the least count of the calibration angle scale. Thus, considering the least count of the calibration scale as 1 deg, the accuracy of the coupler skate encoder system for the experiments described here is  $\pm 0.5$  deg.

Figure 4-2 highlights the coupler skate width against the angle measured by the coupler skate encoder system during door opening and closing operation. Here, the angle refers to the angle of rotation made by the linkage which connects the coupler skates (see section 2). The data depicted in figure 4-2 was obtained by performing experiments on the automatic lift door test jig wherein the coupler skate encoder system was installed on the coupler skate assembly. For the case wherein doors are fully closed such that the coupler skate width is  $W_c = 65$  mm, the angle measured by the coupler skate encoder system is  $32.20 \pm 0.5$  deg. When the doors are fully opened and the coupler skate width is  $W_o = 90$  mm, the angle measured by the coupler skate encoder system is  $0 \pm 0.5$  deg. The doors fully open condition i.e. coupler skate width  $W_o = 90$  mm is the reference condition, thus the sensor angle 0 deg is set at  $W_o = 90$  mm. From figure 4-2, it is observed that the coupler skate encoder system measures the angle of the linkage in the span of 0 deg to 32.20 deg for doors being in fully open and fully closed conditions. Figure 4-2 demonstrates the basic working of the coupler skate encoder system to measure the angle of rotation of coupler linkage during door opening and closing operation.



**Figure 4-2 Coupler skate encoder system data for doors fully opened and closed condition**

Figure 4-3 depicts the coupler skate encoder data for various configurations of coupler skate opening width during door opening operation. The coupler skate opening width was adjusted through a screw-based restriction mechanism such that  $W_o$  was varied in the range 90 mm to 87 mm. For every unique  $W_o$  value, the door open command was given and the corresponding coupler skate linkage angle was measured using a coupler skate encoder system. A specific range such as  $W_o = 90$  mm to 87 mm was selected for these experiments since it is known from an independent study that coupler skate assembly operates successfully at  $W_o = 90$  mm (healthy condition) while it fails to operate the landing lock at  $W_o = 87$  mm (unhealthy condition). At  $W_o = 87.5$  mm, the coupler skate assembly operates intermittently and it becomes unpredictable; it means that  $W_o = 87.5$  mm can be considered as the flag-raising condition i.e. a threshold condition or an indication at which preventive maintenance should be performed.

As highlighted in figure 4-3, the angle measured by the coupler skate encoder for  $W_o = 90$  mm is 0 deg while the angle measured for  $W_o = 87.5$  mm is 5.05 deg and for  $W_o = 87$  mm it is 5.9 deg. It can be observed that the span of a rotation angle of coupler linkage for the coupler skate assembly to transform from being healthy to unhealthy is 5.05 deg. Considering the accuracy of the coupler skate encoder system as  $\pm 0.5$  deg, it can be concluded that the coupler skate encoder system developed and discussed in this article is capable enough to detect any deviation in the performance of the coupler skate assembly even before the complete breakdown kind of situation occurs. In other words, in-case any situation arises wherein the coupler skate width decreases to  $W_o = 87.5$  mm (instead of  $W_o = 90$  mm), the coupler skate encoder system can easily detect the deviation to help the microcontroller system raise the flag for the need of preventive maintenance even before the breakdown occurs.

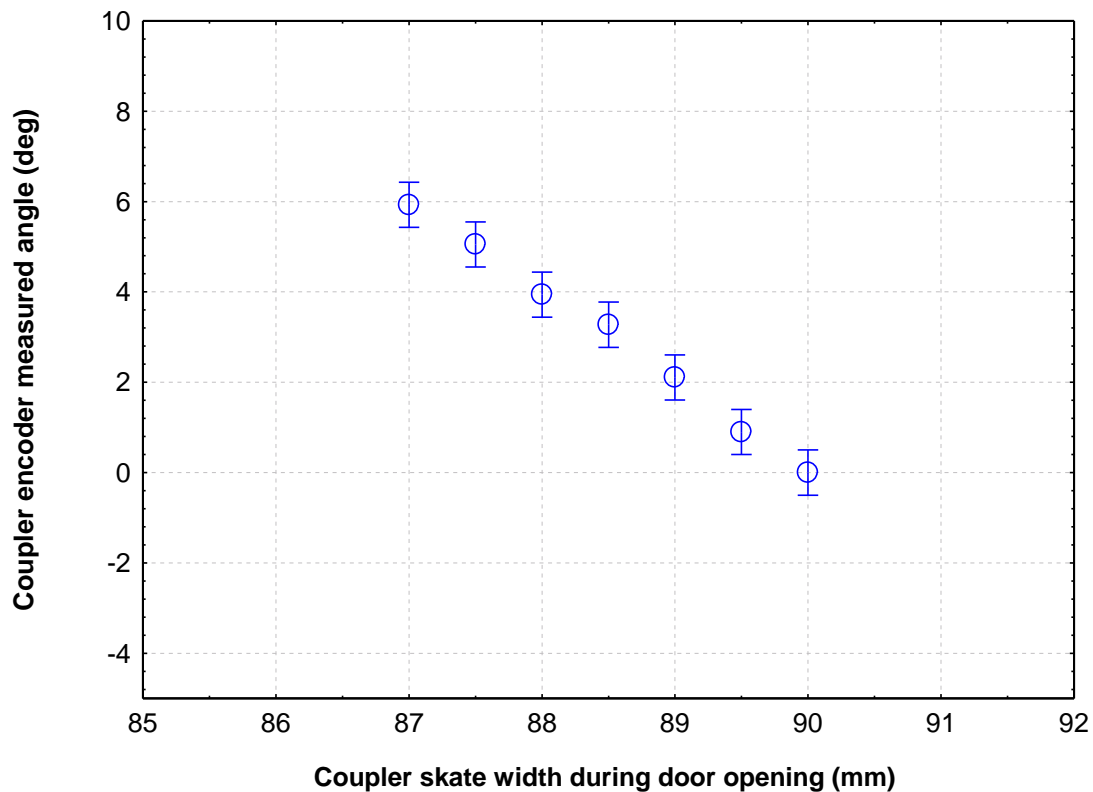
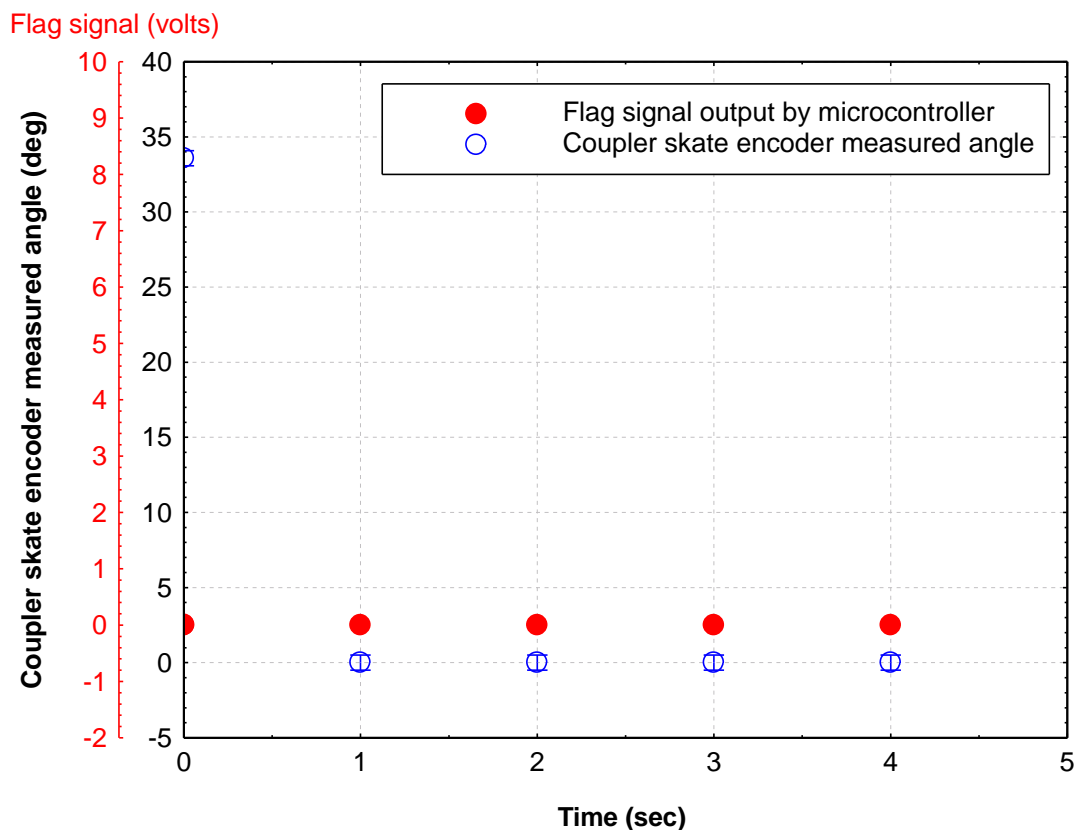


Figure 4-3 Coupler skate encoder angle measurement data versus various coupler skate opening widths

Figure 4-4 and 4-5 demonstrates the proof of concept experiment results (refer section 3.2 for information about experimental set up). Figure 4-4 and 4-5 highlights the coupler skate encoder data against the time in seconds. These experimental data were obtained during door open and door close operation. Also, depicted in the figure 4-4 and 4-5 is the status of flag signal from the microcontroller during door open and close operation. The microcontroller was embedded with an algorithm such that for healthy coupler skate condition the flag signal will remain low (value  $\sim 0$  volts) while for unhealthy coupler skate condition the flag signal value would be high (value  $\sim 5$  volts). Note that, for the demonstration purpose, the unhealthy and healthy condition of the coupler skate assembly was evaluated based on the look-up table fed to the memory of the microcontroller for the door open condition only.



**Figure 4-4 Coupler skate encoder angle measurement and microcontroller flag signal data for door opening and closing operation (Coupler skate assembly in healthy condition)**

Figure 4-4 data corresponds to the experiment wherein the coupler skate assembly was maintained healthy i.e. ( $W_o = 90$  mm, 0 deg). Here, the coupler skate encoder data measured during the door open condition had no deviation from the target value saved in the microcontroller memory, hence no flag signal was indicated by the microcontroller i.e. the output of the microcontroller flag signal remained low.

Figure 4-5 data depicts the experimental results wherein the coupler skate assembly opening width was reduced to  $W_o = 87.5$  mm to simulate an unhealthy condition. Due to reduced coupler skate opening width, the coupler angle measured by coupler skate encoder was 4.37 deg while the expected angle for a healthy coupler skate assembly is 0 deg. Due to the deviation in angle measured by the coupler skate encoder; a high signal (value  $\sim 5$ ) is flagged by the microcontroller indicating an erroneous operation of the coupler skate assembly. Thus, the results highlighted in figure 4-4 and 4-5

demonstrates the possibility of using coupler skate encoder (sensor) to detect abnormal functioning of the coupler skate assembly in real-time.

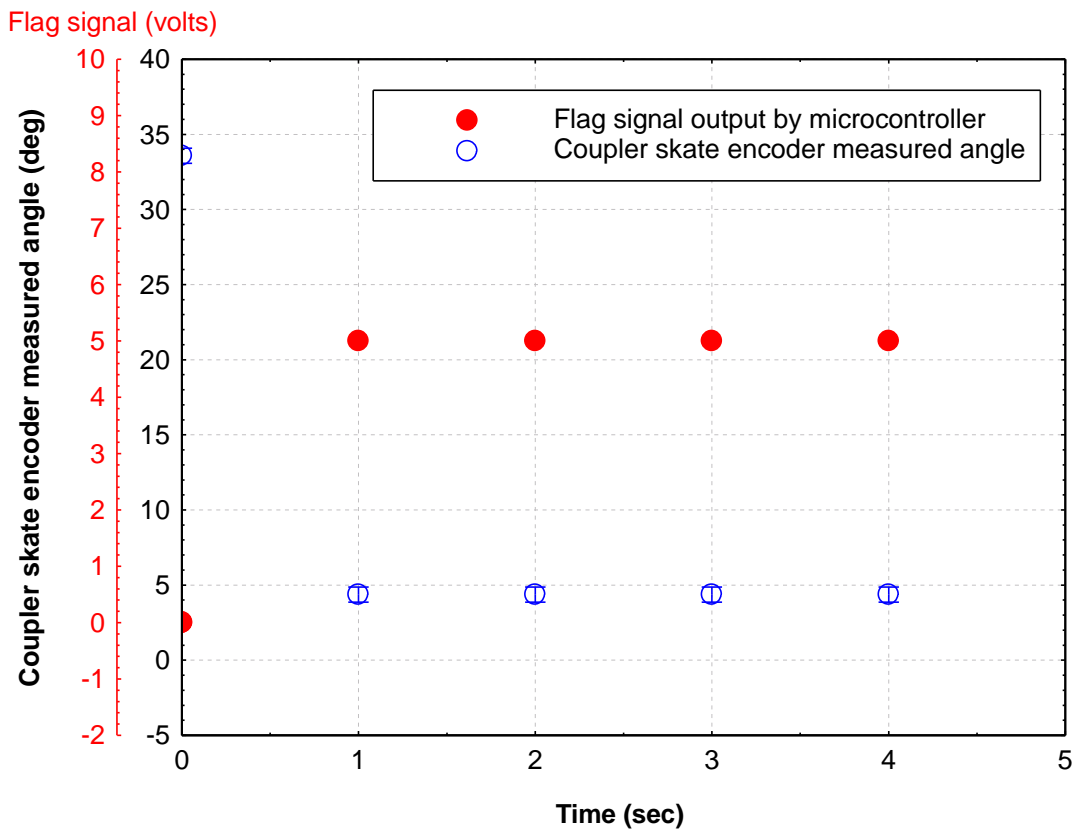


**Figure 4-5 Coupler skate encoder angle measurement and microcontroller flag signal data for door opening and closing operation (Coupler skate assembly in unhealthy condition such that  $W_o = 87.5$  mm)**

## 5 CONCLUSION

A proof-of-concept study of the coupler skate encoder system for monitoring the health of coupler skate assembly (used in automatic door header system of lift) was investigated. In this study, a Hall-effect based sensor was utilized to measure the degree of rotation of coupler skate assembly. The data obtained from the sensor was fed to the microcontroller board to make a necessary decision (i.e. to raise a flag) in the event of any deviation against the known expected value. To evaluate the working principle of the coupler skate encoder system, experiments were performed on an automatic lift door test jig. The results obtained from the experiments are encouraging such that the coupler skate encoder system designed is accurate enough to resolve and detect the smallest degree of deviation in the performance of coupler skate assembly.

## REFERENCES

[1] Michael A., Von Dohre and Tony Cecere, “DOOR OPERATORS”. EDUCATIONAL FOCUS, ELEVATOR WORLD [2003], available at

<https://www.elevatorbooks.com/shop/continuing-education/educational-focus-series/educational-focus-pdf/>

[2] Doug Witham, "PASSENGER ELEVATOR DOOR OPERATORS 101". EDUCATIONAL FOCUS, ELEVATOR WORLD [2003], available at

<https://www.elevatorbooks.com/shop/continuing-education/educational-focus-series/educational-focus-pdf/>

[3] John K. John and K. Subramaniam, "THE ELEVATOR ENTRANCE AND SAFETY PROTECTION". EDUCATIONAL FOCUS, ELEVATOR WORLD [2003], available at

<https://www.elevatorbooks.com/shop/continuing-education/educational-focus-series/educational-focus-pdf/>

[4] AKM sensor [online], Available at

<https://www.akm.com/content/dam/documents/products/rotary-encoder/angle-sensor/em3242/em3242-en-datasheet.pdf>

## **BIOGRAPHICAL DETAILS**

Rohit Nehe is the Head of Electrical and Electronics department at Creestaa Elevators (India) Pvt. Ltd. He obtained his M.S. degree in Mechanical and Aerospace Engineering in 2008 from Syracuse University, NY, USA. Later he obtained his PhD degree in Mechanical Engineering in 2013 from Michigan State University, East Lansing, USA. He has a strong research and academic background in developing diagnostic instruments involving interdisciplinary engineering fields. His current activities at Creestaa Elevators involves research and product development in regards to vertical transportation systems.

Chetan Mahale is a Application Engineer at Creestaa Elevators (India) Pvt. Ltd. He obtained his Bachelor of Engineering degree in Electronics and Telecommunication in 2016 from Savitribai Phule Pune University (SPPU). Later, to gain expertise in Mechatronics engineering field, he obtained his Masters of Technology degree in Mechatronics from SPPU in the year 2018. Since the year 2018 till now (2020), he is actively involved in various new product development projects and applications at Creestaa Elevators (India) Pvt. Ltd.

Babasaheb Patil is a Research & Development Engineer at Creestaa Elevators (India) Pvt. Ltd in the elevator door manufacturing department. He obtained his Bachelor of Engineering degree in Mechanical Engineering in the year 2014 from Mumbai University. He has a diploma degree in computer aided design (CAD) from a private institute based in Pune. His interest and experience lies in design and manufacturing new products related to elevator door assemblies.

# IOT, Magic or Myth?

Rory Smith

The University of Northampton, Northampton, UK

**Keywords:** Internet of things, Machine to Machine, Machine Learning, Artificial Intelligence.

**Abstract.** Through slick videos, magazines, and advertisements, IOT, ML, AI, and M2M have been promoted as a wonderful solution for the lift and escalator industry. This paper reviews the available IOT product offerings by capabilities, and evaluates their efficacy based upon current technology.

The review includes what is now possible, what is not now possible, and what might be possible soon.

Solutions available to the multi-national lift companies and those available to regional and local lift enterprises are also reviewed.

## 1 INTRODUCTION

IoT, the Internet of Things has been promoted as the next big thing for the lift industry. Articles about IoT appear in many types of publications. Advertising commercials appear on television touting the wonders of Cloud computing and Machine Learning (ML).

The November 2019 edition of Elevator World included an article titled *The IOEE: Connecting Equipment, Customers and Passengers*. In addition to explaining Schindler's IOT product, it also describes the many benefits that IoT, Machine Learning (ML), and digitalization will bring to the lift industry.

There is even a magazine, IoT & Elevators, published by Nayar Systems, an IoT company. The magazine is filled with interesting articles on Artificial Intelligence (AI), ML, Smart Cities and connected cities.

The claims in these documents and commercials are not hype, they are true. However, implementing these concepts is not simple.

Because of all the enthusiasm associated with IoT, many product offerings now exist in the lift industry. What these products can and cannot do will be explored.

## 2 IOT AND MAINTENANCE TYPES

### IoT

The **Internet of things (IoT)** is defined in Wikipedia as “a system of interrelated computing devices, mechanical and digital machines, objects, animals or people that are provided with unique identifiers (UIDs) and the ability to transfer data over a network without requiring human-to-human or human-to-computer interaction” [1].

An example of an IoT device would be a temperature sensor located in a lift machine room. The machine room temperature could be viewed on a PC or smart phone

### Maintenance Types

There are several types of lift maintenance where IoT devices can be applied. They are as follows:

- Breakdown maintenance. This type of lift maintenance involves returning a lift to service after it has broken down. Breakdown maintenance is often referred to as Reactive Maintenance.
- Preventive maintenance (PM). This type of maintenance is regularly performed on a lift or piece of equipment to reduce the likelihood of a breakdown [2].
- Usage based maintenance. This is a maintenance strategy based on how much use an asset has experienced. For example, change the oil of a car engine after every 10,000 kilometers of use.
- Condition based maintenance (CBM) is a maintenance method that monitors the condition of critical components or the entire asset in order to determine what maintenance is to be performed and when it should be performed [2].
- Task based maintenance (TBM). TBM is an analysis method that reviews existing PM plans and weeds out duplications and identifies missing tasks. At the conclusion of the analysis a list of tasks is developed that is then used for future maintenance visits [3].
- Predictive maintenance. Predictive maintenance uses ML to issue a recommendation to replace a part or perform a service on a lift or escalator before a breakdown occurs.[4].
- Prescriptive maintenance. This method is a totally automated form of Predictive Maintenance where service tickets are computer generated for every service visit using ML [4].

### 3 IOT GOALS AND OBJECTIVES

There are two perspectives on the goals and objectives of IoT products: those of the building owner or manager, and those of the lift and escalator maintenance provider.

#### **Building Owner/manager's perspective**

Individuals who have had extensive contact with building owners and managers have found that the owners and managers want three things [5,6]:

- The ability to know which lifts are in operation.
- To be notified when a lift breakdown occurs.
- If a lift has broken down, to know if it is occupied.

Whether IoT devices are installed or not, building operators want all their vertical transportation equipment to run trouble free.

#### **Lift maintenance provider's perspective**

Maintenance providers have two objectives [7]:

- Customer satisfaction. If up time can be increased, lifts and escalators run smoothly, and entrapments are reduced, then the customers will be more satisfied.
- Operational efficiency. If the right maintenance tasks are performed at the right time, then efficiency will be increased. The reduction of callbacks also reduces costs.

Accomplishing these objectives will permit maintenance providers to compete based on value and quality rather than on price.

## 4 IOT PRODUCTS

There are many IOT products available in the market. Some products are available to all buyers. The products available from the multinationals are typically available to their present and future clients and are not available to competitors.

The products reviewed represent a cross sectional sample of the products available. The products are neither named nor referenced. In each case the review is based on the product manufacturer's published literature. This review will try to be objective and should not be viewed as either a positive or negative endorsement.

### **Product A, Industrial Router**

Product A is an industrial router that connects to its Virtual Private Network (VPN). The router is available in two versions, wired and wireless. It is described as an Industrial Internet of Things (IIOT) gateway. It is a Machine to Machine (M2M) device.

The product can push data to cloud services such as Microsoft Azure or Amazon Web Services. However, once the data is in the cloud it must be converted to meaningful information by Data Scientists and Domain Experts.

### **Product B, Remote Monitoring System**

Product B is a remote monitoring system that graphically displays the position, motion and door status of the lifts in a building. The graphic data can be viewed on a PC or smart phone. Additionally, this product can issue alerts via email or text messages if there is a problem with the lifts.

This product appears to be designed for building management professionals. It meets the three requirements wanted by building managers described above in Section 3.1. This product can also provide reports that can be used for usage-based maintenance.

A read only interface with the lift controller is required.

### **Product C, Condition Based Monitoring**

Product C uses an accelerometer to monitor the following: travel, ride quality, door operation, car load, leveling, shaft efficiency, number of trips, duty cycles and the condition of traction sheaves.

Both usage-based and condition-based maintenance are possible with this product.

The product is connected to a cloud and does some processing there. The data sent to the cloud makes the use of ML possible.

The product appears to be designed for lift maintenance providers. It is not connected electrically to the lift making it totally secure.

### **Product D, Modular Remote Monitoring with Command and Control**

This product is a modular remote monitoring system that has several optional components.

The base module consists of a cellular modem located in the machine room and a car top module with an accelerometer. The car top module is connected to two of the car call buttons in the car operating panel.

The accelerometer can monitor car and door movements. Movement levels are recorded. If there is a lower level of car movement than normal, the car top unit will send the lift on a test run using the connections to the car call buttons. If the test run is not successful, an alert is sent.

This product can also be connected to compatible light curtains and emergency telephones. The light curtain and phone data are also collected and make the unit more powerful.

An optional I/O board can be connected to the lift controller. This can be used to reset the controller CPU and report such things as “car out of service”.

Both usage-based and condition-based maintenance are possible with this product.

The product is connected to a cloud and does some processing there. The data sent to the cloud makes the use of ML possible.

The product appears to be designed for lift maintenance providers.

Any unit with command and control features is inherently more vulnerable to hacking than read only of isolated systems.

### **Products of the Western Multinational Lift Companies**

Otis, thyssenkrupp Elevator, Schindler and KONE have all announced IoT products. They have also partnered with major ML companies such as Microsoft, GE Predix and IBM Watson.

Their products consist of routers or cellular modems connected to controllers, sensor packages or both. These connections allow them to gather large quantities of data. Their partners can help them to develop the data acquisition, processing and storage architecture as well as providing the cloud processing and ML software to process the collected data.

However, these companies must develop ML algorithms needed for predictive and prescriptive maintenance. These algorithms must be developed by teams made up of Data Scientists and Domain Experts [8]. The efficacy of these products will depend upon the outputs from these teams.

These products appear to be components of premium service offerings.

## **5 CONCLUSIONS**

None of the products reviewed deliver all the potential benefits of Machine Learning, Artificial Intelligence, and IoT. However, all the products deliver some of these benefits.

Each of the products delivers different benefits at different price levels. None of these products is right for everyone. All are most likely ideal for someone.

All the reviewed products are works in progress. All should improve in time. Machine Learning and all learning should lead to improvement.

Because there are so many impressive articles, books and PowerPoints touting the benefits of IoT, one must be cautious when selecting an IoT product.

One must first decide which IoT features are needed. Then, one should ask for live demonstrations of the proposed solution. Anything, no matter how bad, can be made to look fantastic using a PowerPoint.

A live demonstration of a product should usually be closer to reality than a presentation.

When IoT reaches its full potential, it will seem like Magic. It is in the process of forever changing the lift industry.

## REFERENCES

- [1] *Internet of Things* Available from: [https://en.wikipedia.org/wiki/Internet\\_of\\_things](https://en.wikipedia.org/wiki/Internet_of_things) Last accessed Maintenance on: 6 February, 2020
- [2] *Preventive Maintenance* Available from: <https://www.fixsoftware.com/maintenance-strategies/preventative-maintenance/> Last accessed: 6 February 2020
- [3] *Task Based Maintenance* Available from: <https://www.armsreliability.com/page/services/our-methodology/task-based-maintenance-tbm-analysis> Last accessed on: 6 February, 2020
- [4] *The Evolution of Maintenance* Available from: <https://www.ibm.com/blogs/internet-of-things/maintenance-evolution-prescriptive/> Last accessed: 7 February, 2020
- [5] Discussions with Richard Peters, Peters Research, September 2019
- [6] Discussions with Jeff Buntin, thyssenkrupp Elevator, December 2019
- [7] Smith, R (2019) Thyssenkrupp Elevator's Internet of Things *CIO Applications* 8 April 2019 p28.
- [8] Davenport, T. *Big Data @ Work*. Boston: Harvard Business School Press (2014)

## BIOGRAPHICAL DETAILS

Rory Smith is Visiting Professor in Lift Technology at the University of Northampton and a consultant with Peters Research Ltd. He has over 51 years of lift industry experience during which he held positions in research and development, manufacturing, installation, service, modernization, and sales. His areas of special interest are Robotics, Machine Learning, Traffic Analysis, dispatching algorithms, and ride quality. Numerous patents have been awarded for his work.



# Research of Real Time Video Monitoring and Remote Control System of Escalators

Yantai Luo

Shanghai Mitsubishi Elevator Corporation, Japan

**Key Words:** video monitoring; detection; functional safety; remote control

**Abstract.** An escalator is a safe related, heavy-duty special equipment. It is a big challenge for escalator manufacturers to detect a dangerous state or the behaviour of passengers on an escalator by using real-time video monitoring thereby helping the administrators in a security monitoring room to control the escalator remotely at the emergent moment. This hasn't been solved effectively since the escalator was invented 120 years ago. This paper presents some practical methods to overcome the difficulties, which includes following two aspects:

- 1) Detect a dangerous state or the behaviour of passengers, such as accidental falling down, walking in the reversal direction, based on real-time video analysis. To improve the accuracy of detection, this article introduces the method of real-time video analysis which combines optical flow algorithm and image deep learning algorithm.
- 2) Based on functional safety technology, use only one emergency stop button in the security monitoring room to control any of the escalators on which the dangerous state or behaviour of passengers is detected remotely.

The actual run of the system in metro stations demonstrates it can detect a dangerous state or the behaviour of passengers accurately and stably and administrators in security monitoring room can stop the escalator in a safer and more convenient manner. The application result shows that the proposed system has a significant value in lift industry.

## 1. INTRODUCTION

An escalator is a safe related, heavy-duty special equipment, which is widely used in the vertical transportation of subway, light rail, station, airport, wharf, and shopping mall.

In China, with the rapid development of urban subways, the use of escalators for subways has increased rapidly. Taking Shanghai Metro, the largest urban rail transit network in China, as an example, at the end of 2018, the total length of the whole network operation line of Shanghai urban rail transit reached 705km, ranking first in the world, with 2.038 billion passenger trips in the whole year, ranking third in the world<sup>[1]</sup>. The Shanghai Metro has more than 4,000 escalators, which carry more than 30 million passengers a day and bear more than 50% of Shanghai's public transport capacity<sup>[2]</sup>.

Due to the inevitable contact of moving parts with passengers, passenger injuries on escalators account for more than 60% of the total number of rail transit passenger injuries, up to 70 to 80 per month<sup>[3]</sup>. According to statistics, falls account for about 75% of all types of escalator passenger

injuries <sup>[4]</sup>. Therefore, how to detect the fall on the escalator as it happens and stop the escalator remotely and safely by the staff of the control room to prevent major personal injury occurring because of continuous rolling of the fallen passengers is an urgent problem to be solved in the daily operation management of the escalator.

## 2. METHODS

### 2.1 Real-time video analysis

The existing escalator detection system can only detect the operation of traditional machinery, and the monitoring of passenger behaviour mainly depends by way of video surveillance and manual real-time viewing. Due to the wide distribution of escalators, the large number of monitoring, the lack of a large number of human resources to implement real-time monitoring, video surveillance systems can usually only play the role of passive tracing after the accident.

With the development of artificial intelligence image recognition technology, the real-time video analysis related research of escalator passenger behaviour is booming. For example, based on the Openpose<sup>[5]</sup> key point detection algorithm to obtain the human body structure, and the use of the SVM (the Support Vector Machine) classifier to realize the detection and alarm of the pedestrian fall phenomenon in the picture <sup>[6]</sup>, the defect of the algorithm is that it is necessary to detect the key point of the human body, which is easily blocked by the rear passenger or object, and when classifying the human body posture by the SVM, it is difficult to complete the accurate discrimination. The algorithm is based on the human skeleton sequence of the escalator abnormal behavior recognition algorithm. The algorithm firstly detects the passenger face by using the support vector machine which combines the features of the deformable component model and tracks the passenger's motion in the escalator with the improved kernel correlation filter. Then, the human skeleton sequence of the passenger is extracted by using the convolution neural network, and the abnormal behaviour sequence is detected from the passenger skeleton sequence by template matching. Finally, the algorithm uses the dynamic time-regularization to identify the abnormal behaviour sequence based on the five-nearest neighbour method. The optical flow tracking algorithm, and the human object is tracked to define the related abnormal behaviour, and the abnormal behaviour detection is carried out <sup>[7]</sup>. This algorithm only determines the fall through the optical flow tracking, and the misjudgment rate is high.

To achieve a high accuracy, low misjudgment rate, and low cost real-time video method to detect passenger falls on the escalator, this paper proposes a method to first extract the direction of passenger motion based on the dense optical flow method, then group the information eigenvalues of each sub-block motion direction, speed, acceleration and so on in the block which accords with the pixel points in the direction of motion, and then use the SVM classifier to classify the eigenvalues of the matrix in the continuous 1-2 seconds to determine whether the pedestrian in the picture is normal, reverse walking or falling.

The calculation process is as follows:

1. Obtain the first frame image detected by optical flow method
2. Get the second frame image as the current frame image detected by optical flow method
3. The motion direction and displacement of each pixel in the image are calculated by dense optical flow method.

4. Calculate the area of the moving block and the speed of the moving block with the escalator in the third step optical flow diagram displacement distance, mean velocity and variance.
5. Cache the calculated results of step 4 as the feature vector of this frame.
6. Repeat 2,3,4,5 steps using the current frame as the first frame for detection
7. To judge the number of frames with the current pre-frame N frame motion block area > MIN\_S, when the number of frames > K, the preliminary judgment is suspected to fall or reverse walking.
8. The feature matrix composed of n frames was input into the SVM classifier for classification to determine whether it was fall, reverse walking or false alarm.

Feature generation and training specific algorithms:

1) Single frame feature generation:

1. According to the optical flow calculation, the displacement maps of the x-direction and y-direction of the image are obtained respectively:

$$\begin{bmatrix} x_{00} & x_{01} & x_{02} & \dots & x_{0j} \\ x_{10} & x_{11} & x_{12} & \dots & x_{1j} \\ x_{20} & x_{21} & x_{22} & \dots & x_{2j} \\ M & M & M & M & M \\ x_{i0} & x_{i1} & x_{i2} & \dots & x_{ij} \end{bmatrix} \begin{bmatrix} y_{00} & y_{01} & y_{02} & \dots & y_{0j} \\ y_{10} & y_{11} & y_{12} & \dots & y_{1j} \\ y_{20} & y_{21} & y_{22} & \dots & y_{2j} \\ M & M & M & M & M \\ y_{i0} & y_{i1} & y_{i2} & \dots & y_{ij} \end{bmatrix}$$

The downward displacement should be greater than the left and right displacement according to the retrograde and fall movement characteristics of the escalator. Obtain the motion block mask image from the above displacement map:

$$Mask = \begin{bmatrix} m_{00} & m_{01} & m_{02} & \dots & m_{0j} \\ m_{10} & m_{11} & m_{12} & \dots & m_{1j} \\ m_{20} & m_{21} & m_{22} & \dots & m_{2j} \\ M & M & M & M & M \\ m_{i0} & m_{i1} & m_{i2} & \dots & m_{ij} \end{bmatrix} \text{When } y_{ij} \leq 0 \text{ When } m_{ij} = 0 ; \text{ when } y_{ij} > 0 ; \text{ when } x_{ij} < y_{ij} \text{ In}$$

which  $m_{ij} = 0$  Otherwise  $m_{ij} = 1$ .

2. Area extraction of moving blocks

Open operation of mask image; calculate mask image in  $mask^{m_{ij}=1}$ , calculate the area of the connected domain as S;

### 3. CALCULATION OF AVERAGE VERTICAL DISPLACEMENT VELOCITY

Calculate the average velocity of the moving block according to the motion block mask map Mask, displacement map in the y direction.

$$v = \frac{\sum_{i=0; j=0}^{i<H; j<W} y_{ij} \bullet m_{ij}}{\sum_{i=0; j=0}^{i<H; j<W} m_{ij}}$$

3. Velocity variance calculation, based on the average velocity calculated in step 3 to obtain velocity variance:

$$s^2 = \frac{\sum_{i=0; j=0; m_{ij} \neq 0}^{i<H; j<H} (y_{ij} - v)^2}{\sum_{i=0; j=0}^{i<H; j<H} m_{ij}}$$

2) Combination of 25 frame single frame features:

4. The feature vector of 25 consecutive frames is  $25 \times 3 = 75$  eigenvalues

$$F = \left[ [S_0, S_1 \dots S_k], [v_0, v_1 \dots, v_k], [s_0^2, s_1^2, \dots, s_k^2] \right]$$

5. The elements in the three groups of vectors in F are arranged in ascending order respectively to get  $F'$ ;
6. Collect feature vectors  $F'$  in each case for SVM classifier training.
7. Save the classifier's training results for subsequent classification use.

### 3.2 Stop Escalator Remotely

Since it was invented more than 120 years ago, the operation mode of escalators are all local operation, and the practice of attempting remote operation by subway companies all over the world has not been successful for many years. When there is an emergency at the scene (passenger falls on the escalator, congestion at the escalator exit, etc.), it can only rely on the scene personnel to happen to find, on-site emergency operation. In order to ensure the safety of operation, some subway operation companies send more personnel on duty during the peak period and emergency intervention.

- In Moscow Subway, at the side of the escalators, a guard box and an operator on duty is set up. The operator observes the escalators and pushes the emergency stop switch immediately in case of an emergency. The following figure shows:

- Domestic portion MTR Corporation In the peak hour of danger Temporary to be on duty Occurs Emergency Immediate in case of situation Emergency Stop the intervention.



**Figure 1 Moscow Subway, long-term duty personnel**



**Figure 2 Temporary personnel watching escalators at the peak time in China**

If we can realize remote control of escalators in the security monitoring room, especially intelligent awareness and safe and remote control of emergency events, which will greatly accelerate emergency response, and reduce personal injury. But as a specialty equipment, remote control of escalators must be strictly compliant to security standards and regulations, otherwise, if there is a software defect, component failure or EMC defect, it will fail to implement an emergency stop correctly or cause an incorrect emergency stop, which will lead to a more dangerous situation. The emergency stop device shall be an electrical safety device (electric safety device) compliant with EN115-1:2008+A1:2010 5.12.1.2, i.e.: may consist of A) either one or more safety switches, or B) safety circuit (fail-safe circuit), or C) programmable electronic safety related system (PESSRAE).

Currently the world's response strategy is like type A, with a physical emergency stop button for each escalator that conforms to the electrical safety device (EN115-1:2008+A1:2010 5.12.1.2). Operators

manually press the corresponding physical emergency stop button to stop the escalator remotely in the event of a passenger fall occurring, as shown in Figure 3:

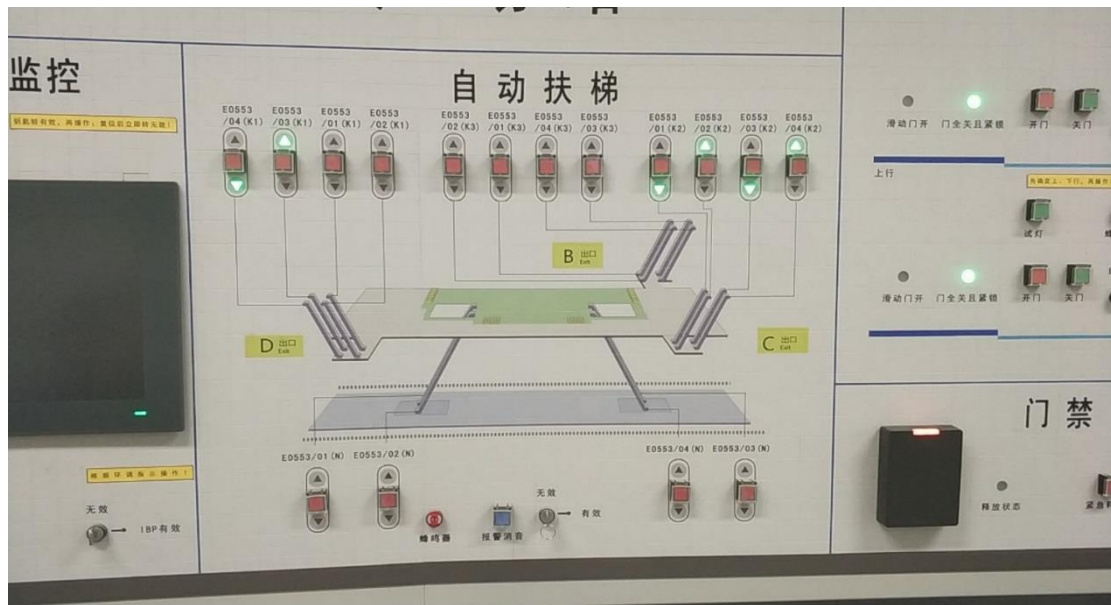


**Figure 3 One actual stop button for each escalator**

This approach has the following disadvantages:

- It's not easy to find accurate buttons when an emergency occurs;
- When the operation error causes further injury, the operator should bear the corresponding safety responsibility, so the operator is not willing to use it, nor dare to use it [8].

This paper proposes a safe and convenient way to stop escalators remotely (i.e. mode C), Operators press only one actual stop button to cut off the safety circuit to stop the escalator on which the dangerous event occurs, through the control of video analysis server and remote control components (which Pass PESSRAE safety certification and obtain type test certificate). As shown in Figure 4:



**Figure 4. Monitor screen and the actual stop button**

The operating procedures are as follows:

1. Video analysis server and remote control components preserves the escalator information when detecting that a passenger is in a dangerous condition on an escalator;
2. Monitor in the security monitoring room display corresponding real-time video according to the information preserved in video analysis server and remote control components;
3. The operator manually confirms that the escalator information is consistent and presses the actual stop button if there are dangerous conditions on the escalator in the video;
4. Video analysis server and remote control device components cut off the corresponding safety circuit of the escalator to stop the escalator.

#### **4. RESULTS**

The system which includes a total of 8 cameras corresponding to 19 escalators, runs from August 2018 to October 2019 In Shanghai Metro Hanzhong Road Station.

##### 1) Successfully capture:

- 32 passenger falls (all passenger falls were successfully captured);
- 738 passenger reverse walking events;

##### 2) Realize safely remote control:

The further personal injury of the passenger is effectively prevented, and the safety is greatly improved.

Take the case that happened at 15:20 on August 17, 2018 as an example, on an up running escalator in Shanghai Metro Hanzhong Road Station, an old lady falls down because of not grasping

the handrail, the operator in the security monitoring room is informed by the monitor, then he presses the actual emergency button to stop the escalator immediately, as shown in figure 5 and figure 6. The time is 14 seconds since the fall happened until the escalator stopped, the time is 26 seconds since the fall happened until the counsel in the station arrived at the escalator.



**Figure 5 Passenger fall detection and remote stop of escalator**



**Figure 6 The counsel in the station arrived at the escalator**

The results show that the system has high accuracy and low misjudgment rate, and the remote stopping escalator is safe and convenient. It has a wide application prospect in the lift industry all over the world.

**REFERENCES**

- [1] Liu Chunjie. Research and Practice of Shanghai Smart Subway [J]. Urban Rail Transit Research,2019(6):1-6.
- [2] Liu Chunjie. Innovation and Practice of Intelligent Control of Shanghai Rail Transit Escalator [J]. China Municipal Engineering,2019(06):1-3+100.
- [3] Long, Sijin,Lu, Jian,Xing, Yingying, et al. An analysis of escalator-related injuries in metro stations in China, 2013-2015[J].Accident Analysis and Prevention,2019,122(Jan.):332-341.
- [4] Filippone, J., Feldman, J. D., Schloss, R. D. and Cooper, D. A.(2002). Elevator and Escalator Accident Reconstruction and Litigation, Lawyers & Judges Publishing Company, Inc.
- [5] M. Andriluka, S. Roth, and B. Schiele. Monocular 3D pose estimation and tracking by detection. In CVPR, 2010.
- [6] Chen Dong. Software development of pedestrian safety monitoring system for electric escalators based on video analysis [D]. Zhejiang University,2019.
- [7] Tian Lianfang, Wu Qichao, du Qiliang, Huang Liguang, Li Miao, Zhang Daming. Identification of the abnormal behavior of walking elevator passengers based on human skeleton sequence [J]. Journal of South China University of Technology (Natural Science),2019,47(04):10-19.
- [8] Yang Guanbao. Escalator energy saving and intelligent monitoring system based on panoramic vision [D]. Zhejiang University of Technology,2011.
- [9] He Cheng. AI Image Recognition and Functional Safety Based Escalator Supervisory and Control System and Related Safety Regulations[J]. China Elevator, 2019,(15):6-8.



# Study on a Vibration Reduction System for Lift Roller Guides

Yosuke Shima<sup>1</sup> and Osamu Furuya<sup>2</sup>

<sup>1</sup>Graduate School of Tokyo Denki University, Ishizaka, Hatoyama-cho, Hiki-gun, Saitama 350-0394 Japan

<sup>2</sup>Division of Mechanical Engineering, School of Science and Engineering, Tokyo Denki University, Ishizaka, Hatoyama-cho, Hiki-gun, Saitama 350-0394 Japan

**Keywords:** Lift, Roller Guides, Vibration Control, Coil Springs, Urethane Elastomer

**Abstract.** Lift roller guides require time and effort for maintenance and replacement, so if they can be extended in life, advantages such as reduced maintenance frequency, cost reduction, and improved reliability can be obtained. In this research, authors propose roller guides that achieve long life by changing the material of the roller and have both ride comfort and durability. To decrease the vibration of lift cabin, an analytical model for calculating the time history response of the lift cabin will be constructed, and the vibration control effect will be verified by simulation incorporating spring and damping elements based on the experimental results. Through analytical and experimental approach, a design way for a roller guide that has optimal riding comfort and durability within the range of safety regulations is proposed.

## 1 INTRODUCTION

In recent years, the number of lifts has been increasing, as facility investment for the new construction of high-rise buildings by redevelopment in urban areas, barrier-free and renewal of old age has become active. Demand for lifts is expected to increase further in the future due to the impact of emerging countries and redevelopment. Roller guides form a part of the car-frame guiding system, the elastic- damping properties of the roller guide shoe (wheel tire), and if included, of additional spring-damper elements provide passive vibration control mechanism installed between the rail in the lift shaft and the cabin on which the person rides, and plays the role of smoothly moving up and down while suppressing vibration. However, with the spread of lifts, there is a shortage of human resources responsible for maintenance. In particular, since roller guides require maintenance and replacement, it is considered meaningful to extend their service life (durability) to reduce maintenance frequency, cost, and reliability. If the rollers are hardened to increase durability, the problem occurs that comfortability and noise will deteriorate. In this study, the problem of vibration and abrasion in the roller guides is focused, and aimed to examine the specification conditions of the roller guides to achieve both comfortability and durability. Specifically, some experiments to investigate the mechanical properties and durability of the roller guides are conducted.

## 2 ROLLER GUIDES

Much of the vibration in the moving cabin of the lift is attributed to the distortion of the guide rail installed in the lift shaft. Figure 1 shows the structure of lift cabin. The main cause of distortion is low accuracy during installation [1], or distortion due to age [2], and existing lifts require drastic renovation for improvement. The distortion of the guide rail propagates inside the cabin along the roller guides, the frame and the rubber mounts. Figure 2 shows the actual roller guides used for the experimental and analytical investigations.

The roller guides handled here are composed of a coil spring, a control arm and a circular roller. The material of the roller part is natural rubber, but it cracks due to wear and eventually peels off. As a countermeasure, it is common to thoroughly implement preventive replacement to increase hardness and durability.

In this research, vibration and durability problems in the roller guides are focused on, and after replacing the material of the roller part to secure the durability, the specification conditions of the roller guide that is compatible with the riding comfort is aimed to examine. Through the analytical and experimental process, the roller guide that achieves both optimum riding comfort and durability within the range that meets safety regulations is designed. Active roller guides are effective in suppressing vibration significantly, and manufacturers are working on development, but there are problems such as high cost and difficulty in adjustment [3].

In this study, the roller guide system that prioritizes compatibility and improves existing passive roller guides to reduce vibration levels at low cost is developed. In the research, the vibration level at which passengers do not feel uncomfortable sets to rms Acc.  $0.1 \text{ m/s}^2$  [4] and sets a displacement as small as possible that does not make contact with other structures as an allowable limit. The roller guides used in this study have a low flatness as shown in Fig. 2. Since a change in mechanical characteristics due to displacement is expected, loading test using a hydraulic servo actuator is conducted. Furthermore, the roller made by urethane elastomer with hardness of JIS-A standard 95 degrees, which has excellent wear resistance, is prototyped and the same experiment is performed. This material is also used in roller guides for railroad track of public transportation system and play facilities, such as Automated Guideway Transit, roller coaster and so on.



Figure 1 Structure of lift cabin

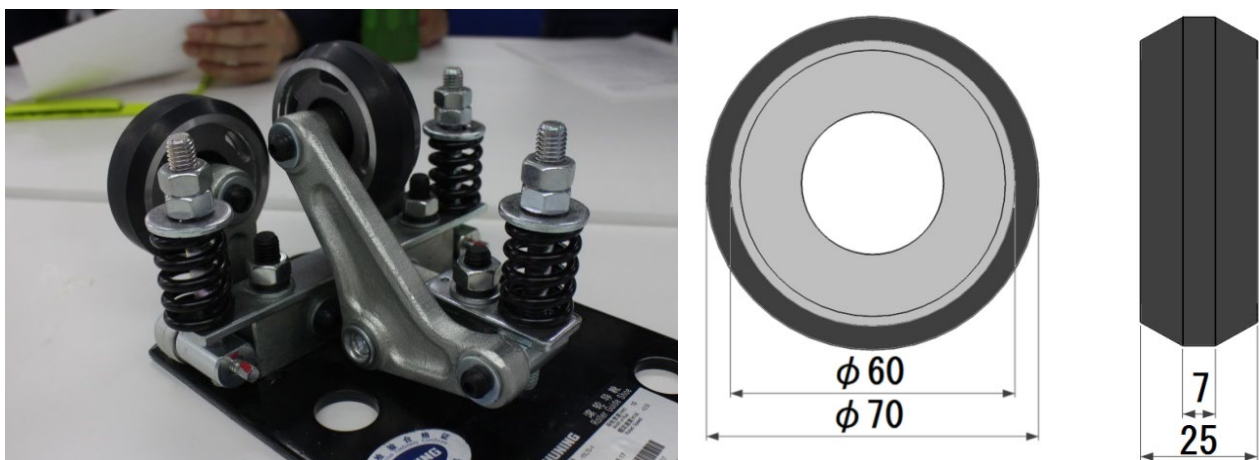


Figure 2 Roller Guides

### 3 ANALYSIS OF LIFT CAR VIBRATION

#### 3.1 Analytical Model

In order to calculate the lateral vibration of the running lift, an analytical model [5] that imitates an actual 6 person ride machine was constructed. In this model, the vibration transmitted from the rail roughness to the cabin via the roller guide, the coil spring, the frame, and the rubber mounts [6] are calculated. An eight-degree-of-freedom analytical model was constructed to calculate the horizontal movement of the four rollers and the horizontal movement and rotation of the frame and cabin. The centre of rotation is same for the frame and the cabin. Waves of the same waveform are input to the upper and lower rollers with a time difference. Acceleration/deceleration of the lift was not included. Figure 3 shows the 8-DOF analytical model. MATLAB2020a was used for the analysis. Figure 4 shows the overview of model.

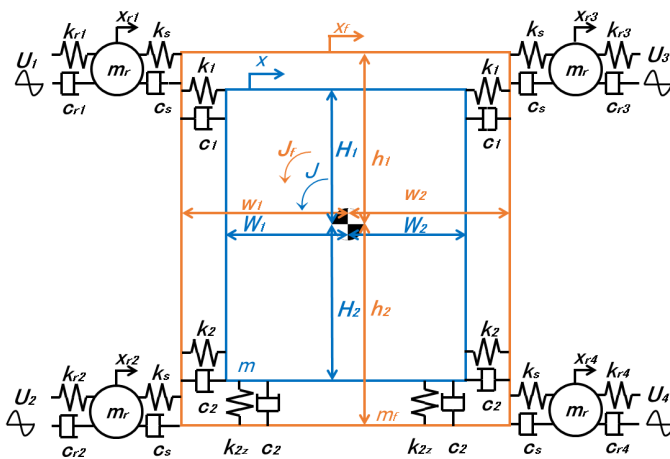


Figure 3 Analytical model

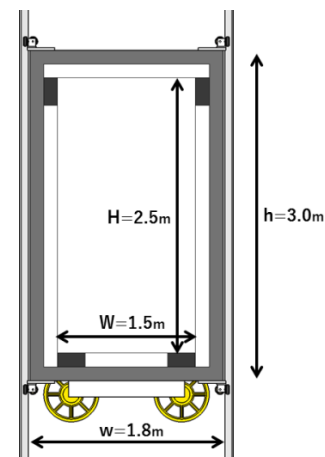


Figure 4 Overview of model

Eq.1 to 8 shows the Equation of Motion (EOM) in this model. In here,

$U_n$ : input displacement,

$k_m$ : stiffness of roller,  $c_m$ : damping coefficient of roller,  $m_r$ : mass of roller,  $x_{r_n}$ : displacement of roller, “n” represents each number from 1 to 4.

$k_s$ : stiffness of coil spring,  $c_s$ : damping coefficient attaching to coil spring,

$k_1$ : stiffness of upper rubber mount,  $c_1$ : damping coefficient of upper rubber mount,

$k_2$ : stiffness of lower rubber mount,  $c_2$ : damping coefficient of lower rubber mount,

$m$ : mass of frame,  $x_f$ : displacement of frame,  $\theta_f$ : rotation of frame,  $J_f$ : Moment of inertia in frame,

$w_1$ : width of frame,  $w_2$ : width of frame,  $h_1$ : height of frame,  $h_2$ : height of frame,

$M$ : mass of cabin,  $x$ : displacement of cabin,  $\theta$ : rotation of cabin,  $J$ : Moment of inertia in cabin,

$W_1$ : width of cabin,  $W_2$ : width of cabin,  $H_1$ : height of cabin,  $H_2$ : height of cabin

In the actual response analysis, the following variables are substituted for the above variables.

$$m = 1200 \text{ kg}, w_1 = 0.9 \text{ m}, w_2 = 0.9 \text{ m}, h_1 = 1.5 \text{ m}, h_2 = 1.5 \text{ m},$$

$$M = 1000 \text{ kg}, W_1 = 0.75 \text{ m}, W_2 = 0.75 \text{ m}, H_1 = 1.25 \text{ m}, H_2 = 1.25 \text{ m}$$

$$k_1 = 400 \text{ N/mm}, k_2 = 400 \text{ N/mm}, k_{2z} = 2000 \text{ N/mm}, c_1 = 400 \text{ N} \cdot \text{s/mm}, c_2 = 400 \text{ N} \cdot \text{s/mm}$$

$$m_r \ddot{x}_{r1} = -k_{r1}(x_{r1} - U_{r1}) - c_{r1}(\dot{x}_{r1} - \dot{U}_{r1}) - k_s(x_{r1} - (x_f - h_1\theta_f)) - c_s(\dot{x}_{r1} - (\dot{x}_f - h_1\dot{\theta}_f)) \quad (1)$$

$$m_r \ddot{x}_{r2} = -k_{r2}(x_{r2} - U_{r2}) - c_{r2}(\dot{x}_{r2} - \dot{U}_{r2}) - k_s(x_{r2} - (x_f + h_2\theta_f)) - c_s(\dot{x}_{r2} - (\dot{x}_f + h_2\dot{\theta}_f)) \quad (2)$$

$$m_r \ddot{x}_{r3} = -k_{r3}(x_{r3} - U_{r3}) - c_{r3}(\dot{x}_{r3} - \dot{U}_{r3}) - k_s(x_{r3} - (x_f - h_1\theta_f)) - c_s(\dot{x}_{r3} - (\dot{x}_f - h_1\dot{\theta}_f)) \quad (3)$$

$$m_r \ddot{x}_{r4} = -k_{r4}(x_{r4} - U_{r4}) - c_{r4}(\dot{x}_{r4} - \dot{U}_{r4}) - k_s(x_{r4} - (x_f + h_2\theta_f)) - c_s(\dot{x}_{r4} - (\dot{x}_f + h_2\dot{\theta}_f)) \quad (4)$$

$$\begin{aligned} m x_f = & -k_s(4x_f - x_{r1} - x_{r2} - x_{r3} - x_{r4}) - c_s(4\dot{x}_f - \dot{x}_{r1} - \dot{x}_{r2} - \dot{x}_{r3} - \dot{x}_{r4}) \\ & + 2k_s(h_1 - h_2)\theta_f + 2c_s(h_1 - h_2)\dot{\theta}_f \\ & - 2(k_1 + k_2)(x_f - x) - 2(c_1 + c_2)(\dot{x}_f - \dot{x}) \\ & + 2(k_1H_1 - k_2H_2)(\theta_f - \theta) + 2(c_1H_1 - c_2H_2)(\dot{\theta}_f - \dot{\theta}) \end{aligned} \quad (5)$$

$$\begin{aligned} J_f \ddot{\theta}_f = & k_s h_1(2x_f - x_{r1} - x_{r3}) - k_s h_2(2x_f - x_{r2} - x_{r4}) \\ & + c_s h_1(2\dot{x}_f - \dot{x}_{r1} - \dot{x}_{r3}) - c_s h_2(2\dot{x}_f - \dot{x}_{r2} - \dot{x}_{r4}) \\ & - 2k_s(h_1^2 + h_2^2)\theta_f - 2c_s(h_1^2 + h_2^2)\dot{\theta}_f \\ & + 2(k_1H_1 - k_2H_2)(x_f - x) + 2(c_1H_1 - c_2H_2)(\dot{x}_f - \dot{x}) \\ & - 2(k_1H_1^2 + k_2H_2^2)(\theta_f - \theta) - 2(c_1H_1^2 + c_2H_2^2)(\dot{\theta}_f - \dot{\theta}) \\ & - k_2(W_1^2 + W_2^2)(\theta_f - \theta) - c_2(W_1^2 + W_2^2)(\dot{\theta}_f - \dot{\theta}) \end{aligned} \quad (6)$$

$$\begin{aligned} M \ddot{x} = & -2(k_1 + k_2)(x - x_f) - 2(c_1 + c_2)(\dot{x} - \dot{x}_f) \\ & + 2(k_1H_1 - k_2H_2)(\theta - \theta_f) + 2(c_1H_1 - c_2H_2)(\dot{\theta} - \dot{\theta}_f) \end{aligned} \quad (7)$$

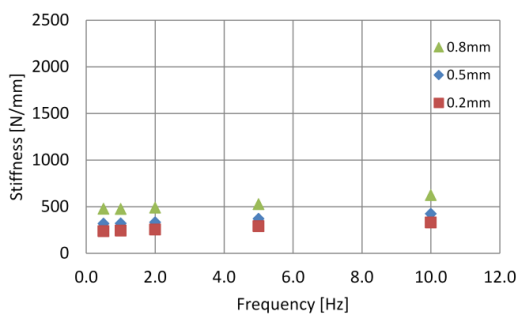
$$\begin{aligned} J \ddot{\theta} = & 2(k_1H_1 - k_2H_2)(x - x_f) + 2(c_1H_1 - c_2H_2)(\dot{x} - \dot{x}_f) \\ & - 2(k_1H_1^2 + k_2H_2^2)(\theta - \theta_f) - 2(c_1H_1^2 + c_2H_2^2)(\dot{\theta} - \dot{\theta}_f) \\ & - k_2(W_1^2 + W_2^2)(\theta - \theta_f) - c_2(W_1^2 + W_2^2)(\dot{\theta} - \dot{\theta}_f) \end{aligned} \quad (8)$$

### 3.2 Modeling on mechanical characteristics for the roller guides

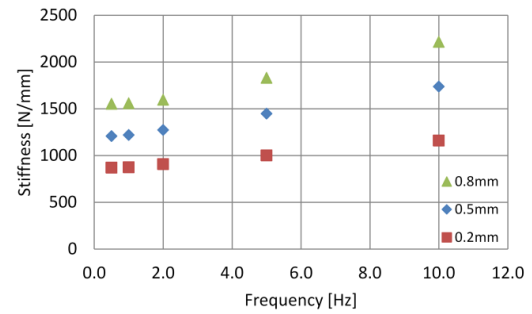
The response displacement of the commonly used rubber roller (hereinafter called “rubber roller”) and the prototyped urethane roller (hereinafter called “urethane roller”) with increased hardness, the stiffness and the damping coefficient dependence on the vibration frequency and displacement, are investigated. In these experiments, mechanical characteristics for the roller guides in a loading experiment [7,8] using a hydraulic servo actuator is investigated, and an operation test using a miniature test apparatus is evaluated. Figures 5 and 6 shows the experimental results. The hardness

and damping coefficient of the urethane roller are about 3 times that of the rubber roller. In addition, the amplitude dependence, which is a characteristic of urethane elastomer with hardness of JIS-A standard 95 degrees, was confirmed.

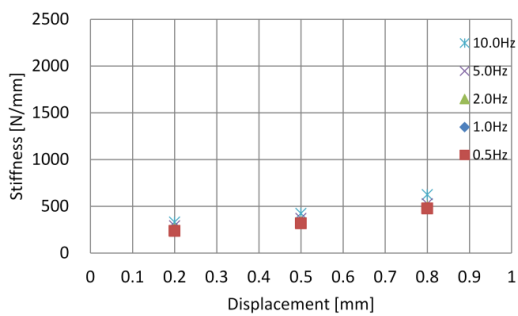
The dependency functions for mechanical characteristic of roller guide in amplitude-dependency and frequency-dependency are obtained from the experimental results. Eq.9 to 12 shows the mechanical characteristics for the roller guides. These formulas are derived from the amplitude dependency and frequency dependency obtained from the loading test of the roller guide. Therefore, in this formula, if the arbitrary frequency and amplitude are substituted as variables, the stiffness and damping coefficient under arbitrary condition are calculated.



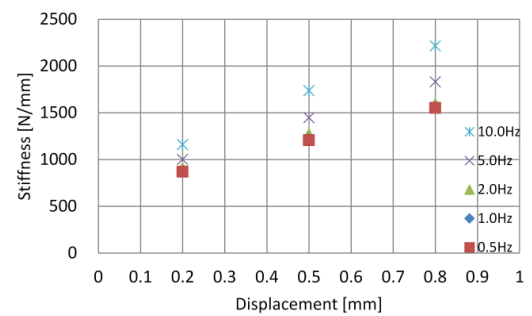
(a) Frequency dependency on stiffness in rubber roller



(c) Frequency dependency on stiffness in urethane roller

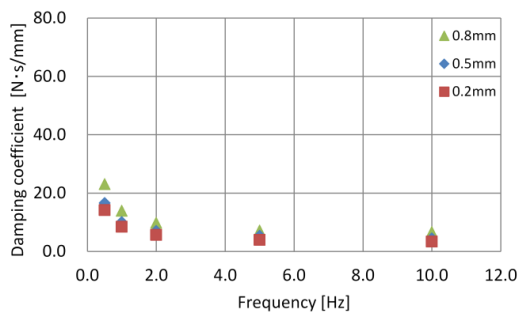


(b) Displacement dependency on stiffness in rubber roller

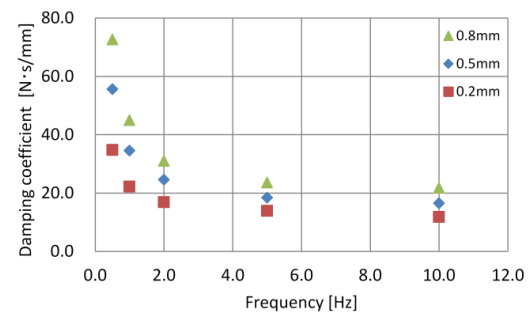


(d) Displacement dependency on stiffness in urethane roller

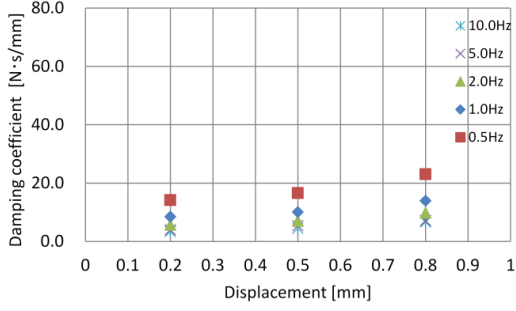
**Figure 5 Comparison between stiffness of rubber roller and urethane roller**



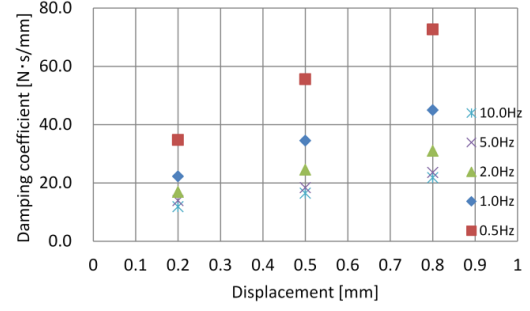
(e) Frequency dependency on damping coefficient in rubber roller



(g) Frequency dependency on damping coefficient in urethane roller



(f) Displacement dependency on damping coefficient in rubber roller



(h) Displacement dependency on damping coefficient in urethane roller

**Figure 6 Comparison between damping coefficient of rubber roller and urethane roller**

In here,  $x_i$ : displacement of input wave [mm],  $f_i$ : vibration frequency [Hz]

Rubber roller

$$k_r = (9.76 f_i + 377) x_i + 7.43 f_i + 148 \text{ [N / mm]} \quad (9)$$

$$c_r = 9.96 f_i^{-0.337} x_i + 6.54 f_i^{-0.525} \text{ [N·s/mm]} \quad (10)$$

Urethane roller

$$k_r = (68.1 f_i + 1060) x_i + 19.2 f_i + 637 \text{ [N / mm]} \quad (11)$$

$$c_r = 39.2 f_i^{-0.465} x_i + 16.2 f_i^{-0.277} \text{ [N·s/mm]} \quad (12)$$

### 3.3 Analytical Result

The vibration reduction effect of the lift cabin is verified using the analytical model introduced in 3.1. Although the running speed set to be arbitrarily in the analytical model, this time it was set to 105m/min as a medium speed. The running speed affects rail bends and interval of gap. Figure 7 shows the input waveform. It is difficult to measure the actual roughness of the rail. Instead of this, the artificial synthetic wave was used to simulate various irregularities of roughness on the rail. Since the main component of the waveform is 5Hz on the left side figure and 2Hz on the right side figure, the parameter  $f_i$  that affects the stiffness and damping of the roller is adjusted to these dominant frequencies. The parameter  $x_i$  changes moment by moment according to the displacement of input. The max displacement of rail roughness is 0.1mm. The wave inputs to the upper, lower, left and right rollers. Furthermore, a sinusoidal wave simulating a maximum rail distortion of 3 mm was synthesized on one side, and the 0.5mm gap was synthesized on both sides. Acceleration on the cabin floor:  $\ddot{x} + H_2 \cdot \ddot{\theta}$ , Displacement:  $x$ , and Rotation:  $\theta$  of the cabin part are obtained by response analysis. Figure 8 shows the vibration waveform when a rubber roller and a urethane roller are installed. The installation of urethane guide rollers improves the strength more than rubber rollers, but the riding comfort may deteriorate, so it is necessary to consider the concept of damping of the entire system. The periodic fluctuations of displacement and rotation are the effects of rail distortion. In the next step, a coil spring is installed between the roller and the cabin to reduce response vibration. Figures 9 and 10 shows the verification of the optimum mechanical characteristics and the vibration waveform at that time. The maximum response of the coil spring stiffness was set to be smaller than

the roller stiffness. Under the condition, the stiffness that satisfies the rms Acc. of  $0.1 \text{ m/s}^2$  is in the range of  $800 \text{ N/mm}$ . It was attempted to reduce vibration by substantially adding damping to the coil spring. As a result, reduction of rms Acc. was confirmed with a damping ratio of 7.5%. Table 1 compares rms Acc. and Max Acc. under each condition. The rms Acc. when using the rubber roller was set to 100% and expressed as the vibration reduction level. As a result, the rms Acc. was reduced by up to 60% by adding the coil spring under the analysis conditions of this time.

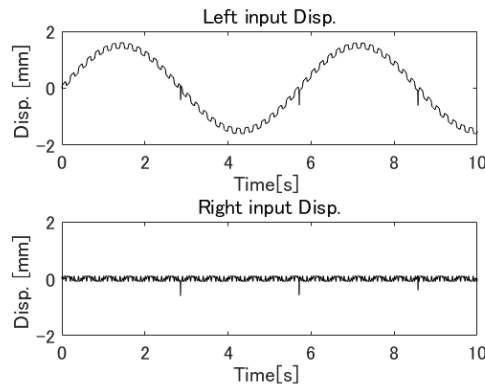


Figure 7 Input waveform

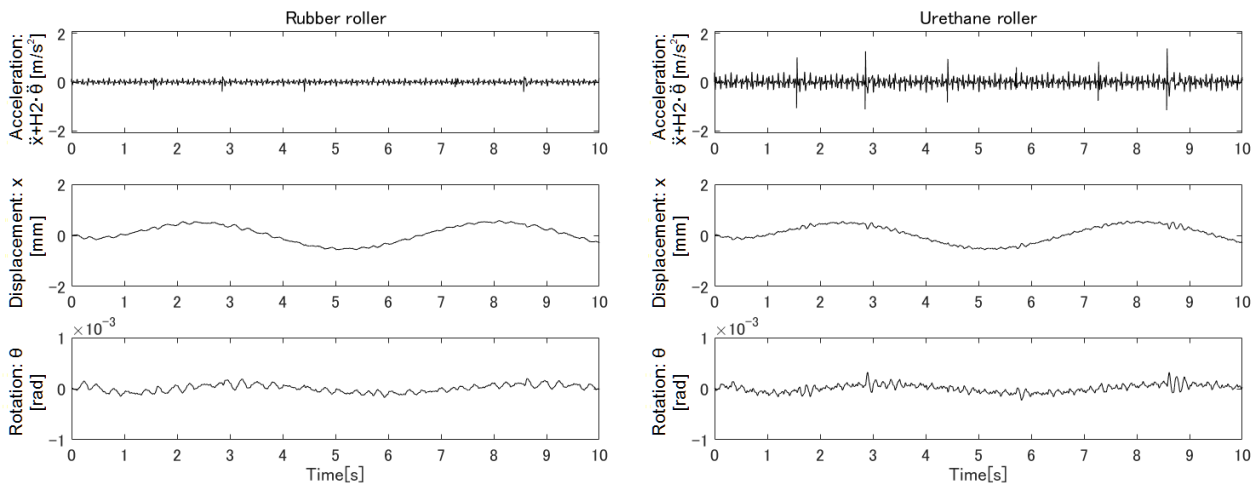
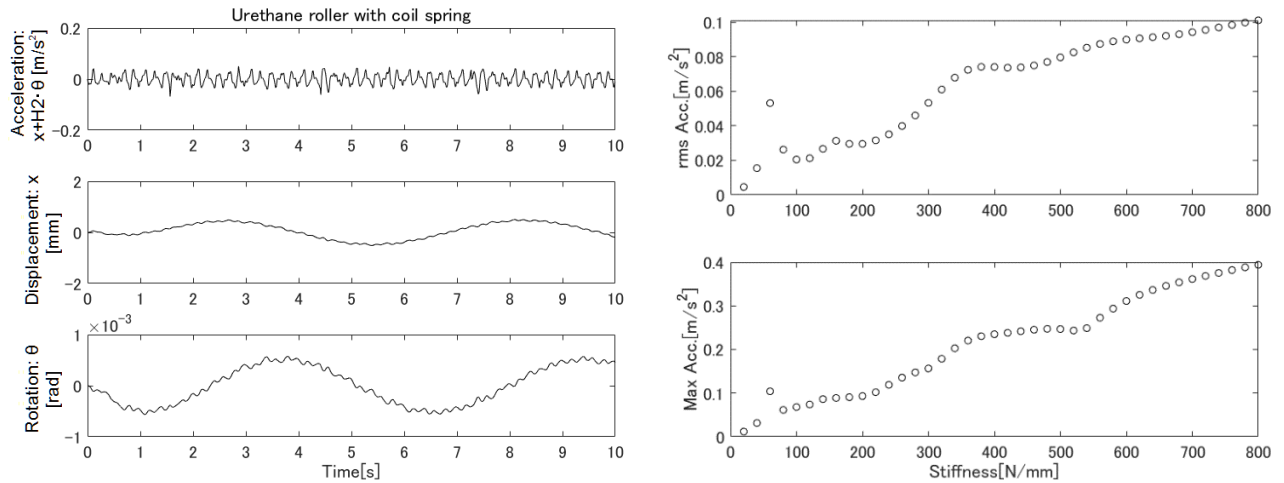
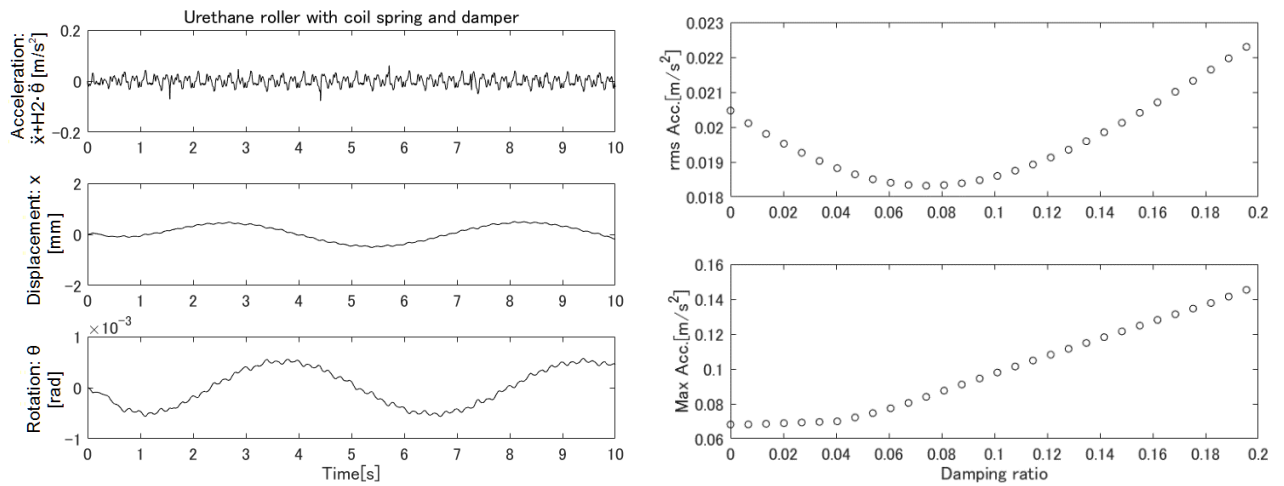


Figure 8 Comparison between rubber roller and urethane roller



**Figure 9 State of optimizing stiffness of coil Spring**



**Figure 10 State of optimizing stiffness of damper**

**Table 1 Response of lift cabin in each situation**

	<b>Rubber roller</b>	<b>Urethane roller</b>	<b>Urethane roller with coil spring</b>	<b>Urethane roller with coil spring and damper</b>
<b>Max Acc. [m/s<sup>2</sup>]</b>	0.400	1.26	0.0682	0.0840
<b>rms Acc. [m/s<sup>2</sup>]</b>	0.0645	0.150	0.0205	0.0183
<b>Vibration level [%]</b>	100	233	31.8	28.4

#### 4 DRIVING EXPERIMENT USING THE MINIATURE TEST SYSTEM FOR ROLLER GUIDES

The experiment using the actual lift is expensive and time-consuming, and it is not realistic to repeat the durability test. In this study, the reduction tester for roller guides was made, and conducted a running test. The experiment equipment consists of a disk that imitates the rail roughness and an iron plate that imitates the cabin. The size of this equipment is 1129 x 930 x 710 mm. By attaching a roller guide to a disk and running it, the horizontal vibration of the cabin and the durability of the roller are verified. Figure 12 shows the overview of the experiment equipment. Shim tape with a width of 10 mm is attached to the disk, and by running in this state, the vibration transmission when overcoming the projection is simulated. The thickness of one shim tape is 0.1mm, and any number of these can be stacked. The cabin can rotate freely in the horizontal and rotational directions by means of linear guides and bearings. An accelerometer (KYOWA AS2GB accelerometer and TEAC es8 data recorder) was attached to the centre of the cabin, and recording was performed at a sampling frequency of 1000Hz. The analytical model is a combination of the frame and cabin of the model introduced in 3.1. Equations (1) to (4) are the same as the model introduced in 3.1, but the equation of the mass part is different. Figure 11 shows the 6-DOF analytical model. Equation (13), (14) shows the equation of motion in mass part.

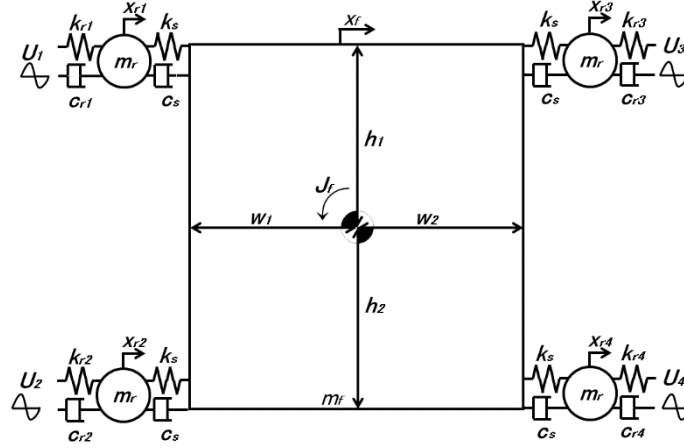


Figure 11 6-DOF analytical model

$$m\ddot{x}_f = -k_s(4x_f - x_{r1} - x_{r2} - x_{r3} - x_{r4}) - c_s(4\dot{x}_f - \dot{x}_{r1} - \dot{x}_{r2} - \dot{x}_{r3} - \dot{x}_{r4}) + 2k_s(h_1 - h_2)\theta_f + 2c_s(h_1 - h_2)\dot{\theta}_f \quad (13)$$

$$J_f\ddot{\theta}_f = k_s h_1(2x_f - x_{r1} - x_{r3}) - k_s h_2(2x_f - x_{r2} - x_{r4}) + c_s h_1(2\dot{x}_f - \dot{x}_{r1} - \dot{x}_{r3}) - c_s h_2(2\dot{x}_f - \dot{x}_{r2} - \dot{x}_{r4}) - 2k_s(h_1^2 + h_2^2)\theta_f - 2c_s(h_1^2 + h_2^2)\dot{\theta}_f \quad (14)$$

Parameter used in the model:  $m = 15$  kg,  $w_1 = 0.125$  m,  $w_2 = 0.125$  m,  $h_1 = 0.115$  m,  $h_2 = 0.115$  m

Figure 13 shows the input waveform and analysis and test results. The waveform that reproduced the protrusion was input to the analysis program for the actual machine and compared with the test results. When comparing the experiment results and the analysis results, the peak waveform periods are shifted. This is probably because the rotation of the disk is unstable due to insufficient torque of the induction motor on the equipment. Although there are other differences in acceleration levels that are thought to be due to the shim mounting method, the reproducibility is generally good, and it can be

used to develop elements such as rollers and springs. In the future, conducting a verification experiment to verify the optimum value calculated using the analysis model and conducting a durability test of roller guides made of different materials are considered.

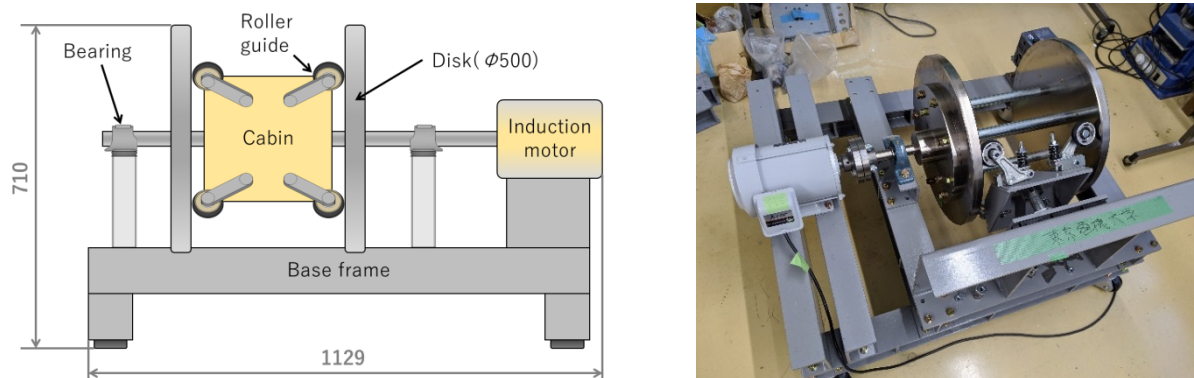


Figure 12 Overview of equipment

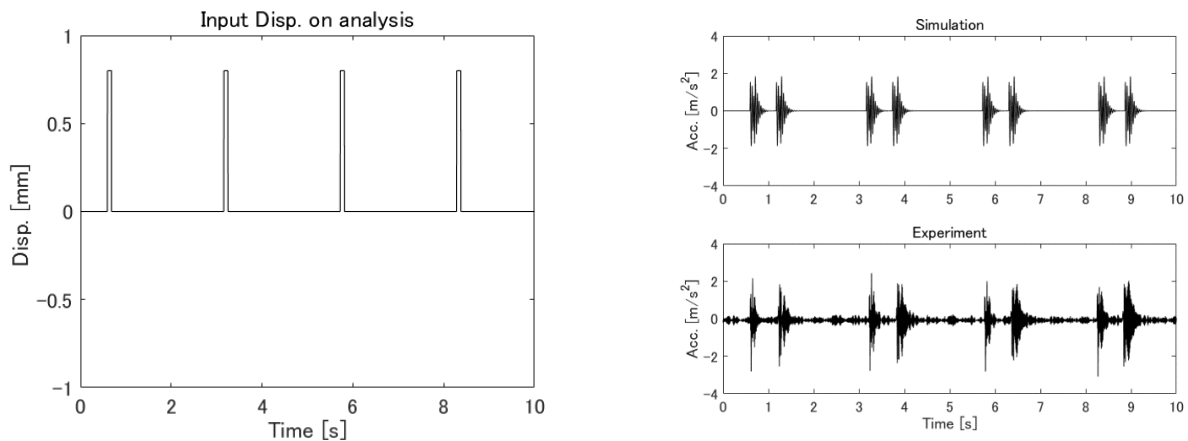


Figure 13 Experiment and Analysis result

## 5 CONCLUSION

In this study, in order to improve the durability of the roller guides and enhance the vibration reduction effect, a simulation analysis was performed using an 8-DOF analysis model. As a result, it was confirmed that the vibration can be sufficiently reduced to 87.7% at maximum by using the coil spring and the damping even if the roller hardened to enhance the durability is used. The Acc. at this time is much lower than  $0.1\text{m/s}^2$ , and it is thought that a comfortable ride for passengers can be realized.

This time, the stiffness of the coil spring was calculated within the range of less than  $800\text{ N/mm}$ . In general, the weight of the cabin is lighter and the response tends to be larger when the number of passengers is smaller than when the passengers are full. The rms Acc. is less than the standard  $0.1\text{ m/s}^2$  even when there is no load. The key point for vibration reduction when using a urethane roller with enhanced durability is the setting of coil spring. Also, by adding damping, it is possible to further suppress rms Acc. while maintaining the same Max Acc. In the actual lift, the stroke of the coil spring is limited because the frame does not come into contact with other structures. In consideration of the deviation of the riding position and the disturbance such as earthquake, the stiffness is set to be larger than the value that can suppress the vibration in the analysis to the greatest extent. In addition, the

waveform used in the simulation is a little worse than that expected in the actual machine, but it can satisfy the ride comfort sufficiently.

Also, a reduction test device for roller guides was manufactured for the durability test. Here, a rail roughness including protrusions was reproduced by placing shims on the surface of the device. Comparing the operation test results with the analytical model simulation results, the reproducibility is generally good despite some problems, and it is considered that it can be used for the element development of rollers and springs.

In the future, a durability experiment of the roller guide using a reduction tester and verifying the vibration reduction effect of the coil spring with damping will be performed. By installing the spring, it can be expected to greatly reduce both acceleration and displacement. Particularly effective in situations where the rail roughness is bad (rough) as verified by simulation. Also, the response in a driving process from start-up to stop will be investigated including increase/decrease of load/eccentricity.

## REFERENCES

- [1] Satoshi Fujita, Hiroshi Kamaike, Motoo Shimoaki, and Keisuke Minagawa, "Elevator and Escalator Engineering", 156-160, (2019) (in Japanese)
- [2] Nobuyoshi Mutoh, Kenkichi Kagomiya, Toshiaki Kurosawa, Masahiro Konya, and Takeki Andoh, "Horizontal Vibration Suppression Method Suitable for Super-High-Speed Elevators", *Transactions on Electrical and Electronic Engineering*, Vol.118-D, No.3, (1998) (in Japanese)
- [3] Naoaki Noguchi, Atsushi Arakawa, Koichi Miyata, Takuya Yoshimura and Seiichi Shin, "Study on Active Vibration Control for High-Speed Elevators". *Journal of System Design and Dynamics*, Vol.5, No.1, 164-179 (2011).
- [4] Kiyoshi Funai, "Technologies of Safety and Ride Comfort for Elevators". *International Association of Traffic and Safety Sciences*, Vol.27, No.2, 31-39 (2002) (in Japanese)
- [5] Hiroyuki Kimura, Mimpei Morishita, Shigeo Nakagaki, "Simulation Techniques for Elevators", *TOSHIBA Review*, Vol.58, 42-45,(2003) (in Japanese)
- [6] Aritomo Nakano, "Types and properties of anti-vibration materials", *Journal of environmental conservation engineering*, Vol.20, No.6, 400-402, (1991) (in Japanese)
- [7] Kazuhito Misaji, Hideki Kato, and Koichi Shibata, "Vibration Analysis of Rubber Vibration Isolators of Vehicle Using the Restoring Force Model of Power Function Type", *Transactions of the Japan society of mechanical engineers. C*, Vol.60, No.578, 679-685, (1994)
- [8] Satoshi Fujita, Osamu Furuya, Yoji Suizu, Yasuhiro Kasahara, Takayuki Teramoto, Haruyuki Kitamura, "Vibration Control of High-Rise Buildings using High-Damping Rubber Damper (2nd Report, Loading Tests and Design Formula for Cylinder-Type High-Damping Rubber Damper)", *Transactions of the Japan society of mechanical engineers. C*, Vol.61, No.585, 1885-1890, (1995) (in Japanese)

## **ACKNOWLEDGEMENT**

The 8-DOF analytical model used in the paper was constructed in cooperation with Mr. Yuya Tase and Mr. Reoya Namiki, Tokyo Denki University. Urethane roller used in the paper was produced by OHTSU CHEMICAL Co., LTD. Reduction tester for roller guides used in the paper was produced by SEC ELEVATOR Co., LTD. The authors would like to express their appreciation for the precious support.

## **BIOGRAPHICAL DETAILS**

Yosuke Shima is master's course student in mechanical engineering of Tokyo Denki University. He researches vibration reduction of lift cabin.

Prof. Osamu Furuya is Professor in Tokyo Denki University. Recently main research object is research and development of vibration reduction for various structures and seismic safety for important facilities.

# Study on Behavior of Escalator During Earthquake

Nayuta SUDO<sup>1</sup>, Satoshi FUJITA<sup>2</sup>, Keisuke Mori<sup>2</sup>, Izumi Nakamura<sup>3</sup>, Shigeki Okamura<sup>4</sup>

<sup>1</sup>Graduate School of Tokyo Denki Univ. Dept. of Mechanical Engineering, Japan

<sup>2</sup>Mitsubishi Electric Corporation Advanced Technology R&D Centre

<sup>3</sup>National Research Institute for Earth Science and Disaster Resilience

<sup>4</sup>Toyama Prefectural University

**Keywords:** Escalator, Quake-resistance, Seismic analysis, non-linear analysis, Seismic evaluation.

**Abstract.** Fall accidents of escalators occurred in 2011, in an earthquake off the Pacific coast of Tohoku. The escalators where the accidents occurred was connecting the second floor to the third floor in commercial facilities of a steel frame building. In general, escalators are set on beams of buildings. Furthermore, one side or both sides of the support are not fixed to prevent damage to the escalator from the interlaminar deformation of the building. However, interlaminar deformation of the building occurred more than expected due to the earthquake. In consequence, the fall accidents occurred because the escalators came off from the beams in the buildings. After the escalator accidents, the seismic standard was revised in Japan. The interlayer displacement angle of buildings is now considered more than before. From this, the overlap allowance is longer, so the possibility of the fall accidents decreases. However, an unfixed part of the escalator may collide with a building beam due to an earthquake. Furthermore, the escalator may transform by the collision and affect their safety. In this study, the dynamic behavior of escalators with building beams during earthquakes are investigated, furthermore, the safety against the revised earthquake resistance standards are confirmed. In this paper, the analysis methods for the safety evaluation is investigated in a three meter lift escalator, which has fallen due to an earthquake. The 3/10 scale model is based on the three meter lift escalator which a top that is not fixed was created. Further, the vibration experiment with the 3/10 scale escalator model was carried out. The behavior of the 3/10 scale escalator model was confirmed during the earthquakes. Moreover the seismic response analysis was carried out with the lumped mass models. The restoring force characteristics of the escalator were modeled in two different methods. The validity of the analysis model was confirmed by comparing the analysis results with the experimental results.

## 1 INTRODUCTION

An escalator is one of the transport equipments that moves people vertically. The escalator is installed in the building and connects floors to other floors. In general, escalators are not fixed to building beams on one or both sides to prevent damage from deformation. However, in the 2011 earthquake off the Pacific coast of Tohoku, four escalator fall accidents occurred [3]. These fall accidents occurred in an escalator installed in a commercial facility of a steel frame building that connected the third floor and the second floor. The fall accident was caused when the escalator was removed from the beam of the building more than expected due the large earthquake. After the escalator accidents, the quake resistance standard was revised in Japan. According to this standard, the layer displacement of buildings to be expected during earthquake is more than before. The layer deformation design angle before the revision of the quake resistance standard had been less than 1/100 [rad]. However, the layer deformation design angle after the revision of the quake resistance standard was 1/40 [rad] in principle. It was 1/24 [rad] when the structural calculation was not done. As a result, the length required for falling accidents was improved. However, the building may be greatly deformed. Furthermore, the escalator may collide with the supporting part of the building due to the increase of the design interlayer deformation angle. In this study, the dynamic behavior of escalators including the collision phenomenon during earthquakes is comprehended. In this paper, a dynamic experiment

is performed with a 3/10 scale escalator truss. Further, a dynamic analysis is performed with two different methods, which are the bilinear model and the differential equation model.

## 2 ESCALATOR DESIGN POLICY

The diagrammatic view of the escalator is shown in Figure 1. The escalator consists of steps, handrails, transport equipment parts and a truss which supports these transportation parts [4]. The overlap between the escalator truss and the building prevents the damage of the escalator by the interlayer deformation. As shown in equation (1), (2) and (3), the length of the overlap allowance is determined by an escalator technology standard in Japan.  $C$  is the gap between the beam of the building and the escalator,  $H$  is the height,  $\gamma$  is the layer deformation angle of building and 20 [mm] is margin of the overlap allowance.

$$B \geq \Sigma\gamma H + 20 \quad (\Sigma\gamma H - C \leq 0) \quad (1)$$

$$B \geq \Sigma\gamma H + 20 \quad (0 \leq \Sigma\gamma H - C \leq 20) \quad (2)$$

$$B \geq 2\Sigma\gamma H - C \quad (20 < \Sigma\gamma H - C) \quad (3)$$

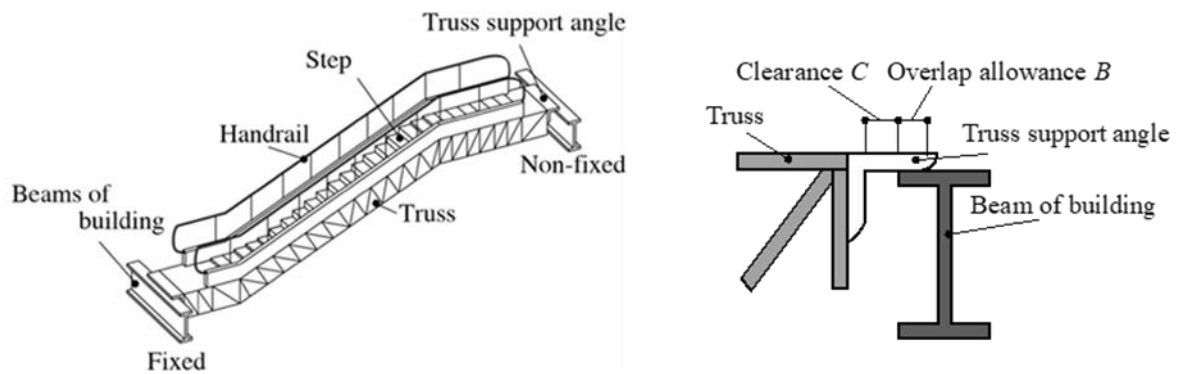


Figure 1 Escalator system and the non-fixed side of the escalator

## 3 VIBRATION EXPERIMENT

A vibration experiment with a 3/10 scale model was conducted. In this experiment, the escalator collides with the building model with the seismic waves. The behavior of the escalator including the collision phenomenon is confirmed.

### 3.1 Specimen

The specimen of the vibration experiment is shown in Figure 2. This specimen is composed of an escalator model and buildings model. This model is a 3/10 scale model of a 3 meter lift escalator where a fall accident occurred. The 3/10 scale model of the escalator uses the similarity rules in Table 1. In Table 1, the subscript f indicates the full scale, further the subscript m indicates after the similarity law. The characteristic of the escalator model and the building model is shown in Table 2. The natural frequency of the escalator period is 0.049 sec. The natural frequency of the building model is 0.223 [s].

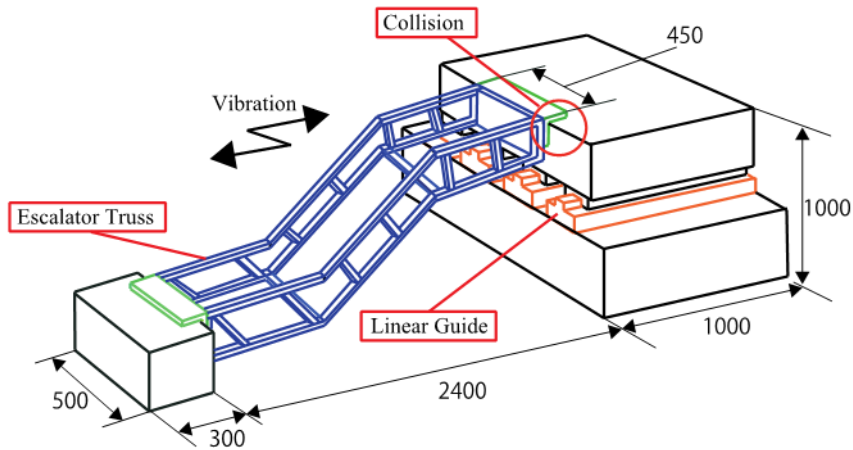


Figure 2 Schematic of specimen

Table 1 Parameter of 0.3 scale models

Length	Mass
$L_m=0.3L_f$	$M_m=0.3^3M_f$

Table 2 Parameter of 0.3 scale models

Escalator				Building		
Mass	1st stiffness	2nd stiffness	Yield disp.	Mass	1st stiffness	Natural period
$m_e$ [kg]	$k_{e1}$ [N/m]	$k_{e2}$ [N/m]	$x_y$ [m]	$m_s$ [kg]	$k_{s1}$ [N/m]	$T_s$ [s]
400	$6.67 \times 10^6$	$-2.4 \times 10^6$	0.0075	2000	$1.59 \times 10^6$	0.223

### 3.2 Input seismic wave

The input seismic wave is shown in Figure 3 [5]. The input seismic waves, which are used in vibration experiments, are scaled by a similarity law with a constant velocity. Accordingly, the acceleration, it is 3.3 times the observed seismic wave moreover 0.3 times the time. In this paper, 0.3 scale of the JMA Kobe NS 25 [kine] and 50 [kine] was used. ([kine] = [cm/s])

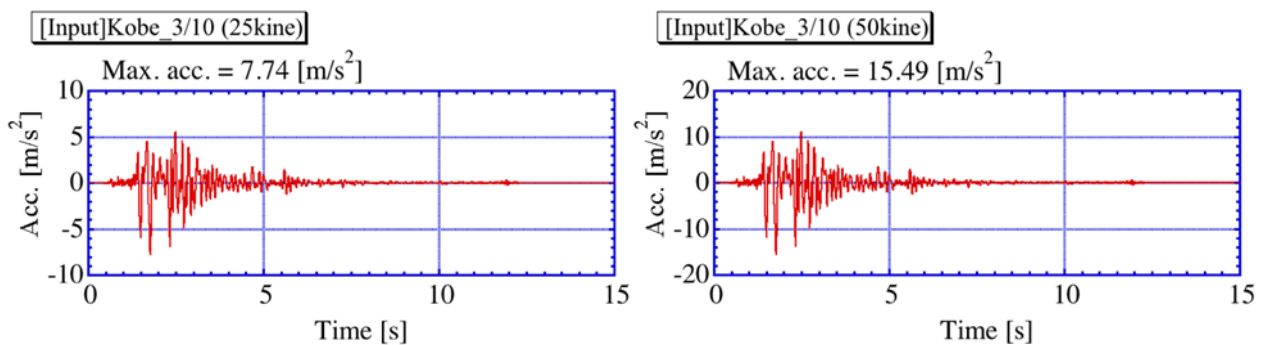


Figure 3 Time history wave the JMA Kobe NS 25 kine and 50 kine

### 3.3 Results of seismic experiments

In the experiment, the acceleration of the shaking table was measured as the input acceleration. The building displacement was measured. Furthermore, the relative displacement between the building and the escalator was measured. In addition, the internal stress of the escalator was measured. The escalator displacement is calculated from the building displacement and the relative displacement. The seismic response in the experiment is shown in Figure 4. The figure shows the experimental results of the non-collision case, the collision case and the buckling case. Additionally, the figure shows the input acceleration, the displacement and the restoring force. In non-collision case, the maximum relative displacement is approximately 23 [mm]. The maximum relative displacement and the maximum building displacement are almost the same. The maximum escalator displacement is less than 1 mm. The escalator displacement is negligible in relative displacement. The relative displacement is mainly the building displacement. Similarly, when a collision occurs, the relative displacement and the building displacement are almost the same. The maximum escalator displacement is approximately 2.5 [mm]. The escalator displacement of the collision case increased than that of the non-collision case. On the other hand, the relative displacement is approximately 25 mm. Regardless of the collision, the relative displacement is mainly the building displacement. In the restoring force characteristics, the deformation does not reach the secondary stiffness. When buckling occurred, the relative displacement exceeded the measurement range. The input wave is more than twice the other two conditions. The building displacement is approximately twice that of the non-collision case. The ratchet deformation occurred in the compression direction on the escalator. Accordingly, the ratchet displacement occurred on the relative displacement. When buckling occurs, the relative displacement is a combination of the building displacement and the escalator displacement. The buckling of the escalator is important in assessing relative displacement. The restoring force characteristic reaches the range of secondary stiffness.

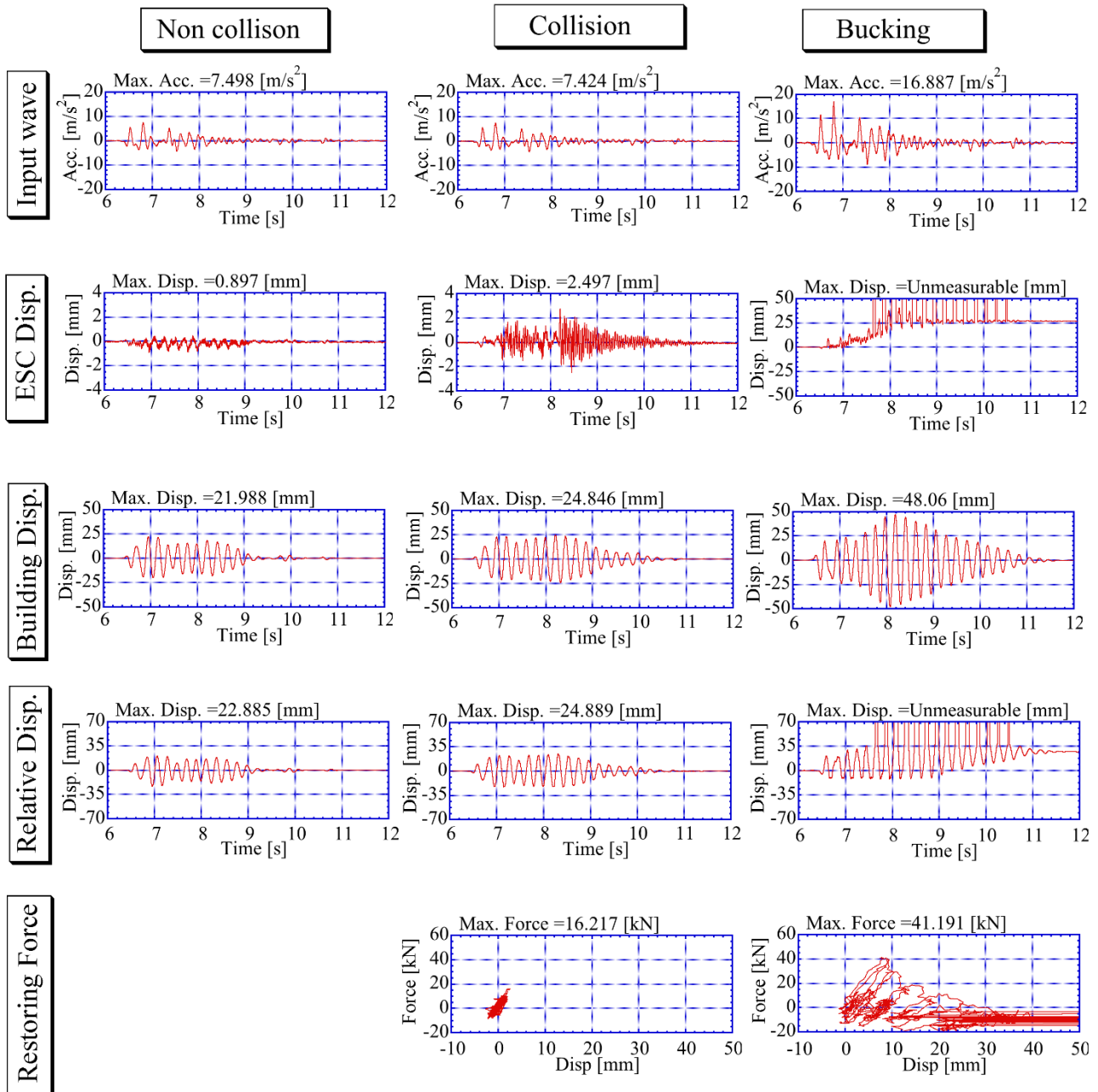


Figure 4 Seismic response experiment result

## 4 DYNAMIC ANALYSIS

### 4.1 Motion equation

#### 4.1.1 Bilinear model

In this analysis, the escalator and the building are each one mass models. In order to reproduce the displacement after buckling, the restoring force of the escalator is modeled by a bilinear model. The analytical model is shown in Figure 5. The characteristics of the escalator trusses and the building is shown in Table 2. In this analysis model, the collision is reproduced by the collision stiffness between the escalator model and the building model. The motion equations are classified into two cases. One is the non-collision case, another is the collision case. In the non-collision case, the motion equations of the escalator model and the building model are the equations (4) and (5). In the collision case, the motion equations are the equations (6) and (7). The transition condition is equation (8). The restoring force of the escalator model is equation (9) and (10). When the escalator displacement exceeded the yield displacement, the stiffness switches. Here,  $m$  is the mass,  $c$  is

the damping,  $k$  is the stiffness, and  $F$  is restoring force. Moreover, the subscript  $e$  is the escalator, the subscript  $s$  is the building, and the subscript  $c$  is the collision stiffness.

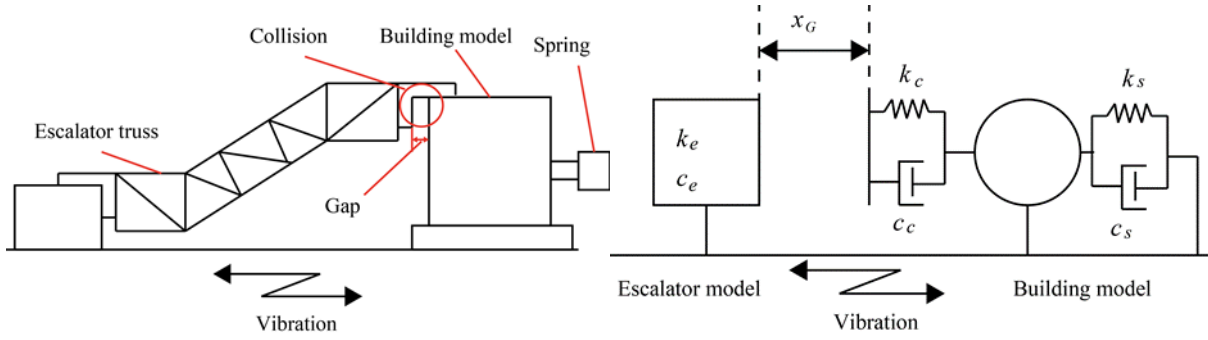


**Figure 5 Analytical model image**

Non collision case

$$\text{Escalator :} \quad m_e(\ddot{x}_e + \ddot{z}) + c_e\dot{x}_e + F_e = 0 \quad (4)$$

$$\text{Building :} \quad m_s(\ddot{x}_s + \ddot{z}) + c_s\dot{x}_s + k_sx_s = 0 \quad (5)$$

Collision case

$$\text{Escalator :} \quad m_e(\ddot{x}_e + \ddot{z}) + c_e\dot{x}_e + F_e + k_c(x_e - x_s - x_G) + c_c(\ddot{x}_e - \ddot{x}_s) = 0 \quad (6)$$

$$\text{Building :} \quad m_s(\ddot{x}_s + \ddot{z}) + c_s\dot{x}_s + k_sx_s - k_c(x_e - x_s - x_G) - c_c(\ddot{x}_e - \ddot{x}_s) = 0 \quad (7)$$

Transition condition case

$$x_G > x_e - x_s \quad (8)$$

$$\text{Restoring force :} \quad F_{e1} = k_{e1}x_e \quad (9)$$

$$\text{After yield restoring force :} \quad F_{e2} = k_{e2}x_e \quad (10)$$

#### 4.1.2 Differential equation model

In this analysis, as in Chapter 4, the escalator and the building are used as mass models. In order to reproduce the displacement after buckling, the restoring force of the escalator is modeled by a differential equation [7]. The characteristics of the escalator trusses and buildings are shown in Table 2. The motion equations are classified into two cases. One is the non-collision case, another is the collision case. In the non-collision case, the motion equations of the escalator model and the building model are the equations (11) and (12). In the collision case, the motion equations are the equations (13) and (14). The restoring force of the escalator model is equation (15). Here,  $m$  is the mass,  $c$  is the damping,  $k$  is the stiffness, and  $F$  is restoring force. Moreover, the subscript  $e$  is the escalator, the subscript  $s$  is the building, and the subscript  $c$  is the collision stiffness.  $T(x)$ ,  $G(x)$  and  $n$  are determined by the resilience properties obtained in the experiment. The values are shown in Table 3.

Non collision case

$$\text{Escalator :} \quad m_e(\ddot{x}_e + \ddot{z}) + c_e\dot{x}_e + F_e = 0 \quad (11)$$

$$\text{Building :} \quad m_s(\ddot{x}_s + \ddot{z}) + c_s\dot{x}_s + k_sx_s = 0 \quad (12)$$

Collision case

$$\text{Escalator : } m_e(\ddot{x}_e + \ddot{z}) + c_e\dot{x}_e + F_e + k_c(x_e - x_s - x_G) + c_c(\ddot{x}_e - \ddot{x}_s) = 0 \quad (13)$$

$$\text{Building : } m_s(\ddot{x}_s + \ddot{z}) + c_s\dot{x}_s + k_s x_s - k_c(x_e - x_s - x_G) - c_c(\ddot{x}_e - \ddot{x}_s) = 0 \quad (14)$$

$$\dot{F}_e = \left[ \begin{array}{l} \left\{ S_{d1} \cdot K_a + (1 - S_{d1}) \cdot \frac{dT(x)}{dx} \right\} \cdot \frac{1 + \text{sgn}(r_k)}{2} \\ + \left\{ S_{d2} \cdot K_b + (1 - S_{d2}) \cdot \frac{dG(x)}{dx} \right\} \cdot \frac{1 - \text{sgn}(r_k)}{2} \end{array} \right] \cdot \dot{x}_e \quad (15)$$

$$S_{d1} = \text{sgn} \left( \frac{T(x) - F_e}{T(x) - G(x)} \right) \cdot \left( 2 \cdot \left| \frac{T(x) - F_e}{T(x) - G(x)} \right| \right)^{\frac{1}{n}} \quad (16)$$

$$S_{d2} = \text{sgn} \left( \frac{F - G(x)}{T(x) - G(x)} \right) \cdot \left( 2 \cdot \left| \frac{F - G(x)}{T(x) - G(x)} \right| \right)^{\frac{1}{n}} \quad (17)$$

**Table 3 Differential equation parameter**

$T(x)$	$G(x)$	$n$
$102188 \times \exp(-108.8 \times x)$	$-102188 \times \exp(108.8 \times x)$	100

## 4.2 Results of seismic response analysis

### 4.2.1 Results of seismic response analysis with bilinear

The result of the seismic response analysis is shown in Figure 6. The figure shows the analysis results of the non-collision case, the collision case and the buckling case. In the non-collision case, the maximum relative displacement is approximately 25 mm. The maximum building displacement is approximately 25 mm. The maximum escalator displacement is less than 1 mm. In this analysis result, the escalator displacement is negligible in relative displacement. The maximum response value and the waveform trend of the experiment can be reproduced with this analysis. However, convergence after the main motion is slow. When collision occurs, the maximum building displacement is approximately 24 mm. The maximum escalator displacement is approximately 3 mm. As in the experiment, the escalator displacement increases than that of the non-collision case. The maximum response value and the waveform trend of the experiment can be reproduced with analysis. In addition, this analysis reproduces the restoring force. In the buckling case, the maximum building displacement is approximately 38 mm. The relative displacement of this analysis is slightly smaller than that of the experimental. However, the waveform trend can be reproduced. The residual displacement of the escalator is 27 mm. The residual displacement of the relative displacement is 27 mm. This analysis results are the same as the experimental results. In addition, the waveform trend of the analysis can replicate the experiment. The maximum relative displacement in this analysis is approximately 59 mm. The restoring force of this analysis reproduces the tendency of the restoring force of the experiment. Accordingly, the behavior of the building and the escalator during earthquakes can be reproduced with a lumped mass model. The behavior of the escalator after buckling can be reproduced with a bilinear model.

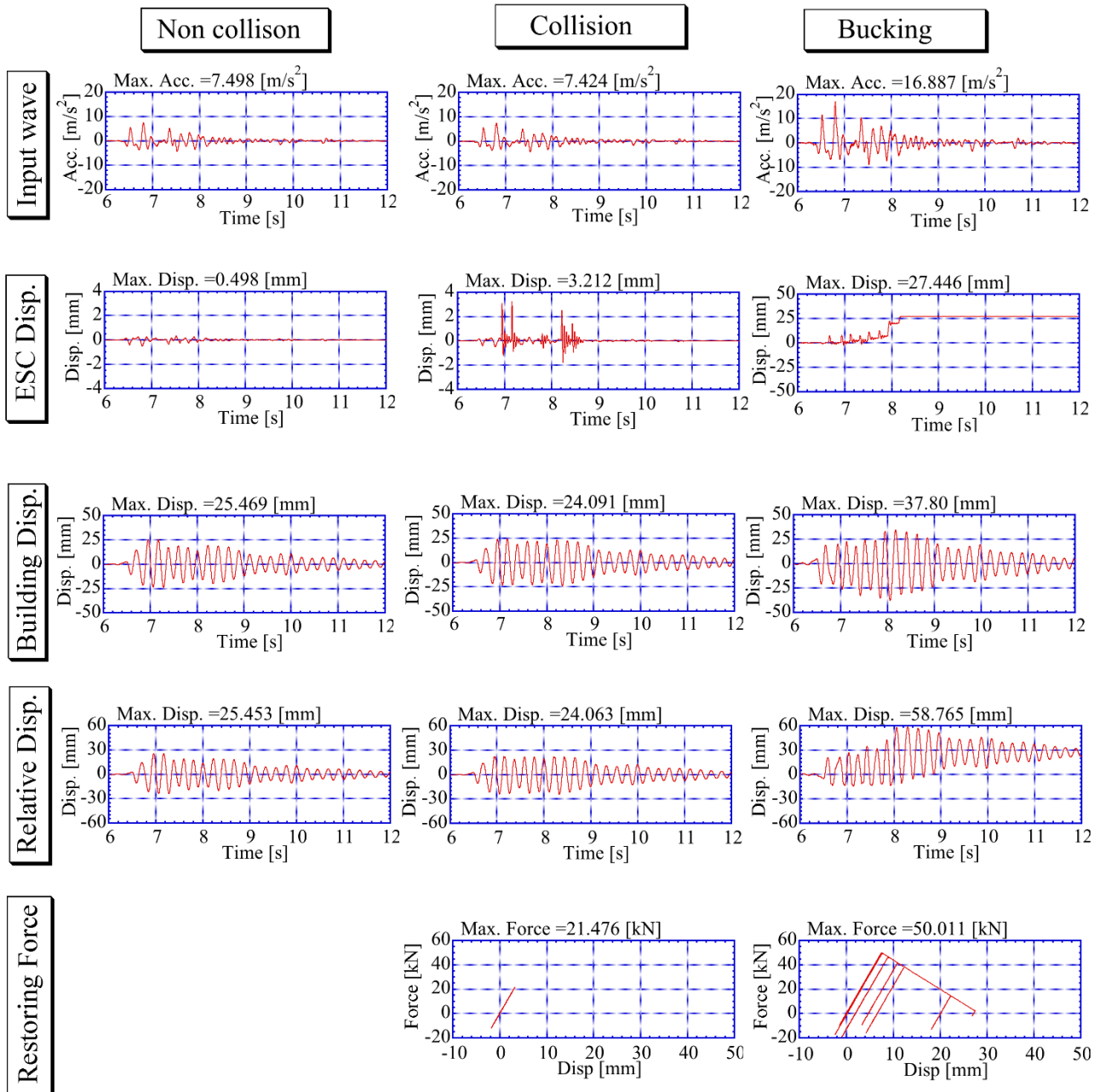


**Figure 6 Seismic response analysis result**

#### 4.2.2 Results of seismic response analysis with differential equations

The result of the seismic response analysis is shown in Figure 7. The figure shows the analysis results of the non-collision case, the collision case and the buckling case. In the non-collision case, the maximum relative displacement is approximately 24 mm. the maximum building displacement is approximately 24 mm. The maximum escalator displacement is less than 1 mm. In this analysis result, the escalator displacement is negligible in relative displacement. The maximum response value and the waveform trend of the experiment can be reproduced with this analysis. When collision occurs, the maximum building displacement is approximately 38 mm. The maximum escalator displacement is approximately 3 mm. As in the experiment, the escalator displacement increases than that of the non-collision case. The maximum response value and the waveform trend of the experiment can be reproduced with this analysis. In addition, the analysis reproduces the restoring force. In the buckling case, the maximum building displacement is approximately 23 mm. The relative displacement of this analysis is slightly smaller than that of the experimental. However, the waveform trend can be

reproduced. The residual displacement of the escalator is 27 mm. The residual displacement of the relative displacement is 27 mm. These analysis results are the same as the experimental results. In addition, the waveform trend of the analysis can replicate the experiment. The maximum relative displacement in the analysis is approximately 60 mm. The restoring force of this analysis reproduces the tendency of the restoring force of the experiment. Accordingly, the behavior of the building and the escalator during earthquakes can be reproduced with a lumped mass model. The behavior of the escalator after buckling can be reproduced with a differential model.

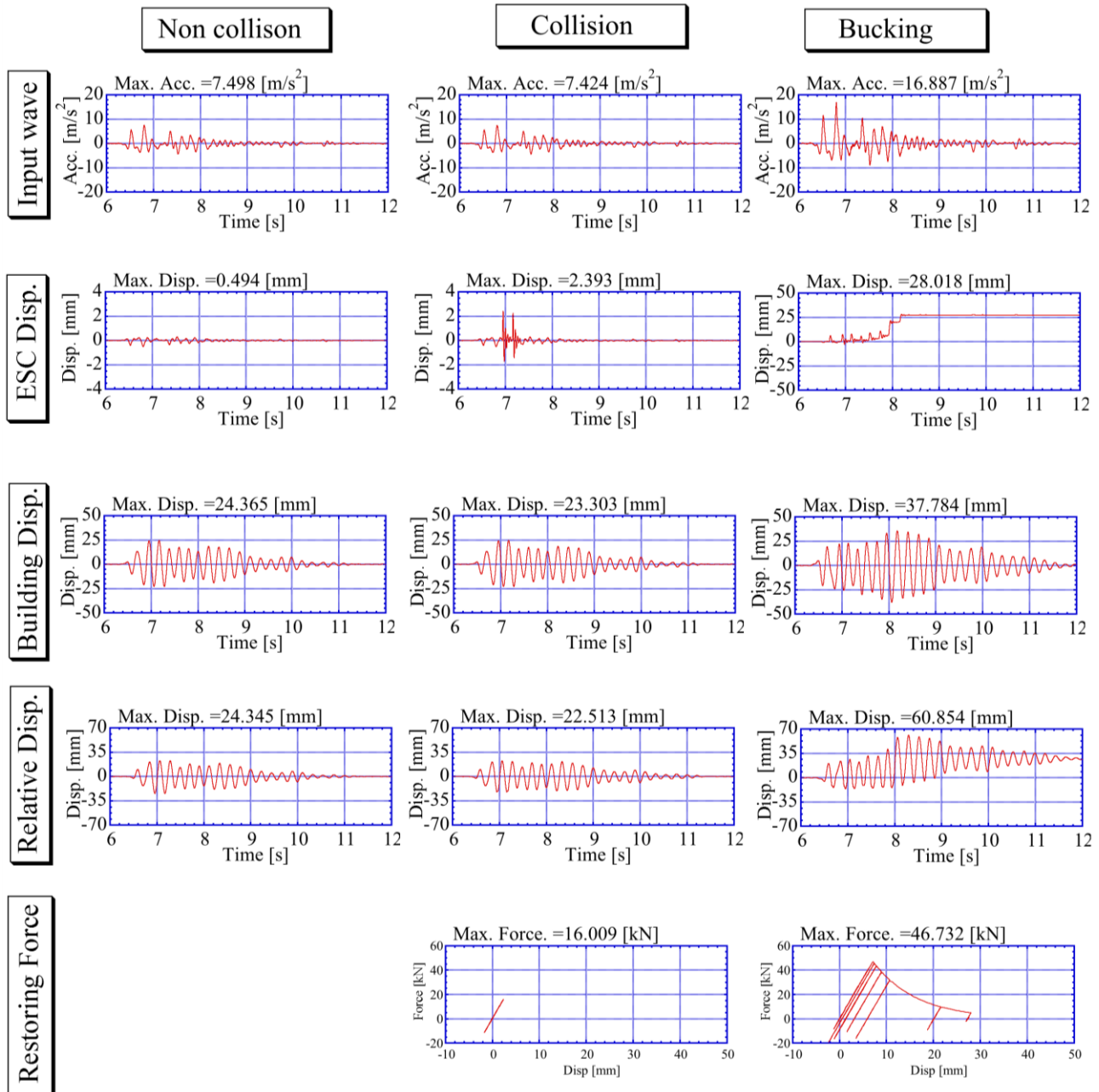


Figure 7 Seismic response analysis result

### 4.3 Comparison of response result at two models

The analytical models were compared. In the non-collision case, the displacement of the building and the displacement of the escalator were the same. Also, in the collision case, the building displacement and the escalator displacement were the same. In the buckling case, the relative displacement is the same, furthermore the maximum value of the response displacement and the tendency of the waveform can be reproduced. Accordingly, both methods are effective for analysis.

## 5 CONCLUSION

In this study, the behavior of the building and the escalator during the earthquake was confirmed with the vibration experiment with the 3/10 scale model. In addition, an analytical model of the escalator including the collision was constructed. The analytical model was studied by modeling the resilience in two different ways. The behavior of the vibration experiment could be reproduced with these analysis models. Furthermore, the restoring force characteristics could be reproduced in the same method. Therefore, the lumped mass model is effective to confirm the behavior of the building and the escalator during earthquakes. The difference of the results with two analytical models are negligible. In addition, a bilinear model and differential equation model is effective to reproducing the behavior of an escalator after buckling.

## REFERENCES

- [1] Tokyo Denki University, Study on ensuring safety of existing escalators against earthquakes, Building standard development promotion project 2014, Survey number:P8, (in Japanese) (2014).
- [2] Keisuke M, Yutaka H, Masahiko N, Takanori Y, Kazutoshi A (2014): Evaluation Method of Residual Load Bearing Capacity for Escalator Truss Structure under Compressive Load Condition.
- [3] Miyata, T., Fujita, S., and Shimoaki, M., Report on Seismic damages of Elevators and Escalators by the Great East Earthquake, Proceedings of the 21th Transportation and Logistics Division Convention No12-79 (2012).
- [4] The Japan building equipment and elevator center foundation, Japan Elevator Association, Elevator/Escalator Engineering Standards 2016version, (2016).
- [5] National research institute for earth science and disaster prevention, Strong-Motion Network (K-NET), available from < <http://www.kyoshin.bosai.go.jp/kyoshin/>>, (accessed on October, 2016).
- [6] Tanaka, Y, Fujita, S, Minagawa, K, Fundamental Study on Development of Simple Analysis Model of Escalator, The Japan Society of Mechanical Engineers, Dynamic and Design Conference, No436 (2014).
- [7] T. Fukazawa, S. Okamura, T. Somaki, T. Miyagawa, T.Yamamoto, T.Watakabe, R. Morobishi and S.Fujita, Proposal of Hysteresis Model using Differential Equation, Struct. Constr. Eng., AIJ, Vol.84, No763, 1231-1241(2019).

## BIOGRAPHICAL DETAILS

Mr Nayuta Sudo is master's course student in mechanical engineering of Tokyo Denki University. He researches vibration behavior of escalator.

# Study on Evacuation Route in Case of Disaster Considering the Fragility of Mechanical Structures

Kazusada Natsu<sup>1</sup> and Osamu Furuya<sup>2</sup>

<sup>1</sup>Graduate School of Tokyo Denki University, Ishizaka, Hatoyama-cho, Hiki-gun, Saitama 350-0394 Japan

<sup>2</sup>Division of Mechanical Engineering, School of Science and Engineering, Tokyo Denki University, Ishizaka, Hatoyama-cho, Hiki-gun, Saitama 350-0394 Japan

**Keywords:** Safety Evacuation, Escalator, Seismic response, Fragility Curve, Dijkstra algorithm

**Abstract.** To improve the evacuation safety of multi-story buildings by escalator, escalator fragility curves were calculated using a probabilistic risk assessment. In order to calculate the damage probability of the escalator and mechanical structure in each story, the time history response analysis of the three storey building model was calculated. A floor model was constructed from graph theory, and a simulation to find a safe evacuation route. The change in the possibility of using the escalator during evacuation due to the revision of the seismic code of the escalator was compared with the old Japanese code in each floor of the building.

## 1 INTRODUCTION

In the earthquake disaster, many industrial facilities suffered frequent equipment damage and their functions stopped. It also led to secondary damage such as breaking of the evacuation route due to falling or scattering of equipment. The seismic code for escalators was revised because of the fall accident of the escalator body in the Great East Japan Earthquake on March 11, 2011. Since the standard was set to make the interstorey drift angle of buildings in the event of an earthquake larger than before, the shortage of the length of the escalator, which is considered to be the main cause of the fall accident, has been improved.

However, the evacuation plan at the time of a disaster is still in accordance with the old seismic standard, and the use of escalators is not stipulated, and it is recommended to avoid using it during evacuation [1]. In many commercial facilities, there is only an escalator in the center of the floor, and the evacuation exit is located far from the center. In such a structure, using an escalator for evacuation can greatly improve safety and efficiency. Therefore, the feasibility of an evacuation plan including an escalator will be examined as a new proposal based on the new standard.

In this research, the durability and the risk (or safety) on the evacuation route were examined by applying the probabilistic risk assessment to the design parameters of escalator and mechanical structures related to evacuation route. The safety of the escalator will be examined by simulating the search for a safe evacuation route in a multi-story building in consideration of the danger of mechanical structures.

## 2 RISK ASSESSMENT

### 2.1 Escalator structure

As shown in Fig.1, the escalator mainly consists of transportation equipment such as steps and handrails, and an escalator truss that supports the transportation equipment. L-shaped support members are attached to both ends of the escalator, and the support members are hung on the building beam and one or both ends are not fixed. Therefore, a supporting method is adopted in which the non-fixed part of the escalator slips during an earthquake and the forced displacement due to the interstorey drift of the building is released [2][3].

In this research, the escalator with fixed lower end and non-fixed upper end, which has the same support method as the escalator in which a fall accident occurs, is targeted. The escalator with fixed lower end and non-fixed upper end is an escalator installed with the supporting member at the lower end of the escalator truss fixed to the building beam and the supporting member at the upper end sliding on the building beam. The part where the support member attached to the escalator truss and the building beam overlap is called the Overlap allowance.

A new standard defines a structure with a low risk of the escalator falling off due to an earthquake or other vibration after the escalator fall accident (Japan Building Equipment/Elevator Center, Japan Elevator Association, 2016). As shown in Table 1, the standard value of the interstorey drift angle before design was 1/100 [rad] or less before revision, whereas the revised standard value was 1/40 [rad], When structural calculation is not performed, it is over 1/24 [rad] [4]. Three standards, 1/100[rad], 1/40[rad], 1/24[rad], are set as Old standard, New standard1, New standard2 in the table. Since the interstorey drift angle is greatly increased, the overlap allowance of escalator increases, and there is a margin for the slide displacement to escape the forced displacement due to the building.

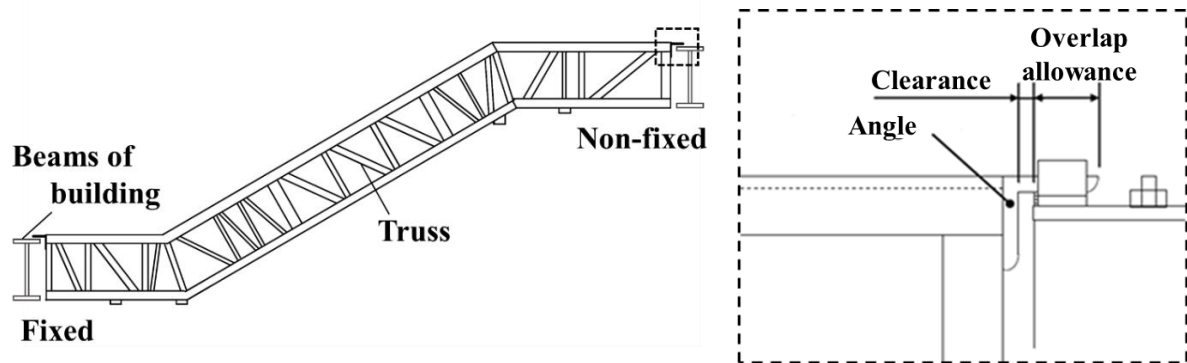


Figure 1 Escalator system and the non-fixed side of the escalator

Table 1 Interstorey drift angle and overlap allowance of the escalator

	Design for the Interstorey drift angle [rad]	Clearance [m]	Overlap allowance [m]
Old standard	1/100	0.03	0.080
New standard 1	1/40		0.245
New standard 2	1/24		0.428

## 2.2 Escalator Fragility curve

In this research, damage evaluation of mechanical structures is performed by a method based on realistic proof strength and realistic response. Model an object to be evaluated, select damage evaluation index, and create a fragility curve that represents the damage probability [5]. The fragility curve is obtained by using the probability density function of proof stress and response. The probability density function is a normal distribution that includes variations in consideration of uncertainty. Letting the average of the data be  $\mu$  and the standard deviation be  $\sigma$ . From these parameters, the probability density function of realistic strength and realistic response is calculated by the following equation (1) (2).

$$f_c(x) = \frac{1}{\sqrt{2\pi}\sigma} e^{-\left[\frac{(x-\mu)^2}{2\sigma^2}\right]} \tag{1}$$

$$f_{Ra}(x_R) = \frac{1}{\sqrt{2\pi}\sigma} e^{-\left[\frac{(x_R-\mu')^2}{2\sigma'^2}\right]} \tag{2}$$

The fragility for an arbitrary value H according to the evaluation index is a cumulative distribution function representing the conditional damage probability, in which the probability density function  $f_c(x)$  of the realistic strength exceeds the probability density function  $f_{Ra}(x_R)$  of the realistic response. It is calculated from equation (3).

$$F(\alpha) = \int_0^\infty f_{Ra}(H, x_R) \left( \int_0^{x_R} f_c(x) dx \right) dx_R \tag{3}$$

The cause of the escalator's fall is considered to be that the escalator fell off the building beam because the non-fixed part of the building slipped a lot due to the unexpected interstorey drift of the building caused by the earthquake motion. Therefore, the three Design for the interstorey drift angle in Table 1 are used as evaluation indices as standard for the possibility of escalator falling. As shown in Fig.2, assuming an escalator with each as a standard for evacuation safety, the probability density distribution is calculated from the statistics based on the slide allowance and the drift angle.

The fragility curve is calculated as shown in Fig.3 from the probability density distribution. The fragility curve that can determine the damage probability of each mechanical structure during vibration is a weight that represents the traffic risk on the evacuation route. If it exceeds the standard value, it is judged that there is a risk for lifting and lowering, so 80-90% is given as a weight. In addition, the 50% reliability curve is applied in consideration of aging deterioration and uncertainty of the structure.

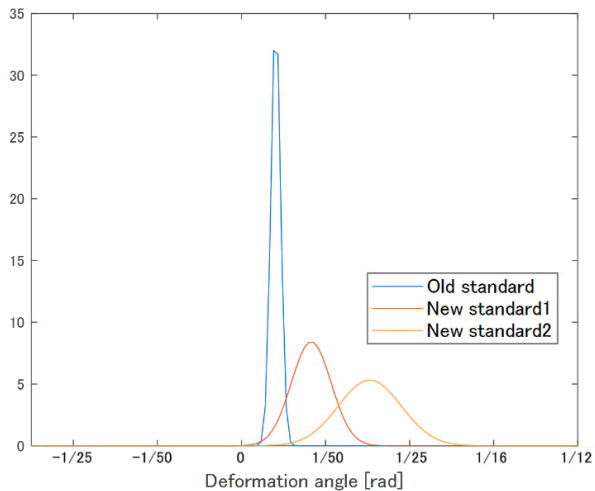


**Figure 2 Probability density distribution of escalator**

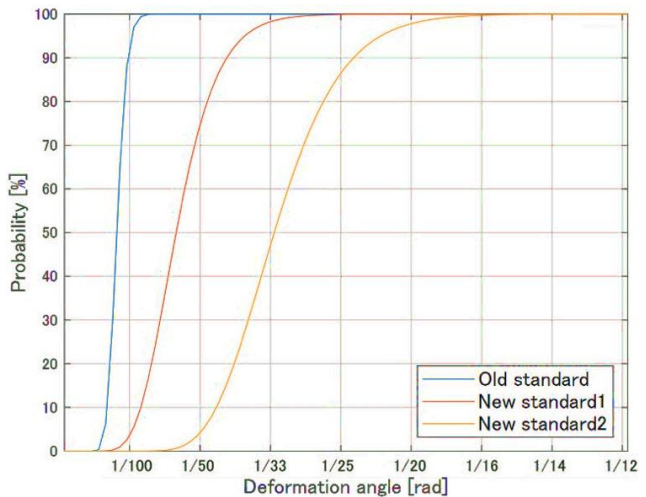


**Figure 3 Fragility curve of escalator**

### 2.3 Other Mechanical structure Fragility curves

At commercial facilities and terminal stations, there are plate glasses, suspended information boards, electronic bulletin boards, and piping. In this research, damage evaluation is shown as these mechanical structures that can be obstacles on the evacuation route.

In plate glass, many small cracks exist on the surface, and stress concentration due to external force is thought to occur at the crack tip. When stress is continuously applied, the crack grows deep and leads to fracture. Destruction occurs at the practical strength of plate glass of about 49 to 98 [N/mm<sup>2</sup>] [6]. Therefore, the calculation was performed when the horizontal axis of the fragility curve in Fig.4 (a) was stress. In a ceiling-mounted structure, it plays the role of holding the hanging bolt (pole) so that it will not fall. Suspension bolt damage is caused by cracks gradually progressing and cross-sectional areas decreasing due to repeated vibration and load [7]. Therefore, as shown in Fig.4 (b), calculation was performed with the horizontal axis of the fragility curve as the stress. As for piping, the structural integrity of the piping used in nuclear facilities has been confirmed [8]. In this research, it is assumed that the structure is used for general building structures, Fig.4 (c) shows the results of piping examination.

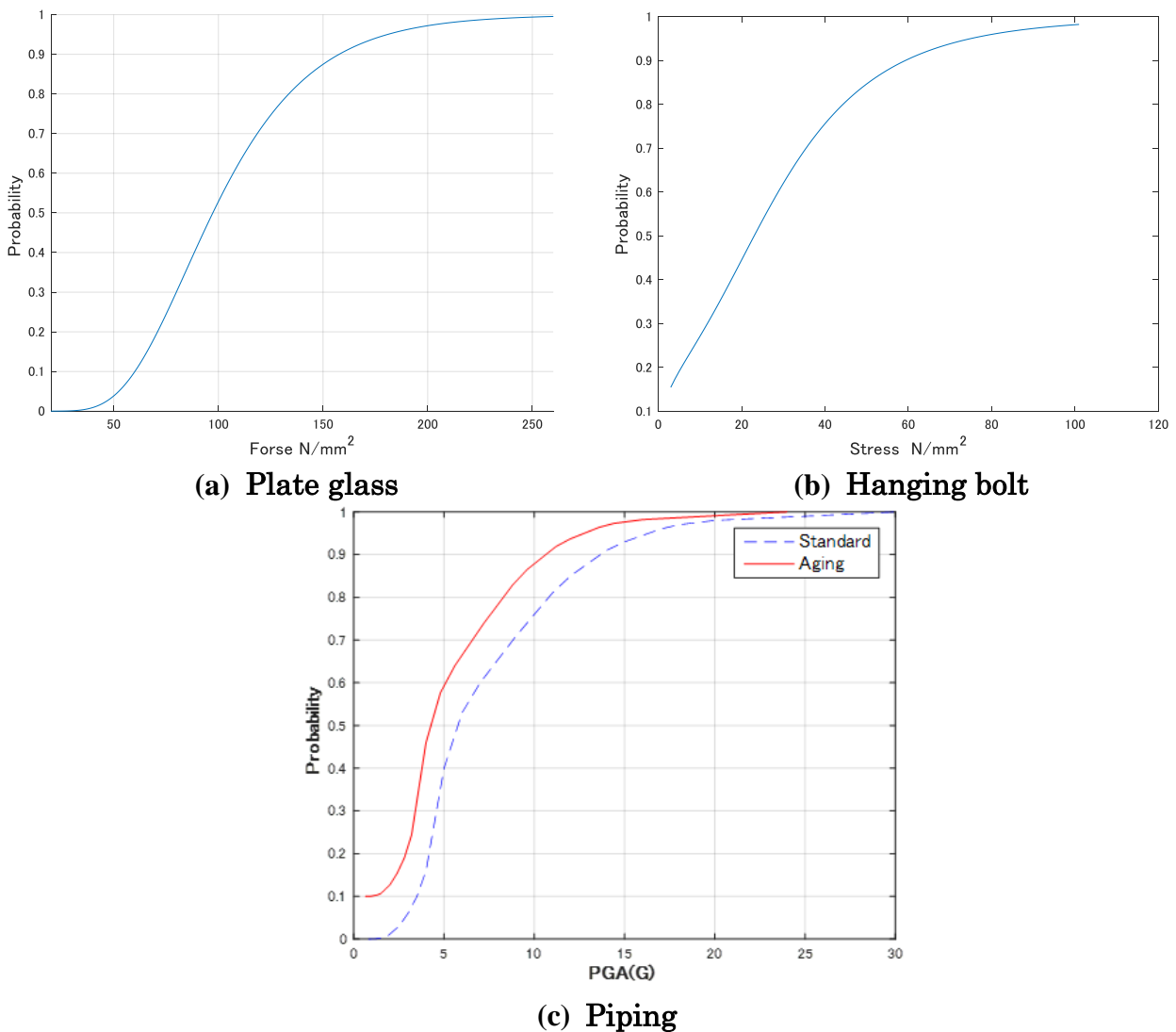


Figure 4 Mechanical structure Fragility curves

### 3 SIMULATION MODEL

#### 3.1 Response analysis using Building model

A time history response analysis of a multi-story building is performed to select the damage state, damage probability, and search conditions for mechanical structures for evacuation route search. The analytical model of the building is assumed to be a steel-framed three-story commercial facility in which the escalator falls. Fig. 5 shows the analytical model of the building model. In Fig.5,  $m_{si}$  is the mass,  $c_{si}$  is the damping coefficient,  $k_{si}$  is the initial stiffness, and  $\ddot{x}_H$  is the ground acceleration. The input ground motion was the K-NET Sendai NS Original wave observed in Sendai City, Miyagi Prefecture during the Tohoku-Pacific Ocean Earthquake [9].

The maximum values of each response are shown in Fig.6. From the maximum interstorey drift angle results, the design interstorey drift angle 1/100 [rad] used in the old standard for calculating the margin is exceeded in the first layer. In the second layer, it can be confirmed that the value is close to 1/40 [rad] of the new standard.

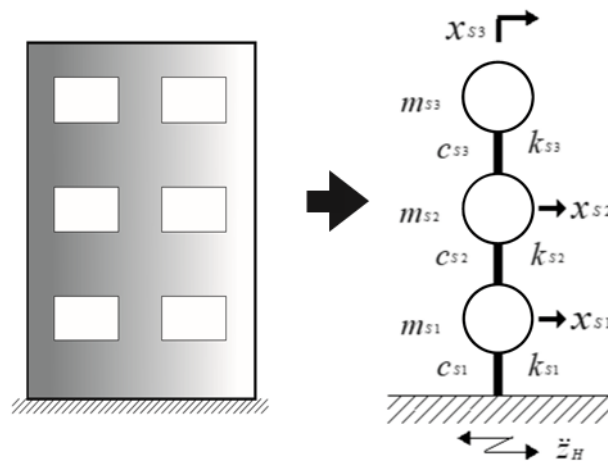


Figure 5 Analytical model of building

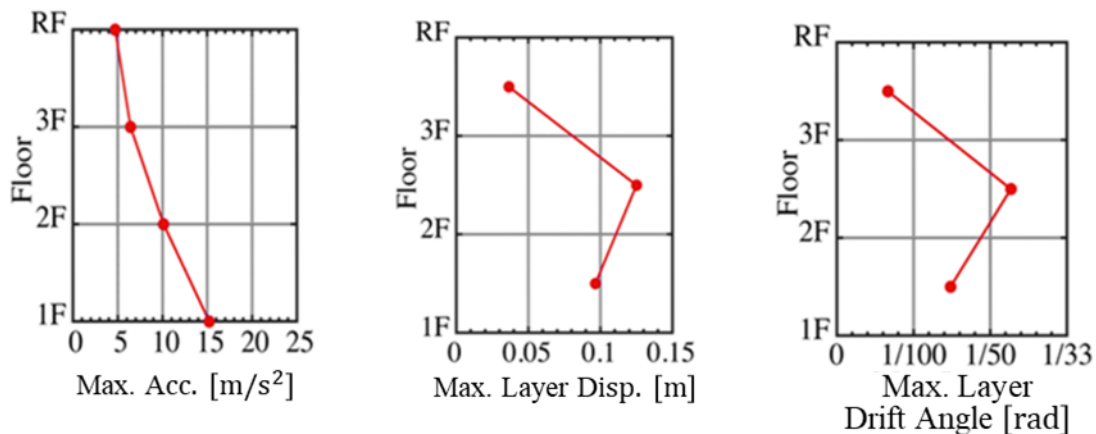


Figure 6 Response values of each layer

#### 3.2 Evacuation route search Simulation model

The evacuation route is evaluated by modeling the floor in the facility using graph theory. This is a method of modeling a phenomenon using points (nodes) dividing a route and line segments (edges) connecting the points, and analyzing its properties and structure.

As a weight, the impassability rate (damage probability × influence coefficient) is given to the edge, and the Dijkstra method is applied in which the route with the lowest total probability is the shortest [10]. The floor model has a simple structure with a staircase and an escalator in the center as an evacuation exit. Figure 7 shows a floor model of the inside of the facility, and Fig.8 shows a network model showing the floor with nodes and edges. It can be confirmed that the escalator located in the center can handle evacuation from both directions toward the center.

The evacuation route is searched from the shortest route. The damage probability is calculated by applying each maximum response value of the 3rd floor building due to the input seismic wave to the fragility curve of the mechanical structure. The impassable rate is calculated from the damage probability and the degree of influence on the passage. In order to compare the evacuation safety of the escalator according to the old standard and the new standard, search between 2F-1F and between 2F-3F with large response values.

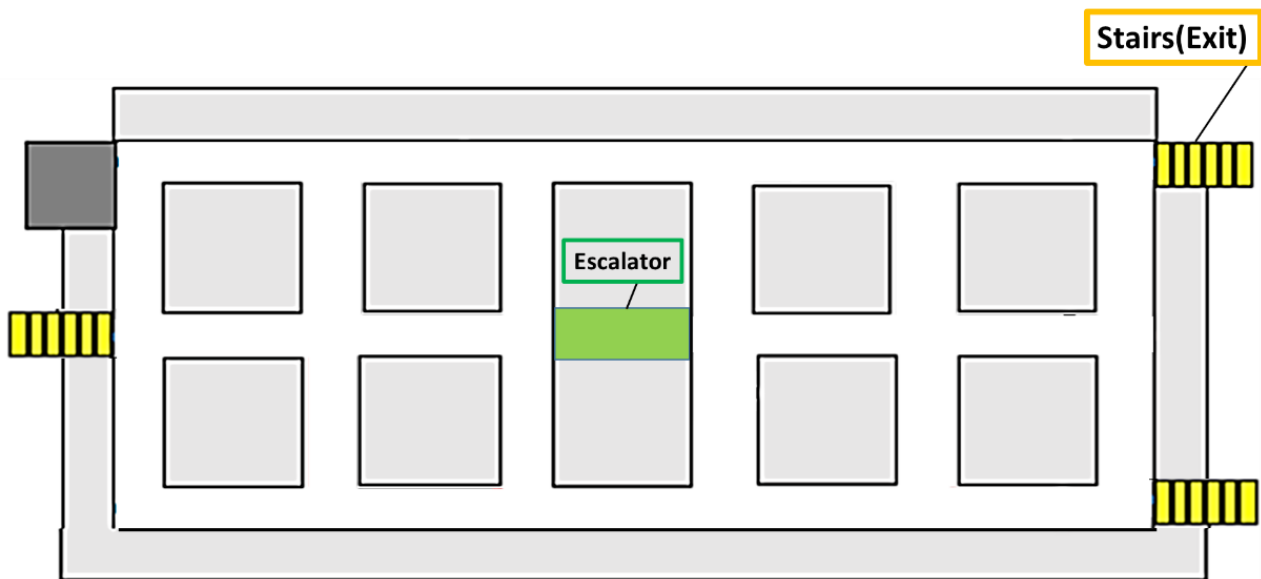


Figure 7 Floor model

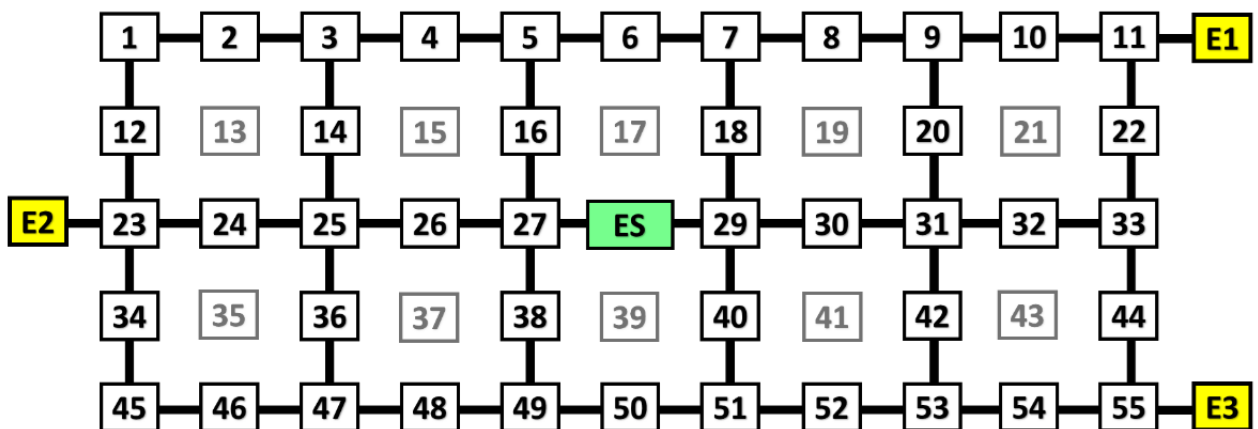


Figure 8 Network model of floor

## 4 EVACUATION ROUTE

### 4.1 Evacuation route focusing on Escalator

The safety of the escalator will be examined according to each standard in order to use it as the exit of the evacuation route. By using the inside of a facility with no obstacles as a model, the performance as an exit is evaluated from the evacuation distance and the risk of escalator. Since there are no obstacles, the safe evacuation route in this model is the shortest route.

Table 2 shows the damage probability of the escalator based on the maximum response value of each layer. At each node, the evacuation probability is calculated by simulating four routes leading to the exit. Probability of evacuation is the probability that the route will reach the exit, and specifies a passable level of 70% or higher. Table 3 shows the maximum evacuation probability for each level when using the escalator for each standard. In the old standard, all are about 20%, so there is a great risk and it is considered impossible to pass. Focusing on New standard 1, the evacuation probability was improved compared with the Old standard, 3F-2F was 33.6%, and 2F-1F was significantly improved at 76.0%. 2F-1F is a value exceeding 70% of the passable level. In New standard 2, the evacuation probability is significantly improved compared to other standards, 92.0% for 3F-2F and 97.6% for 2F-1F. This is a value far exceeding 70% of the passable level in both cases.

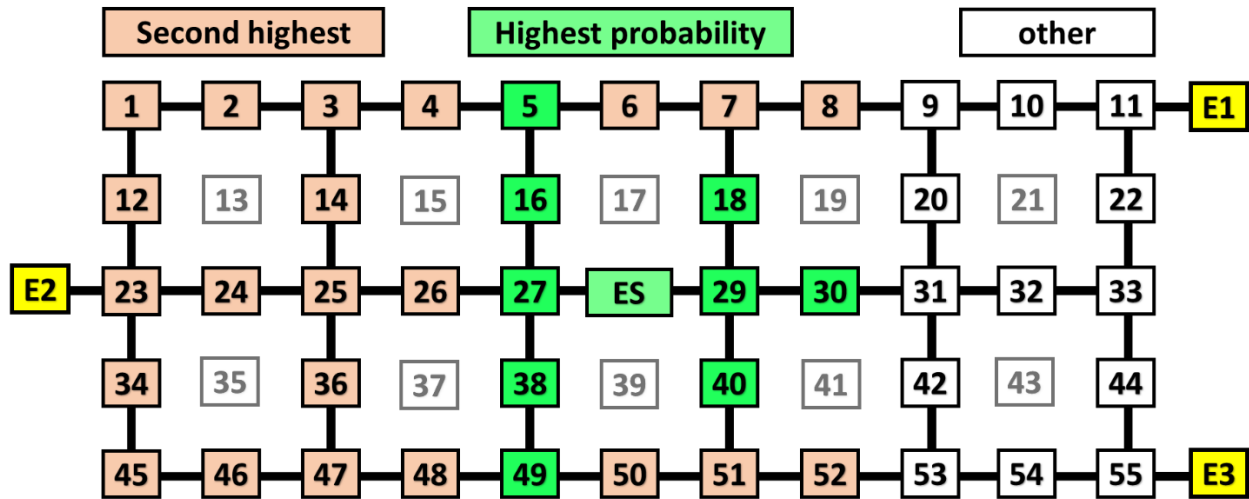
Figure 9 shows the evacuation probability of the shortest route from the escalator of New standard 2 to the exit. It can be seen that the central area (green) has the highest evacuation probability compared to other exits. Even at points away from the center, there are many areas (orange) that show the second highest evacuation probability. Due to the presence of mechanical structures, the second highest route may result in the safest route. In this way, even considering the danger of the escalator, it can be seen that the New standard 2 can function sufficiently as an exit. Especially in the central part of the floor where the stairway exit is not near, the escalator is considered to be effective in the efficiency and safety of evacuation behavior.

**Table 2 Damage probability of escalator**

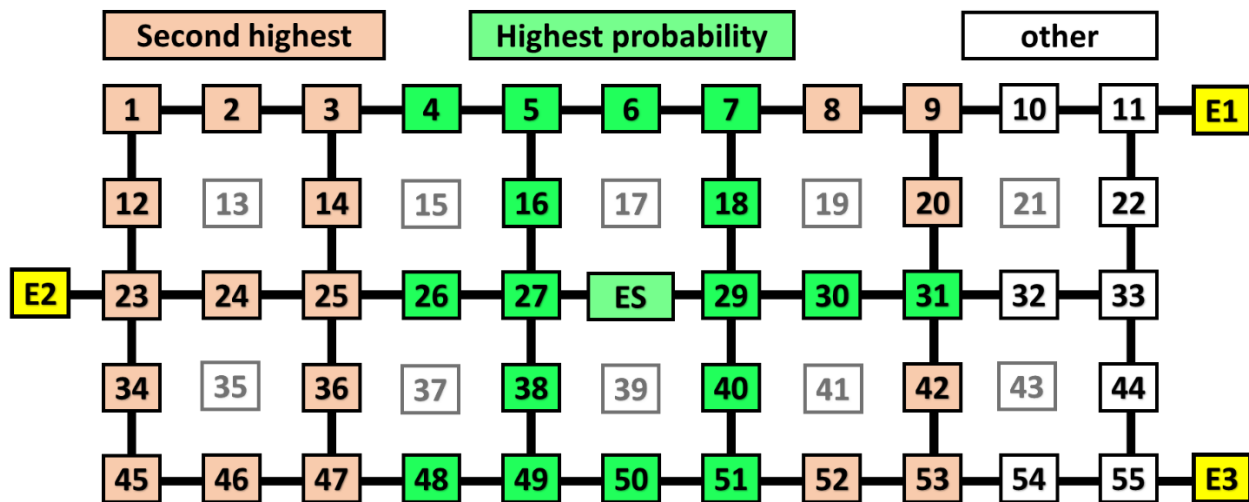
Mechanical structure		3F-2F Damage Probability [%]	2F-1F Damage Probability [%]
Escalator	Old standard	99	99
	New standard1	83	30
	New standard2	10	3

**Table 3 Escalator maximum evacuation probability**

	3F-2F Probability of evacuation [%]	2F-1F Probability of evacuation [%]
Old standard	20.8	20.8
New standard1	33.6	76.0
New standard2	92.0	97.6



(a) 3F-2F nodes



(b) 2F-1F nodes

Figure 9 Nodes with higher escalator probability than other exits

#### 4.2 Evacuation route including mechanical structures

Search for safe evacuation routes under more realistic conditions with mechanical structures inside the facility. A safe route is a route with the highest probability of passage. As shown in Fig.10, the floor model has mechanical structures related to the evacuation route and stairs and escalators.

The search results of the route from node 9 to each exit node are shown below. Figure 11 shows the result of illustrating the evacuation route on the floor. Node 9 is close to both the escalator and E1. This is the place where the escalator can be used as the exit with the second highest evacuation probability depending on the conditions. Table 5 shows each Route with the node number indicating the safest route from the initial position (initial node) to each exit. Table 6 shows the probability of each standard of Route4, which is an evacuation route using an escalator.

As a general tendency, it was confirmed that a route is taken to avoid a structure with a high probability of damage. The layout of the structures is unified, and the evacuation routes do not change by floor due to the balance between impassability and distance. By following the route with the highest evacuation probability, determine the appropriate evacuation route for each floor.

Focusing on Route 4 which uses an escalator, it is impossible to pass because the old standard is about 10% in each case. In New standard 1, which is a general standard, the value is close to 70% of the passable level in 2F-1F. In the new standard 2 which is a strict standard, both are passable levels. It can be confirmed that 3F-2F is the safest route next to Route3, and 2F-1F is the safest route. From these results, it is considered that the escalator based on New standard2, which is the standard when no structural calculation is performed, can make a great contribution to the efficiency and safety of evacuation behavior even in facilities with mechanical structures.

**Table 4 Damage probability of mechanical structure**

Mechanical structure		3F-2F Damage Probability [%]	2F-1F Damage Probability [%]
Escalator	Old standard	99	99
	New standard1	83	30
	New standard2	10	3
Glass		90	80
Pole		14	20
Plumbing		92	75

**Table 5 Evacuation route of simulation result**

	Route	3F-2F Evacuation probability [%]	2F-1F Evacuation probability [%]	Length of the route
Route 1	9-20-31-32-33-22-11-E1	80.86	77.39	7
Route 2	9-8-7-6-5-16-27-38-49-48-47- 36-25-24-23-E2	68.13	63.15	15
Route 3	9-20-31-42-53-54-55-E3	82.80	80.70	7
Route4	9-8-7-18-29- ES	-	-	5

**Table 6 Escalator evacuation probability**

	3F-2F Evacuation probability [%]	2F-1F Evacuation probability [%]
Old standard	18.30	17.70
New standard1	29.60	67.00
New standard2	82.10	87.00

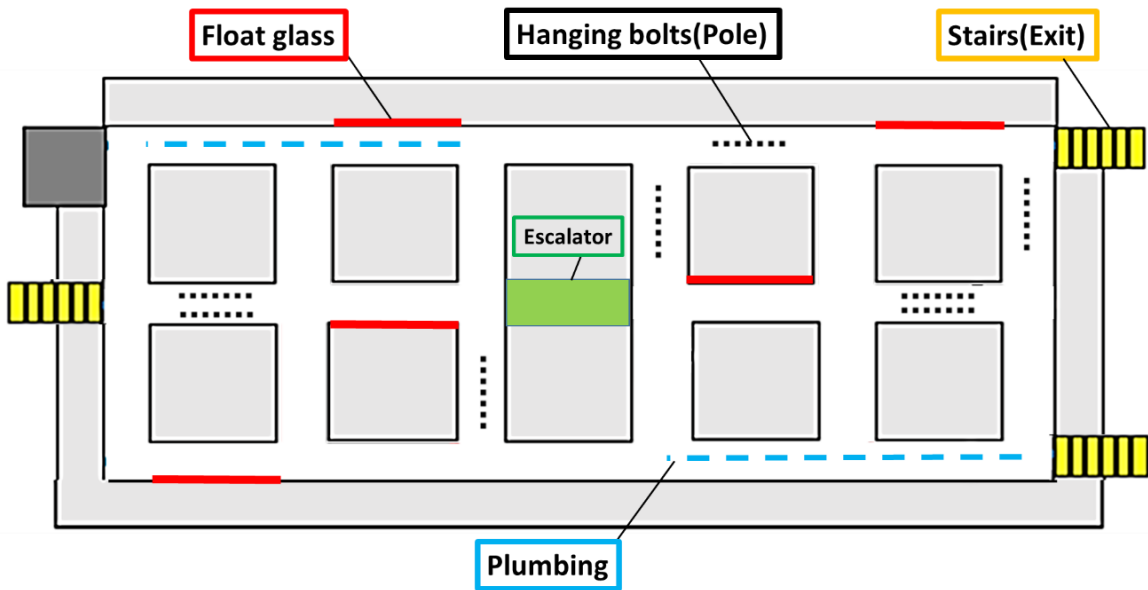


Figure 10 Floor model with mechanical structure

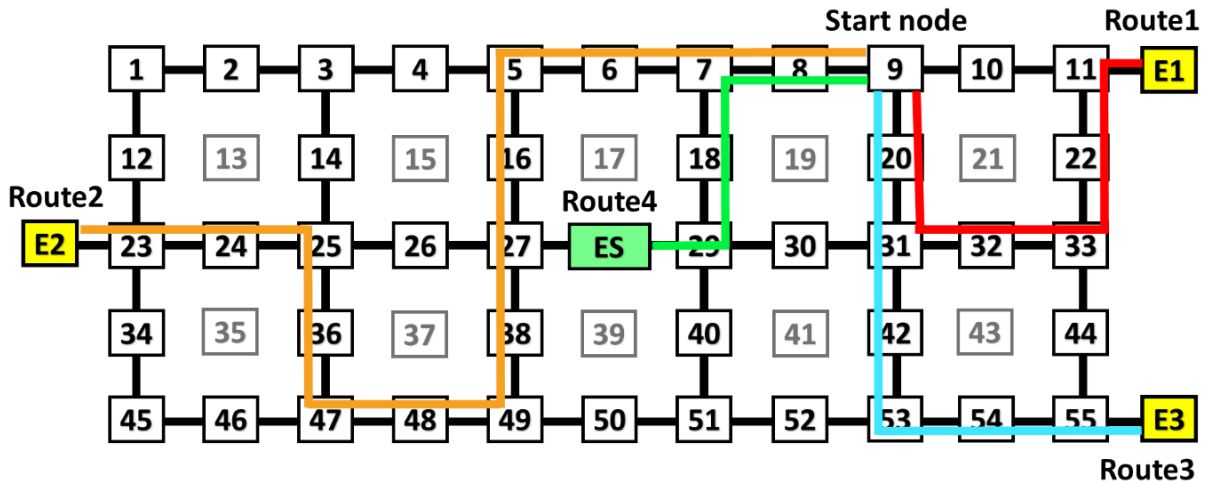


Figure 11 The evacuation route on the floor

## 5 CONCLUSION

In this study, to examine the use of escalators in evacuation planning, a fragility curve was calculated from a probabilistic risk assessment focusing on the falling event. The possibility of the escalator falling was calculated from the maximum response value of the multi-story building. The search for an evacuation route considering the risk of falling was simulated by applying the Dijkstra method to the route with the maximum Passable probability.

From these results, it is conceivable that the escalator will not be able to utilize New standard 1 as an evacuation route in the event of a large-scale earthquake, but it will have sufficient function as an exit at New standard 2 level.

As a future development, we will analyze the escalator slide displacement during an earthquake and make a more accurate evaluation. In addition, it is considered that the fluctuation of probability due to other conditions such as the passage of time and population density will increase. Therefore, considering the degree of influence of the structure on the passage, we plan to study the influence coefficient under a specific damage condition.

## REFERENCES

- [1] National Institute of Advanced Industrial Science and Technology, "Study on evaluation and countermeasure technology for ensuring safety of user's daily activities in architectural space", Vol.37, No.2, 60-78(2012)(in Japanese)
- [2] Satoshi FUJITA, Asami ISHII, "Fundamental study on seismic response of escalator". *Transactions of the JSME*, Vol. 183, No.851, 1-10 (2017) (in Japanese).
- [3] Satoshi FUJITA, Asami ISHII, "A Study on Seismic Response Analysis in Consideration of Non-linear Restoring Force Characteristics of Escalator Truss Structure", *7<sup>th</sup> Symposium on lift & Escalator Technologies*, 1-9, (2017)
- [4] Tokyo Denki University, "How to take safety measures for escalator Consideration about Building standard maintenance promotion business", No.P8, 4-10 (2014) (in Japanese).
- [5] Japan Atomic Energy Society, "Implementation standard for probabilistic risk assessment due to earthquakes for nuclear power plants". *Atomic Energy Society of Japan Standard*, 1-10 (2015) (in Japanese).
- [6] Taro MORIYA, Syou NARUSE, Masatoshi KATO, Jinhen TASHIRO, "Glass engineering handbook", *Asakura Publishing*, 194-203, (1963) (in Japanese).
- [7] Kazuya TAKEDA, Tyohiro NISHIKAWA, Teturo YAMASHITA, Kazumasa Ohashi, "Experimental study on seismic performance of ceiling suspension pipes and suspension bolts in building equipment", *Air Conditioning and Sanitary Engineering Society*, No.208, 21-26, (2014) (in Japanese).
- [8] Yoshihito YAMAGUCHI, "Evaluation of soundness of aged piping considering earthquake exceeding design assumption", *Japan Atomic Energy Agency Safety Research Center*, 13-16, (2017) (in Japanese).
- [9] Satoshi FUJITA, Kimiaki KONO, Asami ISHII, "Study on the behavior of escalator in case of huge earthquake", *Dynamic and Design Conference*, 1-10, (2017) (in Japanese).
- [10] Rikio ONODERA, "Basics of graph theory", *Morikita Publishing*, 7-11, (2007) (in Japanese).

## CREDITS

The 3 DOF analytical model used in the paper was constructed cooperation with Mr. Kimiaki Kono, Tokyo Denki University. Mechanical structure parameters used in the paper was produced by Mr.Kazuya Matushima & Mr.Kohei Numazawa, Tokyo Denki University. The authors would like to express our gratitude for providing us with the precious data.

## BIOGRAPHICAL DETAILS

Kazusada Natsu is master's course student in mechanical engineering of Tokyo Denki University. He researches Safe evacuation routes including mechanical structures.

Prof. Osamu Furuya is Professor in Tokyo Denki University. Recently main research object is research and development of vibration reduction for various structures and seismic safety for important facilities.



# The Maximum Number of Passengers Boarding a Lift in Office Buildings Based on Automated Passenger Counts

Tiina Laine<sup>1</sup> and Janne Sorsa<sup>2</sup>

<sup>1</sup>KONE Industrial Ltd, Hissikatu 3, FI-05830 Hyvinkää, Finland

<sup>2</sup>KONE Industrial Ltd, Keilasatama 3, FI-02150 Espoo, Finland

**Keywords:** lift passenger behaviour, car capacity factor, automated passenger counts, handling capacity ratio, level of service.

**Abstract.** While a lift is serving a landing but is already carrying several passengers, the passengers on the landing need to decide whether to board the lift or wait for the next. The boarding decision is made by contrasting the space available in the car to the required space, which assumedly depends on physical, behavioural and social factors. As already observed in the 1960s, passengers do not typically fill a lift up to its rated passenger capacity, i.e., the maximum number of passengers in a lift car that must not be exceeded due to lift safety standards. If, in lift traffic design, the maximum number of passengers in a lift car is assumed to equal rated passenger capacity, the lift group may not reach its required handling capacity in practice. Regardless the known contradiction, the maximum number of passengers accepting to board a lift has not been studied systematically. This paper aims at filling the gap by analysing automated passenger counts in three existing office buildings. Car capacity factor is defined as the ratio of maximum passenger count in a lift to rated passenger capacity. The highest car capacity factors are derived for different traffic conditions as well as related to both handling capacity and pedestrian level of service criteria. The results indicate diverse behaviours when passengers are about to board a lift.

## 1 INTRODUCTION

As a part of their journey in a multi-storey building, lift passengers routinely decide whether they board a lift that already carries several passengers or wait for the next lift. To board a lift, passengers require free space to satisfy not only their physical needs but also personal preferences. Factors that affect the behaviour may include, but are not limited to, culture, gender, building type, social group, time of day and experienced waiting times. Lift safety standards restrict *maximum available car area* for a lift with a particular *rated load* [1,2]. It has been observed already in the 1960s that passengers do not typically fill lifts up to their capacities although behaviour varies depending on rated load and time of day [3].

Regardless the early observations, it is surprising that the maximum number of passengers accepting to board a lift has not been studied systematically. The assumed maximum number of passengers accommodated by a lift, i.e., *passenger capacity*, is one of the key parameters in lift traffic design, which aims at defining a suitable lift installation for a building, e.g., the number of lifts as well as their rated loads and speeds [e.g. 4]. If passenger capacity assumed in the design is higher than passengers actually accept, the lifts may not be able to transport as many passengers as indicated. In contrast, if more passengers than assumed by passenger capacity accept to board in practice, the lift installation may be somewhat oversized with respect to the demand.

Passenger capacity can be defined either as *rated* or *area-based passenger capacity*. Rated passenger capacity is typically obtained by dividing rated load by average passenger mass, e.g., 75 kg in Europe. Maximum available car area per passenger in a lift loaded up to its rated passenger capacity decreases as rated load increases [1,2]. For example, area per passenger equals 0.20 m<sup>2</sup> for an 800 kg lift and 0.16 m<sup>2</sup> for a 2000 kg lift. On the other hand, area-based passenger capacity can be derived by dividing maximum available car area by the area required by an average passenger, where the area of a design ellipse, 0.21 m<sup>2</sup>, is typically assumed. The design ellipse was derived

using the 95<sup>th</sup> percentile body depth and shoulder width of male laborers in the USA to allow for personal articles, psychological preferences and body sway [5]. If a passenger is modelled by the design ellipse, standard-sized lift cars can accommodate passengers from 57% to 70% of their rated passenger capacities for a 2000 kg lift and an 800 kg lift, respectively [6]. Thus, depending on the method, passenger capacity of a 2000 kg lift can be either 26, 20 or 15 passengers.

This paper studies the maximum number of passengers accepting to board a lift in three office buildings operating under normal circumstances. Required data was collected by *Lift Performance Analyser* (LPA), which is a stand-alone sensor device temporarily installed in a lift [7]. The LPA detects floor levels when the lift stops and acceleration rates using an accelerometer, which allows to calculate lift group *handling capacity* with measured lift performance times. In addition, it uses 3D camera technology with human detection algorithms to identify boarding and alighting passengers with greater than 95% accuracy. The passenger counts are used to derive car capacity factors and handling capacity ratios, which define how full a lift is and how close to handling capacity measured passenger demand is, respectively.

## 2 DEFINITIONS

The stop-wise counts of passenger transfers recorded by the LPA yield the number of passengers carried by a lift at any time. More formally, let  $S$  denote the set of lift stops, which is indexed by  $i$ . It is assumed that the stops are ordered by the time of occurrence so that  $i - 1$  refers to the stop preceding stop  $i$ . Furthermore, the number of alighting and boarding passengers during a stop are denoted by  $a_i$  and  $b_i$ . The number of passengers,  $p_i$ , inside the lift after stop  $i$  evolves cumulatively,

$$p_i = p_{i-1} - a_i + b_i. \quad (1)$$

Stops are associated with period  $T$  of fixed length. Period length of five minutes is assumed unless stated otherwise. For example,  $T$  may refer to a five-minute period 10:55-11:00 excluding the end time. The period, to which a stop belongs, is determined by the time of arrival at the stop-floor. Car capacity factor  $CCF$  is defined as the ratio of maximum number of passengers to rated passenger capacity  $PC$  among the set of stops  $S_T$  during period  $T$ ,

$$CCF_T = 100\% \times \max_{i \in S_T} p_i / PC. \quad (2)$$

The number of passengers in a lift can also be related to maximum available car area  $CA$ , which is described by available area per passenger  $APP$ :

$$APP_T = CA / \max_{i \in S_T} p_i. \quad (3)$$

The maximum available car area is defined by safety standards. Area per passenger allows to classify lifts according to pedestrian level of service criteria for waiting and queuing areas [5]. For example, human touch zone, i.e., LOS E, corresponds to an occupancy of 0.19-0.28 m<sup>2</sup> per person.

Passenger demand  $PD_T$  equals the sum of all boarding passengers,

$$PD_T = \sum_{i \in S_T} b_i. \quad (4)$$

Handling capacity  $HC5$  defines the maximum sustainable number of passengers per five minutes that a lift group can transport for uppeak traffic with under an average loading of 80% of rated passenger capacity. Handling capacity ratio  $HCR$  for a five-minute period  $T$  is the ratio of passenger demand and handling capacity [8,9],

$$HCR_T = 100\% \times PD_T / HC5. \quad (5)$$

Handling capacity ratio may exceed 100% since a full collective lift group has higher handling capacity in mixed and downpeak traffic than in uppeak traffic [e.g. 10]. Handling capacity ratio can also be calculated for periods longer than five minutes by properly scaling passenger demand.

### 3 STUDIED BUILDINGS AND LIFTS

Site surveys were conducted during 2018 and 2019 in three European office buildings with typical lift car sizes (see Table 1 for details).

**Table 1 Office A, B and C building data**

	<b>Office A</b>	<b>Office B</b>	<b>Office C</b>
<b>Region</b>	South Europe	South Europe	Central Europe
<b>Predominant religion</b>	Islam	Islam	Christian
<b>Tenancy</b>	Single	Multiple	One big tenant
<b>Absence rate [%]</b>	20	Unknown	20
<b>Number of floors</b>	29	29	15
<b>Measurement time</b>	6:35...19:59	6:48...18:59	6:45...20:00
<b>Morning peak</b>	8:30...9:30	8:30...9:30	8:30...9:30
<b>Lunch peak</b>	12:00...13:45	11:55...13:40	11:55...14:35
<b>Evening peak</b>	17:55...18:25	17:50...18:20	16:55...17:25
<b>Number of lifts in group</b>	6	6	5
<b>Group control</b>	Full collective	Full collective	Full collective
<b>Rated speed [m/s]</b>	2.5	2.5	2.5
<b>Rated load [kg]</b>	A1...A4, A6: 1000 A5: 1200	B2...B6: 800 B1: 1000	C2, C3: 1200 C1, C4, C5: 1500
<b>Rated passenger capacity [persons]</b>	A1...A4, A6: 13 A5: 16	B2...B6: 10 B1: 13	C2, C3: 16 C1, C4, C5: 20
<b>Area per passenger at capacity [m<sup>2</sup>]</b>	A1...A4, A6: 0.185 A5: 0.175	B2...B6: 0.200 B1: 0.185	C2, C3: 0.175 C1, C4, C5: 0.170
<b>Lift shape</b>	Long and narrow	Long and narrow	Varying widths and depths
<b>Handling Capacity [persons/5-min]</b>	95 (79 without A6)	91	109
<b>Personal accessories</b>	No moving aids, summer clothing	No moving aids, summer clothing	Normal
<b>Passenger waiting times</b>	Unsatisfactory	Excellent	Satisfactory

The chosen buildings were also high enough so that lifts played the key role in vertical transportation. In other respects, the buildings were chosen relatively randomly. Office A building management had reported traffic problems and asked for a survey. Office B was known to have

good passenger service quality and was chosen for comparison purposes since it is very similar to Office A. In both cases, building management allowed LPAs to be installed in lifts for collecting data, but observations were limited to the main entrance floor due to their security policy. Office C is located in another part of Europe than offices A and B. The lifts of Office C were on the limit of being able to satisfy the passenger demand.

Data collection started before 7 a.m. and ended by 8 p.m. at the latest. Periods that were included in morning uppeak, mid-day lunch-peak and evening downpeak, were decided when analysing data and seeing when the peaks take place in each building. In Office B, data was collected for one day only, while Office A and C were studied for a couple of days. According to the observations, all lifts in the buildings were in normal use, but the sensor in lift A6 failed during the second day.

Table 2 presents average and maximum handling capacity ratios across the 5-minute periods of the defined peak times, where day 2 results for Office A are based on only five lifts. During morning uppeak in Office A, maximum handling capacity ratio exceeded 100%, which also implies that peak passenger demand exceeded handling capacity. Accordingly, peak demand in the morning in Office B is clearly below handling capacity even during the worst 5-minute period. In Office C, morning peak demand is about the same as handling capacity during the first two measurement days but exceeds it during the last measurement day.

According to the definition of handling capacity ratio, also passenger demands at other times of the day are compared to uppeak handling capacity. With full collective control, a lift group can handle higher passenger demands in lunch-peak and downpeak than in uppeak. Therefore, handling capacity ratios greater than 100% do not necessarily indicate insufficient handling capacity.

**Table 2 Average and maximum handling capacity ratios during peak times**

Building	Day	Average <i>HCR</i> [%]			Maximum <i>HCR</i> [%]		
		Morning	Lunch	Evening	Morning	Lunch	Evening
A	1	81	102	91	108	130	137
	2	73	85	67	102	121	135
B	1	48	59	56	70	109	90
C	1	67	73	75	96	117	111
	2	69	81	75	94	120	102
	3	65	79	76	107	104	103

In Office A and B, evening peak passenger demands were about 30% higher than in the morning implying rather fixed times to leave the office. The sharpness of evening peak was a bit surprising. In Office C, evening peak passenger demands were on average 6% greater than in the morning. Office A seems similar to Office C based on the ratio of lunch-peak handling capacity ratio to the one of uppeak. This may arise from the tenancy: Office A was a single-tenant office, and Office C had one big tenant occupying most floors. On the other hand, Office B was a multi-tenant office. In these single-tenant offices, the highest passenger demands during lunch-peak were about 20% greater than during uppeak, but in the multi-tenant office the difference was even more than 50%. However, strong conclusions cannot be made based on this amount of data.

#### 4 MAXIMUM CAR CAPACITY FACTORS

Table 3, 4 and 5 present the highest measured car capacity factors and the respective minimum areas per passenger in Office A, B and C, respectively. The densities are further classified by pedestrian level of service criteria. The maximum car capacity factors are also averaged across the lifts. However, average areas per passenger cannot be given due to different car sizes.

According to the measurements, passengers seem to accept the highest car capacity factors during lunch-peak. Car capacity factors are also higher during downpeak than during uppeak. This does not necessarily mean that people would be more eager going for lunch or to home than coming to work. The trend might arise from passengers’ previous experiences on waiting for a lift. At the main lobby, passengers know that the next lift will arrive soon. On normal office floors, passengers may expect that the next lift will arrive only after a long wait. Alternatively, during lunch-peak, passengers often travel in socially connected groups, which may motivate the group to board even a crowded lift as a whole [11].

**Table 3 Maximum car capacity factors and minimum areas per passenger in Office A**

Day	Lift	Maximum CCF [%]			Minimum APP [m <sup>2</sup> ] and LOS		
		Morning	Lunch	Evening	Morning	Lunch	Evening
1	A1	69	92	100	0.267 (E)	0.200 (E)	0.185 (F)
	A2	85	100	85	0.218 (E)	0.185 (F)	0.218 (E)
	A3	77	100	85	0.240 (E)	0.185 (F)	0.218 (E)
	A4	85	85	92	0.218 (E)	0.218 (E)	0.218 (E)
	A5	69	81	88	0.255 (E)	0.215 (E)	0.200 (E)
	A6	92	92	92	0.200 (E)	0.200 (E)	0.200 (E)
	<i>Average</i>	79	92	90			
2	A1	85	100	100	0.218 (E)	0.185 (F)	0.185 (F)
	A2	92	108	85	0.200 (E)	0.171 (F)	0.218 (E)
	A3	85	108	100	0.218 (E)	0.171 (F)	0.185 (F)
	A4	92	100	108	0.200 (E)	0.185 (F)	0.171 (F)
	A5	69	88	94	0.255 (E)	0.200 (E)	0.187 (F)
	<i>Average</i>	85	101	97			

As Office A did not have sufficient handling capacity, car capacity factor exceeded 80% many times and even reached 100% occasionally. At minimum, area per passenger dropped below 0.19 m<sup>2</sup>. Accordingly, level of service degraded to class F. The results indicate differing behavioural patterns between the measurement days. Both average and maximum handling capacity ratios were greater during day 1 than during day 2. On the contrary, passengers accepted higher car capacity factors during day 2, which could have occurred due to long waiting times experienced during day 1. This observation could also result from random variation.

**Table 4 Maximum car capacity factors and minimum areas per passenger in Office B**

Lift	Maximum CCF [%]			Minimum APP [m <sup>2</sup> ] and LOS		
	Morning	Lunch	Evening	Morning	Lunch	Evening
B1	69	69	62	0.267 (E)	0.267 (E)	0.300 (D)
B2	60	90	70	0.333 (D)	0.222 (E)	0.286 (D)
B3	70	80	80	0.286 (D)	0.250 (E)	0.250 (E)
B4	60	70	70	0.333 (D)	0.286 (D)	0.286 (D)
B5	70	80	100	0.286 (D)	0.250 (E)	0.200 (E)
B6	80	80	70	0.250 (E)	0.250 (E)	0.286 (D)
<i>Average</i>	68	78	75			

**Table 5 Maximum car capacity factors and minimum areas per passenger in Office C**

Day	Lift	Maximum CCF [%]			Minimum APP [m <sup>2</sup> ] and LOS		
		Morning	Lunch	Evening	Morning	Lunch	Evening
1	C1	75	70	75	0.227 (E)	0.243 (E)	0.227 (E)
	C2	88	94	75	0.200 (E)	0.187 (F)	0.233 (E)
	C3	69	106	81	0.255 (E)	0.165 (F)	0.215 (E)
	C4	60	65	65	0.283 (D)	0.262 (E)	0.262 (E)
	C5	70	70	70	0.243 (E)	0.243 (E)	0.243 (E)
	<i>Average</i>	72	81	73			
2	C1	65	70	65	0.262 (E)	0.243 (E)	0.262 (E)
	C2	81	75	69	0.215 (E)	0.233 (E)	0.255 (E)
	C3	75	88	-	0.233 (E)	0.200 (E)	-
	C4	85	70	80	0.200 (E)	0.243 (E)	0.213 (E)
	C5	60	60	70	0.283 (D)	0.283 (D)	0.243 (E)
	<i>Average</i>	73	73	71			
3	C1	60	65	80	0.283 (D)	0.262 (E)	0.213 (E)
	C2	81	81	88	0.215 (E)	0.215 (E)	0.200 (E)
	C3	88	81	94	0.200 (E)	0.215 (E)	0.187 (F)
	C4	65	80	80	0.262 (E)	0.213 (E)	0.213 (E)
	C5	60	65	80	0.283 (D)	0.262 (E)	0.213 (E)
	<i>Average</i>	71	75	84			

In Office B, peak passenger demands did not exceed handling capacity. As a result, car capacity factors rarely exceeded 80% and level of service never degraded to F. On the other hand, the lifts were the smallest among the studied buildings, which implies the largest area per passenger with a car capacity factor of 100%.

Fig. 1, 2 and 3 present maximum car capacity factors measured for each lift in Office A, B and C at different times of the first measurement day. The other days were quite similar to the first day but with some exceptions. In Office A, car capacity factor temporarily exceeded 80% several times and in several lifts during the first measurement day. The second day provided similar data with the exception that car capacity factor also exceeded 100%. In Office B, 80% car capacity factor was rarely exceeded. In Office C, over 80% car capacity factor was measured a couple of times per day. Also over 100% car capacity factors were observed during the first day for several sequential starts of lift C3, which did not happen during the other measurement days.

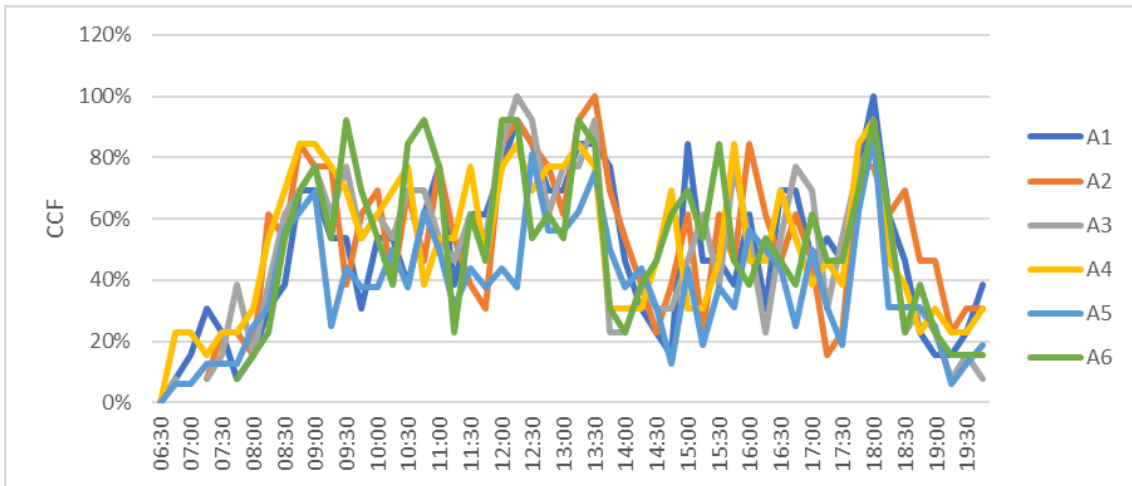


**Figure 1 Office A maximum car capacity factors for each 15-minute period**

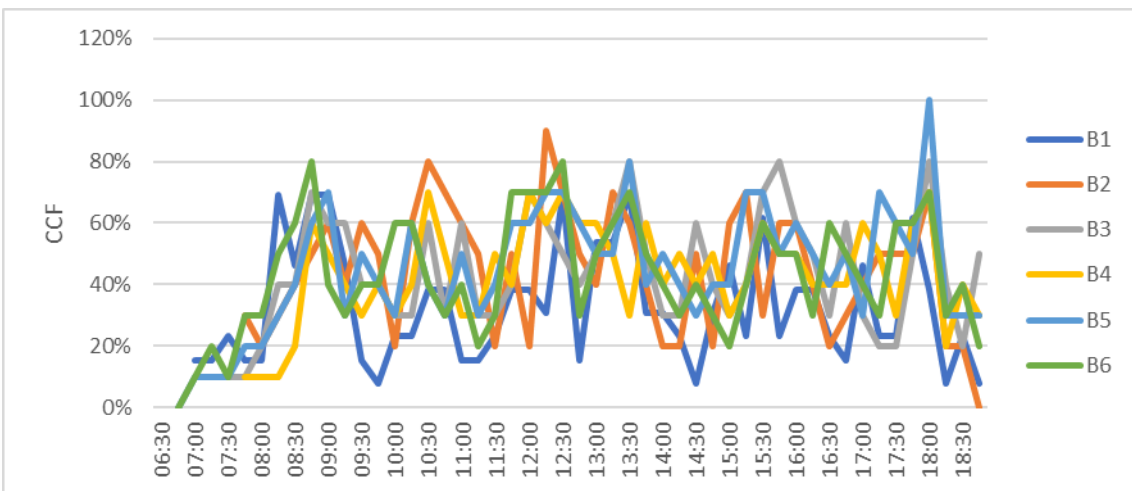


**Figure 2 Office B maximum car capacity factors for each 15-minute period**

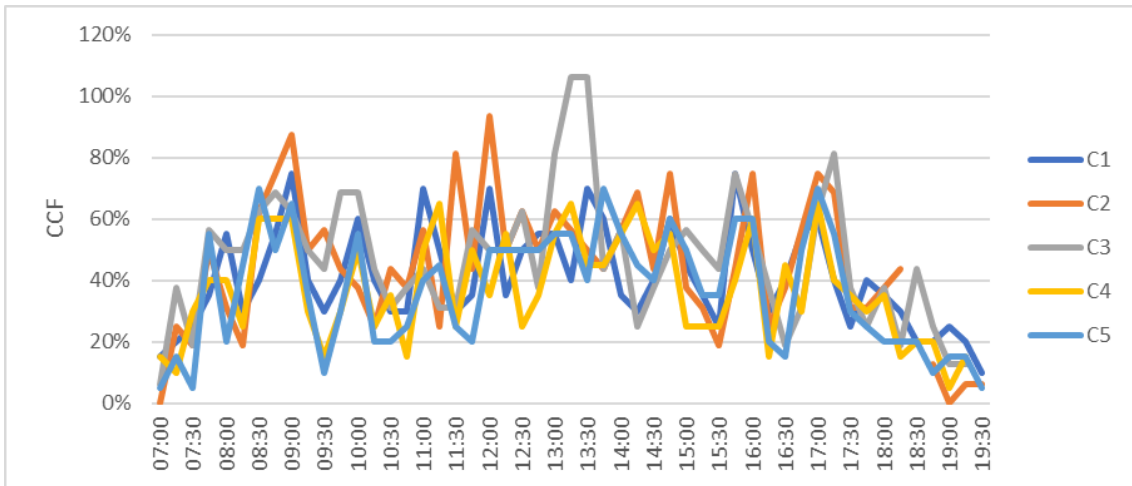


Figure 3 Office C maximum car capacity factors for each 15-minute periods

### 5 THE EFFECT OF CAR SIZE ON CAR CAPACITY FACTORS

Fig. 4, 5 and 6 show car capacity factors for different rated loads for 15-minute periods of a day. The values represent averages across the maximums of lifts with the same rated load and measurement days. The figures also present handling capacity ratios, to which observed car capacity factors seem to be related. It is worth noticing that the 15-minute periods and the averaging smooth the peak values from the previously shown values.

In each office, the larger cars have clearly lower car capacity factors compared to the smaller cars. This observation confirms the known effect of safety standards on available car area, but the posed limits are not necessarily the only reasons. If a lift group contains lifts with different sizes and especially if they look equally narrow, passengers do not necessarily realize the additional space in the larger lifts.

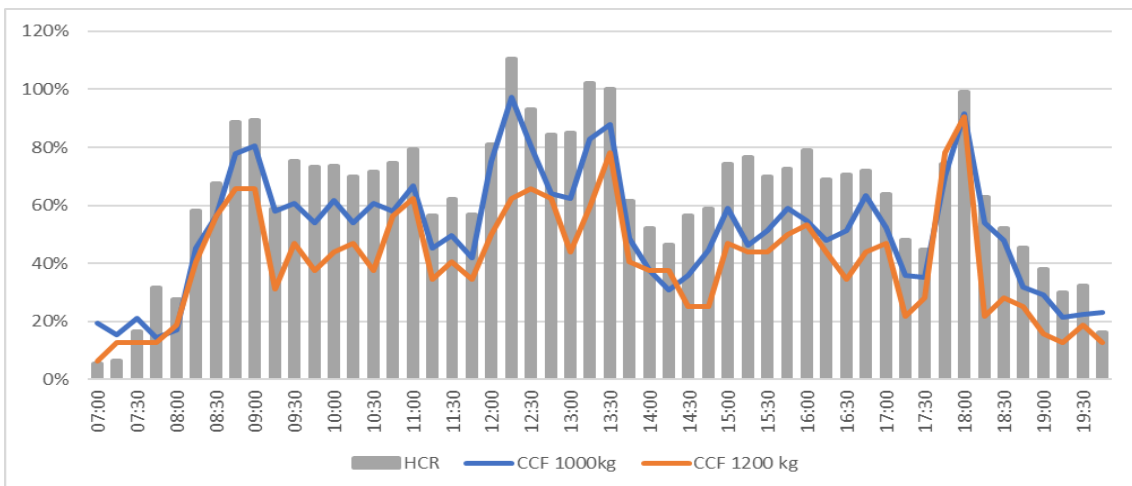


Figure 4 Average of maximum car capacity factors for 1000 kg and 1200 kg lifts in Office A

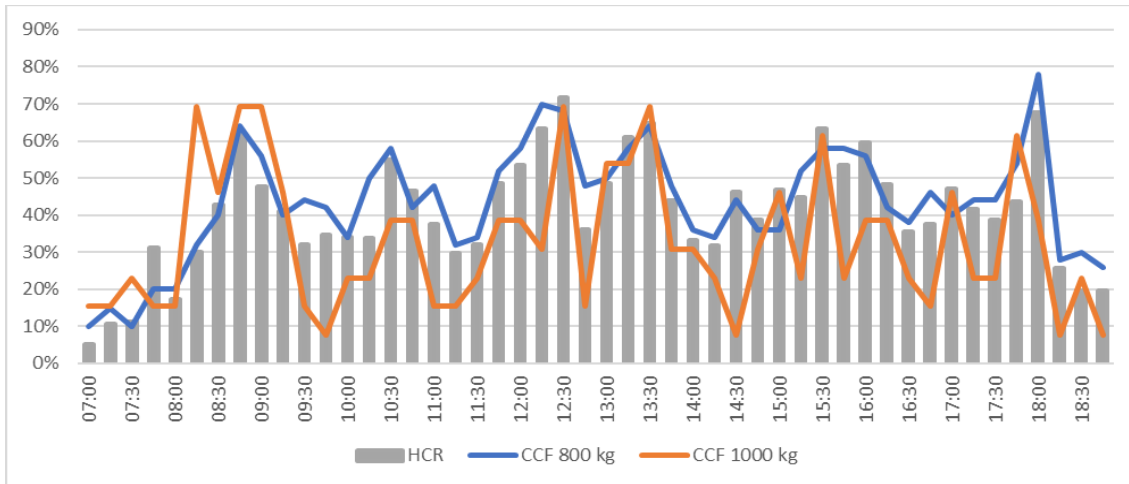


Figure 5 Average of maximum car capacity factors for 800 kg and 1000 kg lifts in Office B

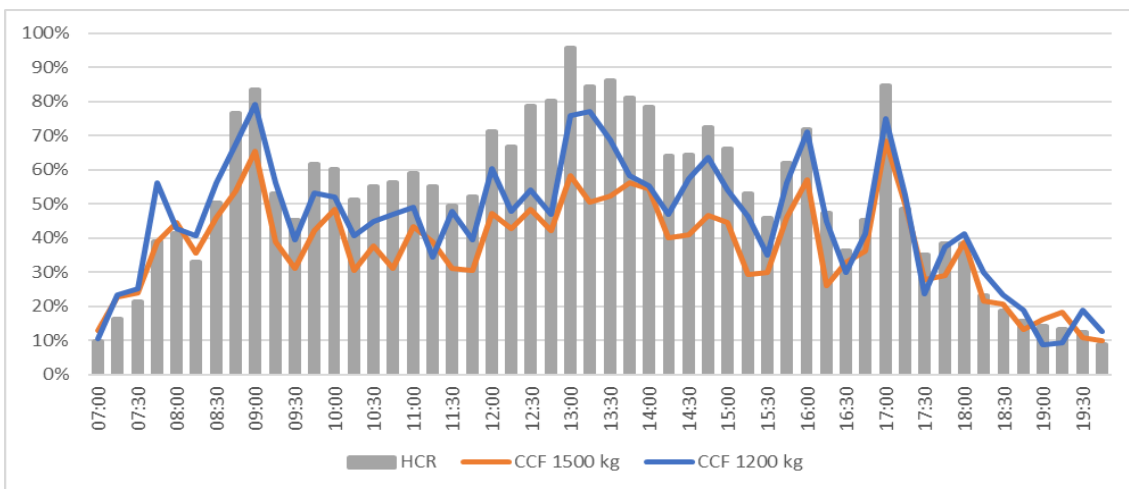


Figure 6 Average of maximum car capacity factors for 1200 kg and 1500 kg lifts in Office C

## 6 CONCLUSION

In this paper, the maximum number of passengers accepting to board a lift was studied in three office buildings. Sensor devices were installed in the lifts to automatically count and record the number of boarding and alighting passengers during each stop. Car capacity factors and handling capacity ratios were derived from the passenger counts for different times of a day. Car capacity factor was defined as the ratio of the maximum number of passengers in a lift to the rated passenger capacity. Handling capacity ratio, on the other hand, relates passenger demand within a period to lift group handling capacity. These quantities help in normalizing observations across different factors such as region, cultural background, city, neighbourhood, building, tenant, time of day and lift type.

The results show that passengers repeatedly boarded lifts until car capacity factor reached about 80%, which roughly corresponded to an area of 0.21 m<sup>2</sup> per passenger. These values could be used as safe defaults when defining passenger capacity in lift traffic design at least in Europe. However, lifts were also filled up to their rated passenger capacities, which may be acceptable in some regions. Furthermore, passengers also accepted higher densities in lifts during midday lunch-peak and evening downpeak compared to morning uppeak. Therefore, local rather than global guidance on defining passenger capacity should be sought during the design process to ensure that the lifts can comfortably accommodate the assumed number of passengers and the size of the lift installation does not become excessive.

At least one lift in each studied group had higher rated load compared to the others. An important finding was that the larger lifts of the groups were consistently loaded to lower car capacity factors than the smaller ones. This result may arise from available car areas per passenger in fully loaded cars. Alternatively, passengers may not be able to recognize the additional space in the larger cars if the cars are narrow and about equal in width. This raises a doubt whether lift traffic design should be conducted according to the smallest car size of a group. Such a precaution may not be necessary if the larger cars are also wider than the smaller ones but may be necessary in the case of equal car widths.

Ideally, lift traffic design is based on realistic assumptions on lift passenger behaviour. Data analysis as shown in this paper can be used to derive passenger capacities but should be extended to a wider range of geographical areas and building types. The data analysis should be accompanied with behavioural observations, which could reveal the reasons and conditions why passengers accept or refuse to board a lift. Such results could help developing lift traffic simulation models further. Since the used in-car sensors cannot detect passengers in lift lobbies, lobby sensors could complement the data acquired with the in-car sensors.

## REFERENCES

- [1] ASME, *ASME A17.1/CSA B44-2016 – Handbook on Safety Code for Elevators and Escalators*. The American Society of Mechanical Engineers, the United States of America (2016).
- [2] CEN, *EN 81-20:2014 – Safety rules for the construction and installation of lifts - Lifts for the transport of persons and goods - Part 20: Passenger and goods passenger lifts*. European Committee for Standardization, Belgium (2014).
- [3] G.R. Strakosch, and R.S. Caporale, *The Vertical Transportation Handbook, 4th Edition*. John Wiley, New Jersey (2010).
- [4] ISO, *ISO 8100-32:2020 – Lifts for the transportation of persons and goods – Part 32: Planning and selection of passenger lifts to be installed in office, hotel and residential buildings*. International Organization for Standardization, Switzerland (2020).
- [5] J.J. Fruin, *Pedestrian Planning and Design*. Metropolitan Association of Urban Designers and Environmental Planners (1971).
- [6] J. Sorsa, M. Ruokokoski, and M-L. Siikonen, “Human Body Size in Lift Traffic Design”. *Proceedings of 4th Symposium on Lift and Escalator Technologies*, Northampton (2014).
- [7] D. Batey, and M. Kontturi, “Traffic analysis for high rise buildings to be modernized”. *Elevator Technology 21 – Proceedings of Elevcon 2016*, IAAE, 26-35 (2016).
- [8] M-L. Siikonen, J. Sorsa, and H. Hakala, “Impact of traffic on annual elevator energy consumption”. *Elevator Technology 18 – Proceedings of Elevcon 2010*, IAAE, 344-353 (2010).
- [9] N. Segercrantz, *Impact of traffic on annual elevator energy consumption in high-rise buildings*. Bachelor's thesis, Aalto University Faculty of Information and Natural Sciences, Department of Applied Physics (2010).
- [10] G.C. Barney, *Elevator Traffic Handbook: Theory and Practice*. Spon Press, London (2003).
- [11] J-M. Kuusinen, J. Sorsa, M-L. Siikonen, and H. Ehtamo, “A study on the arrival process of lift passengers in a multi-storey office building”. *Building Services Engineering Research and Technology*, Vol. 33, No. 4, 437-449 (2012).

## **BIOGRAPHICAL DETAILS**

Tiina Laine is an expert in People Flow Planning and has been working for KONE Major Projects since 2008. She's located in Finland supporting projects globally. She graduated 2007 as Master of Science (Tech.) from Helsinki University of Technology, Department of Mechanical engineering. She's been involved in planning many of world highest towers and trained also new lift traffic specialists.

Janne Sorsa is the head of People Flow Planning in KONE Major Projects. He obtained the degree of D.Sc. (Tech.) in operations research in 2017 from Aalto University School of Science. He has developed optimization models and numerical algorithms for lift group control systems. His research interests include all aspects of modelling people flow in buildings such as transport planning, simulation, behaviour, human factors and evacuation.



# The Passenger Input to Escalator Accidents

David Cooper

LECS (UK) Ltd & University of Northampton

**Keywords:** accident, escalator, human factors, falls, entrapments, injury

**Abstract.** The number of accidents occurring on escalators and moving walks around the world is increasing. This paper looks at some typical and non-typical accidents and will investigate the passenger input into the event. It is known that many accidents occur as a result of intended misuse and/or miscreant behavior however it has been found that some accidents occur as a result of totally innocent input by the passenger. To some in the industry the action of the passenger is obviously dangerous and leads to the event but some accidents are as a result of chance and often bad luck.

## 1.0 INPUTS INTO ESCALATOR ACCIDENTS

Dr Lutfi Al Sharif, in his paper entitled “Escalator Human Factors: Passenger behavior, accidents & design” [1] created a Venn diagram identifying the three inputs to escalator passenger accidents. These were:

- Design
- Maintenance, Inspection & Operation
- Passenger Behavior

The Venn diagram can be seen below (Fig 1) with the section entitled “Passenger Behaviour” highlighted in yellow.

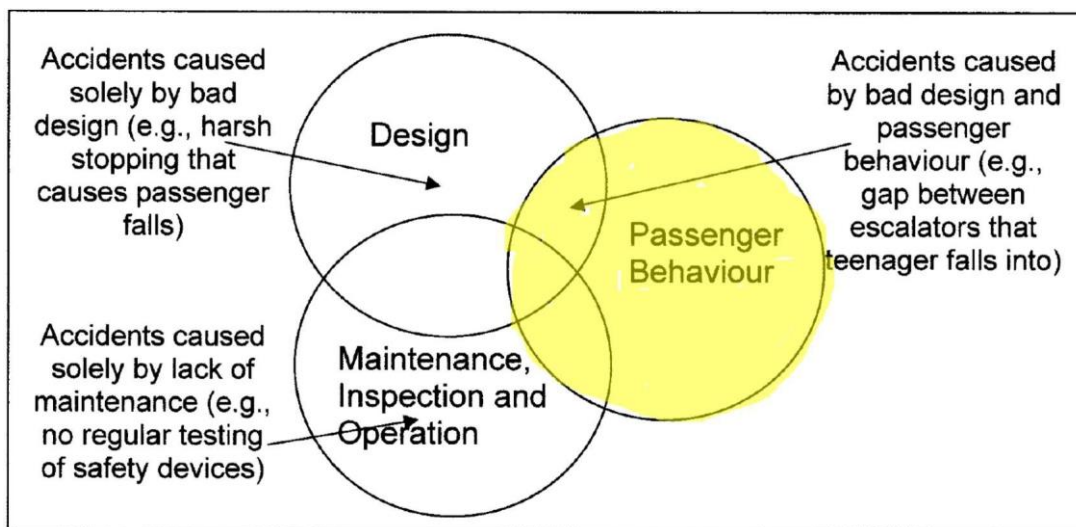


**Fig 1: Al Sharif Venn Diagram [1]**

The number of escalator accidents involving personal injury occurring are rising and litigation following accidents is similarly increasing. The works of Gerk [1], Cooper [2], White [3] and Owen [4] indicate this is the case.

When litigation occurs the contribution of all three elements of the Venn diagram will be taken into consideration and escalator owners (the defendants) will want to promote the actions of the passenger as primary causation whereas the claimant (generally the injured party) will want to

point towards defects in design and/or maintenance, inspection & operation.

Whilst accidents occur that involve a single element of the Venn diagram very often there will be two or three of the elements involved.

## 2.0 PASSENGER BEHAVIOR

The purpose of this paper is to identify examples of passenger behaviors that contribute to escalator accidents.

In cases where passenger actions have been either causative or contributory to the accident they can generally be categorized as

1.1.1 Intended Misuse

1.1.2 Unintended Misuse

This categorization is troublesome as some may argue that a person getting on an escalator with luggage or using a walking stick would not be aware of the potential risk of a runaway suitcase causing a cascade fall or a walking stick tip under load being across the joint between two steps when they go into transition.

The troublesome element is when a passenger repeats the same unintentional error and a similar accident occurs where a further risk category can be introduced of willful negligence.

Owners very often rely on CCTV footage when defending legal actions and this can be extremely helpful in any analysis post incident. The following photographs refer



**Photo 1: Wheelchair user about to board an escalator**



**Photo 2: Miscreant youths riding the handrail**



**Photo 3: Child riding handrail**



**Photo 4: Youth holding onto handrail external to the step band**



**Photo 5: Youth sliding down the centre deck**



**Photo 6: Person struggling with a luggage cart**

The passenger input into these events is obvious yet it may be argued that in photo 4 the child was of an age so as not to be aware of the danger he was putting himself in.

Similarly, the lady in photo 7 may well be oblivious to the risk she is placing herself (and indeed others below her on the escalator) in.

The one thing for sure is that once the people in the photographs have had an accident, they are unlikely to repeat their actions.

Some accidents involving passengers can be defined as being completely innocent with no deliberate input into causation but nevertheless an accident occurs.

These include footwear entrapment where the passenger has no idea that the wearing of such items can end in a serious accident.

It is true to say that there is a secondary component to the accident over and above the innocent wearing of footwear in as much as their feet must have been in a position of danger for the accident to occur.

There are a very few numbers of escalator owners who mark where a passenger should stand on an escalator step so how would a passenger know? You aren't taught at school where to stand! That having been said there are many asset owners who have or are still trying to improve the situation. The HSE PM34 document "Safety in the use of escalators" [6] was intended to educate passengers and its replacement SAFed EMW [9] features all aspects of escalator safety.



**Photo 7: Footwear entrapment**



**Photo 8: Footwear entrapment**

Other accidents where the innocent action of a passenger result in injury. In the incident below the young girl bent over to pick up a coin she had dropped and her hair went between steps and became entangled. Amore common occurrence is shoe lace entrapment.



Ordeal over: Hayley Young recovering at home after her hunt for 10p almost ended in traged

Escalator terror as girl of nine is trapped by her hair

**Fig 2: Hair Entrapment**

### 3.0 ACCIDENT PREVENTION

A way of preventing accidents is education and/or signage however even such an approach can be criticized as it could be construed that you are actually educating a person to misbehave and if they are of an adventurous character it may promote miscreant behavior.

Similarly, signage can be criticized as being an invitation to misbehave and where do you stop when it comes to pointing out potential hazards? Signage is very often ignored by a passenger and is often used in a legal argument to simply say “we pointed out the risk in advance”.

EN115-1 (2017) Annex G [7] introduces some standard signage that should be posted which is limited to 4 signs:

- G1 Small children should be held firmly
- G2 Dogs shall be carried
- G3 Use the handrail
- G4 Pushchairs not permitted



Figure G.4 — Prohibition sign "Push chairs not permitted"

**Fig 3: Sign from annex G of EN115-1 (2017) [7]**

This is very limiting and does not cover many of the passenger contribution to accidents.

In addition, owners of escalators have for many years introduced their own signage for risks post incident:



**Photo 9: Bespoke Signage**

#### **4.0 MITIGATION**

As the number of litigation cases increases escalator owners need to be aware of the need to maintain documentary evidence of risk assessments, proper design, appropriate specification and sound maintenance.

In many cases the only argument is that it was the actions of the injured party (or someone else on the escalator that caused the injury) as a form of defence. This may be a sole contributory factor or a combination of factors such as those detailed in the Al-Sharif Venn diagram in Fig 1.

When it comes to mitigation for an escalator owner in situations where obvious misuse isn't involved there are a number of issues that very often get introduced but require supporting evidence, these include:

- Condition of footwear
- Alcohol Intoxication
- Drugs
- Luggage
- Rushing
- Using a mobile phone
- Devices that cause unbalance at transition
- Leaning over the side

Tripping or losing balance on an escalator can also lead to an entrapment which results in serious injury however this does not necessarily mean that there is a defect.

Hand injuries as a result of entrapment on escalators is a common accident so much so that Dr Campbell Reid, a surgeon, published a paper entitled "Escalator injuries of the hand" [8]

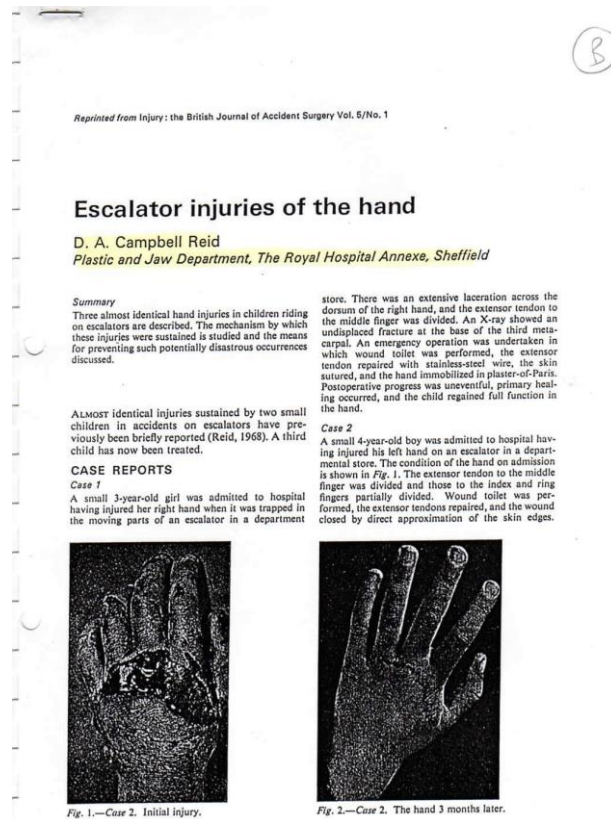


**Fig 4: Medical paper on escalator injuries of the hand [8]**

As with all risk management strategies the options available are to eliminate the risk or manage the risk.

Given that the risk in this context is the risk of a civil action against an escalator owner after an incident the current general strategy of owners is to attempt to mitigate the risk by apportioning blame towards the passenger. That is not a sound strategy when it comes to trying to achieve ALARP (as low as reasonably practicable)

Mistakes that escalator owners often make are that they leave themselves open to criticism for a number of reasons that may not be causative of the incident, including:

- Failure to maintain documentation
- Failure to maintain
- Failure to undertake periodic thorough examinations
- Failure to risk assess
- Failure to train staff
- Failure to specify adequately
- Failure to specify consistently
- Failure to follow procedures after an accident

Legal teams will ask for disclosure and the inability to demonstrate sound custodianship may open up a gap in the defence argument.

The fact of the matter is that the input by way of passenger actions to an accident may be as a result of easily identifiable misuse or by way of an innocent act or omission.

Escalator owners need to protect themselves against potential claims as a result of passenger inputs and the best option is to try and educate passengers. In the past documents such as the HSE PM34 [6] document “Safety in the use of escalators” aimed at educating passengers but in reality, such a

document never got to land on the breakfast table of most homes! The SAFed EMW guidance document [9] gives good advice but, again, it doesn't reach the coalface it only reaches those that are already well versed in escalator technology and safety.

In the UK LEIA have produced the "Liam loves escalators" [10] campaign and the SAFED EMW guidance [9] also provides good guidance. In addition, TfL have undertaken extensive research into improving escalator safety [11] as have other owners such as BAA [5] but still accidents are on the increase [2][3][4][5].

The US elevator & escalator safety foundation reaches school age children and educates them in how to use an escalator safely by attendance at educational establishments. Perhaps this is the only way the industry will reach those that need to be educated and hopefully they will pass on that education.

## REFERENCES

- [1] Al-Sharif, "Escalator Human Factors: Passenger behavior, accidents & design", DNK
- [2] Gerk, J.G. "An inquiry of contributory factors in escalator accidents in the USA 1920-2001" (2001) University of Northampton.
- [3] Cooper D., "Escalator runaways" Proc. 10th Symposium on Lift and Escalator Technologies, Northampton, September 2019 (available at <https://liftsymposium.org/download/LiftandEscalatorSymposiumProceedings2019>)
- [4] White, C: Escalator accident statistics and safety. 1983 (private paper)
- [5] Owen, A (2004) Review of escalator safety in UK airports. BAA
- [6] HSE Guidance note PM34 "Safety in the use of escalators"
- [7] BS EN 115-1:2017, Safety of escalators and moving walks. Construction and installation
- [8] Campbell-Reid, Escalator injuries of the Hand, DNK
- [9] SAFed (2018) Guidelines for the safe operation of escalators and moving walks Issue 3 (London: Safety Assessment Federation) (available at <http://www.safed.co.uk/technical-guides/machinery-lift-and-crane>)
- [10] [www.leia.co.uk/safety/liam-loves-safety-campaign](http://www.leia.co.uk/safety/liam-loves-safety-campaign)
- [11] TFL (2016) Safety, Accessibility & Sustainability Panel, Improving Escalator Safety (available at <http://content.tfl.gov.uk/sasp-20163006-part-1-item10-improving-escalator-safety.pdf>)

## BIOGRAPHICAL DETAILS

EurIng David Cooper

BSc (Hons), MSc, MPhil, CEng, FIET, FCIBSE, FRSA, FCGI, FSOE

David is a Chartered Engineer and Chairs the Educational Trust that manages these Symposiums. He has been in the lift & escalator industry since he left school in 1980. His MSc in lift engineering was awarded by University College Northampton and his dissertation was a study into accidents on escalators involving shopping trolleys His MPhil was awarded by the University of Northampton and his thesis was a study into accidents involving minors falling over the sides of escalators.

# The Round Trip Time Simulation: Monte Carlo Implementation and Consistency with Other Techniques

Matthew Appleby, Richard Peters

Peters Research Ltd, Great Missenden, HP16 9AZ, UK

**Keywords:** Monte Carlo simulation, Lift Traffic Analysis, Calculation, Simulation, Round Trip Time

**Abstract.** Currently, the two main paradigms of lift traffic analysis applied by the lift industry are Round Trip Time (RTT) calculations and dispatcher-based simulations. General Analysis (GA) RTT allows classical uppeak RTT to be extended to account for complex scenarios such as mixed traffic patterns.

Now, Monte Carlo Simulation (MCS) will allow GA RTT to be extended to account for even more complex scenarios such as destination control. MCS sits in between the calculation and simulation paradigms; individual round trips are simulated, and the process is repeated many times to determine standard parameters including average number of stops, capacity factors and round trip time. In this paper, the authors discuss the implementation of MCS within lift traffic analysis software and demonstrate its consistency with classical RTT, GA RTT and full dispatcher-based simulation. The implementation allows MCS to fit within current design methodologies used in lift traffic analysis.

## 1 INTRODUCTION

A Round Trip Time (RTT) calculation determines the average time taken for a lift to complete a full round trip of the building based on a set of equations and input parameters. A RTT calculation will always produce the same set of results if the same equations and input parameters are used.

The uppeak RTT models a building where passengers are travelling only from the ground floor to their destination floor. This is the simplest form of traffic analysis which continues to be applied widely [1] [2].

The General Analysis (GA) RTT calculation [2] [3] extends the uppeak RTT model to account for multiple entrance floors and mixed (incoming, outgoing and interfloor) traffic. The GA fits neatly into the standard lift traffic analysis methodology as it takes a similar, although extended, set of inputs and produces a similar set of outputs.

Dispatcher based simulation [2] extends traffic analysis further, accounting for more complex circumstances by modelling the whole process of each individual calling a lift and travelling to their destination. The simulation is assessing every passenger trip rather than extrapolating results from a single average round trip of the lift.

Simulation is a powerful tool and can be used to model complex systems not easily analysed by RTT calculations, e.g. destination control, cars sharing a shaft [4] [5] [6]. However, the complexity of simulation tools means that they are normally based on proprietary intellectual property, and are not transparent or verifiable [7]. Hence CIBSE Guide D's recommendation [1] that practitioners should begin their planning exercise with a RTT before moving to simulation, paying careful attention to any major differences in design outcomes.

Monte Carlo Simulation (MCS) sits in between the calculation and simulation paradigms; individual round trips are simulated, and the process is repeated many times to determine standard parameters. MCS has created a lot of research interest in recent years [8] [9] [10] as it allows the modelling of complex systems without the need to apply dispatcher based simulation.

This paper addresses the implementation of MCS within lift traffic analysis software with a view to widen its application beyond the research community. The implementation allows MCS to fit within current design methodologies used in lift traffic analysis. Consistency with RTT calculations and dispatcher-based simulation for uppeak traffic is demonstrated.

## 2 IMPLEMENTING MONTE CARLO SIMULATION

This chapter describes the process of simulating a round trip. For a full MCS, these steps must be repeated a significant number of times to find an average RTT.

### 2.1 Generating Passengers

The first step in a MCS is to create a set of passengers and decide their origins and destinations. The approach proposed by Al-Sharif for MCS applies an Origin Destination matrix [11] [10]. This starts with a table containing the probabilities of a passenger going from an origin (row) to a destination (column) which sums to 1, see the example in Figure 1.

Origin / Destination	G	1	2	3	4	5
G	0	0.07	0.07	0.07	0.07	0.07
1	0.05	0	0.02	0.02	0.02	0.02
2	0.05	0.02	0	0.02	0.02	0.02
3	0.05	0.02	0.02	0	0.02	0.02
4	0.05	0.02	0.02	0.02	0	0.02
5	0.05	0.02	0.02	0.02	0.02	0

**Figure 1 Probability Density Function of the Origin Destination Matrix**

This is translated into a cumulative distribution function of the origin destination matrix by adding each value to the value of the element in the next box as shown in Figure 2.

Origin / Destination	G	1	2	3	4	5
G	0	0.07	0.14	0.21	0.28	0.35
1	0.4	0.4	0.42	0.44	0.46	0.48
2	0.53	0.55	0.55	0.57	0.59	0.61
3	0.66	0.68	0.7	0.7	0.72	0.74
4	0.79	0.81	0.83	0.85	0.85	0.87
5	0.92	0.94	0.96	0.98	1	1

**Figure 2 Cumulative Distribution Function of the Origin Destination Matrix**

For each passenger to be served in the round trip, a random number between 0 and 1 is generated. In the cumulative distribution function of the origin destination matrix, the first number that is greater than or equal to the random number is used to determine the origin and the destination of passenger.

Figure 3 shows the random number generated, and the resulting passenger origin/destination for eight passengers.

Random:	0.41	0.57	0.05	0.88	0.94	0.30	0.82	0.18
Origin	1	2	G	5	5	G	4	G
Destination	2	3	1	G	1	5	2	3

**Figure 3 List of passengers**

### 2.2 Building Stop List

The next step is to sort the passenger into up traffic and down traffic and to add their stops to a set of lists, see Figure 4.

U <sub>p</sub>	1	2	2	3	0	1	0	5	0	3
D <sub>own</sub>	5	0	5	1	4	2				

**Figure 4 Stops segmented into up and down**

Next, each value in the up list is sorted into ascending order and each value in the down list is sorted into descending order, see Figure 5.

U <sub>p</sub>	0	0	0	1	1	2	2	3	3	5
D <sub>own</sub>	5	5	4	2	1	0				

**Figure 5 Stops sorted ascending then descending**

Repeating values in both lists can be removed as the lift does not need to know the number of passengers, all it needs is a list of floors to stop at. Finally, the two lists are concatenated together into one list of stops which if the lift travels around, every passenger will be delivered to their required floor, see Figure 6.

Stops	0	1	2	3	5	4	2	1	0
-------	---	---	---	---	---	---	---	---	---

**Figure 6 List of stops**

### 2.3 Round Trip Time

The list of stops provides the basis for calculating the lift round trip accounting for travel time between the stops, doors times and passenger transfer times.

The process of generating passengers and calculating the round trip time is repeated multiple times yielding many round trip time values. The average of the individual round trip time values is reported as the MCS round trip time.

### 3 IMPLIMENTING THE RTT SIMULATION

#### 3.1 The challenge with applying MCS

The MCS as described in the previous section follows the traditional RTT calculation by assuming the number of passengers loading the car at ground floor is a pre-determined number. Once the round trip time is determined, the handling capacity of the system can be calculated.

This is the only practical approach for manual uppeak RTT calculations. It has a number of limitations including:

- the handling capacity resulting from filling the car may be more than the anticipated passenger demand for this installation, yielding a pessimistic result for round trip time, interval, and car loading
- if the building has multiple entrance floors or interfloor traffic, a fully loaded car at the start of the RTT may prevent additional passengers loading at higher floors.

These issues are solved in traffic analysis software [2] by asking the user to enter the required passenger demand. The calculation then determines how full the car will be at every level to determine the maximum car loading. The inputs and outputs are effectively reversed, see Table 1. This reversal of inputs and output also aligns calculation with dispatcher based simulation.

**Table 1 Reversal of inputs and outputs for advanced traffic analysis**

<b>Analysis type</b>	<b>Input</b>	<b>Output</b>
uppeak RTT calculation and MCS	car loading <i>expressed in persons or as a capacity factor</i>	handling capacity <i>how many people can be transported per unit time</i>
enhanced uppeak, general analysis and dispatcher based simulation <sup>1</sup>	passenger demand <i>the rate at which people arrive persons per 5 minutes</i>	capacity factor <i>how full the car considered will be as a %.</i>

#### 3.2 Generating passengers

An equivalent, but more widely used approach than the Origin Destination matrix applies the concept of arrival rates and destination probabilities [3] [2]. This combines passenger demand (how many people want to use the lift for a given unit of time) with a destination probability matrix which determines what proportion of the people arrive on the different floors and where they want to travel.

Consider a passenger demand of 13% with a traffic mix of 45% incoming, 45% outgoing and 10 % interfloor traffic. With ground and 5 upper floors populated by 80 people per floor, the arrival rate - destination probability table [12] is as presented in Table 2

---

<sup>1</sup> In simulation there is also a capacity factor input to limit car loading for a specific car size according to practical limitations. However, the analogous car loading in comparison to RTT calculations is reported as a simulation result.

**Table 2 Arrival rate – destination probability table example**

Origin	Arrival Rate (persons per 5 minutes)	Destination Probabilities (%)					
		Ground	Level 1	Level 2	Level 3	Level 4	Level 5
<b>Ground</b>	27.0	0.00	20.00	20.00	20.00	20.00	20.00
<b>Level 1</b>	6.6	81.82	0.00	4.55	4.55	4.55	4.55
<b>Level 2</b>	6.6	81.82	4.55	0.00	4.55	4.55	4.55
<b>Level 3</b>	6.6	81.82	4.55	4.55	0.00	4.55	4.55
<b>Level 4</b>	6.6	81.82	4.55	4.55	4.55	0.00	4.55
<b>Level 5</b>	6.6	81.82	4.55	4.55	4.55	4.55	0.00

A first estimate of round trip time  $RTT_1$  is required before a list of passengers can be generated for the MCS. This estimate will be revised the MCS repeated until the estimate is the same or very close to the round trip time calculated by MCS.

$$\text{Number of passengers transported } i = \sum[\text{Arrival Rate}] \cdot \frac{RTT_i}{\text{Number of lifts}}$$

If the first estimate of  $RTT_1$  is 120 seconds, and the software is considering a three lift group, then the number of passengers used in the first MCS simulation based on Table 2 will be:

$$\text{Number of passengers transported } _1 = \frac{(27.0 + (6.6 \cdot 5))}{300} \cdot \frac{120}{3} = 8.0$$

The origin and destination of passengers can be generated as described in section 2.1 or as they would be for simulation [13] to create a table equivalent to Figure 3. The approach needs to allow for fractions of passengers. For example, if the number of passengers to be transported was 7.5, in half of the MCS calculations the number of passengers generated would be 7, and in the other half 8.

The software runs the MCS for many trials, each with a different passenger list, and assuming  $RTT_1$ . This yields an improved RTT estimate,  $RTT_2$ . The process is repeated until  $RTT_{i+1} \approx RTT_i$ . Interval is calculated by dividing the RTT by the number of lifts. Capacity Factor is determined by calculating the peak car loading in a round trip as a percentage of the available capacity. The Capacity Factor reported is the mean value of all the trials.

To convey the underlying approach of the application of MCS within the software [2], the authors have chosen to label this analysis type as RTT Simulation (RTTS).

#### 4 COMPARISON OF RESULTS

To compare results, consider Example 4.1 from CIBSE Guide D [1] which is modelling the uppeak in an office building with 14 floors above ground. For a full set of parameters, refer to the Guide. The solution under consideration is a six 1600 kg car group with a rated speed of 2.5 m/s. The passenger demand is 12% uppeak (100% incoming).

Applying the computer program [2] the results for the four different analysis techniques are given in Table 3.

For the RTT Simulation, each MCS was based on 1000 trials. For the dispatcher simulation a group control dispatcher was selected with an uppeak mode which returned all empty cars to the ground floor and cycled their doors. Ten two hour simulations with the first 15 minutes and last 5 minutes disregarded to remove start and end effects.

**Table 3 Comparison of results for CIBSE Guide D Example 4.1**

	<b>Upeak</b>	<b>General Analysis</b>	<b>RTT Simulation</b>	<b>Dispatcher Simulation</b>
<b>Interval (s)</b>	27.1	26.4	27.2	25.3
<b>Capacity Factor by area (%)</b>	71.6	69.6	71.1	66.8
<b>Number of Stops (including ground)</b>	9.3	9	9.5	Not available
<b>Highest Reversal Floor (1 is ground floor)</b>	14.4	14.2	13.4	Not available

The results demonstrate consistency between the different analysis techniques for the uppeak traffic condition.

## 5 DESTINATION CONTROL

### 5.1 Types of control

All the analysis methods in the previous sections assume conventional control. In conventional control, the passenger presses either an up or a down button when they arrive at their origin floor. Once they get in the lift, they select their destination floor and the lift then takes them to that floor. This means that the dispatcher has to make the assignment decision based on the origin and direction of travel alone as it does not yet know the destination. In all RTT calculations, the lifts are assumed to have the same round trip time.

In destination control, improved uppeak handling capacity is achieved through dispatching algorithms that divide the traffic so that passengers travelling to the same destination ride the lifts together. This reduced the average number of stops, and thus the RTT.

### 5.2 The allocator

For MCS, this division of traffic can be modelled by introducing an allocator and having multiple epochs [10]. Instead of modeling a single round trip, or with MCS a single round trip multiple times, the traffic for  $e$  round trips is considered where  $e$  is the number of epochs. Passengers for  $e$  round trips is generated. Then traffic is separated into  $e$  groups according to the allocator logic.

An allocator uses transparent, straight forward rules to approximate the dispatcher logic. For destination control, Al-Sharif et al [10] considered two forms of allocator. The origin allocator sorts incoming traffic into ascending order of origin and outgoing traffic into descending order of origin. This allocator works well for incoming traffic. The destination allocator sorts incoming traffic into ascending order of destination and outgoing traffic into descending order of destination. This works well for outgoing traffic. Once sorted, the traffic is divided as equally as possible between the  $e$  epochs.

In the author's implementation, these two allocators have been combined: incoming traffic is sorted by destination and outgoing traffic is sorted by origin. Although achieved through detailed internal modelling in a dispatcher, this allocator reflects the outcome of a typical destination control algorithm.

In Al-Sharif et al [10] the number of epochs was assumed to be the number of lifts. However, they can be different, particularly in large groups. If the number of lifts is six and the number of epochs was six, then the allocator is assuming that only one in six lifts will be available to the passenger travelling up from the ground floor. This yields a lower interval and larger handling capacity, but longer waiting times.

### 5.3 Results

Table 4 shows the results for Example 4.1 for one to six epochs and a Dispatcher simulation applying the Destination Control (ACA) [2] algorithm configured for ‘time to destination optimisation’.

**Table 4 Comparison of results for RTTS and Dispatch simulation applying Destination Control**

	RTT Simulation						Dispatcher Simulation
	<i>e</i> =1	<i>e</i> =2	<i>e</i> =3	<i>e</i> =4	<i>e</i> =5	<i>e</i> =6	
<b>Interval (s)</b>	27.2	19.1	16.3	14.6	13.4	12.9	15.9
<b>Capacity Factor by area (%)</b>	71.1	50.4	43.5	38.5	35.6	33.6	41.9
<b>Number of Stops (including ground)</b>	9.5	6.3	5.1	4.4	4.0	3.7	Not available
<b>Highest Reversal Floor (1 is ground floor)</b>	13.4	10.6	9.7	9.3	8.6	8.8	Not available

The greater the number of epochs, the more opportunity there is for grouping passengers travelling to common destinations. Hence with increasing numbers of epochs, all RTTS results trend down (get better) as a reduced number of stops and highest reversal floor yields a lower round trip time, interval, and loading.

However, Table 4 results hide that with increased epochs passenger waiting times will increase as the passenger has to wait for their allocated lift instead of the next lift to depart. A real destination control dispatcher is making a tradeoff which account for waiting time, transit time times, and in some instances, required handling capacity to satisfy passenger demand.

In this example, the closest comparison between the RTT simulation and the Destination Control (ACA) algorithm is when there are three epochs. This is analogous to a look ahead factor [14] of three, i.e. the dispatcher will consider the next three lifts in its allocation of a new passenger. This would be a reasonable assumption to balance the competing factors being considered in many destination control algorithms.

Different destination control dispatcher options could be modeled by changing the number of epochs, e.g.  $e=1$  would reasonably correspond waiting time optimisation. In the example above, increasing the number of epochs to  $e=3$  brings the results closer to ‘time to destination optimisation’. For maximum theoretical handling capacity, and some level of ‘anti-saturation control’,  $e=number\ of\ lifts$  would be a reasonable representation.

## 6 CONCLUSION

Monte Carlo Simulation (MCS) is a technique used to tackle problems in many fields spanning finance, engineering, physical sciences and even gaming. It can be used when estimating the value of a variable that is dependent on a set of random input variables.

The application of MCS to lift traffic analysis is relatively new. However, the need to provide analysis of increasing complex systems without developing increasing complex formulae make it an attractive approach to benchmark dispatcher based simulation results.

To work within an existing lift traffic software design paradigm, MCS needed to be applied in a way where the user inputs the required passenger demand and tests a pre-determined lift configuration. This adds complexity to software code but simplifies its application for the user.

Consistency of results for uppeak traffic has been demonstrated between established traffic analysis techniques and MCS. If assumptions are consistent, the results should be similar.

For the analysis destination control, dispatching decisions need to be made which consider more than one average round trip. These decisions have been simplified and included in an ‘allocator’. How this traffic is divided, reflects different modes of operation in destination control systems. Consistency of results for uppeak traffic has been demonstrated between a dispatcher simulation with a destination control algorithm and a MCS using three epochs.

Consistency between MCS and dispatcher based simulation for mixed traffic will depend on how well the allocator reflects the underlying principles of the dispatcher. Further work is required to understand the correlation of results for mixed traffic, and to understand the relationship between interval and waiting time in the context of MCS.

MCS sits in between the RTT calculation and dispatcher based simulation paradigms. To convey the underlying approach of the application of MCS to lifts, the term RTT Simulation (RTTS) has been chosen to label the implementation described in this paper.

The application of MCS and RTTS is likely to become more prevalent as engineers seek new ways to analyse more complex lift systems. It also provides insights into the limits of an idealised dispatcher which informs dispatcher design.

## ACKNOWLEDGMENTS

The authors are grateful for the pioneering work of Dr Al-Sharif in the introduction of MCS to traffic analysis, and to Maria Abbi for her early contribution to the software implementation.

## REFERENCES

- [1] CIBSE, “CIBSE Guide D: 2015, Chapter 3 and 4,” London, Chartered Institution of Building Service Engineers, 2015.
- [2] Peters Research Ltd, “Elevate Traffic Analysis and Simulation Software,” [Online]. Available: [www.peters-research.com](http://www.peters-research.com).
- [3] P. R. D, “Lift Traffic Analysis: Formulae for the General Case,” *Building Services Engineering Research and Technology*, vol. 11, no. 2, 1990.
- [4] R. Smith and R. Peters, “Analysis of Elevator Performance and Passenger Demand with Destination Control,” in *Elevator Technology 17, Proceedings of ELEVCON*, Thessaloniki, 2008.
- [5] R. Smith and R. D. Peters, “Enhancements to the ETD Dispatcher Algorithm,” in *Elevator Technology 14*, 2004.
- [6] S. Gerstenmeyer and R. D. Peters, “Multicar Dispatching,” in *6th Symposium of Lift and Escalator Technologies*, Northampton, 2016.
- [7] B. GC, “Can lift traffic simulators be verifiable, transparent, repeatable & reproducible,” in *10th Symposium on Lift and Escalator Technologies*, Northampton, 2019.

- [8] L. Al-Sharif, O. F. Abdel Aal and A. M. Abu Alqumsan, “The Use Of Monte Carlo Simulation To Evaluate The Passenger Average Travelling Time Under Up-Peak Traffic Conditions”.
- [9] S. Gerstenmeyer, “Traffic Analysis for a Multi Car Lift System Used as Local Group,” in *9th Symposium on Lift and Escalator Technologies*, Northampton, 2018.
- [10] L. Al-Sharif and R. D. Peters, “Using the Monte Carlo Simulation to Evaluate the Round-Trip Time Under Destination Group Control,” in *9th Symposium of Lift and Escalator Technologies*, Northampton, 2018.
- [11] L. Al-Sharif and A. M. Abu Alqumsan, “An integrated framework for elevator traffic design under general traffic conditions using origin destination matrices, virtual interval, and the Monte Carlo simulation method,” *Building Services Engineering Research and Technology* 36.
- [12] Peters Research Ltd, “Elevate Advanced Training Course Example,” Peters Research Ltd, Great Missenden, 2020.
- [13] R. D. Peters, L. Al-Sharif, A. Hammoudeh, E. Alniemi and A. Salman, “A Systematic Methodology for the Generation of Lift Passengers under a Poisson Batch Arrival Process,” in *5th Symposium on Lift and Escalator Technologies*, Northampton, 2015.
- [14] G. C. Barney and S. M. dos Santos, in *Elevator Traffic Analysis Design and Control*, London, Peter Peregrinus, 1985.

## BIOGRAPHICAL DETAILS

Matthew Appleby is a Software Engineer with Peters Research Ltd. He is part of the team working on enhancements to Elevate and related software projects. He joined Peters Research in 2019 and is studying part time for a Digital Degree Apprenticeship.

Richard Peters has a degree in Electrical Engineering and a Doctorate for research in Vertical Transportation. He is a director of Peters Research Ltd and a Visiting Professor at the University of Northampton. He has been awarded Fellowship of the Institution of Engineering and Technology, and of the Chartered Institution of Building Services Engineers. Dr Peters is the principal author of Elevate, elevator traffic analysis and simulation software.



# The Use of Lifts in Offices in Social Distancing Environments

Jochem Wit

Deerns Netherlands

**Keywords:** COVID-19, social distancing, optimization, traffic handling, lobby capacity, waiting times.

**Abstract.** This paper addresses the potential remaining lift capacity for high-rise office buildings when limiting the number of passengers per car to only two persons due to social distancing restrictions in the COVID-19 era. It describes an array of measures that have to be taken to guarantee personal safety and sufficient distance, namely by eliminating crossing traffic and optimising the potential use of the lift system. Both the waiting time and the lobby capacity can be decisive when searching for the optimum. Without proper measures only about 20-30% of the original population can usually be served. With major measures and by successfully reducing peak flows the new maximum population can be increased to about 40-60% of the original population.

## 1 INTRODUCTION

In the spring of 2020 most office buildings were temporarily abandoned due to national lockdowns as a result of the global outbreak of the COVID-19 virus. To avoid further spreading in crowded working environments the majority of office workers have since then been working from home and have not been able to visit their offices on a daily basis. Since the summer of 2020 most countries have gradually released the restrictions for outside activities but still hold back on indoor activities with large densities of people in areas with possibly insufficient ventilation capacity. In most public buildings social distancing of 1.5-2.0 m between individuals must be maintained and most companies transfer these restrictions to their office environment to minimise the risk of an outbreak in their personnel. Apart from the significant reduction in floor capacity in terms of usable desks the social distancing rules also reduce the practical capacity of lifts, stairs, corridors and lobbies. This paper offers an overview of the outcome of several lift studies that were performed for existing office buildings to determine the limitations and points of attention due to social distancing in lifts and lift lobbies.

## 2 POPULATION

The outcome of several building studies shows that social distancing restrictions in offices can result in a significant reduction of available desks and supporting services. The population that can actually return to work safely within the new settings appears to be in a range of 50%-65% of the original population, depending on the offices type, the lay-out of the building and its floors and the original office floor density. The higher the original density of desks per floor area was (one desk per 6-8 m<sup>2</sup> net floor area is not uncommon in open-plan offices nowadays), the higher the density reduction factor will be. The number depends very much on the lay-out and orientation of the desk clusters per floor: how many desks per cluster can be used safely, can these clusters be moved or rearranged to provide more distance, are there any corners of the office area that have to be closed off to avoid deadlocks and facilitate one-way traffic flows? It also depends highly on how far the owner/employer is willing to invest to alter the lay-out temporarily and provide safety measures such as protective screens and organise additional cleaning/disinfecting service rounds. Additionally, in some cases the lay-out of general services such as restaurants, toilet areas, cloakrooms and pantries provide a maximum on a floor or even building scale on top of the local limitations. Reduced availability of stairwells might limit the population due to safety implications in case of evacuation. And then there is the issue of the remaining lift capacity, that reduces the maximum returning population even further.

### 3 LIFT AND LOBBY CAPACITY

There are two main reasons why the transportation capacity of the original lift system will decrease significantly in a social distancing office environment:

- Reduction of the maximum car load to no more than 2-3 persons per car, thus reducing the fundamental transportation capacity of the lift system;
- Reduction of the lobby capacity for waiting persons due to loss of maximum density and/or loss of waiting area due to newly required traffic corridors.

Compared to the regular car loading in common 1,275 – 1,800 kg lifts in office buildings the loss of capacity in a lift car due to social distancing can be up to 75-90%. This is a huge decrease of transportation capacity from the original design. Luckily there are mitigating circumstances that improve the potential significantly, such as lower cycle times and less interference from two-directional and interfloor traffic. Please refer to sections 4-6 for a further substantiation of this effect.

Regarding the lift lobby the common area capacity will typically reduce from a range between approximately 0,5 m<sup>2</sup> (crush capacity) and 0,75 m<sup>2</sup> (normal capacity) per person under normal conditions to a range between approximately 2,5 m<sup>2</sup> (no cross traffic) to 3,0 m<sup>2</sup> (limited cross flow) per waiting person under social distancing conditions. This too is a reduction in capacity of 70-85%. These values already take into account that several corners of the area will not be used efficiently.

The loss in waiting capacity will be urgently noticeable through the forming of significantly longer queues than normal. The loss of transportation capacity will add to the problem indirectly by processing significantly less people per time unit than previously. The combined effect will result in huge levels of congestion in the waiting areas and corridors leading up to these areas, if the original population were to be given access to the building. This is exactly what needs to be avoided in a social distancing environment and that is why the visiting population has to be reduced to restore balance in the system for buildings that rely heavily in the lift system.

The limitations mentioned above force us to reconsider both the conventional traffic handling capacity of the lift configuration - based on (increased) waiting time criteria - and the available lobby area – considering the required (decreased) queue lengths potential. Both capacities can be the limiting factor in social distancing lift analyses.

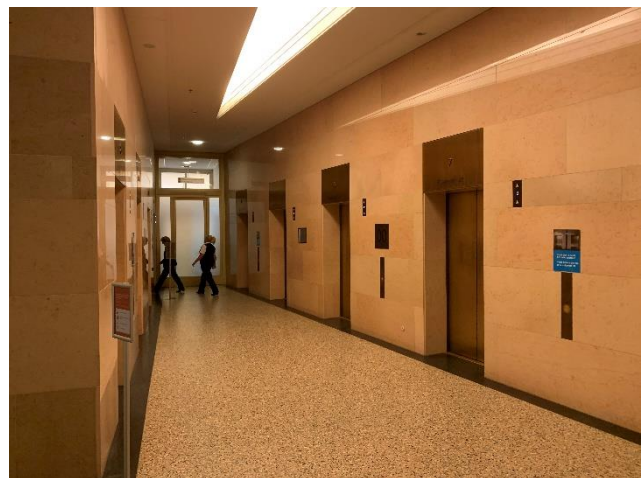


**Figure 1: Empty lift lobbies during the COVID-19 period. Will they soon fill up again with reduced queuing density?**

#### 4 PRIMARY MEASURES (HOW TO BOOST POTENTIAL)

For boosting the remaining traffic handling capacity in office buildings to allow a population as high as possible to safely return to the building, the following (mainly organisational) measures should be considered:

- **Increasing the use of stairs:** Mandatory use of stairs for the bottom 3-5 floors should be introduced, assuming that proper solutions for the transportation of mobility impaired persons (MIP) and goods are available (see below). The stairs should be used in one direction only, unless they are at least 2 meters wide or can be divided into an upward and a downward lane by temporary screens. This is necessary to guarantee safe distance between the people using it: passing each other will usually not be possible within normal stairs width. Additionally some stairs may have to be closed off completely (for instance if they exit into the lift lobby thus jeopardizing the main traffic flow) or made accessible in one direction only;
- **Eliminating interfloor traffic:** If possible within single tenant situations (or multi-tenant with multiple floors per tenant) interfloor traffic in the lifts should be eliminated as much as possible. This means that the use of stairs between floors becomes mandatory. This measure is necessary to keep the cycle time of the lifts for primary home floor traffic as low as possible, and to prevent stops with already filled cars when conventional controls without a (modifiable) car weighing device are present. Please refer to section 5 for a further explanation;
- **Reducing and spreading meeting traffic:** It will remain important to meet online as much as possible, due to the reduced capacity of meeting rooms and to avoid hourly meeting traffic peaks. It is vital to avoid unnecessary interfloor traffic peaks on the whole hours. This can be solved by making sure that half of the meeting facilities can only be booked on the whole hours and the other half only on the half hours. This results in a halving of the internal meeting peaks. The alternating schedule can be realized by programming 30 minute disinfection breaks in between the meetings;
- **Avoiding crossing traffic flows:** Crossing flows in the lift lobbies should be avoided as much as possible, to maximise floor area and prevent door transfer time delays due to people waiting for counterflow traffic. This is necessary to avoid dense flows in two directions through a common lobby, resulting in a major reduction of waiting area capacity and or risk of a breach in the safety distancing between people. This may require eliminating the lunch peak traffic, providing separate floors for incoming and outgoing traffic and opening/closing secondary entrances:
  - **Eliminating lunch peak traffic:** Lunch traffic does not only burden lift group controllers the most these days, it also results in unwanted two-way traffic in lobbies. It is advisable to consider eliminating two-way lunch traffic as a whole by introducing mandatory lunch in the workplace, unless incoming traffic and outgoing traffic can be vertically separated (see below). So preferably the restaurant(s) and any other decentralised facilities (coffee corners and take-away points) should be closed off. If necessary, lunch boxes can be delivered on the office floors in the morning with a separate goods lift;
  - **Vertically separating incoming and outgoing traffic lobbies:** If the incoming and outgoing traffic during lunch break can be vertically separated on different levels, two lobbies (one for incoming and one for outgoing traffic) should be used. Lunch traffic will then however remain dominant for the analysis and the achievable remaining population. A benefit here is that the lobby capacity will probably not be the limiting factor anymore. On the other hand, traffic between the two separated floors will not be possible, so alternative measures for MIP and goods traffic might be necessary. The separation can be advantageous for the morning up peak and the afternoon down peak as well, since no counter traffic routes have to be organised in the main lobbies;



population. This reduction should preferably be realised by closing off the highest floor(s). For office buildings with 10 or more floors above the ground floor a significant reduction of the visiting population and/or populated floors will be necessary to guarantee safe working and traveling conditions for the population. These buildings require bespoke analysing of the traffic handling with the available lift and lobby system.

## 5 SECONDARY MEASURES (HOW TO MAKE IT WORK)

The following secondary measures will probably be required to guarantee safe use of the lifts from a social distancing perspective and make the processes as described in section 4 work properly:

- **Reducing the car load:** Reduction of the maximum car load to 2-3 people through adjusting the load bypass thresholds (when using a weighing device with conventional controls) and/or the controller settings (when using destination control) will be necessary. For upwards traffic from the main lobbies this can also be organised by emphasising and upholding the limited car loading rules to the users, but especially for downwards traffic it is crucial that the car load is limited to 2-3 persons to avoid unnecessary stops, resulting in loss of capacity and irritation for the users. When using destination control this can be done from within the intelligent control system, but if there is a conventional control system this will not always be possible. A load weighing device with a load bypass system will not always be available and if there is one it is not self-evident that it can be adjusted to function properly and reliably in the 150-225 kg range. Possibly a (costly and time consuming) modification of the car and counterweight balancing or other sensing devices (infrared detection) are required. If this is not addressed, interfloor traffic and/or the otherwise rather harmless afternoon down peak could become dominant in the capacity and quality experience of the users due to a series of unnecessary and frustrating stops. In these rare cases down traffic should be forced to use the stairs or concentrate on transfer levels to be collected by lifts with dedicated service zones;
- **Identifying waiting zones on the floor:** Although it would be best to rely on the discipline and common sense of the population, it is recommended to provide visual reference areas or waiting spots on the floor in the main lobbies (mandatory guidance). On the upper floors the density in the lift lobbies will be minimal and personal discipline will be sufficient;
- **Improve circulation and guarantee safety distances:** Within small lobbies and especially when two-way traffic or through traffic in the lobbies is unavoidable, mandatory routing and safe zones should be provided by using screens to separate the waiting areas (with circles or 1.5-2.0 m marking on the floor) from the circulation areas;
- **Reducing delays:** The door and sensor delay settings should be improved when they are not already maximized. The chance of extra people embarking late resulting in door re-openings is limited within the new social distancing game rules, assuming the population and traffic is organized professionally and people behave respectfully;
- **Rearranging panels:** Due to conflicting waiting and circulation areas it is possible that hall call panels or destination selection panels (when placed inside the lobby) have to be moved or deactivated if they interfere with the optimal use of the lobby and would introduce more people interacting within social distance limits than strictly necessary. Thus an optimal arrangement of flows versus waiting spots can be achieved in an environment where panel use will be less intense and with a more predictable rhythm;
- **Emphasizing the required discipline and responsible behaviour:** The importance of each person's own responsibility in maintaining a safe distance to others, playing by the rules and behaving respectfully cannot be overemphasized. The same applies to placing one call per person with destination control systems: this becomes even more important than it already was. Everybody shall have to place an individual call, there is no room for ghost passengers.

## 6 CAPACITY BOOSTING

In section 3 it was stated that the theoretical reduction of traffic handling capacity can be approximately 75-90% of the original capacity due to the limited number of people in the cars. In practice, the remaining values can be significantly better due to the following effects:

- A substantial reduction of lift cycle times due to the fact that the lifts will be making significantly less stops during their cycle and will also have a lower average reversal floor. The reduction depends on the number of floors and the original car loading. For buildings with more than 10 floors and cars with a nominal load of 1,275 – 1,800 kg the number of stops per cycle will typically reduce to approximately only 15-30% of the original number. The average reversal floor will reduce to 70-75% of the original floor height. On the other hand, transfer times will be longer and door sensor times will have to be as well. Please refer to the end of this section for the logic behind this. In the conducted studies so far, the resulting cycle time of lifts with reduced car loading proved to be 20-40% lower;
- There will be a significant reduction in disruptive interfloor traffic, which results in an additional reduction of the cycle times. The effect depends on the tenancy of the building: within a multi-tenant setting the effect will be limited (especially if there are multiple tenants per floor instead of multiple floors per tenant), but in a single tenant situation this effect can provide 5-10% extra traffic handling capacity;
- Due to the above effect the transit times for passengers will be substantially lower and due to that trade-off a rise of waiting times can be acceptable, assuming that the lobby capacity is sufficient. A rise of the average waiting time from for instance 40 to 60 seconds could be acceptable in the new social distancing working culture, if that time loss is earned back during the trip. With appropriate communication about the measures and the procedures the people will understand and accept the new balance;
- If possible, the lunch peak should be eliminated by mandatory lunch breaks on the office destination floors. This eliminates the traffic peak that is dominant nowadays in offices, reducing the traffic handling issue to the lesser challenging morning up peak. This provides room for a more efficient traffic handling of a slightly higher population in the less dense morning traffic profile;
- The traditional peak flow densities in buildings will most likely reduce slightly due to the desire of (a part of) the original population to avoid crowds. Even without mandatory peak flow reduction by for instance introducing fixed time slots for working and lunching hours, it may be expected that morning peak flows reduce from 11-14% per 5 minutes to 9-11% per 5 minutes and lunch peak flows from 12-16% to 10-13% per 5 minutes. The bandwidth is mainly due to differences between single and multi-tenant buildings, locations in the direct vicinity of public transportation hubs and/or lunch facilities that are not on the main entrance floors (resulting in additional lunch traffic between the restaurant and the entrances/exits for people enjoying a lunch break stroll);
- Finally, the new maximum population will probably be significantly lower due to area restrictions for safe working conditions. If the population reduces to the earlier mentioned 50-65% of the original capacity, the remaining traffic handling capacity proportionally increases will approximately 50%-100%.

Depending on the situation in the office tower, two extra measures can be considered to boost the up peak traffic handling compared to the pre-corona situation even more:

- If the lift capacity is dominant: reduce the number of home floors, for instance by closing off stops on basement (parking) levels or podium amenities levels. Be aware that this might be necessary anyway in case there are conventional controls present and the car load weighing device cannot be modified to a 2-3 person threshold;

- If the lobby capacity is dominant: introduce multiple home floors, for instance by allowing basement (parking) traffic or encouraging traffic from podium amenities levels. This requires destination control or a car load weighing device that can be modified to a 2-3 person threshold.

Please be aware that when using lift simulation software to determine the remaining population that can be handled in relation to the lobby capacity there is a potential discrepancy to consider between simulation and reality when using destination control. This is caused by the queuing discipline and organisation, that can be significantly different than usual, for instance when using single line queues (without overtaking possibilities) or split queues (partially in the lobby after the destination control panels and partially outside of the lobby before these panels):

- In case of split queues there will be a lag of information and thus a reduction of the intelligence potential of the lift controller. Within destination control systems the controller can choose to assign people who have arrived later to shortly incoming cars, thus skipping the queue (not First in First Out which is more applicable to conventional traffic handling). This is done to reduce the number of destinations per trip and optimise coincident calls. Within social distancing settings this is not always possible, so the number of selected calls can never exceed the lobby capacity and destinations are possibly given later. In reality the controller will not be aware of the queue that might be present behind the selection panel, in the simulation software it usually does. This results in simulation outcome that are potentially too positive, since the simulation controller knows all the destinations of created agents in advance;
- Even within the lift lobby it might prove to be practically impossible to transfer to an assigned lift through the already waiting people before their lift leaves. This might result in extra delays through efficiency loss (not all spots on the floor will be occupied) and longer embarking times within the lobby.

## 7 FLATTENING THE CURVES

Apart from the traffic handling and capacity boosting measures presented in sections 4-6 it can also be advantageous to influence the demand side. Corresponding to the global COVID-19 strategy to “*flatten the curve*” to protect health care capacity one could likewise ease the pressure on lift systems by spreading out the demand over longer peak periods. See figure 3 for an illustration. Common peak flow percentages and potential values under social distancing restrictions are:

- Common peak flow values in offices will be between 11-14% per 5 minutes during the up peak and 12-16% per 5 minutes during the lunch peak, depending on a multi- or single tenancy, fixed or flexible working hours and/or direct connections to public transportation hubs;
- Due to the probable reluctance of office workers and hopefully their desire to avoid high densities it can be expected that the population will spread their working and lunch times within the social distancing era more than before. They will probably flatten the curve to possibly 9-11% and 10-13% respectively without the building facility manager having to organize mandatory working shifts to reduce peak values;
- If an even greater reduction of the peak flow density is required in the building to increase the maximum population mandatory working and lunching time slots will be inevitable. Even then a peak of 6-8% and 8-10% during up and lunch peak respectively will probably be the minimum due to other external influences and practical limitations that become dominant. These could be school opening times, public transportation peaks, internal meeting schedules and unavoidable lunch flocking. When mandatory time blocks are introduced for the lunching peak this should not be done per individual floor to avoid congestion in the destination floors lobbies. It would be better to lunch by vertical zone, horizontal zone (North-South or East-

West) or in alphabetical order. This could be slightly disadvantageous for the waiting times, but it prevents undesirable queues in the destination lobbies;

- The outgoing afternoon peak will usually not be relevant in office buildings due to lower peak percentages and scattered traffic in multiple lobbies. There is however one exception if the lifts have conventional controls and a load weighing device is not present or cannot be modified to a 150-225 kg zone with sufficient reliability. In that case the down peak can become dominant after all. Please refer to section 5 for an explanation.

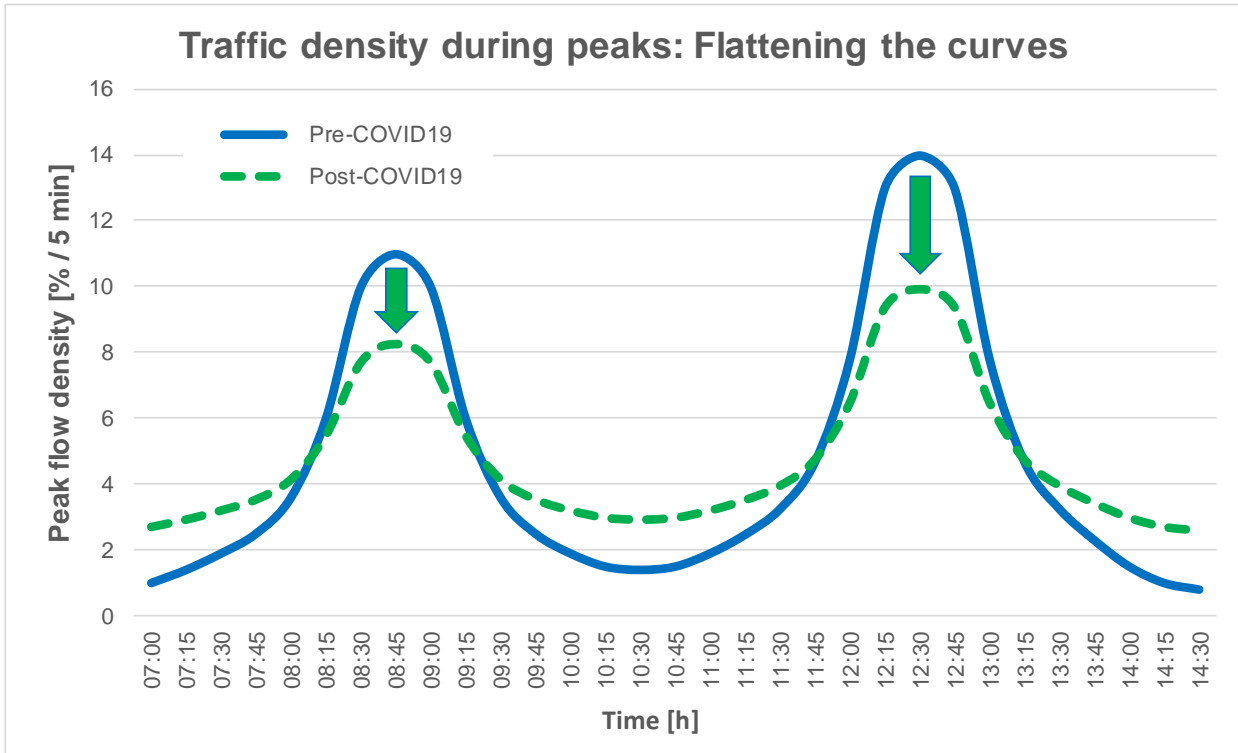


**Figure 3: Flattening the curves: Will this happen automatically or does it have to be enforced to optimise lift capacity utilisation?**

## 8 CASE STUDIES

During the COVID-19 pandemic several building studies were performed to determine the potential population that could safely return within social distancing restrictions. Amongst others a national high-rise headquarters and two high-rise ministries asked Deerns to determine how many people could still be allowed in the buildings and how long the queues for the lifts would become, assuming that within social distancing there would only be room for 2 or 3 people in the lifts? They also wanted to know what would be required in terms of organizational measures (traffic flows, use of stairs, peak reduction) and technical measures (lift controls, switching off stops and/or panels, adjusting car loads) to be able to use the building and the lifts safely?

After analysis by means of extensive lift simulations, it has been found that without forced spreading of work times, in most cases about 30-40% of the original population could return to these offices, assuming that the original traffic peaks would slightly reduce due to natural spreading. By moving to forced working time distribution, approximately 40-60% of the original occupation could be welcomed back again. In order to achieve these numbers at the head office the lobby capacity on the ground floor had to be limited to a maximum of 12 people and several destination selection panels had to be switched off. An important additional condition for the re-occupation of this building was that the opposing traffic had to be split during the lunch peak: ascending traffic

will soon leave from the ground floor while descending traffic gets out on the 1<sup>st</sup> floor and continues down the stairs. In the ministries, the lunch peak will have to be eliminated completely (by providing lunch at the workplace) and the main floor of the high-rise lift groups will be moved to the 2<sup>nd</sup> floor, in order to make better use of the capacity of the lobby (which will only fit approximately 20 people).

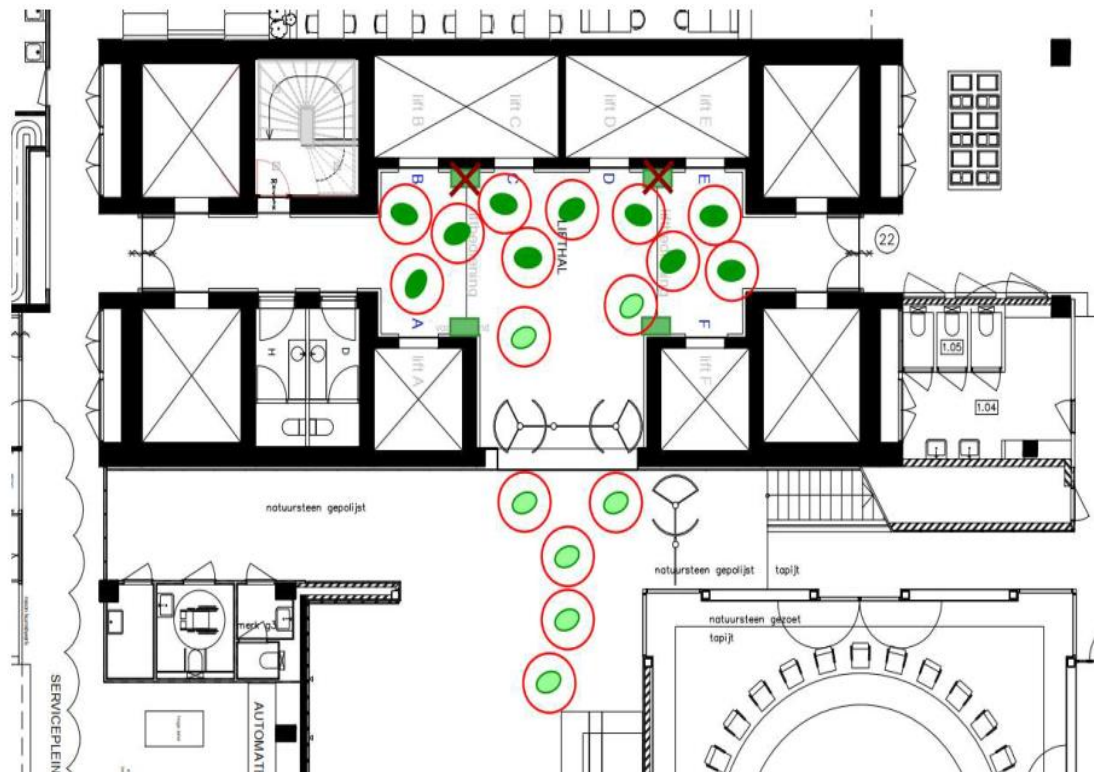


**Figure 4: Example of a lift lobby with frontal orientation, a limited number of waiting positions, reduced number of panels and split queues.**

From one of these cases figure 4 shows an example of a lift lobby with a remaining queuing capacity of approximately 12 persons, split queues (partially in the lift lobby and partially in the general entrance area) and a reduced number of destination selection panels. In this case lunch traffic had to be vertically split to optimise lobby capacity.

Figure 5 shows an example of a waiting time and queuing length graph, used to determine which of these is dominant for the maximum population to allow back into the building. In this particular case an increased average waiting time value of 50 seconds was acceptable and the remaining traffic handling capacity of the lift group proved to be approximately 22 people per 5 minutes. This traffic intensity would result in an average queue length of approximately 5 persons in the lift lobby, but with stochastic variations up to a maximum value of 14 people. Would the maximum lobby capacity here have been no more than for instance 10 people, the allowed passenger flow should not have exceeded approximately 19 persons per 5 minutes. The corresponding average waiting time would then only be approximately 28 seconds. For reference, this particular lift group would normally provide handling capacity for approximately 50 people per 5 minutes, resulting in a remaining traffic handling capacity of only 38-44% of the original value.

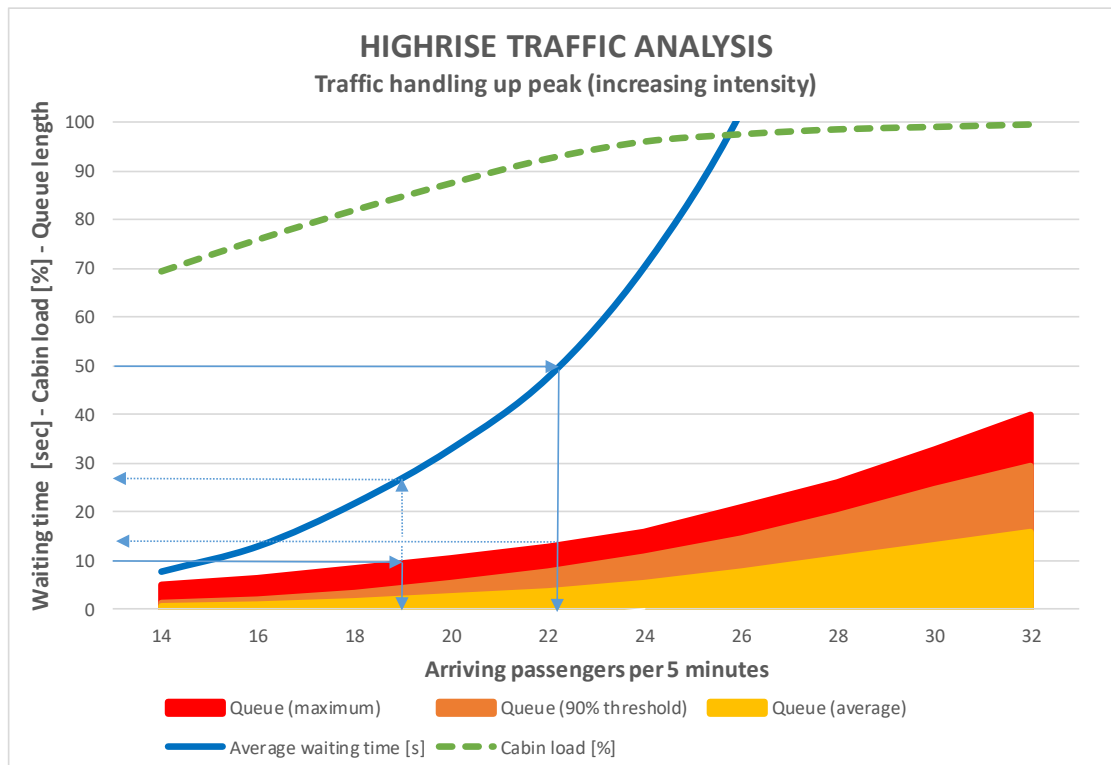


**Figure 5: Example graph of a capacity analysis for restricted lift capacity during social distancing (waiting time and queuing length).**

## 9 CONCLUSIONS AND FUTURE PROSPECTS

Analysing the remaining traffic handling capacity and the scope and depth of technical and organisational measures for social distancing lift optimisation is always bespoke work, especially for high-rise buildings. It involves the lift configuration, the building lay-out, the lobby lay-out, the stair configuration, the peak flows, the tenancy (single or multi), the number of home floors and the range of organizational measures the client is willing to accept. For buildings up to about 6-8 floors the lifts are generally not dominant and buildings can generally fill up to their maximum social distancing population when enforcing optimised stair use. For buildings from 8-10 floors above the ground floor the lifts become dominant and the maximum population decreases.

From several practical cases and simulation studies the following main bandwidths were found for traffic handling with reduced car loading in office buildings with 10 or more destination floors:

- Without measures or with only slight adjustments about **20-30%** of the original population can usually be served;
- With major measures (mandatory use of stairs for lower floors and interfloor traffic, no lunch peak or a vertical traffic split for incoming/outgoing lunch traffic, closing off several higher floors, raising the home floor for highrise lifts et cetera) the population can be increased to about **30-40%** of the original population;
- By reducing peak flows through mandatory time schedules for working and lunching hours the population can be increased to about **40-60%** of the original population;
- For most buildings this adds up to about **70-90%** of the newly reduced social distancing population. When a reduction of this revised population is necessary due to the lifts and/or lobby capacity it is best realised by closing off the highest possible floor(s).

The question that remains is if we will soon (if ever) return to the original pre-COVID19 densities of office populations. A permanent higher fraction of workers from home and lower overall densities for offices are very probable in the near future. It is too early to say if we will ever be designing for densities based on 6-10 m<sup>2</sup> per person again. Will tenants respond by transferring to smaller offices, resulting in more tenants per floor and higher density mixes in existing multi-tenant buildings? A migration of office users to smaller floor plates seems very likely.

To prepare for future circumstances requiring social distancing one might want to consider pandemic proof building designs which provide a fundamental separation between incoming/upward and outgoing/downward traffic. This could require separate stairwells and lift lobbies for incoming and outgoing traffic (vertically stacked) as well as stairwells not directly connected to crowded lift lobbies. This could also have an effect on the required lift lobby area and the need for additional stairs and escalators for splitting inbound and outbound traffic vertically.

These measures could as a side effect increase the lift capacity but also provide more health focus and liveliness in the building, assuming that the stairs connecting to the entrance area are designed to be attractive and wide to accommodate traffic flows at an appropriate distance.

## REFERENCES

- [1] M. Bruil, & C. Rentier, *Vuistregel voor bepaling huisvestingscapaciteit met de 1,5 meter richtlijn bij gebruik van liften* (2020)

## BIOGRAPHICAL DETAILS

Jochem Wit received his MSc degree in Mechanical Engineering with honours from the Technical University of Delft in 1995. He is a transportation and lift logistics consultant at Deerns. He specialises in lift capacity analyses, simulations and logistical studies for the optimal dimensioning of lift groups in high-rise buildings, complex stacked buildings and hospitals. In recent years he has focussed on evacuation using lifts and solving saturation problems in under lifted / over populated buildings. He works at the Transportation & Logistics department of Deerns, an expert group in the field of building related transportation equipment. Jochem Wit was a member of the Technical Committee of the Dutch High-rise Covenant and chairman of the Technical Subcommittee for Vertical Transportation.



# Using the Inter-Linked Monte Carlo Simulation Method (iL-MCS) to Calculate the Value of the Elevator Round Trip Time to Reflect the Random Nature of Passenger Destinations

Lutfi Al-Sharif, Noor Toghoj, Ammar Hakam

The University of Jordan, Amman 11942, Jordan

**Keywords:** Monte Carlo simulation, interlinked Monte Carlo simulation, elevator, lift, round trip time, interval, elevator traffic engineering

**Abstract.** The Monte Carlo Simulation method (MCS) has been successfully used to find the value of the elevator round trip time under general traffic conditions. It has also been extended to find the value of the round-trip time under destination group control. This paper extends the application of the method by introducing the so-called “interlinked Monte Carlo Simulation” method (iL-MCS). In the conventional MCS method, the trials are not linked, and each trial is completely independent of the other trials. The new suggested method (iL-MCS) links the trials such that the end conditions of one trial affect the initial conditions of the following trial. This “interlinking” allows the method to reflect the effect of the random passenger destinations on the value of the round-trip time. It can even be extended to quantify the effect of elevator bunching on the value of the round-trip time and hence the loss in handling capacity due to the effects of elevator bunching. Examples will be coded in MATLAB and presented to illustrate the method and its results.

## 1. INTRODUCTION

The elevator round trip time has for a long time formed the basis of sizing and selecting the number and speed of elevators in a building [1] following the assessment of demand [2]. Even with the advent of simulation, most designers still use the round-trip time as the basis for the initial phase of the design based on calculation and then follow it up with simulation runs to refine the final design.

The calculation of the value of the round trip time has traditionally been based on using an equation that was developed and expanded in the 1980s [3] which relies on the elevator kinematic equations ([4], [5]). The main drawback of this equation is that it is only applicable and correct in a special set of conditions such as incoming traffic, independent passenger decisions, rated speed attained in one floor jump and a single entrance. A number of researchers have attempted to extend the application of this equation to more general cases ([6], [7], [8]). An attempt was also made to extend the equation to accurately incorporate all of these special conditions [9].

One of the most important successes in this area was the application of the Monte Carlo simulation method to find the value of the round-trip time under incoming traffic conditions [10] and then under general traffic conditions [11]. It was also used to find the value of the average travelling time [12]. In one of the latest papers, it was used to evaluate the round-trip time for hypothetical traffic systems ([13], [14], [15]) and even under destination group control [16].

In all these papers that used the Monte Carlo simulation to find the value of the round-trip time, the trials were completely independent. Each trial was kept separate from the preceding and the succeeding trials. This paper introduces the concept of interlinking the consecutive trials in order to better reflect the randomness in the elevator traffic system. Specifically, this paper *interlinks* the trials in order to reflect the effect of the variability in the value of the round-trip time that is caused only by the randomness of the passenger destination.

It is worth mentioning that this paper will not take into consideration the randomness in the arrival times of the passengers (assumed to follow a Poisson distribution). This would be the scope of a future paper.

The way in which the Monte Carlo simulation has been applied to the evaluation of the round-trip time has been based on generating random passenger origins and destinations. These origins and destination are then used in order to calculate the exact value of the round trip time for this trial (or scenario) by calculating the kinematics of movement of the car to get to the required floors, the door opening and closing time, and the passenger transfer time into and out of the car. This value of the round-trip time is stored in an array. The process is repeated for many trials (denoted as  $n$ , say 10 000 trials). The value of the round-trip time for each trial (or scenario) is stored in the same array. At the end of the  $n$  trials, the average value of the round-trip time is taken as representative of the true value.

A similar process will be followed in this paper, but with the difference that the number of passengers generated in each trial is not constant, but dependent on the previous value of the round-trip time. The car capacity will be assumed to be limited, thus better reflecting the reality of the fluctuations in the value of the load in the elevator car.

The second section will identify the two sources of randomness in elevator traffic systems. The third section takes one of these sources of randomness and further discusses the two-way complex inter-dependence between the number of passengers boarding the elevator car and the value of the resultant round-trip time. The fourth section evaluates the value of the round-trip time under interlinked Monte Carlo simulation conditions, assuming an unlimited car capacity. "Unlimited car capacity" means that whatever the number of passengers waiting at the landing can board the car and are not restricted by the physical car capacity. The fifth section shows that the analysis would always converge to the same average value of the round-trip time regardless of the starting conditions. The sixth section explores the effect of limiting the car capacity on both the value of the passengers in the car and the overall handling capacity. Conclusions are drawn in the seventh section.

## **2. THE TWO SOURCES OF RANDOMNESS IN ELEVATOR TRAFFIC SYSTEMS**

The two sources of randomness in elevator traffic systems are the following:

1. The first source of randomness in the arrival times of the individual passengers. It has long been recognized that the arrival of passengers for service follows a Poisson distribution (more precisely, the number of passengers arriving in a specified period of time follows a Poisson distribution, and this random variable is a discrete random variable). It is more common to model this process by examining the inter-arrival time between consecutive passengers, which follows an exponential distribution, whereby the random variable is a continuous random variable. This source of randomness is not considered in this paper. For simplicity, the inter-arrival time is assumed to be constant.
2. The second source of randomness in elevator traffic systems is the randomness of the passenger origin and destination floors. In the general case, it is assumed that the passenger origin and destination selections are independent. When the building under consideration has a single entrance and the type of traffic is incoming only, the origin floor is the same for all passengers and the source of randomness is the passenger destination floors. Each passenger is assumed to select a destination based on the probability density function for the floor destinations, which is based on the number of occupants in each floor.

These two sources are the source of all randomness in the elevator traffic system, and any other display of randomness in the elevator has its roots in one or both of these two sources. For example,

the variability of the round trip is caused by the random passenger destinations (2<sup>nd</sup> source above) and the variability of the number of passengers boarding the elevator car (which is caused by both the first and second sources above).

It is also worth remembering that the variability of the round-trip time for each elevator will lead to the time between the successive arrivals of the elevators at the landings being variable, a phenomenon known as bunching ([17], [18]). It is widely accepted that bunching can lead to the loss of handling capacity and the increase in the passengers waiting time. In extreme, cases, bunching can lead to the reversal of the sequence of elevator movements around the building (i.e., with four elevators in the group, and assuming they start in the sequence of A, B, C and D, this could later become A, C, B, D).

In this paper, only the second source of randomness is modelled (and more specifically, the passenger destinations only, as the building under consideration has only one entrance and the type of traffic is incoming only). Its effects on the variability in the value of the round-trip time, number of passengers boarding the elevator car and the passengers left queuing behind at the landing are all explored.

The other source of randomness is not considered in this paper and will be the subject of a future paper.

### **3. THE COMPLICATED INTER-DEPENDENCE BETWEEN THE NUMBER OF PASSENGERS BOARDING THE CAR IN A ROUND TRIP AND THE VALUE OF THE ROUND TRIP TIME**

The randomness of the passenger destinations result in the variability of the value of the round-trip time. When the round-trip time varies, this means that the elevator car will take longer than normal or shorter than normal to return to the main entrance (or to any landing) for the next round-trip. This variability means that more passengers will have accumulated at the landing (when the round trip time is longer than its average value) or fewer passengers would have accumulated at the landing (when the round-trip time is shorter than its average value). If the elevator car has unlimited capacity, then it is assumed that the elevator car can take all of these passengers. This variability in the number of passengers boarding the car will then, in turn, lead to the variability of the value of the round-trip time...and so on. This inter-dependence between the number of passengers boarding the car in each round trip and the value of the round trip time is best represented by using the Inter-linked Monte Carlo simulation, where the value of the round trip time in each trial is used to determine the number of passengers in the following round is neatly capture by consecutive numerical trials.

So this is a two way effect: The increase in the number of passengers boarding the elevator car in a round trip will generally increase the value of the round trip; and the increase in the value of the round trip means that more passengers “accumulate” waiting at the landings waiting to board that elevator car. The decrease in one variable will also then lead to a decrease in the other.

However, this vicious cycle is broken by the randomness of the passenger destinations. For example, even if the number of passengers in a round trip is large, they could all be heading to coincident lower floors in the building leading to a smaller value of round-trip time. Alternatively, even if the number of passengers is small in a round-trip, they could all be heading to non-coincidental floor in the upper part of the building, leading to a larger value of the round-trip time.

#### 4. THE NUMBER OF PASSENGERS IN THE CAR IN EACH TRIAL ASSUMING UNLIMITED CAR CAPACITY

In this section, the car capacity is assumed to be unlimited. The consequence of this simplifying assumption is that no passengers are left behind in each round trip and thus no passengers need to be “carried-over” to the next round trip. In section 6, this assumption is removed, and the effect of the limited car capacity is further explored, which results in passengers being left behind at the landing and being “carried-over” to the next round-trip trial. It is interesting to note that adding this feature to the Monte Carlo simulation method, represents an action that moves the system nearer to the characteristics of discrete time-simulation (or time dependent simulation).

Under the conventional Monte Carlo simulation trials, it is assumed that the number of passengers is constant in each trial (10 passengers in this case). In order to allow the reader to have a visual base to compare the following graphs to, this trivial assumption has been shown in Figure 1 assuming constant passenger arrival rate.

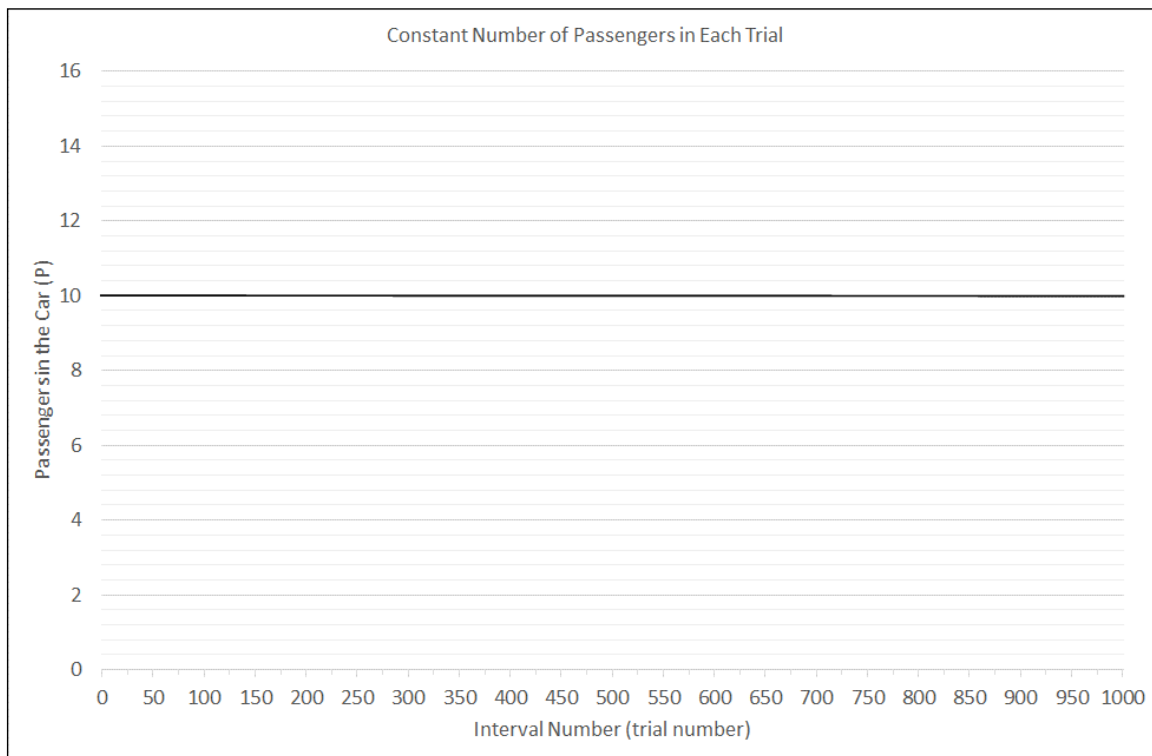


**Figure 1: The number of passengers in the car is constant in each trial.**

The next figure shows how “interlinking” the consecutive Monte Carlo simulation trials alters the value of the passengers boarding the elevator in each round trip. The value of the passengers boarding the elevator car in each round trip only depends on the value of the round trip in the previous trial. It is remarkably interesting to note the average value of passengers remains around 10 (which is the original value on which the building was designed and the number of elevators base). This phenomenon can also be seen in the next section, where the value of passengers always “gravitates” towards the design value of passengers ( $P=10$ ) regardless of the initial value.

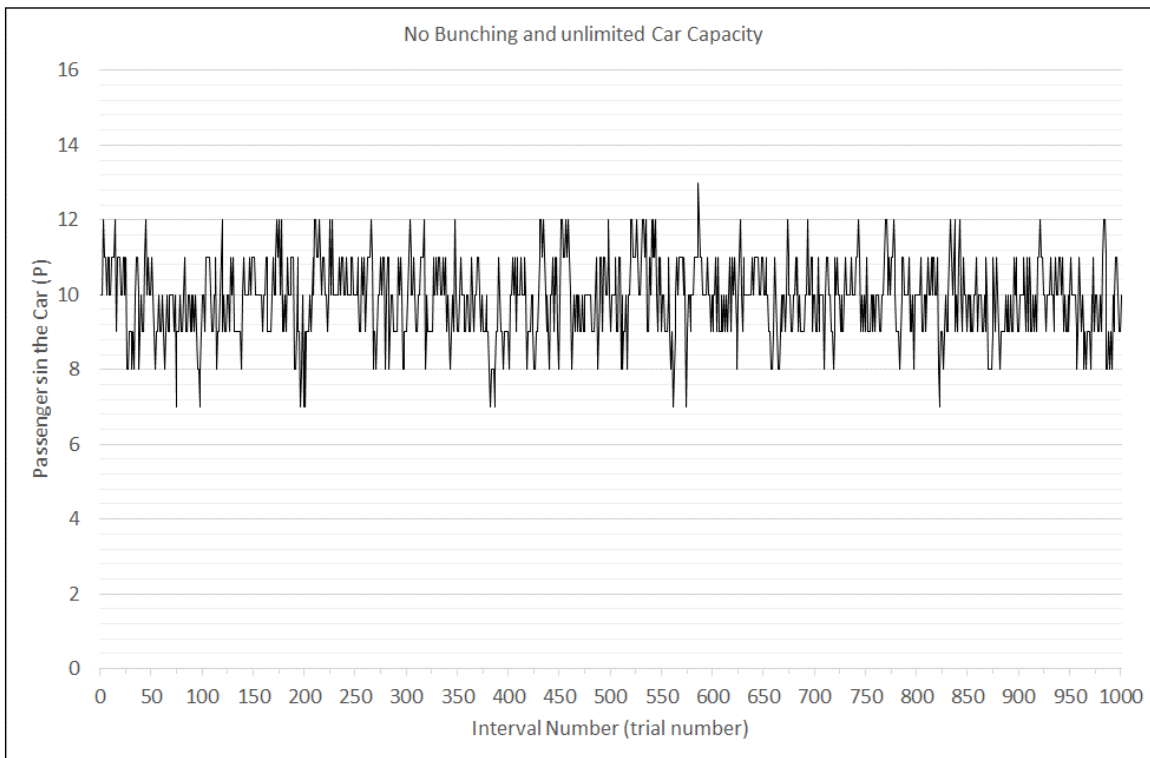


**Figure 2: The number of passengers in the car in each trial without bunching and with unlimited car capacity.**

The effect of bunching is then taken into consideration in the next figure (Figure 3). The “swings” in the number of passengers boarding is much larger than the case because this case considers both the value of the round trip time in the most recent trial as well as the difference between the values of the round trips for the latest two trials (which is a representation of the effects of bunching). Nevertheless, it is also remarkable to note that the average value of the passengers boarding the car is still equal to the design value of  $P=10$  passengers.

The effect of bunching is taken into consideration as follows. The value of the previous round trip time is subtracted from the current value of the round-trip time. This is then divided by the number of elevators in the group in order to convert it from round-trip to interval. If the result is positive, it means that the current interval is longer than the previous interval and that there are more passengers arriving compared to the previous interval. If the result is negative, it means that fewer passengers would have arrived in the current interval compared to the previous interval. The difference between the two intervals is converted to units of passengers by multiplying the time difference by the arrival rate in units of passengers per second (i.e.,  $\lambda$ ). This provides the adjustment in the number of passengers. If positive the number is added to the number of passengers carried over to the next trial. If negative, it is subtracted from the number of passengers carried out to the next trial.

This algorithm recognizes the fact that the direct reason for bunching is the variability in the value of the round trip time in consecutive intervals.

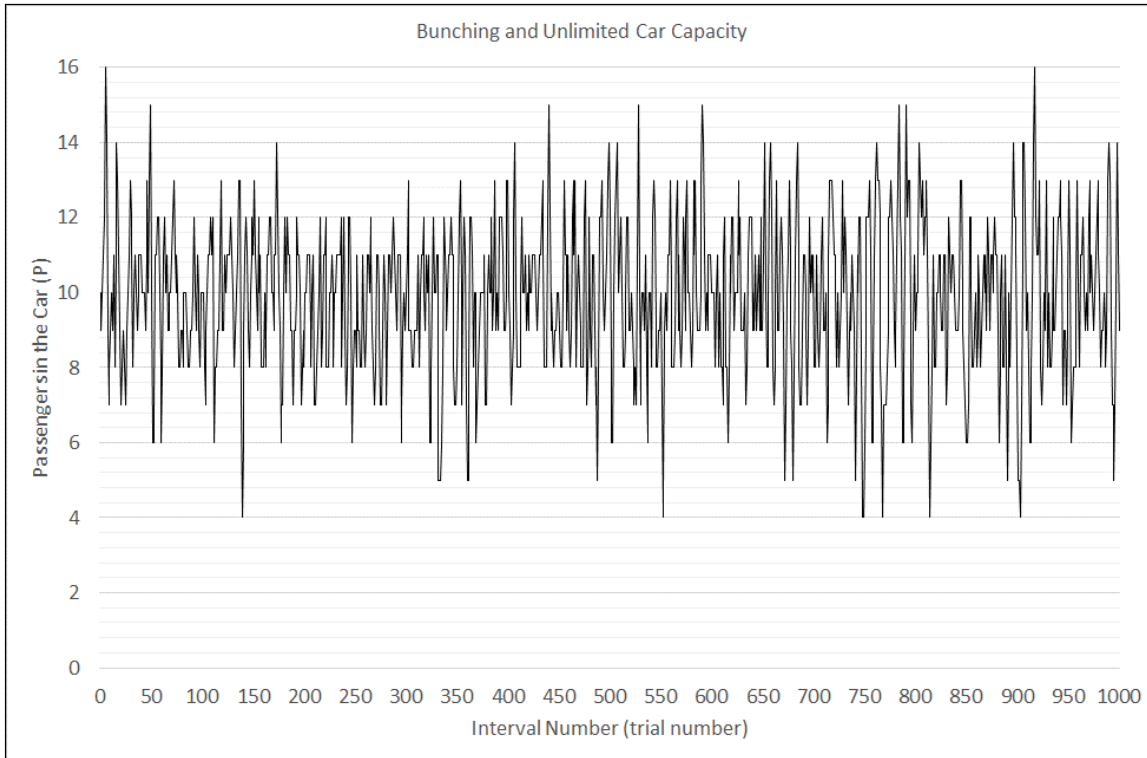


**Figure 3: The number of passengers in the car in each trial with bunching and assuming unlimited car capacity.**

It is worth noting that despite the variability on the value of the passengers board the car under the three setups (conventional MCS without interlinking; interlinked MCS without the effect of bunching; interlinked MCS with the effect of bunching) and the variability in the value of the round trip time under the three setups, the average value of the number of passengers boarding the elevator car is the same for the three setups as well as the average value of the round trip time. This is shown in the table below (Table 1).

It is worth noting that the original design of this building used 10 passengers ( $P_{des}=10$  passengers) and results in a design value for the round trip time of 133.5782333 s, and a design handling capacity of 12.477% of the population of the building, which has 900 residents.

**Table 1: Average values of passengers boarding the elevator car and the average value of the round trip time under the conventional MCS and the two interlinked MCS algorithms.**

Setup	MCS (constant car load)*	iLMCS unlimited car capacity without bunching	iLMCS unlimited car capacity with bunching
P	10.0	9.958	9.855
RTT (s)	133.57	133.02	131.6

\* The design values for the building assuming 5 elevators in the group.

The most important conclusion from this section is the following: Despite the random variations in the value of the round trip time (caused by the passenger destination selections) and the random variations in the number of passengers boarding the elevator car in each round trip, these variations will not lead to a loss in the handling capacity of the elevator traffic system if the elevator car is

assumed to have unlimited capacity. The average values of these two random variables will still converge to the same value assumed during the design process.

### 5. CONVERGENCE REGARDLESS OF THE INITIAL VALUE OF P

This section examines the convergence of the trials in the interlinked case. The question can be posed as follows: Do the future values of the round-trip time and the number of passengers in the car depend on the initial value used in the first trial? Or would these values converge to the correct value after enough trials?

In order to examine this point, the initial value of the number of passengers in the car was varied for the building under questions above and below the design value for the number of passengers in the car (which is  $P=10$  in this case). Values of 1 passenger, 10 passengers and 20 passengers were used. The system was run for 100 successive interlined trials. This was done for both the bunching interlinked case and the non-bunching interlinked case.

It is interesting to note that in both cases and regardless of the initial value for  $P$ , the trials quickly converged to the expected value of  $P$  (i.e.,  $P=10$ ) after a small number of trials (Figure 4 and Figure 5).

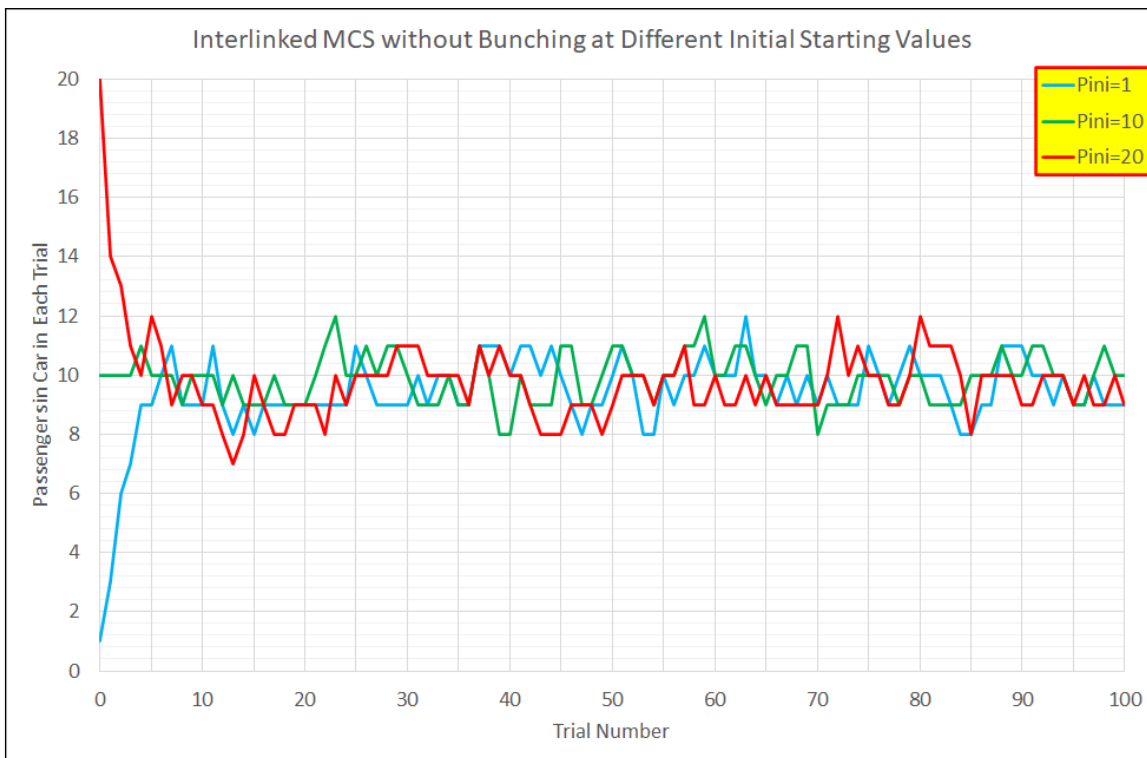
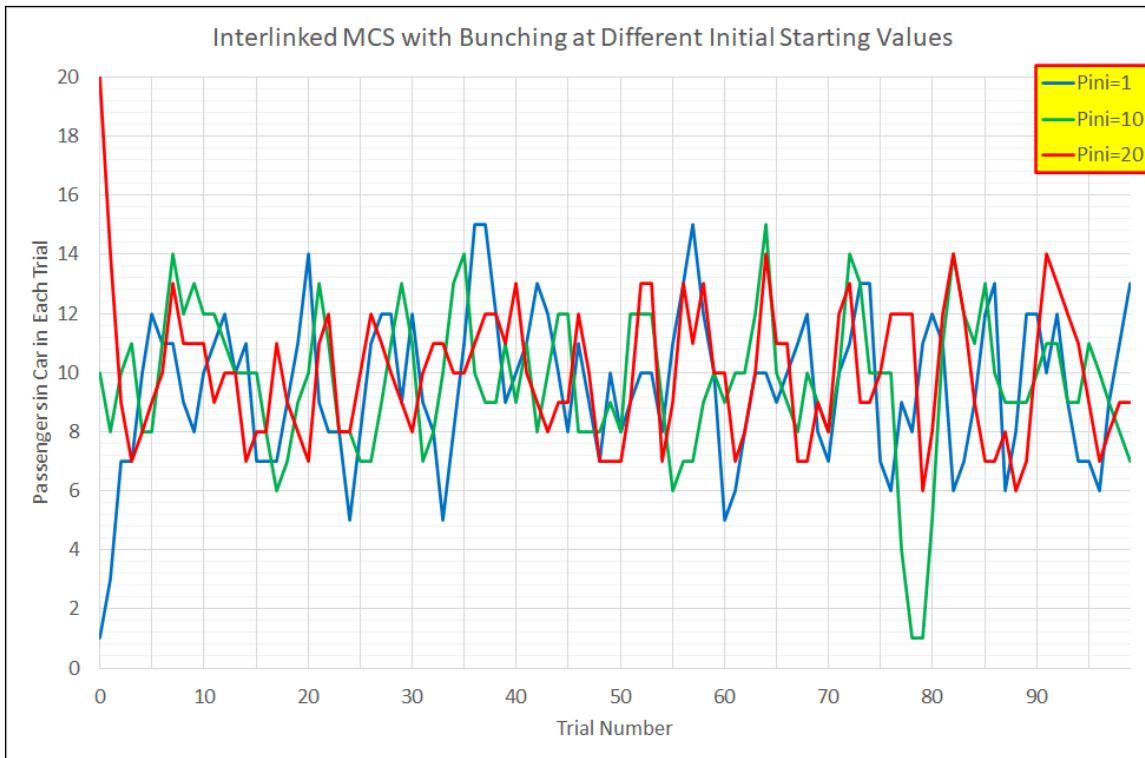


Figure 4: Convergence to the same value of  $P$  with different initial values not reflecting the effect of bunching.



**Figure 5: Convergence to the same value of P with different initial values including the effect of bunching.**

This *self-correcting mechanism* is remarkably interesting in understanding the variation in the value of the round-trip-time around its mean value. However, it is important to note that this is only possible under the assumption of unlimited car capacity.

## 6. THE EVOLUTION OF THE QUEUE LENGTH BASED ON THE RATED OR ENLARGED CAR CAPACITY

In this section, it will be assumed that the car capacity is limited, in order to understand its effect on the system performance. Since the car capacity will be assumed to be restricted, a number of passengers might not be able to board the elevator car in each round trip and will be “carried-over” to the next trial. Thus it is possible for queues to start developing at the landing.

Thus, the passenger queue length at the landing(s) is examined. By definition, the inter-linked nature of this method of Monte Carlo simulation means that the number of passengers carried over from trial to the next is effectively the number of passengers left behind and “carried over” to the next trial.

To investigate the passenger queue length, 100 consecutive interlinked trials were run and the data gathered for the number of passengers in the queue collected. Each one of these series of 100 trials was then repeated 1000 times. These 1000 runs will be denoted as an “ensemble” a term that is borrowed from weather forecasting (in weather forecasting, a large number of forecasts are run each with a slightly different initial value, and the results are called an ensemble). By taking the average of all the runs in the ensemble, a smooth run of 100 consecutive interlinked trials is produced.

This results in good convergence and shows a repeatable result that is shown in Figure 6. Four graphs are shown, each one showing the number of passengers in the queue over 100 consecutive trials.

It is clear from the plot that when the car capacity is limited to the design number of passengers (Pdes), the number of passengers in the queue increases continuously. However, when the car capacity is increased by just one passenger, the queue length does not increase continuously, but stabilizes at a constant value.

The figures also show the effect of taking bunching into consideration, where this causes a slight increase in the length of the queue.

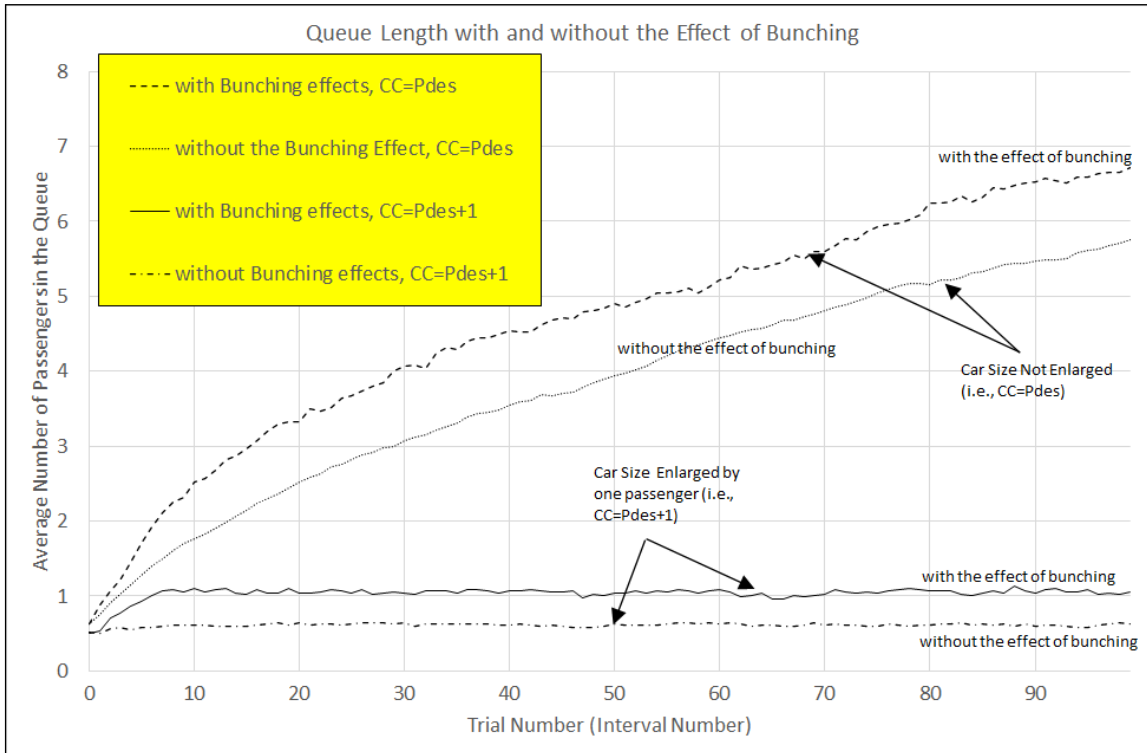


**Figure 6: The passenger queue length with and without the effect of bunching.**

This example clearly shows the importance of enlarging the elevator car capacity by a small amount in order to allow the queue length to stabilize. In this case, it was sufficient to increase it by one passenger, but further analysis is required on a number of different buildings in order to draw any firm conclusions about the required enlargement of the car capacity and its dependence on the parameters of the system being designed.

Another effect that can be observed when the results are further analysed is the actual achieved handling capacity. By processing the number of passengers in the car in each trial and the actual round-trip time, the actual handling capacity in each trial can be calculated. The average handling capacity is shown in Table 2 over all the 100 trials (averaged from the ensemble). It can be seen that bunching reduces the actual handling capacity below the design handling capacity. Limiting the elevator car size at the design number of passengers (Pdes) also causes a loss in the handling capacity from the design handling capacity of 12.477%.

**Table 2: The calculated actual handling capacity under four setups.**

Car capacity	Handling Capacity (HC%)	
	Without the effects of bunching	With the effects of bunching
CC=Pdes= 10	12.41%	12.39%
CC=Pdes+1=11	12.47%	12.46%

It is important to state that this building was based on the use of 10 passengers, a round trip time 133.5782333 s, and five elevators resulting in a design handling capacity of 12.477%. The building has 60 persons per floor over 15 floors, with a total population of 900 persons. The traffic was assumed to be incoming.

## 7. CONCLUSIONS

The Monte Carlo simulation has been successfully used to find the value of the elevator round trip time under general conditions, such as the multiple entrances, general traffic conditions, and rated speed not attained in one floor jump. It has also been used to find the value of the passenger transit time as well as the round-trip time under destination group control.

This paper has extended the use of the Monte Carlo simulation method in order to allow it to reflect the random nature of the passenger boarding the elevator in each round trip and the random variations in the value of the round trip. This has been done by inter-linking the consecutive trials by using the final value from one trial as the starting value for the next trial.

It has been shown that, despite the random variations in the value of the passengers boarding the car in each round and the random variation in the value of the round trip time, the average value of these remains equal to the design value of the elevator traffic system. It was also shown that as long as the car capacity is assumed to be unlimited, the handling capacity of the elevator traffic system is not reduced due to these random variations.

When the car capacity was limited to the design value of the passengers (Pdes), a slight reduction was observed in the handling capacity coupled with an increasing passenger queue at the landing. By increasing the car capacity by just one passenger, the handling capacity was restored, and the queue nearly disappeared. Although the required enlargement could be different for different systems and buildings, the general conclusion is that an increase in the car capacity from the design value is necessary in order to overcome the detrimental effects that could result from the random variations in the value of the number of passengers boarding the elevator car and the random variations in the value of the round trip time.

This paper has only addressed the effects of the randomness of the passenger destinations. Future papers will address the random effect of the passenger exact arrivals in time. Further research is also needed to identify the effects of enlarging the car capacity and how it impacts the queue length at the landing.

## BIOGRAPHICAL NOTES

Lutfi Al-Sharif is currently Professor of Electrical Engineering at Al-Hussein Technical University in Amman/Jordan and jointly Professor of Building Transportation Systems at of the Department of Mechatronics Engineering, The University of Jordan. He received his Ph.D. in elevator traffic analysis in 1992 from the University of Manchester, U.K. He worked for 10 years for London Underground, London, United Kingdom in the area of elevators and escalators.

In 2002, he formed Al-Sharif VTC Ltd, a vertical transportation consultancy based in London, United Kingdom. He has over 30 papers published in peer reviewed journals the area of vertical transportation systems and is co-inventor of four patents and co-author of the 2<sup>nd</sup> edition of the Elevator Traffic Handbook.

He is also a visiting professor at the University of Northampton (UK), member of the management committee of the annual Symposium on Lift & Escalator Technologies and a consultant for Peters Research Ltd.

He is a passionate believer in making higher education simple and accessible for engineering students and has a You Tube channel on engineering that has more than 55 000 subscribers and around 8 million views. He has also been working as a member of the METHODS Erasmus+ Project that aims to improve teaching methods in higher education in Jordan and Palestine. He is also the author of the Mechatronics Engineering Module on Saylor.org.

## REFERENCES

- [1] Barney G C and Al-Sharif L. Elevator Traffic Handbook: Theory and Practice. Routledge. 2016.
- [2] Al-Sharif L. Introduction and Assessing Demand in Elevator Traffic Systems (METE I). Lift Report 2014; 40(4): 16-24. July/August 2014.
- [3] Barney G C and Dos Santos S M. Elevator Traffic Analysis, Design and Control. Peter Peregrinus Ltd., revised 2nd edition, 1985.
- [4] Peters R D. Ideal Lift Kinematics. *Elevator Technology* 6, IAEE Publications, 1995.
- [5] Al-Sharif L. Intermediate Elevator Kinematics and Preferred Numbers (METE III). Lift Report 2014; 40(6): 20-31. Nov/Dec 2014.
- [6] Peters R D. *Vertical Transportation Planning in Buildings*. Ph.D. Thesis, Brunel University, Department of Electrical Engineering, February 1998.
- [7] Al-Sharif L. The effect of multiple entrances on the elevator round trip time under up-peak traffic. *Mathematical and Computer Modelling* 2010; 52(3-4): 545-555.
- [8] N.R. Roschier, M.J. Kaakinen, "New formulae for elevator round trip time calculations", *Elevator World* supplement, 1978.
- [9] Al-Sharif L and Abu Alqumsan A M. Stepwise derivation and verification of a universal elevator round trip time formula for general traffic conditions. *Building Services Engineering Research and Technology* 2015; 36(3): 311-330. doi: 10.1177/0143624414542111.
- [10] Al-Sharif L, Aldahiyat H M and Alkurdi L M. The use of Monte Carlo simulation in evaluating the elevator round trip time under up-peak traffic conditions and conventional group

control. *Building Services Engineering Research and Technology* 2012; 33(3): 319–338. doi:10.1177/0143624411414837.

[11] Al-Sharif L and Abu Alqumsan A M. An Integrated Framework for Elevator Traffic Design under General Traffic Conditions Using Origin Destination Matrices, Virtual Interval and the Monte Carlo Simulation Method. *Building Services Engineering Research and Technology* 2015; 36(6): 728-750.

[12] Al-Sharif L, Abdel Aal O F and Abu Alqumsan A M. Evaluating the Elevator Passenger Average Travelling Time under Incoming Traffic Conditions using Analytical Formulae and the Monte Carlo Method. *Elevator World* 2013; 61(6): 110-123. June 2013.

[13] So A, Al-Sharif L and Hammoudeh A. Traffic analysis of a simplified two-dimensional elevator system. *Building Services Engineering Research and Technology*. 2015; 36(5): 567-579. doi:10.1177/0143624414568728.

[14] So A, Al-Sharif L and Hammoudeh A. Concept design and derivation of the round trip time for a general two-dimensional elevator traffic system. *Journal of Building Engineering* 2016; 5(2016): 165-177.

[15] So A, Al-Sharif L and Hammoudeh A T. Analysis of possible two dimensional elevator traffic systems in large buildings. *Elevator Technology 20* 2014; 20:51-61. Paris, France, July 2014.

[16] Al-Sharif L and Peters R D. Using the Monte Carlo Simulation to Evaluate the Round-Trip Time under Destination Group Control. 9<sup>th</sup> Symposium on Lift & Escalator Technologies, Northampton, United Kingdom. September 2018.

[17] Al-Sharif L. Bunching in lifts: Why does bunching in lifts increase waiting time? *Elevator World (Mobile, AL, USA)* 1996; 44(11): 75–77.

[18] Al-Sharif L. Bunching in Lift Systems. *Elevator Technology* 5 1993; 5: 88-97. The International Association of Elevator Engineers (Brussels, Belgium), the proceedings of the 5th International Congress on Elevator Technologies, Elevcon '93, Vienna, Austria, November 1993.